ESCUELA INTERNACIONAL DE DOCTORADO
(CEINDO)

PROGRAMA EN CIENCIA Y TECNOLOGIA DE LA SALUD

UNIVERSIDAD CEU

FACULTAD DE FARMACIA
DEPARTAMENTO DE QUÍMICA Y BIOQUÍMICA

TESIS DOCTORAL

LRRK2 inhibitors as effective drugs for the treatment of neurodegenerative diseases

Presentada por

Josefa Zaldivar Diez de Bonilla

Directores:

Ana Martínez Gil

Carmen Gil Ayuso-Gontán

Madrid, 2018

ACKNOWLEDGEMENTS

PREFACE

INDEX

ABBREVIATION LIST……...**1**

RESUMEN…….....**7**

INTRODUCTION……...**13**

1. Neurodegenerative diseases and kinase proteins: general overview……..**15**

2. LRRK2 general overview……...**19**

3. New roles for LRRK2……**23**

3.1. The implication of LRRK2 in regulating adult neurogenesis……....**23**

3.2. The relationship between LRRK2 and tau…….....**25**

3.2.1. Direct and indirect phosphorylation of tau by LRRK2…….……..**29**

3.2.2. Tau aggregates in *post mortem* studies in patients carrying *LRRK2* mutations……..……**31**

3.3. LRRK2 and retinal neurodegenerations……...…….**33**

3.3.1. Retinal neurodegenerations…….**34**

4. LRRK2 inhibitors……..……..**36**

4.1. Introduction to chemical genetics……...…**36**

4.2. Non-selective LRRK2 inhibitors……**37**

4.3. Selective LRRK2 inhibitors……..….**39**

4.3.1. Diaminopyrimidine derivatives…….....**39**

4.3.2. Indolinone derivatives……**42**

4.3.3. Other scaffolds……..……...**43**

4.4. Final considerations when designing new LRRK2 inhibitors……**45**

OBJECTIVES……..**47**

RESULTS AND DISCUSSION……..**51**

1. Design and synthesis of new LRRK2 inhibitors……...**53**

1.1. Introduction and background……..……**53**

1.1.1. Indolinone derivatives..……...**54**

1.1.2. Triazolo-pyrimidine derivatives…….……**55**

1.1.3. Benzothiazole derivatives……**55**

1.2. Objectives……...**57**

1.3. LRRK2 homology model and docking studies……..**58**

1.3.1. Construction of the homology model……..**58**

1.3.2. Docking studies……...**60**

1.4. Design, synthesis, enzymatic evaluation and structure-activity-relationships of new indolinone derivatives……**63**

1.4.1. Design of new indolinone derivatives……**63**

1.4.2. Synthesis of new indolinone-piperazine derivatives……...**64**

1.4.3. Enzymatic evaluation on LRRK2, structure-activity-relationships and docking studies……...……..**66**

1.4.4. Detailed study of the isomeric equilibrium in the indolinone derivatives synthesized……**68**

1.5. Design and synthesis of new LRRK2 inhibitors based on the benzothiazole scaffold……..**71**

1.5.1. Synthesis of *N*-(benzothiazole-2yl)-4-morpholine benzamide derivatives……..……**71**

1.5.2. Synthesis of *N*-(6-fluorbenzothiazole-2yl)-aryl derivatives……**73**

1.5.3. Enzymatic evaluation on LRRK2, structure-activity-relationships and docking studies……...……..**74**

1.6. Determination of the blood-brain-barrier permeability……..**78**

1.6.1. *In vitro* parallel artificial membrane permeability assay……**78**

1.7. Conclusions……**81**

2. LRRK2 inhibitors as pro-neurogenic agents……**83**

2.1. Introduction……**83**

2.2. Objectives……**84**

2.3. Wnt signaling modulation……**85**

2.3.1. Background of the assay employed……**85**

2.3.2. Results and discussion……**86**

2.4. Neurosphere proliferation assay……**91**

2.4.1. Background of the assay employed……**91**

2.4.2. Results and discussion……**92**

2.5. Neurosphere differentiation assay……**96**

2.5.1. Background of the assay employed……**96**

2.5.2. Results and discussion……**96**

2.6. Conclusions……**100**

3. LRRK2 inhibitors as anti phospho-tau agents……**103**

3.1. Introduction……**103**

3.2. Objectives……**104**

3.3. Tau-neuroprotection assay……**105**

3.3.1. Validation of the assay……**105**

3.3.2. Tau neuroprotection assay for triazolo-pyrimidine and benzothiazole LRRK2 inhibitors……**108**

3.4. Ngn2-transfected-A152T-derived neurons assay……**110**

3.4.1. Background of the assay employed……...**110**

3.4.2. Results and discussion……...**112**

3.5. 6-weeks differentiation A152T assay……...**117**

3.5.1. Background of the assay employed……...**117**

3.5.2. Results and discussion……...**118**

3.6. *In vivo* models of tauopathies……...**120**

3.6.1. GMR-MAPT. V337M *Drosophila melanogaster* model……..**120**

3.6.2. Tauopathy rodent model……**124**

3.7. Conclusions……..**130**

4. LRRK2 as a therapeutic target for retinitis pigmentosa……...**131**

4.1. Introduction……..**131**

4.1.1. The *rd10* mouse model……..**131**

4.2. Background……...**136**

4.3. Objectives……**141**

4.4. Analysis of the expression of LRRK2 in retina……**141**

4.5. Determination of the neuroprotective effect of indolinone **23** in the photoreceptor layer in *rd10* mice……**142**

4.6. Determination of the anti-inflammatory effect of indolinone **23** on activated microglia……..……..**144**

4.7. Conclusions……..**146**

CONCLUSIONS……**147**

DIFUSSION OF RESULTS……**151**

EXPERIMENTAL SECTION……**155**

1. Computational studies……..**157**

1.1. Homology models……**157**

1.2. Docking studies……**158**

1.3. Quantum mechanics minimizations……**158**

2. Chemistry……...**159**

2.1. Synthesis of indolinone derivatives……..**160**

2.2. Synthesis of benzothiazole derivatives……**164**

3. Biology……**175**

3.1. *In vitro* experiments**...**……...**175**

3.1.1. Enzymatic activity ……**175**

3.1.2. CNS Penetration: *in vitro* parallel artificial membrane permeability assay……..……..…**175**

3.1.3. Neural progenitor cells (NPCs) experiments ……**176**

3.1.4. Neurosphere cultures……..……...**177**

3.1.5. SH-SY5Y cultures……..……...**181**

3.1.6. Ngn2-transfected-A152T-derived neurons assay……..**181**

3.1.7. 6-weeks-differentiated A152T-derived neurons assay……..**183**

3.2. *In vivo* experiments……...……**184**

3.2.1. GMR-MAPT. V337M *Drosophila melanogaster* model……..**184**

3.2.2. *Rd10* mouse model……..……..**185**

REFERENCES……..**187**

ABBREVIATION LIST

- AcOEt: ethyl acetate
- AD: Alzheimer's disease
- ADME: absorption-distribution-metabolism-excretion
- ADMET: absorption-distribution-metabolism-excretion-toxicology
- AGD: agyrophilic grain disease
- ALS: amyotrophic lateral sclerosis
- ANK: ankyrin
- ARM: armadillo
- BBB: blood-brain barrier
- BSA: bovine serum albumin
- CBD: cortico basal degeneration
- CDK5: cyclin-dependent-like kinase 5
- ^{13}C-NMR: ^{13}C-nuclear magnetic resonance
- CNS: central nervous system
- COR: carboxy-terminal of a ras of complex
- CTE: chronic traumatic encephalopathy
- DAPI: 2-(4-amidinophenyl)-1H-indole-6-carboxamidine
- DFT: density fuctional theory
- DMAP: 4-(dimethylamino)pyridine
- DMEM: Dulbecco´s modified Eagle´s medium
- DNA: deoxyribonucleic acid
- DVL1: disheveled 1
- Dcx: double cortin
- EDTA: ethylenediaminetetraacetic acid
- EDCI: N-(3-dimethylaminopropyl)-N´-ethylcarbodiimide
- EGF: epidermal growth factor
- EtOH: ethanol
- ESI: electrospray ionization
- FBD: familial British dementia
- FBS: fetal bovine sreum
- FCG: forward chemical genetics
- FDD: familial Danish dementia
- FGF: fibroblast growth factor

- FG: forward genetics
- FTD: frontotemporal dementia
- FTLD: frontotemporal lobar degeneration
- FTDP-17: frontotemporal dementia with parkinsonism linked to chromosome 17
- GCC: ganglionic cell layer
- GDP: guanosine diphosphate
- GFAP: glial fibrillary acidic protein
- GGT: globular glial tauopathy
- GM: glia of Müller
- GSK-3β: glycogen-synthase kinase 3β
- GTP: guanosine triphosphate
- HEK: human embryonic kidney
- Hex: hexane
- ^{1}H-NMR: ^{1}H-nuclear magnetic resonance
- HTS: high-through-put screening
- HOBT: hydroxybenzotriazole
- HPLC: high-performance-liquid-choromatography
- HRMS: high resolution mass spectrometry
- IBA-1: ionized calcium-binding adapter molecule 1
- INL: inner nuclear layer
- IPL: inner plexiform layer
- iPSC: induced-pluripotent stem cells
- JAK2: janus kinase 2
- LRP6: low-density lipoprotein receptor-related protein 6
- LRR: leucine-rich repeats
- LRRK2: leucine-rich-repeat kinase 2
- MAPT: microtubule-associated tau
- MTT: 3-(4,5-dimethylthiazol-2-yl)-2,5-diphenyltetrazolium bromide
- MS: mass spectrometry
- NFTs: neurofibrillary tangles
- Ngn2: neurogenin 2
- NOR: novel object recognition
- NPC: neural progenitor cells

- NSC: neural stem cells
- OA: okadaic acid
- ONL: outer nuclear layer
- OPL: outer plexiform layer
- PBS: phosphate buffer saline
- PD: Parkinson´s disease
- PDE6: phosphodiesterease 6
- PFA: paraformaldehyde
- PTMs: posttranslational modifications
- PP2A: protein phosphatase 2A
- PSP: progressive supranuclear palsy
- PyBOP: benzotriazol-1-yl-oxytripyrrolidinophosphonium hexafluorophosphate
- q-PCR: quantitative polymerase chain reaction
- RCG: reverse chemical genetics
- RD: retinal dystrophies
- RGC: retinal ganglionic cells
- RMSD: root mean square deviation
- RNA: ribonucleic acid
- ROC: ras of complex
- ROCK: rho-associated-coiled-coil-containing kinase
- ROS: reactive oxygen species
- RP: retinitis pigmentosa
- RPE: retinal pigment ephitelium
- r.t.: room temperature
- rt- PCR: real-time polymerase chain reaction
- SAR: structure-activity relationships
- SD: standard deviation
- SDS: sodic dodecilsulfate
- SEM: standard error of the mean
- SGV: subgranular zone
- SOD1: superoxide dismutase 1
- SVZ: subventricular zone
- TCF/LEF: T-cel factor/lymphoid enhancer factor

- THF: tetrahydrofuran
- TIE2: tyrosin protein kinase receptor 2
- TLC: thin-layer chromatography
- TNFα: tumor necrosis factor-α
- WB: western blot
- WT: wild type

RESUMEN

El tratamiento de las enfermedades neurodegenerativas, como la enfermedad de Alzheimer o la enfermedad de Parkinson entre otras, es uno de los grandes retos del siglo XXI. Esto se debe al gran número de pacientes afectados debido al aumento en la esperanza de vida. Se trata de enfermedades devastadoras en las que la calidad de vida de los enfermos empeora drásticamente. Asimismo, tienen un gran impacto social debido al gasto que suponen para la sanidad pública y las familias. Por todo ello, es de vital importancia encontrar nuevos fármacos eficaces que sean capaces de frenar el avance de estas enfermedades y no sólo de paliar los síntomas de las mismas.

Este tipo de patologías se caracterizan por ser enfermedades multifactoriales en las que se ven implicados varios procesos biológicos. La etiología de estas enfermedades es aún desconocida pero se han descrito distintos eventos comunes a todas ellas entre los cuales destacan el estrés oxidativo, la neuroinflamación, la excitotixidad del glutamato y disrupciones en el proceso de plegamiento de las proteínas.

La fase final en la biosíntesis de las proteínas corresponde a las modificaciones post-trasduccionales. Estas modificaciones post-transduccionales juegan un papel fundamental en el correcto plegamiento de las proteínas. Una de las más relevantes en la fisiología humana es la fosforilación. El proceso de fosforilación supone un equilibrio entre la función de diversas proteínas quinasas y las fosfatasas. Existen varias quinasas que fosforilan a diversas proteínas implicadas en los mecanismos de neurodegeneración. Una de éstas es la quinasa rica en repeticiones de leucina, LRRK2 (del inglés leucine-rich-repeat kinase 2).

LRRK2 fue descubierta en 2002 y se ha convertido en una de las dianas más estudiadas en el campo de la enfermedad de Parkinson, ya que las mutaciones en el gen que codifica esta proteína son la primera causa genética de esta enfermedad. LRRK2 es una proteína compleja con siete dominios diferentes que ejerce una actividad tanto GTPasa como ATPasa. Sin embargo, el papel que juega esta enzima en diferentes vías de señalización neuropatológicas es más extenso y por tanto, podría jugar un papel importante en otras enfermedades neurodegenerativas.

Por ello, nos planteamos como objetivo principal de ésta tesis estudiar el papel que juega LRRK2 fuera de la enfermedad de Parkinson mediante una estrategia de química genética.

Para ello, en primer lugar y dado que no existe una estructura cristalográfica del dominio quinasa de LRRK2, se construyó un modelo de homología. Este modelo permitió el estudio del modo de unión de una familia de inhibidores de LRRK2 que ya había sido sintetizada en el grupo de investigación además de guiar el diseño de una nueva familia de inhibidores derivados de benzotiazol que ha sido sintetizada en este trabajo.

De esta manera utilizando esta pequeña pero estructuralmente diversa colección de inhibidores de LRRK2, se ha podido estudiar en distintos modelos *in vitro* e *in vivo*, la implicación de este enzima en la neurogénesis en adulto, en la fosforilación de tau y en la retinosis pigmentaria. En relación a la activación de la neurogénesis en adulto que podría compensar la muerte neuronal que ocurre en las enfermedades neurodegenerativas, se ha visto que algunos de los inhibidores actúan como moduladores positivos de la vía de señalización de Wnt (una de las principales vías neurogénicas) en un modelo que utiliza progenitores neuronales humanos obtenidos a partir de células pluripotenciales inducidas de adultos sanos. Asímismo, estos inhibidores con potencial neurogénico fueron probados *in vitro* en neuroesferas obtenidas a partir de la zona subventricular de ratones adultos y se comprobó que los mismos eran capaces de promover la proliferación de los progenitores neurales. Finalmente, los inhibidores más prometedores fueron estudiados en experimentos de diferenciación utilizando estas mismas neuroesferas y se pudo observar como algunos de ellos eran capaces de promover el linaje neuronal y fundamentalmente oligodendrocítico. Esta interesante actividad biológica de los inhibidores de LRRK2, hace pensar que este diana puede jugar un papel interesante en la esclerosis múltiple.

Por otro lado, se decidió estudiar si la inhibición farmacológica de LRRK2 podría ejercer efecto en la fosforilación de tau. Esta hipótesis se basó en el hecho descrito sobre la fosforilación de tau *in vitro* como *in vivo* por LRRK2 tanto de una manera directa como indirecta. Para confirmar esta hipótesis, la quimioteca de inhibidores de LRRK2 se evaluó en un ensayo de neuroprotección desarrollado en este trabajo mediante el cual se induce neurotoxicidad por incremento de la fosoforilación de tau en células de neuroblastoma humano. Los inhibidores de LRRK2 demostraron tener un efecto neuroprotector en este modelo. Asímismo, estos compuestos fueron probados en un modelo celular de demencia fronto-temporal en el cual se utilizan neuronas glutamatérgicas obtenidas a partir de las células pluripotentes inducidas de un paciente afectado de esta enfermedad y portador de una mutación en el gen que codifica la proteína tau y que consecuentemente provoca la

hiperfosforilación de la misma. Algunos inhibidores fueron capaces de reducir la fosforilación de tau en las dendritas así como la acumulación patológica de tau total en el soma de estas neuronas. En un siguiente paso, los compuestos más interesantes fueron probados en un segundo modelo celular de demencia fronto-temporal en el que a partir de las mismas células pluripotentes inducidas del mismo paciente se obtuvo un cultivo neuronal mixto en el que había neuronas dopaminérgicas, colinérgicas, glutamatérgicas y serotonérgicas, entre otras. En este segundo modelo se determinó cómo estos inhibidores de LRRK2 eran capaces de reducir la fosforilación de tau en distinto grado y medida en distintos epítopos. Un grupo reducido de estos inhibidores prometedores fueron probados en un modelo *in vivo* de *Drosophila* en el cual se expresa una forma humana mutada de la proteína tau en el ojo de la mosca. Consecuentemente se desencadena un fenotipo patológico en el ojo de esta. En un ensayo cualitativo se determinó cómo uno de los inhibidores de LRRK2 es capaz de revertir dicho fenotipo. Finalmente, uno de los inhibidores más prometedores fue probado en un modelo de tauopatía murino en el cual se induce la expresión de tau humana mutada en el lado ipsilateral del hipocampo. Con este modelo se determinó que el inhibidor es capaz de alcanzar el cerebro ya que se produce una bajada en los niveles de fosforilación de tau en el hipocampo, a la vez que una mejora de la cognición en estos animales.

El último campo en el que se decidió estudiar el papel de LRRK2 fue en las degeneraciones retinianas, en concreto, la retinosis pigmentaria. Ya se había visto en el grupo que la glúcogeno-quinasa-3β (GSK3-β) juega un papel importante en este tipo de patologías y dado que LRRK2 está muy relacionada con la misma, se decidió estudiar si podría estar también implicada. En un primer lugar, se determinó que en un modelo de roedor de esta enfermedad (*rd10*), la expresión de LRRK2 aumenta a medida que avanza el proceso neurodegenerativo. En un segundo lugar, se estudió cómo en animales que habían sido tratados con uno de los inhibidores de LRRK2 había una tendencia a neuroproteger la capa de fotorreceptores así como una bajada importante de la neuroinflamación que se da en la retina como consecuencia de la enfermedad.

Estos resultados abren un nuevo horizonte terapéutico para los inhibidores de LRRK2, ya que se muestra que esta enzima puede ser una diana interesante para promover la neurogénesis en adulto con una especial implicación en la esclerósis múltiple, en tauopatías y también en retinosis pigmentaria

INTRODUCTION

1. Neurodegenerative diseases and kinase proteins: general overview

The search of effective treatments for neurodegenerative diseases is one of the most urgent clinical and social needs today given their widespread and devastating nature. As most neurodegenerative disorders are age-dependent, due to longer life expectancy the prevalence of these diseases, including Alzheimer´s (AD) and Parkinson´s diseases (PD) among others, increases daily[1, 2]. Given their largely complex unknown etiology and the lack of effective treatments there is a critical need to better understand the underlying disease pathophysiology and discover effective disease-modifying targets for their treatment. The most important neurodegenerative diseases by the number of patients are AD, PD, amyotrophic lateral sclerosis (ALS) and tauopathies[3].

In 1807, James Parkinson firstly described "the shaking palsy" which nowadays is kwon as PD[4]. In 1906, Alois Alzheimer, firstly described AD as a "peculiar severe disease process of the cerebral cortex"[5]. More than two hundred years ago since the first documentation of this type of diseases, some aspects of their pathology have been discovered or understood, however big gaps of knowledge continue to exist[6]. Currently, is known that the molecular mechanisms behind PD and AD are complex and involve several theories or hypothesis where many diverse factors interrelate. However, none of these postulates alone is able to clarify the pathophysioly behind these diseases[7]. Thus, neurodegenerative diseases can be considered as multifactorial diseases where many more studies are required[8].

Beside all the research that still needs to be done three main events have become evident in the etiology of neurodegenerative diseases: the excitotoxicity effect mediated by an excess of glutamate, neuroinflammation and oxidative stress.

- Excitotoxic effect. High levels of glutamate in the synaptic cleft lead to a massive entry of Ca^{2+} into the neuron. This big increase in the Ca^{2+} concentration promotes the activation of phospholipases, proteases and endonucleases among other enzymes which overcomes in damages in the cytoskeleton, cellular membrane and DNA[9].

- Neuroinflammation. The role of neuroinflammation is a double-edged sword and its effects depend on the control of the response[10]. The principal component of neuroinflammation is the activation of the microglia that is the resident innate immune cells in the Central Nervous System (CNS) and provides the first line of defense. They can sense a wide range of stimuli that disrupt the microenvironment of the brain including CNS trauma, ischemia, infection agents, toxic insults and autoimmune injuries. Activation of the microglia is normally a beneficial effect and its action is stopped whenever the homeostasis of the brain has been reestablished. However, escaping from its tight control, the response can become exaggerated and destructive, and turns into chronic persistent inflammation that drives progressive neurodegeneration. Thus, regardless of the type of the initial lesion, neuronal damage and uncontrolled inflammation amplify each other, including a vicious self-propagating cycle that causes the chronic progression of neurodegenerative diseases[11].

- Oxidative stress. Oxidative stress is the result of unregulated production of reactive oxygen species (ROS), such as hydrogen peroxide, nitric oxide, superoxide and hydroxyl radicals. One of the consequences of normal aging is the increase of copper and iron in the brain. This situation could lead to hypermetallation of proteins that normally bind to ROS; therefore, the concentration of ROS inside the brain will rise up[12].

These three events may change the brain microenvironment and therefore, they may interfere with the protein folding process (**Figure 1**)[13]. Normally, after their biosynthesis, most of the proteins must be converted into tightly folded compact structures in order to carry out function in proper way. However, under some circumstances such as ageing, mutation and environmental stress (i.e. glutamate excitotoxicity, neuroinflammation and oxidative stress), proteins deviates from their normal folding pathway that leads to the formation of protein aggregates[14].

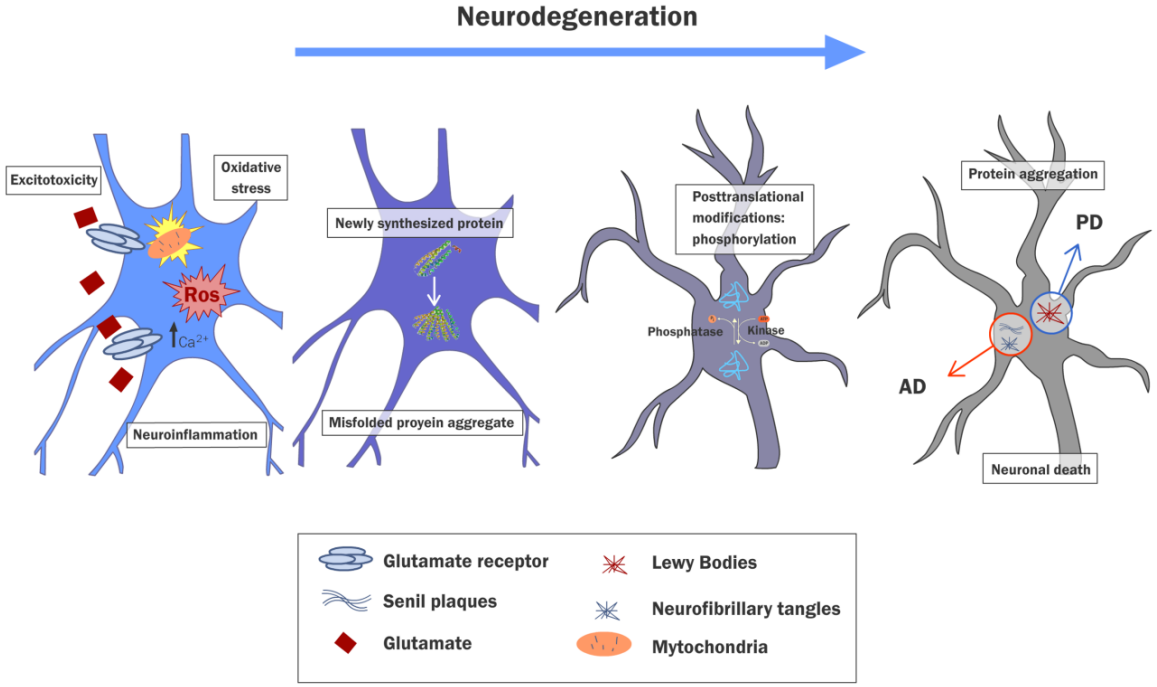

Figure 1. *Common molecular mechanisms leading to protein aggregation in neurodegenerative diseases.*

Thus, due to protein misfolding highly soluble proteins are gradually converted into insoluble, filamentous polymers which contain the characteristic cross-β-pleated sheet structures. These filamentous structures accumulate as amyloid fibrils which later deposit in the nucleus or cytoplasm of affected neurons or in the extracellular space. Eventually the accumulation of filamentous structures will lead to neuronal death[15]. The type of protein that aggregates depends on the type of disease and is summarized in **Table 1**. AD is characterized by two types of lesions, neurofibrillary tangles (NFTs) composed by aberrantly phosphorylated tau and senile plaques which are aggregates of β-amyloid[16]. In PD, inclusions of α-synuclein known as Lewy Bodies are found especially in the *substantia nigra* affecting mainly dopaminergic neurons[17]. In ALS, a mutated form of the superoxide dismutase 1 (SOD1) enzyme aggregates as well as aggregates of RNA-binding proteins and ubiquitin are found in the cytosol of the neuron[18].

Posttranslational modifications (PTMs) such as phosphorylation, ubiquitination or sumoylation, which alter the conformation and/or biological function of proteins, can also affect protein concentration, folding, localization and, ultimately, aggregation. Thereby, they play a critical role in neurodegenerative disorders[19].

Table 1. *Most abundant protein aggregates in neurodegenerative diseases.*

Disease	Protein/peptide	Characteristic pathology	Most affected regions
AD	i)Aβ-peptide (1-40/1-42) ii)Tau iii)α-synuclein	i)Senile plaques ii)NFTs iii)Lewy bodies	i)cortex, hippocampus, forebrain and brain stem ii)same as above iii)same as above
PD	i)α-synuclein ii)Parkin (DJ-1, PINK1)	i)Lewy bodies ii)Lewy bodies	i)*Substantia nigra* and cortex ii)*Substantia nigra*
ALS	Superoxide dismutase (SOD1), RNA binding proteins (TDP43, FUS, TAF15) and Ubiquitin	Hyaline inclusions, bonnia bodies and axonal spheroids	Spinal motor neurons and motor cortex
Primary tauopathies: Pick disease, progressive supranuclear palsy (PSP), corticobasal degeneration (CBD), argyrophilic grain disease (AGD), sporadic multiple system tauopathy with dementia, fontotemporal dementia with parkinsonism linked to chromosome 17 (FTDP-17) and globular glial taupathy (GGT)	Tau	Pick bodies	Frontal and temporal lobes of the cortex and hippocampus

Phosphorylation affects protein conformation, function and fate in many different ways: it may be required for proper protein folding; it may induce conformational changes that can result in lower or higher catalytic activity; it may precede or function as a recognition signal for further PTMs, such as ubiquitination; it may alter the subcellular localization and it may modify protein-protein interactions[20]. In PD, α-synuclein present in Lewy Bodies is phosphorylated in Ser129[21] and in AD and other tauopathies hyperphosphorylation of tau at multiple epitopes causes its misfolding and aggregation[22]. Therefore, phosphorylation has emerged as a key molecular target for neurodegenerative diseases. Phosphorylation is an interplay between kinases and phosphatases and thus kinases have become important targets for disease-modifying therapies to prevent neurodegeneration[23]. There are around 2000 kinase proteins encoded from more than 500 genes, contributing to approximately 1.7% of the human genome[24]. These enzymes are specific for serine, threonine and tyrosine, which means that they specifically phosphorylate the substrate in these amino acids. In the past two decades, protein kinases have emerged as prominent drug targets which are being pursued by pharma and academia. Previously thought to be non-druggable, presently more than 40 kinase inhibitors, including small molecules and antibodies, have been approved by the Food and Drug Agency [25]. While the

development of kinase inhibitors is still mainly concentrated in the field of oncology, a number of kinase-targeting candidate therapeutics have entered various stages of clinical evaluation for CNS indications[26]. Currently, among the most important established kinase targets for CNS diseases are: glycogen-synthase-kinase-3 (GSK-3), leucine-rich-repeat-kinase-2 (LRRK2), p38 mitogen-activated-protein-kinases (MAPKs), dual-specificity-tyrosine-phophorylation-regulated kinase 1A (DYRK1A), cyclin-dependent-like-kinase (CDK5), and rho-associated-coiled-coil-containing-kinase (ROCK)[23].

2. LRRK2 general overview

LRRK2 is an enigmatic enzyme that has been placed as one of the most highly pursued targets for PD. The discovery of LRRK2 in 2002, began with the identification of a gene defect localized to chromosome 12 in a family from Japan with autosomal dominant inherited Parkinson´s disease that did not carry any of the known PD mutations at that time and the locus was designated PARK8[27]. Before the discovery of LRRK2, known Mendelian forms of PD were early-onset forms, typically starting in the 30s, with either autosomal recessive [*PARK2* (parkin), *PARK6* (PINK-1), *PARK7* (DJ-1)] or dominant [*PARK1* (α-synuclein)] patterns of inheritance[28]. In contrast, only two years later, two independent groups identified mutations in *LRRK2* as the cause of *PARK8* PD[29, 30] by finding several families in Asia, the United States, and Europe that develop a dominantly inherited form of the disease that, similar to the original Japanese family, starting in the 50s or 60s and followed a course typical of the sporadic form.

LRRK2 is an unusually large protein (2527 amino acids) classified as a member of the ROCO superfamily which is characterized by the presence of a tandem Ras of complex (ROC) C-domain, kinase domains and carboxy-terminal of Roc (COR) sequence which links them[31]. In addition, domains related to protein-protein interaction are found: armadillo (ARM), ankyrin (ANK), leucine-rich repeats (LRR) and WD40 domains. In an overall view, the N-terminal region of LRRK2 will be formed by the ARM domain[32], the ANK domain compromising 7 ankryrin-type repeats and then 13 leucine-rich repeats in the LRR domain[33], followed by the catalytic domain with both GTPase and activity (ROC-COR-Kinase) and finally the WD40 domain which is consisted by C-terminal repeats[34]. A full crystal structure of human LRRK2 is not available yet, only the Roc domain is available[35]. However, giving the importance of having a structure of the kinase domain that allows the

design of kinase inhibitors, as well as the other domains, different crystallographic strategies have been employed. The resulted structures can be categorized in three different groups and have been deposited in the Protein Data Bank (**Figure 2**):

- Structure from a homology model using the kinase ERK2 as a template[36] (Figure 2A).
- Structures from the prokaryotic analogue *Chlorobium tepidum*: one of the leucine rich domain[37] and two of the Roc-COR domain[38] (Figure 2B).
- Surrogate crystals (Figure 2C): two structures have been obtained from punctual mutations on *Dictyostelium discoideum* Roco4 kinase to generate humanized Roco4 kinase which its active site resembles the human LRRK2 kinase domain[39], furthermore, this humanized Roco4 kinase was mutated in specific residues which correlate with human LRRK2 pathogenic mutations generating four structures more[40]; three crystals employing MST3 which is a kinase that its ATP-binding site has a 73% similarity to and it has been crystallized with three different LRRK2 inhibitors[41]; and finally four-teen LRRK2 kinase domain surrogate crystals obtained by the introduction of point mutations into checkpoint kinase 1 (CHK1) cocrystalysed with known literature LRRK2 inhibitors as well as new inhibitors described in that work[42].

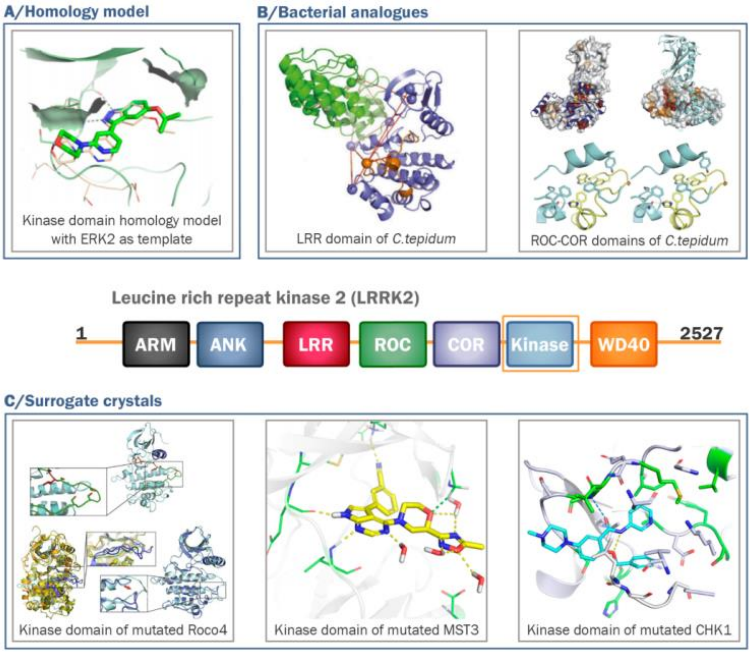

Figure 2. *Schematic representation of LRRK2 domains and crystal structures available.*

About 50 disease-associated mutations in *LRRK2* have been reported in familial or sporadic cases of Parkinson´s disease. The various dominant mutations in *LRRK2* result in changes concentrated in the central region of the protein. This region includes the ROC, the COR domain and the kinase domain. By contrast, mutations outside the catalytic domain have not shown to be involved in the pathology[43]. *LRRK2* mutations are the most common genetic cause of PD, accounting for 4% of familial PD and 1% of sporadic PD.

Furthermore, in North African Arabs the prevalence of *LRRK2* mutations rise up to 40% of all PD cases[44]. *LRRK2* mutations are autosomal and dominant as both homozygous and heterozygous have a same risk of disease. Five of them are definitely considered pathogenic:

- G2019S: is the most prevalent one as it is present in 85% of the patients carrying *LRRK2* mutations. It has been demonstrated that it increases the kinase activity up to 7-fold compared with the wild-type protein[43].
- R1441C, R1441G, Y1699C and I2020T: are much less common as they have only been identified in a small number of patients. Their role is controversial as some authors believe that they increase GTPase activity and others proposed the opposite effect[44]. Very curiously, R1441G mutation is most prevalent in the Basque Country and is rare outside northern Spain (**Figure 3**). It is hypothesized that it originated in the Basque population and the dispersion of the mutation occurred through short-range gene flow and was largely limited to nearby regions, thus, is popularly known as the "Basque mutation"[45].

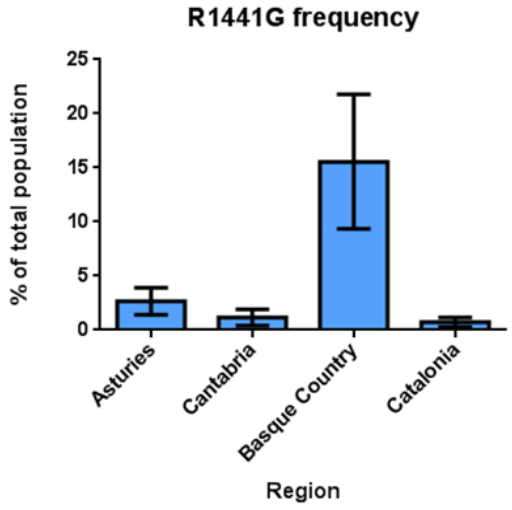

Figure 3. *Geographical distribution of the prevalence of R1441G mutation in Spain.*

The physiological functions of LRRK2 could be related to its two enzymatic activities: the kinase domain could catalyze phosphorylation and the ROC-GTPase domain is involved in GTP-GDP hydrolysis. In addition, to those catalytic functions, multiple protein-protein interaction regions indicate that LRRK2 may act as a scaffolding protein contributing to the formation of a multiprotein signaling complex[46]. However, the precise function of LRRK2 remains largely unknown. This is at least partially related that earlier research has mainly focused only on the role of LRRK2 in neurons, in which endogenous expression is low[47]. Many studies have, therefore, relied on overexpression of LRRK2 in non-physiologically relevant cell lines or animal models, but these approaches generate results that do not necessarily reflect the normal physiological interactome of LRRK2. A big step in trying to elucidate the physiological role of this protein was the discovery that RabGTPases may be substrates of LRRK2 catalytic activity[48]. However, in a target engagement context two LRRK2 auto-phosphorylation sites have been used as a measurement of LRRK2 activity: Ser935 and Ser1292. However, some authors report that Ser935 is not a direct LRRK2 auto-phosphorylation site[49]. Furthermore, one report that compared LRRK2 Ser935 and Ser1292 phosphorylation showed that the same LRRK2 inhibitor affected differently at these epitopes[41]. Therefore, the extent to which LRRK2 Ser935 and Ser1292 de-phosphorylation correlates with enzyme occupancy by an inhibitor should be interpreted with caution[50]. New experiments show that a possible better way of measuring LRRK2 activity and thus, LRRK2 inhibitor engagement is by measuring the phosphorylation of Rab10[51, 52].

Despite this outstanding work, there is evidence growing nearly in day to day basis implicating LRRK2 in remarkably diverse pathways. In an effort of trying to highlight the most important ones, the following LRRK2 implications may be listed: regulation of transcription[53], regulation of translation[54], mitochondrial function[55], neurite outgrowth[56], cytoskeletal dynamic[57], vesicle trafficking[58], autophagic protein degradation[47] and inflammation[59] (**Figure 4**). In the context of cellular localization, LRRK2 is consistently found in intracellular membranous structures including mitochondria[60], the endolysosomal system[61], the endoplasmic reticulum[62] and Golgi[63]. At a tissue level, LRRK2 in highly expressed in the lung and in kidneys[64]. In the brain is mostly found in the dopaminergic neurons of the *substantia nigra*[64].

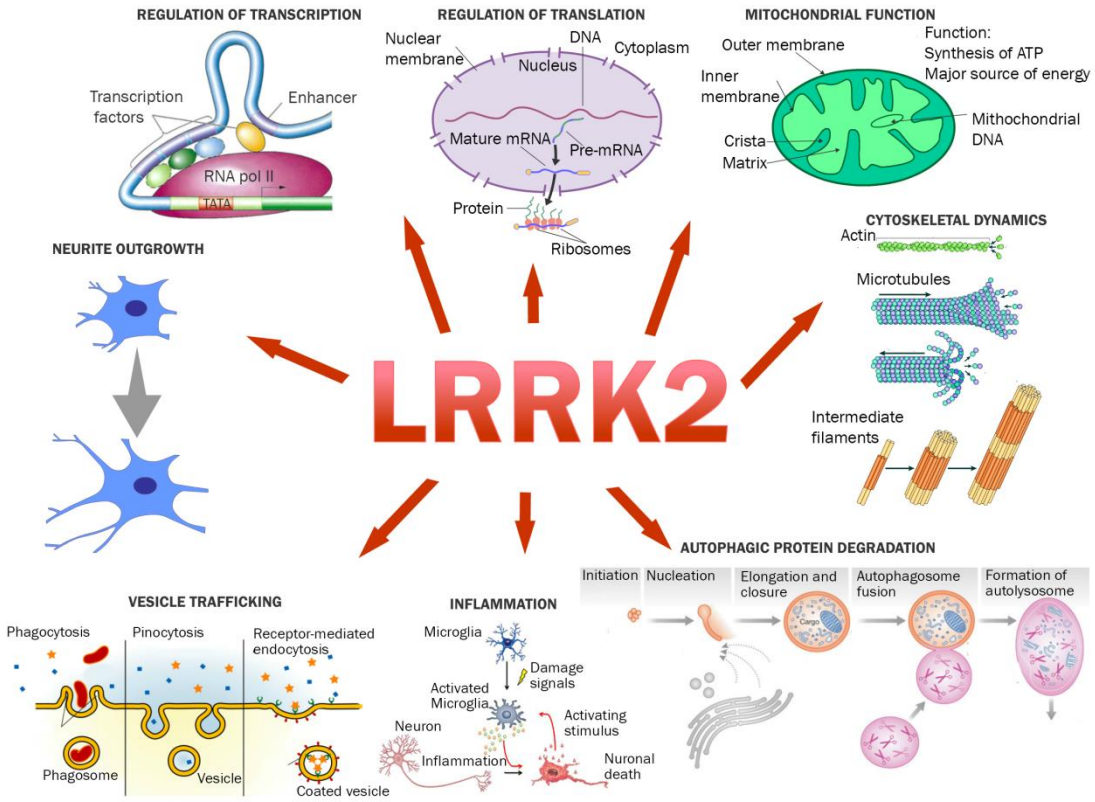

Figure 4. *Schematic representation of the main biological process in which LRRK2 is involved.*

LRRK2 physiology and pathology is a field that is growing exponentially since its discover in 2002[65]. LRRK2 research has progressed significantly in recent years with more reports of LRRK2 interactors and the development of more specific and sophisticated LRRK2 kinase inhibitors. The extent of PD association, the nature of its implied functional pathways together with its active kinase domain makes LRRK2 an attractive pharmacological target in the quest of new PD therapeutic[66]. However, the pathophysiology of LRRK2 is much more complicated and it can be related to other neurodegenerative disorders. Three important aspects and more recently reported are described in detail in order to argument the hypothesis that LRRK2 inhibitors could be used for other neurodegenerative diseases outside the PD spectrum.

3. New roles for LRRK2

3.1. The implication of LRRK2 in regulating adult neurogenesis

Since the time of the pioneering discoveries reported in 1962 by Joseph Altman regarding the formation of new neurons in the adult mammalian brain,[67] significant

progress has been made in terms of demonstrating the potential of activating adult neurogenesis[68]. The fact that new neurons are born in the adult brain has profound implications for our understanding of brain function and pathology as it raises the possibility that the nervous system has an intrinsic repair capacity[69]. Given evidence suggesting that neurogenesis is impaired in many neurodegenerative diseases, therapeutic approaches that stimulate neurogenesis may have potential to stimulate repair and even recovery, thereby, providing innovative disease-modifying treatments[70, 71].

Adult neurogenesis is observed mainly in two areas of the brain: the ventricular-subventricular zone (SVZ) along the walls of the lateral ventricles, and the subgranular zone (SGV) of the dentate gyrus in the hippocampus[72]. The magnitude of the formation of new neurons in the human brain was assessed with the outstanding work of K. L. Spalding *et al*. in which by measuring the concentration of nuclear-bomb-test-derived ^{14}C in genomic DNA, they found that 700 new neurons are added in each human hippocampus per day, corresponding to approximately an annual turnover of 1.75%[73].

Given the complexity of the signaling pathways involved in neurogenesis, there are many potential molecular targets for controlling neurogenesis, although the majority remains to be investigated. Wnt/β-catenin signaling is known as one of the major players in all stages of brain development while more recently it has been proved to be also involved in neural differentiation of pluripotent stem cells with an important role in the adult brain[74]. Using a Wnt signaling reporter mouse[75], Wnt/β-catenin signaling activity has been observed in neural stem cells (NSC) and neural progenitor cells (NPC) of the SVZ, moreover it is upregulated as an endogenous repairing mechanism in ischemic stroke[76] and traumatic nerve injury models[77].

Growing evidence suggests that deficiencies in Wnt signaling in the adult brain may be linked to the etiology of several neurodegenerative diseases, including AD and PD[78]. Furthermore, Wnt/β-catenin activation with specific small molecules modulators, such as some glycogen synthase kinase-3β (GSK-3β) inhibitors, have provided a preclinical way to promote neuroregeneration in ageing mouse models of PD by rescuing midbrain dopaminergic stem cells[79]. Taken together, these data suggest that pharmacological modulation of the Wnt signaling in the brain might lead to new therapeutic strategies for neurological diseases[80].

LRRK2 plays a key role in Wnt signaling[81] with reported direct physical interactions between low-density lipoprotein receptor-related protein 6 (LRP6), the cytoplasmic phosphoproteins known as DVL1 (Dishevelled 1) and the β-catenin destruction complex[82] (**Figure 5**). Furthermore, pathogenic mutations in LRRK2 (R1441C, Y1699C and G2019S) weakened these interactions with Wnt pathway components[83]. In contrast, the PD protective LRRK2 variant R1398H enhances Wnt signaling activity[84]. Furthermore, overexpression of the PD-related mutant G2019S LRRK2 protein has been shown to cause defects in adult neurogenesis at the level of cell proliferation, neurite outgrowth and generation of newborn neurons[85].

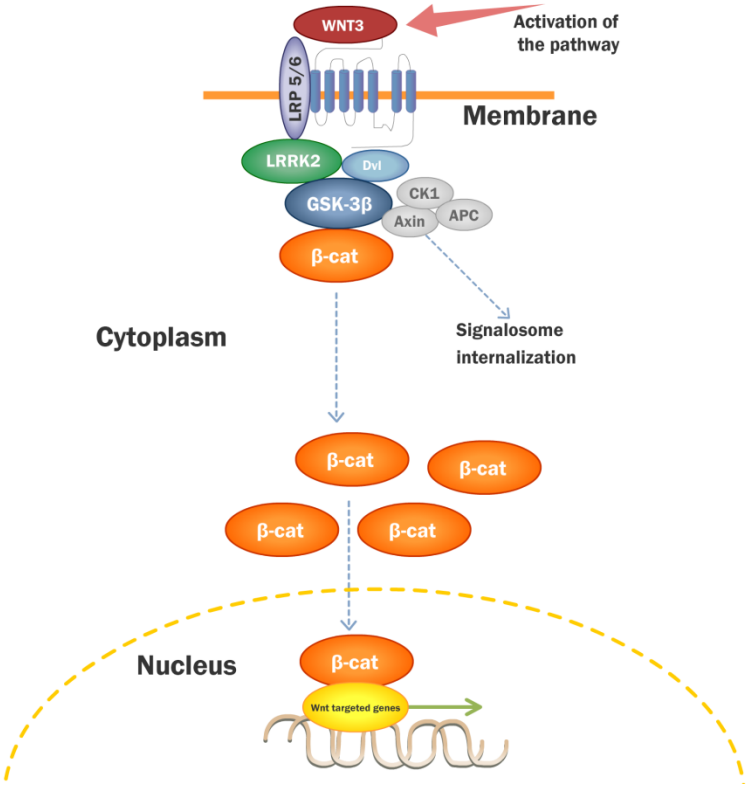

Figure 5. *Schematic representation of the role of LRRK2 in the Wnt signaling cascade*.

Finally, neural stem cells (NSCs) derived from human induced pluripotent stem cells (iPSC) containing the LRRK2 G2019S mutation showed increased susceptibility to proteosomal stress, as well as passage-dependent deficiencies in nuclear-envelope organization, clonal expansion and neuronal differentiation[86].

3.2. The relationship between LRRK2 and tau

In the mideighties when tau protein was identified as the major molecular component of NFTs in AD, it soon was reported that fibrillary tau pathology is not

restricted to AD. The term "tauopathy" was used for the first time in 1997 to describe the concept of "familial multiple system tauopathy with presenile dementia"[87]. Now the term is used to refer to a group of sporadic or familial neurodegenerative disorders that all are characterized by filamentous accumulations of hyperphosphorylated tau protein in neurons or neurons and glial cells[88-92].

Tauopathies can be classified according to different criteria. Here is shown the classification depending on whether tau pathology is considered the major contributing factor to the neurodegeneration or associated with other pathologies and the classification according to the type of tau isoform that aggregates are given[87].

Classification according to the role of tau in the disease: primary vs secondary tauopathies

- Primary tauopathies are defined as "neurodegenerative diseases where neuronal or neuronal and glial filamentous tau inclusions are the salient neuropathological feature"[93]. The term of primary tauopathies which can also be named as frontotemporal lobar degeneration (FTLD) (both terms can be used interchangeable) is used as an umbrella term that groups several different neurodegenerative diseases characterized by predominant destruction of the frontal and temporal lobes[94-97]. This group comprises Pick disease, PSP, CBD, AGD, sporadic multiple system tauopathy with dementia, frontotemporal dementia (FTD) with microtubule-associated tau (MAPT) gene mutation also called FTD with parkinsonism linked to chromosome 17 (FTDP-17) , and globular glial tauopathy (GGT).
- Secondary tauopathies are characterized by tau pathology in association with other types of pathology[93]. They represent a heterogeneous group of disorders of very diverse etiology in which AD is the secondary tauopathy most studied. Some of these disorders are caused by environmental factors, such as, chronic traumatic encephalopathy[98] (CTE), among others. On the other hand, some secondary tauopathies are clearly genetically associated. Some examples are: trisonomy 21 in Down´s Syndrome[99], mutations of the prion protein gene in some forms of the Gerstman-Sträussler-Scheinker syndrome[100], or mutations in the BRI2 gene in familial British dementia (FBD) and familial Danish dementia (FDD)[101].

- Classification according to the tau isoform pattern (**Table 2**):

Tau protein is encoded by a single gene, *MAPT*, on chromosome 17, but expressed in different isoforms due to alternative splicing of pre-RNA[102]. In the human brain, tau exons 2, 3 and 10 are alternatively spliced, giving rise to six different isoforms[103]. Tau isoforms differ by the presence of three or four repetitive domains in the C-terminal part (3R, 4R) in combination with the presence or absence of one or two amino acid inserts in the amino region (ON, 1N, 2N). Based on the ratio of the 3R and 4R tau isoforms involved in the fibrillary lesions, four types of tauopathies have been distinguished[104].

Table 2. *Classification of tauopathies according to the isoform pattern.*

Class I	Class II	Class III	Class IV
Equal proportion of 3R and 4R	Predominant 4R	Predominant 3R	Short ON3R
AD	PSP	Pick disease	Myotonic distrophy
Down´s syndrome	CBD	Some cases of FTDP-17	
Parkinsonism-dementia complex of Guam	AGD		
Pick disease type C	GGT		
CTE	Ageing-related tau astrogliopathy		
Some cases of FTDP-17	Some cases of FTDP-17		

A very important aspect regarding to tau pathophysiology are the mutations in the gene coding for tau (*MAPT).* More than 50 mutations in *MAPT* gene have been described so far[105]. Tau gene mutations are pathogenic as they perturb RNA splicing, impair tau functions and promote tau fibrillization[106]. The clinical manifestations among the different mutations are very heterogeneous and even different individuals with the same mutation may develop different pathological features which leads to think that additional genetic and epigenetic factors are important[105]. Three of the most important ones as they have enable the possibility of developing cellular and animal models for tauopathies are P301L[107] A152T[108] and V337M[109].

But how is the connection between tau physiology and neurodegeneration? The tau-microtubule hypothesis is a well stablished theory that tries to relate neuronal death in tauopathies to tau hyperphosphorylation[110, 111]. In the adult brain tau is mainly bound to tubulin to promote its polymerization, to regulate stability of microtubules and to determine microtubule spacing[112]. In physiological conditions, more than 80% of tau is bound to microtubules in a “kiss and hop” manner[113]. However, in pathological conditions, tau

becomes hyperphosphorylated[114]. This hyperphosphorylation reduces its microtubule-binding ability and thus detaches from the microtubules[115]. As a result, the microtubules begin to break down and therefore, the axonal transport is disrupted[116]. Free tau is re-distributed from the axon to the cell body[117] where it accumulates on the shape of immunocytochemical detectable features known as "pre-tangle"[118]. Subsequent steps apparently involve conformational changes towards the formation of β-sheet aggregates and the subsequent self-aggregation towards larger filaments to form NFTs (**Figure 6**)[119].

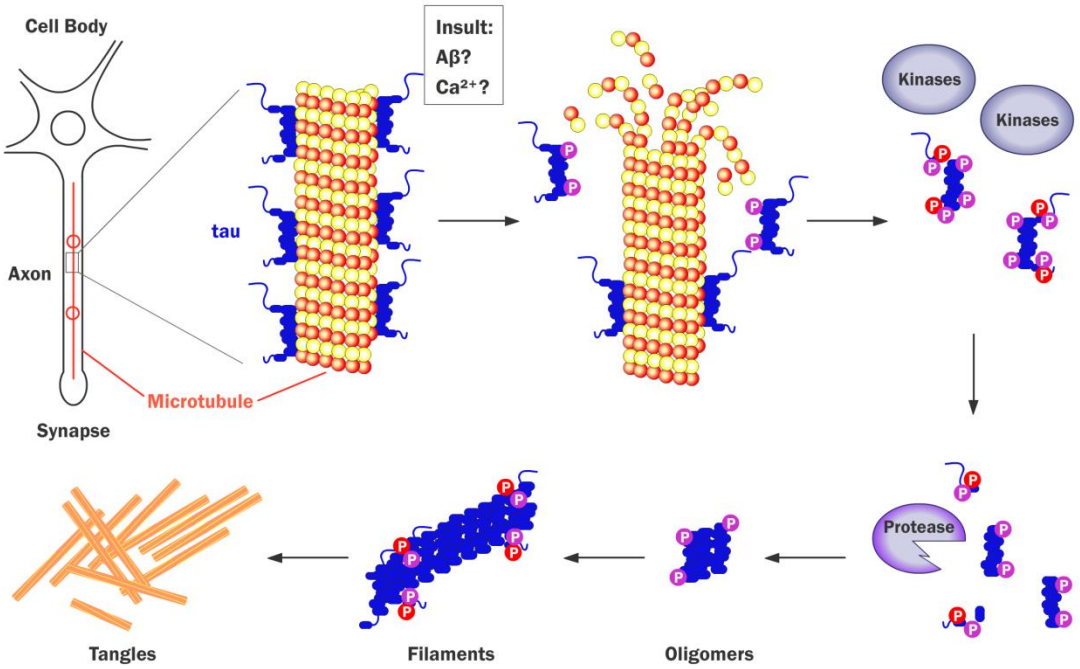

Figure 6. *Pathological tau hyperphosphorylation.*

Beside all this evidence, it still remains unclear how physiological tau converts into pathological tau. Many researchers are trying to elucidate this path and some of the more update trends indicate that is not the large supramolecular fibrillary tau aggregates but probably the soluble prefibrillar oligomeric tau what represents the toxic tau species[120]. Furthermore, other authors claim and therefore, generating more general doubt that the pathogenic role of tau is at the synapse whereas tau aggregates are only late manifestations of the disease[91] and very recently it has been shown for the first time in humans that tau spreads between connected neurons[121]. It is an extremely complex pathway; however, what seems clear is that a mild decrease at tau phosphorylation may lead to neuroprotection.

The possible connection between LRRK2 and tau can be studied at two different levels. The first one is the direct and indirect phosphorylation of tau by LRRK2 and the second one the presence of tau aggregates in patients carrying LRRK2 mutations.

3.2.1. Direct and indirect phosphorylation of tau by LRRK2

There is evidence that suggest that LRRK2 phosphorylates tau directly and indirectly both *in vitro* and *in vivo* (**Figure 7**). It has been demonstrated using LRRK2-transfected SH-5YSY cells that LRRK2 directly phosphorylates tubulin-associated tau in Thr181 but does not phosphorylate free tau[122]. Furthermore, co-transfected COS-1 cells with LRRK2-I2020T and 4R tau showed an increase in phosphorylation at Thr231 and Thr181 compared to wildtype[123]. In addition, in co-transfected HEK 293T cells with LRRK2-G2019S and 0N3R tau it was reported that Thr149 and Thr153 were among the most abundant phosphorylation epitopes[124]. In an *in vivo* context, using wild-type (WT) LRRK2 transgenic mice crossed with transgenic Tg4510 mice that express human mutant (P301L)/0N4R tau known as LRRK2/Tau_{P301L}, accumulation and phosphorylation of insoluble tau was increased. Phosphorylation at Thr149, Thr205 and Ser199/Ser202/Thr205 was significantly increased compared to tau_{P301L} mice, however, phosphorylation at Thr153 did not reach statistical significance[124]. The effect of LRRK2 phosphorylation of tau may be dependent by the presence of microtubules as it was shown *in vitro* using kinase reactions experiments[125]. Phosphorylation of tau at Thr153 and Thr205 by LRRK2 is enhanced in the presence of microtubules and the G2019S mutation increases this effect[125]. In another murine model, G2019S-LRRK2 an increased level of tau phosphorylation at Ser396/404 was observed[126].

Since phosphorylation at Ser396 is preferentially targeted by GSK-3β[127], it was speculated that LRRK2 may regulate this process through GSK-3β-dependent mechanisms. This hypothesis was confirmed by F. Kawakami, *et al.* by showing that LRRK2 directly interacts with GSK-3β, this interaction enhances the kinase activity of GSK-3β and finally phosphorylation of tau at Ser396 is increased in LRRK2-overexpressing SH-SY5Y cells[128]. This work suggests that upon interaction with LRRK2, GSK-3β undergoes a conformational change, thus activating its intrinsic kinase activity. Another fact to take in consideration in the context of indirect phosphorylation of LRRK2 *via* GSK-3β, is the fact that G2019S expression in *Drosophila* leads to mislocalization of axonal tau in dendrites which causes dendrite degeneration. The mechanism of action is thought to be that

hyperactivated G2019S promotes tau phosphorylation at the T212 site by the *Drosophila* glycogen synthase kinase 3β homolog Shaggy (Sgg) and therefore inducing hyperphosphorylation and mislocalization of tau with resultant dendrite degeneration[129].

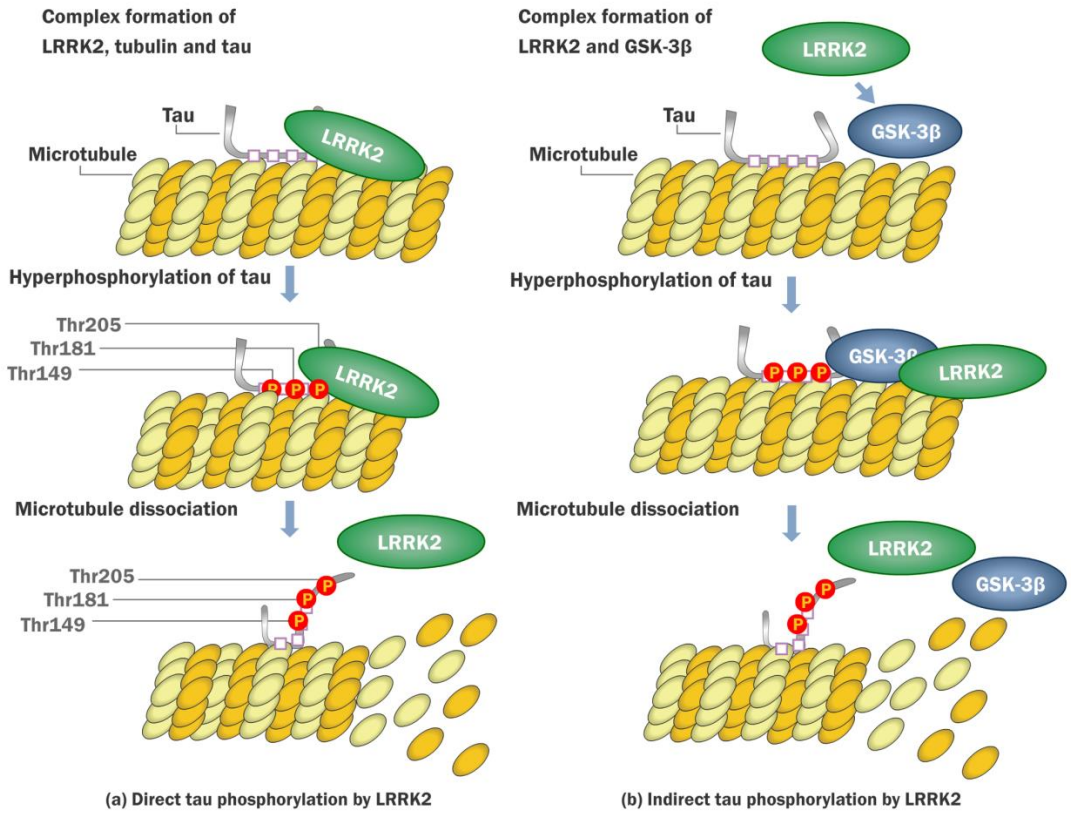

Figure 7. *LRRK2-mediated phosphorylation of tau.*

In 2015, in an outstanding work done by E. Ohta, *et al.* using I2020T mutant LRRK2 iPCS-derived neurons tau phosphorylation at Ser202/Thr205 and Thr231/Ser235 was increased compared to healthy controls and this effect is supposed to be through GSK-3β activation as a decrease in phosphorylation of Ser9 and an increase at Tyr216 of GSK-3β which corresponds respectively to the inactivated and hyperactivated forms of the enzyme[130]. This effect was reverted using CHIR-99021 and LRRK2-IN-1, two small molecules inhibitors of GSK3-β and LRRK2 respectevely[130]. The effect of LRRK2 in upregulating phosphorylation of GSK-3β at Ser9 was further confirmed in *Drosophila*[131]. The expression of LRRK2-G2019S in *Drosophila* leads to neurite degeneration and this effect is rescued by lovastatin by increasing the phosphorylation of Ser9 of GSK-3β and therefore, inhibiting GSK-3β activity and phosphorylation of tau. However, the hypothesis that tau may be a direct substrate of LRRK2 phosphorylation was refracted suggesting that

LRRK2 facilitates tau phosphorylation as a scaffold protein rather than by direct phosphorylation of tau[132].

At a cellular level but from a different perspective, it is important to mention that the interaction between LRRK2 and tau promotes the accumulation and aggregation of non-monomeric and high-molecular weight tau species in co-transfected HEK293 cells with LRRK2 and tau cDNA[133]. In addition, LRRK2 increases tau secretion, possibly as a consequence of an impairment of tau proteosomal degradation[133].

3.2.2. Tau aggregates in *post mortem* studies in patients carrying *LRRK2* mutations

During the last years tau aggregates have been reported in *post mortem* studies of patients carrying different LRRK2 mutations (**Figure 8**). The first evidence of tau pathology in PD patients was found in 2005 only one year after the discovery of LRRK2, in a patient carrying Y1699C-LRRK2[134].

Tau immunohistochemistry showed neuro-fibrillary tangles (NFTs) in the hippocampus, subiculum, entorhinal and transentorhinal cortices suggesting the possibility for the first time that LRRK2 may interact directly or indirectly with other pathways than α-synuclein that lead to neurodegeneration[134]. Very surprising in 2006 tau pathology was reported in a patient carrying R1441C-*LRRK2* mutation suffering from PSP. However, only this case was found among a population of 242 PSP patients and the conclusion reached from this study was that this *LRRK2* variant may not contribute in susceptibility of PSP[135]. In the same year, the case of a patient carrying G2019S-*LRRK2* mutation that showed tau pathology was reported. This was the case of a man diagnosed with PD with no cognitive decline. The inmunopathological study revealed no Lewy bodies in any section but tau 4R immunohistochemistry was positive following a pattern of distribution in the brain typical of PSP. Furthermore, tau 3R immunostaining was consistent with early Alzheimer-type pathology[136]. In 2007, LRRK2 was reported to colocalize with tau in oligodendroglial colied bodies and intracytoplasmic neuronal inclusions in eight members of a family with a specific genetic form (N279K) of frontotemporal dementia[137]. In 2012 several cases of tau pathology were reported in patients carrying *LRRK2* mutations. The first case was a PD G2019S-*LRRK2* mutation carrier, who was reported to show with diffuse Lewy body pathology but tau inclusions and amyloid pathology consistent with advanced AD[138]. Secondly, six patients carrying I2020T-*LRRK2* mutation showed 3R and 4R tau-positive

lesions in the brainstem, hippocampus and amygdala[123]. Thirdly, *LRRK2* mutation N1437H carrier showed mild tau pathology[139]. And finally, in that same year a very interesting case was reported of a patient carrying both G2019S-*LRRK2* mutation and H1/H1 haplotype of *MAPT* which is strongly associated as a risk factor of PSP, therefore, the *MAPT* haplotype may have represented a predisposing factor for tauopathy upon which increased LRRK2 kinase activity acted resulting in toxic aggregation of tau[140].

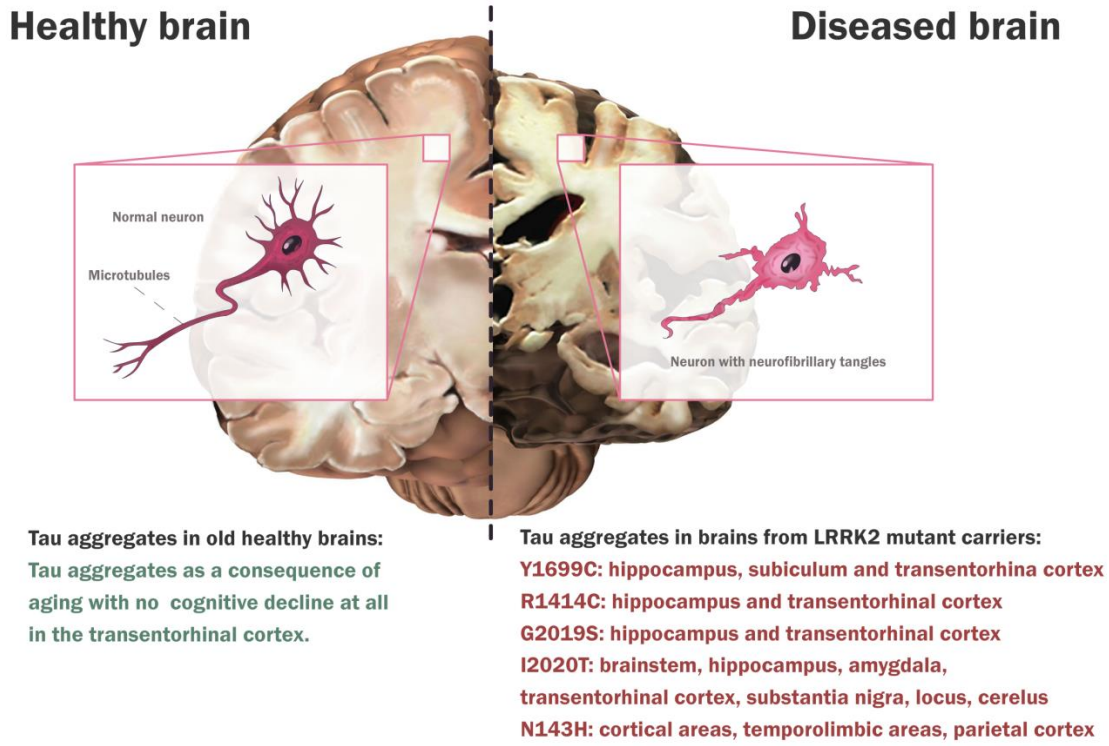

Figure 8. *Localization of tau aggregates in post-mortem studies of LRRK2 mutants carriers: Y1699C[134], R1414C[138], G2019S[140], I2020T[123], N143H[139].*

In 2015, in the same work of E. Ohta, *et al.* in the postmortem analysis of the same patient from who the iPSCs were obtained, tau pathology in the form of pre-tangles was seen in anatomical regions of pyramidal cell layers, transentorhinal cortex, *substantia nigra* and *locus ceruleus* in a grade closer to AD pathology than to normal sporadic form of PD. Consistent with this observation, inmunohistochemical staining exhibited higher level of tau phosphorylation at Ser202/Thr205 in neurons of the hippocampus, *substantia nigra* and *locus ceruleus*[130].

Finally but very interesting, is the fact decreased levels of total tau and p-tau is reported in cerebrospinal fluid in asymptomatic and symptomatic *LRRK2* mutation carriers suggesting that tau metabolism in the brain is dysfunctional due to LRRK2 activity[141].

3.3. LRRK2 and retinal neurodegenerations

A very innovative application in which LRRK2 may play an interesting role is in retinal neurodegenerations. The relationship between LRRK2 and retinal dystrophies has been poorly studied and there is no publication till the present in which a connection between this target and visual neurodegeneration diseases is shown. However, as the optic nerve and the retina are parts of the CNS and LRRK2 plays an important pathogenic role in CNS diseases, it opens a new field in research by trying to determine if LRRK2 may play a role in retinal neurodegenerations.

Optic nerve and retina are considered parts of the CNS as they develop from the diencephalon during embryonic development[142]. The retina comprises a complex network of 5 different types of neurons: photoreceptors, bipolar cells, amacrine cells, horizontal cells and retinal ganglionic cells (RGC). The retina processes the visual stimuli into electric stimuli that reach the RCG whose axons will subsequently form the optic nerve[143]. These axons further carry the action potential to the lateral geniculate nucleous and the superior colliculus which eventually reaches the higher visual processing centers[144]. As the optic nerve exits the globe, similar to all fiber tracts of the CNS, it gets covered with myelin produced by oligodendrocytes and all the three meninges: pia mater, arachnoid and dura mater.

Despite their diverse morphology, RGC and CNS neurons display similar properties as both comprise a cell body, dendrites and an axon. Furthermore, the eye is a unique privileged site, where there is a collection of cytokines and inside the eye specific immune responses occur similarly to the ones in the CNS. The blood-retinal barrier and blood-brain barrier (BBB) are similar to each other as they are both composed of non-fenestrated endothelial cells that are firmly connected by tight junctions. The aqueous humor and cerebrospinal fluid are similar in composition and anti-inflammatory reactions, and in any acute inflammation of either the brain or the eye, there will be a rise in intracranial pressure and intraocular pressure, respectively[145].

Due to these similarities and to this complex network of neurons any insult to the CNS such as neurotoxic environment due to oxidative stress, immune attack or deprivation of neurotrophic factor, result in a hostile environment for the neighboring neuron which was not involved in the inciting factor[146]. This phenomenon is known as secondary

degeneration which holds the potential to manifests itself into damage to optic nerve and subsequent neurons[147,148]. Therefore, not only various CNS pathologies can have ocular manifestations that often precede conventional diagnosis[149] but also various eye-specific pathologies share characteristics such as neuroinflammation[150] of other CNS pathologies. From all this evidence, the eye can be considered as the window of the brain and the retina a valuable model to study the CNS (**Figure 9**)[151]. Trying to understand the precise mechanisms of neuroinflammation and neuronal death in these two systems could improve our understanding and guide the search of new therapeutic approaches for neurodegenerative diseases.

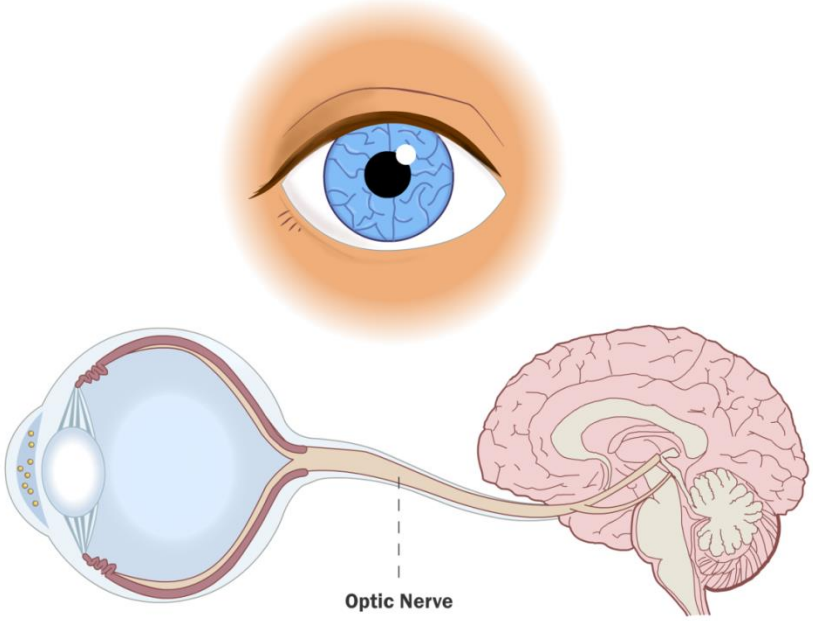

Figure 9. *The eye as a window to the CNS.*

3.3.1. Retinal neurodegenerations

The etiology and pathogenesis behind retinal dystrophies (RD) such as age-related macular degeneration, glaucoma, diabetic retinopathy and retinitis pigmentosa (RP) are different. However, the final outcome is the same, impairment of diverse retinal cell types which leads to vision loss. The reason for this common mechanism is because at the cellular and molecular level, the response to retinal injury is similar leading to morphological and functional impairment of the retina[152]. They represent a major cause of blindness and a public health challenge. Till the present, there is no neuroprotective treatment available, despite that many research lines are devoted to clearly elucidate their pathology and to develop effective treatments including very innovative strategies such as

cellular therapy, gene therapy and retinal implants[153]. Photoreceptors (rods and cons) are the primary cellular units in the retina that convert the light stimuli to a neural action potential, and therefore, RD can be categorized into broad groups depending on the type of photoreceptor affected. RD groups can include rod-dominated diseases, cone-dominated diseases and generalized retinal degenerations involving both. In addition, syndromic forms whereby the phenotype extends outside the retina are also found.

RP is the most prevalent form of RD. RP is a progressive non-syndromic rod-cone disease. RP comprises a group of genetically heterogeneous retinal disorders in which more than 60 pathogenic genes have been found[154]. At a cellular level, these genetic defects lead to apoptosis of the photoreceptors which is evident from the thinning of the outer nuclear layer of the retina and pigmented deposits[155]. Clinical manifestations evolve from progressive deterioration of the ability to see in dim light causing night blindness, followed by "tunnel vision" phenomenon in which the peripheral vision slowly encroaches toward the center of the visual field to finally lead to complete blindness (**Figure 10**)[156].

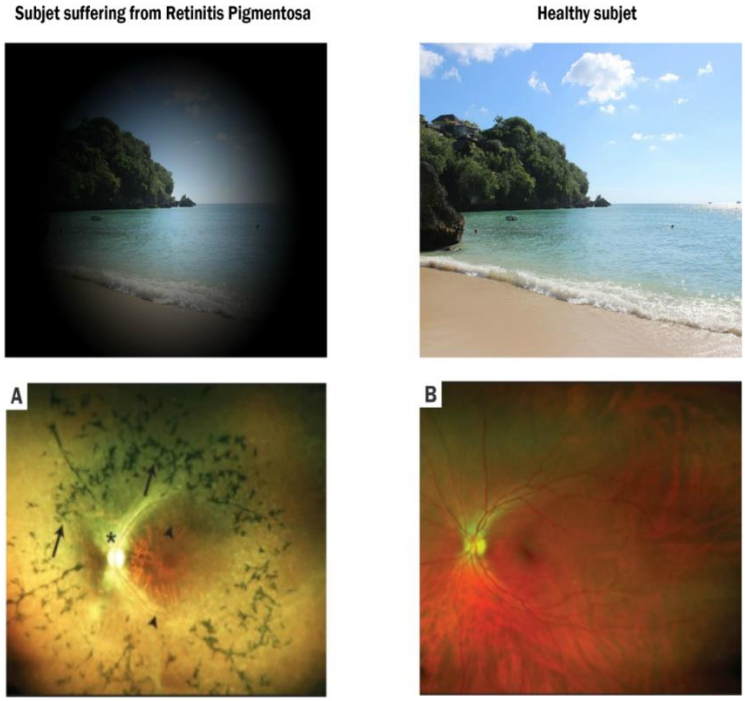

Figure 10. *Clinical and molecular manifestations of RP.*

Both the progression of visual loss and the onset of the disease vary within individuals. By average, RP patients are legally blind by the age of 40. RP is categorized as a rare disease, with a prevalence reported in one case out of 3000 - 4000 individuals[157].

4. LRRK2 inhibitors

4.1. Introduction to chemical genetics

As many biological functions of LRRK2 are still unknown it is of high importance to generate chemically diverse LRRK2 inhibitors in order to interrogate in detail all the implications of the pharmacological inhibition of LRRK2 could have following a chemical genetic approach. Chemical genetics, in the simplest terms, can be defined as a "genetics" study using "chemical" tools. Classical genetics may study a gene function by directly removing a gene product(s), proteins (genetic knockout), from the organism. In contrast, chemical genetics indirectly studies a gene's role by altering the activity of the cognate protein, using small molecule inhibitors analogously to the genetic knockout[158]. The use of small molecule probes can confer a number of advantages over conventional genetic manipulations. First, the effects of small molecules on the function of a target protein are conditional and thus usually rapid and reversible[159]. Second, by varying the concentration of a small molecule probe and its binding mode to the protein, it may be possible to tune the activity of the protein in a refined way[160]. Third, by using more than one small molecular probe or molecular probes with dual activities, the function of multiple proteins may be independently modulated[160]. As in classical genetics, chemical genetics is divided into two approaches, forward and reverse (**Figure 11**). Forward chemical genetics (FCG) operates "from effect to cause" or from phenotype to genotype (genetic sequence)" whereas the target of the small molecule modulator is not known at the outset of the study. A library of compounds is phenotypically screened with the aim of finding an active ligand. When it is found subsequent identification of the protein that the active ligand targets is performed which is the most challenged step[161]. In the same context, reverse chemical genetics (RCG) begins with a known protein, analogous to a specific gene selection. This known protein is then screened with vast pools of library compounds to identify functional ligands that either stimulate or inhibit the target protein. Once a specific ligand is identified, it is introduced to a cell or organism and the resulting changes in phenotype are studied[158].

Therefore, both FCG and RCG strategies are very interesting and successful approaches to interrogate the biological functions of a target. This methodology can be applied to LRRK2 with the aim of synthesizing a LRRK2 inhibitor chemolibrary to gain light in the biological functions in which this protein is involved.

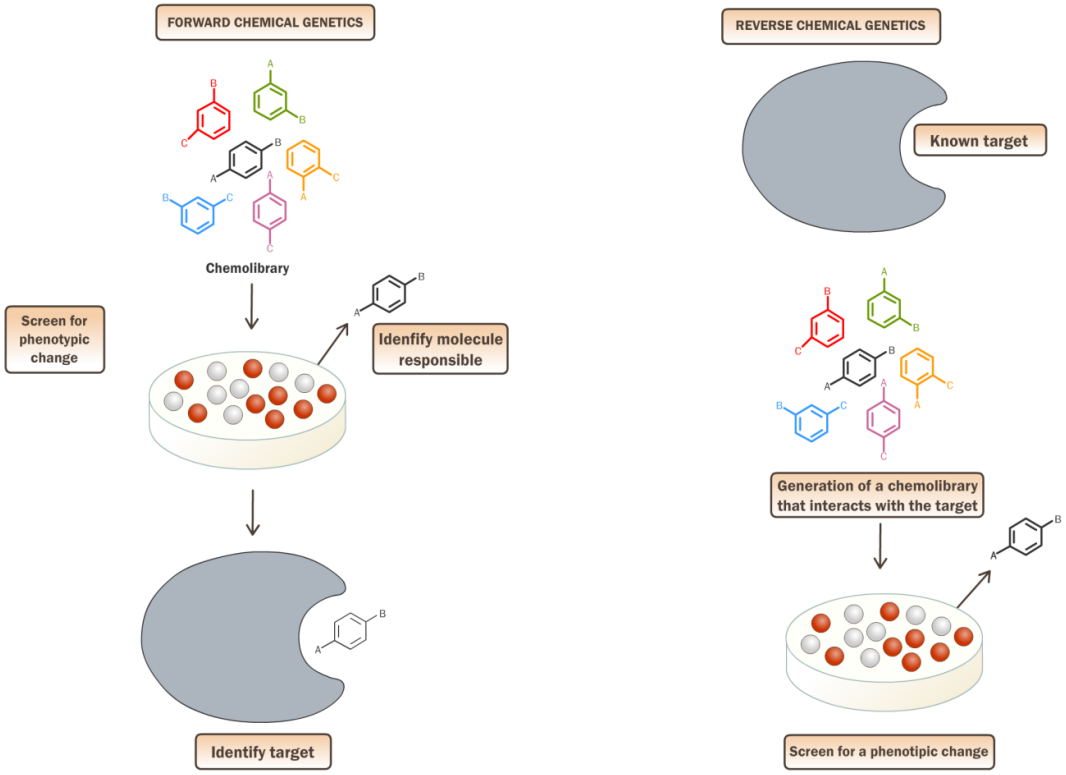

Figure 11. *Forward chemical genetics and reverse chemical genetics.*

4.2. Non-selective LRRK2 inhibitors

With all the evidence shown above linking LRRK2 to neurological disorders in and out the CNS and the lack of disease modifying treatments, has resulted in great interest to develop LRRK2 inhibitors. Due to the clear genetic link between LRRK2 and PD it becomes obvious that developing a potent, specific and with good pharmacokinetic properties LRRK2 inhibitor could be a neuroprotective treatment for PD. Big efforts have been done with the aim of finding small molecules that are able to bring LRRK2 enzymatic function back to normal, not only in the wild-type protein but also in some of its pathogenic mutations especially G2019S as it is the most prevalent one. Groups ranging from academics, biotech companies, and big pharmaceutical industries have all engaged in identifying LRRK2 kinase inhibitors. Leveraging the existing knowledge surrounding kinase drug discovery and linking their internal expertise, multiple chemotypes have been disclosed[162]. The brief but very productive history of LRRK2 inhibitors (**Figure 12**) till the present is an example of outstanding work from medicinal chemists both from academia and industry trying to overcome all the issues that have emerged along the difficult but

extremely important and necessary of developing a LRRK2 inhibitor that reaches the market as a disease-modifying treatment for neurodegenerative diseases.

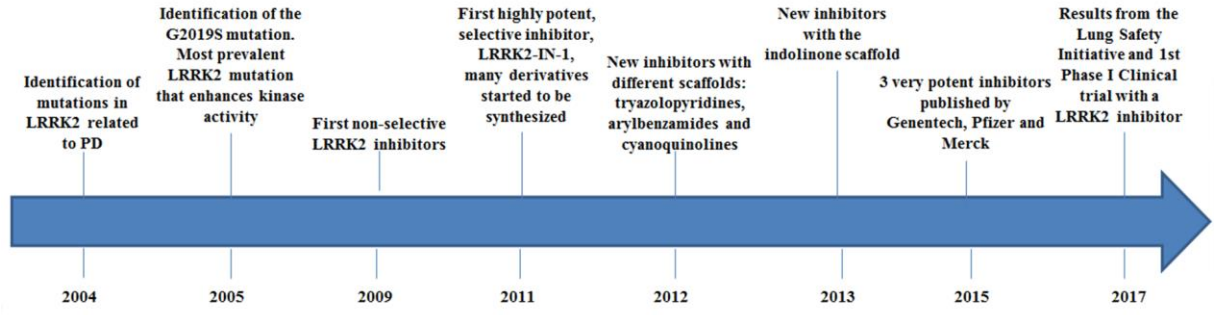

Figure 12. *Chronogram of the most relevant discoveries in the history of LRRK2 inhibitors.*

Initial studies in 2009 identified several classes of nonselective kinase inhibitors (**Figure 13**)[163, 164] These early LRRK2 hits known as: H-1152 (**1**), Y-27632 (**2**) and Sunitinib (**3**) were found using a commercial kit of kinase inhibitors screened in the recombinant enzyme LRRK2 wt and G2019S mutant. These molecules are competitive inhibitors interacting with the ATP binding site of kinases and possibly due to that fact, they do not show selectivity among other kinases[163]. Owing to their promiscuity further development of these compounds was not continued.

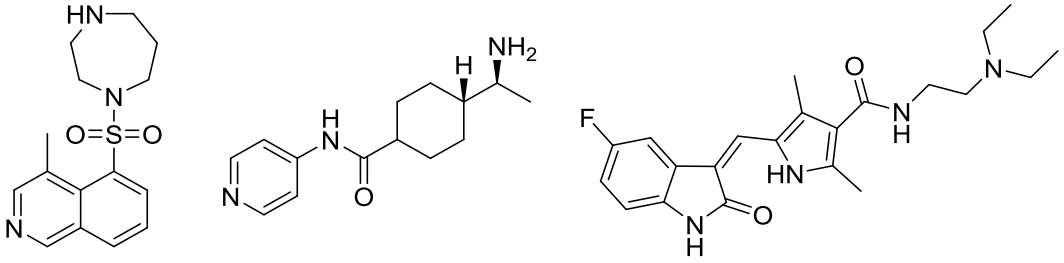

H-1152 (1) **Y-27632 (2)** **Sunitinib (3)**

	1	**2**	**3**
IC_{50} LRRK2 wt (µM)	0.24	2.30	0.08
IC_{50} LRRK2 G2019S (µM)	0.15	1.00	0.02
Selectivity	NO	NO	NO

Figure 13. *Chemical structure and biological activity of compounds **1 - 3.***

4.3. Selective LRRK2 inhibitors

After the disclosure of the first non-selective LRRK2 inhibitors several selective inhibitors were published. In order to summarize in this work the most important findings, the selective LRRK2 inhibitors are organized by scaffolds. Three groups are defined: the first one is the group of aminopyrimidine derivatives, indolinone derivatives form the second group and the last one other scaffolds (triazolopyridine, arylbenzamide, pyrrolopyrimidine-benzonitrile and indazole derivatives) are collected. All of these selective LRRK2 inhibitors are competitive inhibitors that are thought to bind in the catalytic domain of LRRK2, although competitive studies have not been published for all of them (**Figure 14**). Till the present no allosteric LRRK2 inhibitor has been reported.

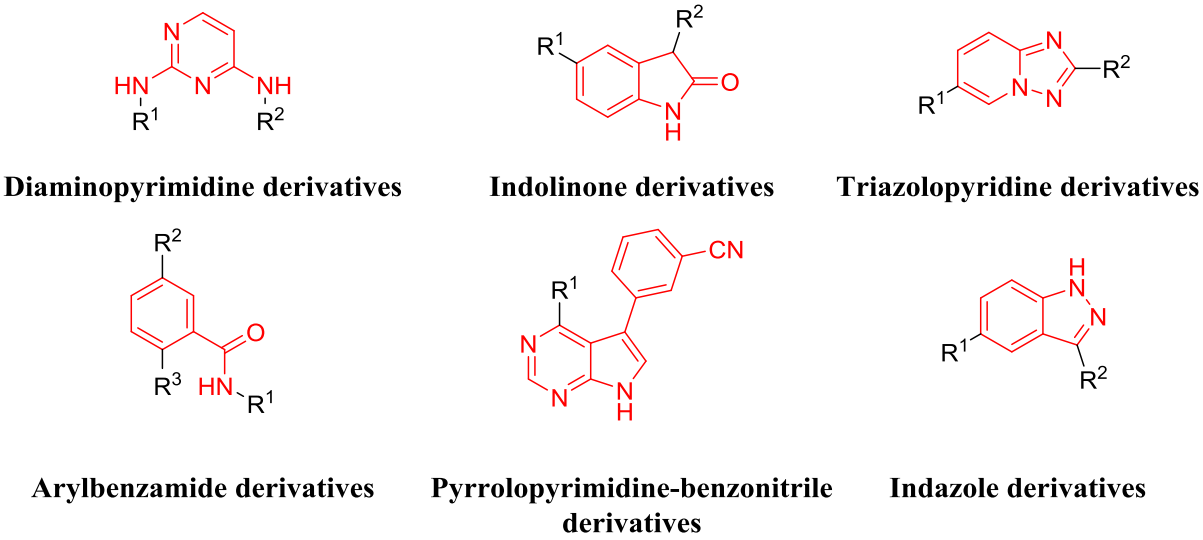

Figure 14. *Chemical scaffolds used as LRRK2 inhibitors.*

4.3.1. Diaminopyrimidine derivatives

In 2011, the first selective LRRK2 inhibitor published was LRRK2-IN-1 (**4**). LRRK2-IN-1 (**4**) is a diaminopyrimidine derivative that demonstrated its ability to inhibit both *in vitro* and *in vivo*[165]. LRRK2-IN-1(**4**) rapidly suppresses LRRK2 kinase activity *in vivo* leading to dephosphorylation of Ser910/Ser935. However, even though it showed an improved selectivity profile it still show equipotent activity against ERK5, DCAMKL, PLK1 and PLK4. This off-target activity has been found to lead to misinterpretation in biological assays especially when testing the effects of LRRK2-IN-1 (**4**) in neurite outgrowth and inflammation[166]. Moreover, LRRK2-IN-1 (**4**) showed bad absorption-

distribution-metabolism-excretion (ADME) properties due to its high levels of plasma protein binding and its inability to cross the blood-brain-barrier. Apart from these facts LRRK2-IN-1 (**4**) was very useful as a pharmacological tool to further understand the role of LRRK2 in neurodegenerative pathologies.

Since the publication of LRRK2-IN-1 (**4**), many more derivatives were synthesized containing the diaminopyrimidine scaffold: CZC-25146[167] (**5**), CZC-54252[167] (**6**), TAE684[168] (**7**) and HG-10-102-01[169] (**8**) (**Figure 15**). Following that same train of thought, the pharmaceutical company Genentech found in a high-through-put screening (HTS) campaign another diaminopyrimidine[170] hit (**9**) (**Figure 15**). Although compound **8** showed excellent biochemical potency and physochemical properties compatible for crossing the BBB, significant improvement of the selectivity was needed.

Therefore, this series of compound went through several rounds of optimization in which it was found that a trifluormethyl group at position 5 of the pyrimidine ring and also alkylation of one of the amino groups are favorable for the activity. Furthermore, substitution at different position of the phenyl ring attached to the diaminopyrimidine moiety is necessary to achieve selectivity among other kinases. These modifications lead to compound GNE-7915[171] (**10**).

Later on, in an effort to reduce size, improve aqueous solubility and to eliminate a potential reactive metabolite derived from the aniline moiety a medicinal chemistry program was started using aminopyrazoles as aniline bioisosteres. Substitution of one of the nitrogen atoms of the aminopyrazole ring lead to the discovery of GNE-0877[172] (**11**) (**Figure 15**), which is highly efficient, with ADME properties suitable for multiday efficacy and toxicity studies and excellent selectivity profile. However, the biggest issue was found when both compounds **10** and **11** were tested in nonhuman primates (NHP) and accumulation of lamellar bodies in type II pneumocytes of the lung were found and could potentially lead to respiratory difficulties[173].

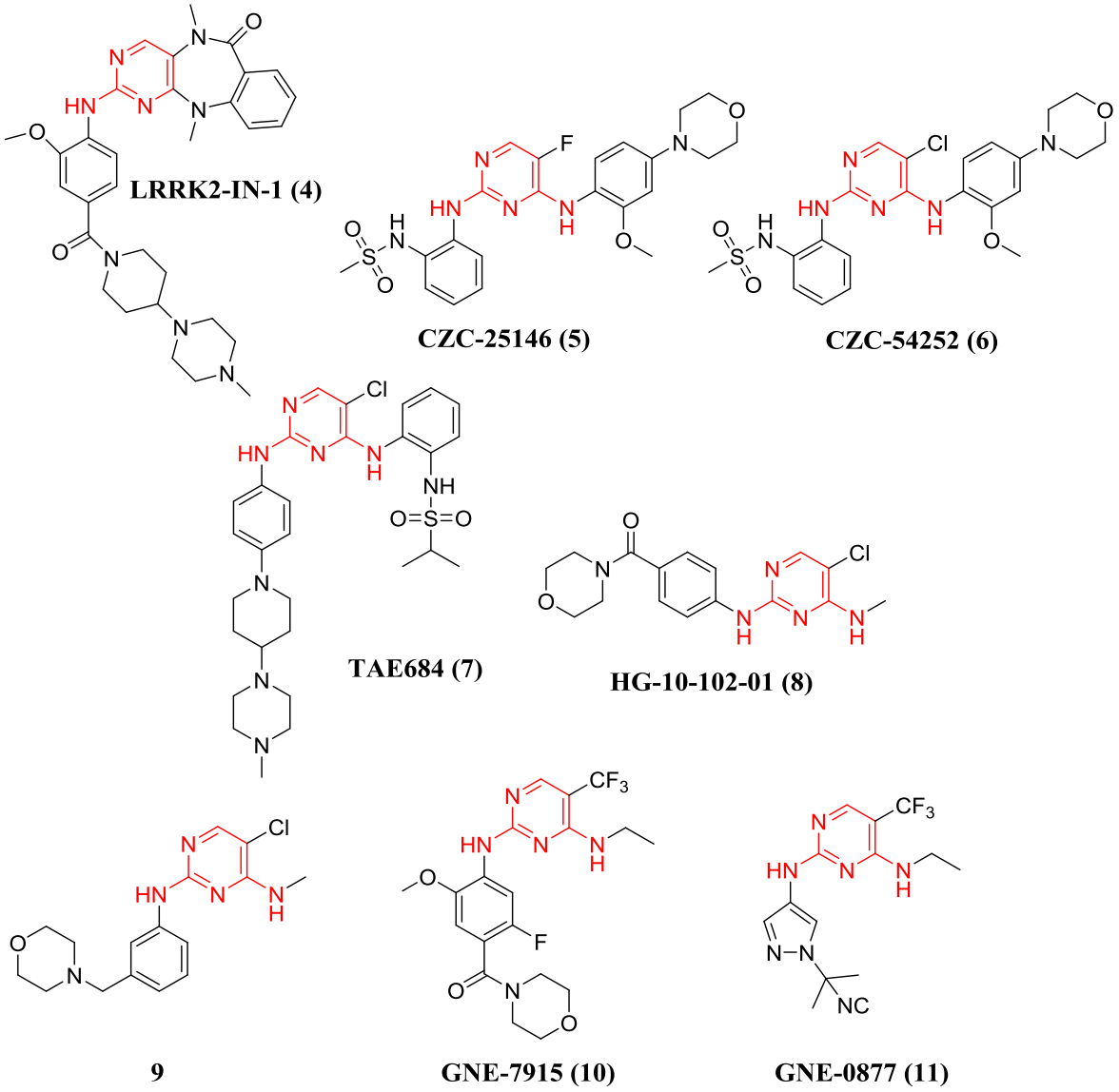

	LRRK2-IN-1 (4)	5	6	7	8	9	10	11
IC_{50} LRRK2 wt (μM)	0.013	4.760	1.280	7.800	0.020	0.006	0.009	0.003
IC_{50} LRRK2 G2019S (μM)	0.006	0.007	0.002	0.006	0.003	0.003	0.004	0.001
Selectivity	Acceptable	Good	Good	Acceptable	Good	Bad	Good	Good
Off-target effects	YES	NO	NO	YES	NO	-	NO	YES
ADMET properties	Bad	Bad	Bad	Good	Acceptable	Acceptable	Bad	Bad
CNS permeable	NO	NO	NO	NO	YES	YES	YES	YES
In vitro activity	YES	YES	YES	YES	YES	Not tested	YES	YES
PK	Bad	Bad	Bad	Acceptable	Acceptable	Acceptable	Good	Good
In vivo activity	YES	Not tested	Not tested	YES	YES	Not tested	Good	YES
CNS *in vivo* activity	NO	Not tested	Not tested	NO	YES	Not tested	Not tested	YES

Figure 15. *Diaminopyrimidine derivative: chemical structures and biological properties.*

4.3.2. Indolinone derivatives

Another scaffold which has been successful in the LRRK2 field is the indolinone one (**Figure 14**). The idea of using this core came from the discovery of Sunitinib (**3**) as a LRRK2 inhibitor. In August 2013 a group from Novartis started a medicinal program which led to the discovery of the indolinone analogues **12** and **13** (**Figure 16**)[174]. Although, the biological properties of theses inhibitors seem promising, they showed some off-target effects as they also inhibit Anaplastic Lymphoma Kinase (ALK), Vascular Endothelial growth factor receptor 2 (VEGF) and Platelet derived growth factor receptor-α (PDGFra)[174]. Further development of these compounds has not been published yet. Later on, in August 2014 Göring *et al.* described the promising indolinone derivatives **14** and **15**. However, the main drawback of these compounds was their toxicity evaluated in zebra fish embryos (**Figure 16**)[175].

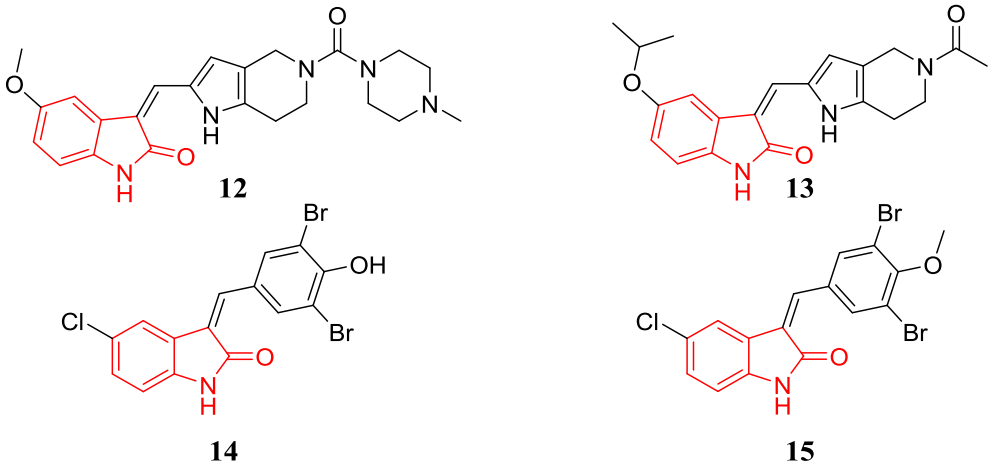

	12	**13**	**14**	**15**
IC_{50} LRRK2wt (µM)	0.009	0.004	0.015	0.046
IC_{50} LRRK2 G2019S(µM)	Data not reported	Data not reported	0.010	0.064
Selectivity	Acceptable	Acceptable	Good	Data not reported
Off-target effects	YES	YES	NO	Data not reported
ADMET properties	Good	Good	Good	Bad
CNS permeable	Yes	Yes	Not tested	Not tested
In vitro activity	Data not reported	Data not reported	Not tested	Not tested
Pharmacokinetics	Good	Good	Not tested	Not tested
In vivo activity	Data not reported	Data not reported	Not tested	Not tested
CNS *in vivo* activity	Data not reported	Data not reported	Not tested	Not tested

Figure 16. *Indolinone derivatives: chemical structures and biological properties.*

4.3.3. Other scaffolds

- Triazolopyridine derivatives

In the same HTS campaign by Genentech in which the diaminopyrimidine derivative (**9**) was found, another LRRK2 hit was found containing the triazolopyridine scaffold (**16**) (**Figure 17**)[170]. However, this scaffold was abandoned due to poor drug metabolism and pharmacokinetic properties associated with the phenol moiety[176].

- Arylbenzamide derivatives

In September 2012 a new LRRK2 inhibitor GSK2578215A (**17**) (**Figure 17**) was published by GlaxoSmithKline[177]. Compound **17** is highly potent and selective, but, it failed to show target engagement in the brain[177]. In 2014, another arylbenzamide derivative, BMPPB-32 (**18**) was published (**Figure 17**)[178]. The design of this compound was not included in the publication but it showed to be potent and selective. Furthermore, it was able to restore visual function in a *Drosophila* PD model[178].

- Pyrrolopyrimidine-benzonitrile derivatives

In January 2015 Pfizer published a new LRRK2 inhibitor, PF-06447475 (**19**) which has a pyrrolopyrimidine-benzonitrile moiety in its structure (**Figure 17**)[41]. Derivative **19** is a highly potent, selective, brain penetrant and *in vivo* active LRRK2 inhibitor BAC-transgenic WT LRRK2 and BAC-transgenic G2019S LRRK2 mice, however, due to pharmacokinetic concerns in higher species this compound was not taken into clinical trials (**Figure 17**)[41].

- Indazole derivatives

In September 2015 Merck Research Laboratories published their first work on MLi-2 (**20**), a potent, selective and centrally active LRRK2 inhibitor (**Figure 17**)[179]. Benzo-pyrazole derivative **20** exhibits good IC_{50} values *in vitro* (0.76 nM), good dephosphorylation of pSer935 in a cellular assay (IC_{50}= 1.4 nM) and good binding measured by a radioligand assay (IC_{50}=3.4 nM). Furthermore, it was able to reduce phosphorylation of Ser935 in the brain; however, similar morphologic changes in the lung consistent with enlarged type II pneumocytes were observed (**Figure 17**)[179]. The chemistry and the structure-activity-relationship (SAR) of this series were published in 2017[36]. The

medicinal chemistry program that led to the discovery of compound **20** started with a HTS campaign of the Merck in-house library in which 3,5-disubstituted indazoles were found as hit compounds. Optimization of these hits were performed varying the nature of the substituents at positions 3 and 5 which finally raised the conclusion that aromatic substitution is needed at position 3 whereas alkylic substitution is needed at position 5 in order to achieve good ligand efficiency, low efflux ratio of P-glycoprotein and good hepatocyte clearance.

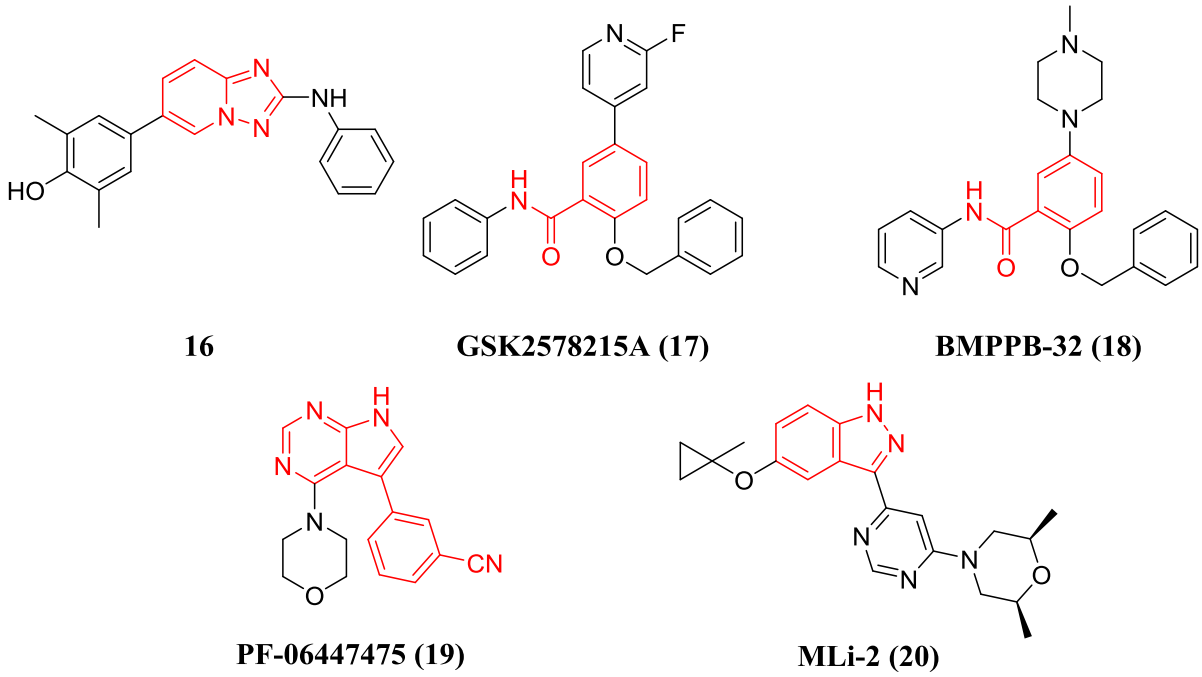

16 **GSK2578215A (17)** **BMPPB-32 (18)**

PF-06447475 (19) **MLi-2 (20)**

	16	**17**	**18**	**19**	**20**
IC_{50} LRRK2wt(μM)	0.02	0.011	0.001	0.003	0.001
IC_{50} LRRK2 G2019S (μM)	Data not reported	0.009	0.006	0.011	0.001
Selectivity	Bad	Good	Good	Good	Good
Off-target effects	YES	NO	NO	NO	YES
ADMET properties	Bad	Good	Good	Good	Bad
CNS permeable	Not tested	YES	Not tested	YES	YES
In vitro activity	Not tested	YES	YES	YES	YES
Pharmacokinetics	Bad	Good	Good	Bad	Good
In vivo activity	Not tested	NO	YES	YES	YES
CNS *in vivo* activity	Not tested	NO	Not tested	YES	YES

Figure 17. *Other scaffolds: chemical structures and biological properties.*

4.4. Final considerations when designing new LRRK2 inhibitors

Big efforts have been done in designing and synthesizing LRRK2 inhibitors both from academia and industry. It has been a fruitful but very difficult path especially when big concerns were raised regarding possible toxic effects that LRRK2 inhibition may have in the lung. The three chemotypes which have been so far progressed furthest: diaminopyrimidine derivative from Genentech (**9**), pyrrolopyrimidine-benzonitrile derivative from Pfizer (**19**) and indazole derivative from Merck (**20**) have shown on-target safety issue regarding the formation of type II pneumocytes in the lungs which has also been noted but without any lung functional impairment in NHP[180]. As a consequence, the Michael J. Fox Foundation (MJFF) sponsored a pre-competitive consortium, the Lung Safety Initiative (LSI) in Genentech, Merck, and Pfizer. Each company provided a key tool compound, of differing chemotypes, for a two week NHP lung safety toxicology study to fully assess the potential of this lung finding. While the full results remain to be published, poster presentations indicated that all compounds did exhibit this lung finding[181]. However, there appeared to be a dose response to this observation and the vacuolation was completely reversible within 2 weeks of the termination of drug dosing. Hence the path forward for a LRRK2 kinase inhibitor appears to be possible[162]. A big step was announced by Denali Therapeutics Inc, which reported on the 20th of December 2017 by a press communication that its LRRK2 inhibitor, DNL201, achieved, on average, greater than 90% inhibition of LRRK2 kinase activity observed at peak and greater than 50% inhibition at drug levels at the highest multiple dose tested in a healthy volunteer Phase 1 study. In the ongoing studies in healthy volunteers, Denali is investigation safety and tolerability, pharmacokinetics and paharmacodynamics in blood and in CSF and characterizing a biomarker to estimate target engagement in the brain. However, the structure of this compound is not disclosed yet.

Beside these achievements, it is important to synthesize new LRRK2 inhibitors with different scaffolds to have a significant battery of available tools to be employed for the elucidation of the functions of LRRK2. Analyzing the successes and the failures in designing LRRK2 inhibitors two important challenges need to be taken in consideration:

- The first challenge and it is applicable for any CNS-targeted drug discovery programme is effective penetration of the BBB. It is estimated that only 2% of small-molecule drugs are able to effectively cross the BBB[182]. The physicochemical properties of a drug considerably influence passive diffusion across biological

membranes[183,184] and the potential to serve as a substrate for the P-glycoprotein (PGP) efflux transporter[185]. If one examines CNS market drugs it becomes clear that low molecular weight, good lipophilicity, low number of hydrogen-bond donors and low pK_a are crucial for brain permeability.

- The second biggest challenge is selectivity and it is of crucial importance when designing any kinase inhibitor. The catalytic domain is highly conserved along the human kinome, therefore, it is important to find drugs that can specifically interact with the desired kinase, in order to stop nonspecific problems. Most kinase inhibitors occupy the kinase domain. An interesting design strategy for gaining selectivity is targeting regions outside the ATP-binding site using non-competitive or allosteric inhibitors[26]. Till the present there is none allosteric LRRK2 inhibitors published.

OBJECTIVES

The search of effective treatments for neurodegenerative diseases is one of the most urgent clinical and social needs today given their widespread and devastating nature.

The etiology behind neurodegenerative diseases is still unclear. However, posttranslational modifications such as phosphorylation interfere in protein misfolding and therefore, they play a critical role in neurodegeneration. In that sense, kinases have emerged as important targets for disease-modifying therapies.

Although LRRK2 is one of the most highly pursued kinase target in this field because the clear genetic relationship between mutations in the gene that codes for this enzyme and PD, the role of LRRK2 in the brain is much more complex, poorly understood and goes beyond the PD spectrum.

Therefore, the main goal of this thesis is to explore new biological mechanisms in which LRRK2 is involved, particularly focusing in three applications: the role of LRRK2 in adult neurogenesis, the role of LRRK2 in tau phosphorylation and a potential role of LRRK2 in retinal degenerations. The methodology chosen will be a reverse chemical genetic approach synthesizing a small LRRK2-inhibitor chemolibrary that will be used to interrogate these new biological pathways.

The specific objectives to accomplish this goal are:

1. Study of the binding mode by computational studies of a family of new LRRK2 inhibitors based on the indolinone scaffold previously synthesized in the group.

2. Design and synthesis of a new family of LRRK2 inhibitors using rational design based on previous inhibitors and with the help of computational studies.

3. Evaluation of the LRRK2 inhibitors synthesized in cellular models of adult neurogenesis.

4. Evaluation of the LRRK2 inhibitors synthesized in cellular models of tauopathies and in *in vivo* models.

5. *In vivo* evaluation of a LRRK2 inhibitor in a mouse model of retinitis pigmentosa.

RESULTS AND DISCUSSION

1. Design and synthesis of new LRRK2 inhibitors

1.1. Introduction and background

The biological function of a known protein may be studied using a chemical genetic approach which implies the use of small molecules able to interact with it[161]. This strategy has been followed to interrogate some functions of LRRK2 in different pathological conditions from PD. In this case, a reverse chemical genetic approach[158] will be followed. The first step will be the generation of a diverse chemolibrary of LRRK2 inhibitors and then, their biological activity in different cellular and *in vivo* assays will be used to determine new roles for LRRK2 outside the PD spectrum. Furthermore, these new small molecules that have proved to be valuable pharmacological tools may be optimized in different medicinal-chemistry programs to increase their drug-like properties. This strategy offers the potential to have new drug candidates for further development.

With that goal in mind, in 2013 a medicinal-chemistry program was set up in the group for the design and synthesis of new LRRK2 inhibitors. These previous experiments have led to the discovery of three different families of new LRRK2 inhibitors (indolinone, triazolo-pyrimidine and benzothiazole derivatives) that are at different stages of development.

1.1.1. Indolinone derivatives

The first approach was to develop new LRRK2 inhibitors containing the indolinone core, present in previous LRRK2 inhibitors[174, 175]. Several compounds were synthesized and were enzymatically evaluated as potential LRRK2 inhibitors. Among them, 24 new indolinone derivatives (**21 - 44**) showed interesting activities in LRRK2 (wt) and G2019S mutant even in the nanomolar range (**Table 3**)[186].

Table 3. *Chemical structures and enzymatic activity (LRRK2wt and LRRK2-G2019S) of indolinone derivatives synthesized* ***21 - 44****.*

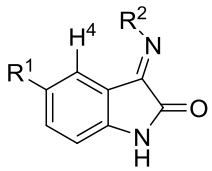

Compound	R^1	R^2	IC_{50} LRRK2wt (μM)	IC_{50} LRRK2 G2019S (μM)	*E*:*Z* ratio
21	H	$N(Ph)_2$	0.11	0.29	95:5
22	Cl	$N(Ph)_2$	0.01	0.05	85:15
23	Br	$N(Ph)_2$	0.02	0.03	91:9
24	OMe	$N(Ph)_2$	0.13	0.31	100:0
25	F	$N(Ph)_2$	0.02	0.12	96:4
26	H	N(Bn)(Ph)	3.83	3.67	44:56
27	H	Piperidine	1.34	2.21	44:56
28	F	Piperidine	1.50	2.01	30:70
29	Cl	Piperidine	0.28	0.57	30:70
30	Br	Piperidine	0.49	0.54	21:79
31	OMe	Piperidine	0.76	1.11	41:59
32	H	Morpholine	1.70	6.68	24:76
33	F	Morpholine	3.65	5.40	30:70
34	Cl	Morpholine	1.20	1.46	26:74
35	Br	Morpholine	1.33	1.02	17:83
36	I	Morpholine	0.55	0.51	30:70
37	OMe	Morpholine	0.76	1.11	38:62
38	OCF_3	Morpholine	8.74	7.49	12:88
39	H	4-OMe-Ph-	2.17	2.33	83:17
40	H	Ph	3.65	2.98	83:17
41	H	2-F-Ph-	2.34	3.29	67:33
42	H	4-F-Ph-	3.18	3.69	67:33
43	H	4-NO_2-Ph-	7.27	7.27	64:36
44	H	4-$N(Me)_2$-Ph-	3.79	3.11	76:24

1.1.2. Triazolo-pyrimidine derivatives

The second approach was the design and synthesis of new LRRK2 inhibitors containing the triazolo-pyrimidine scaffold which was previously reported as privileged feature for protein kinase inhibition[170]. Five different compounds **(45 - 49)** were synthesized and enzymatically evaluated finding activities in the micromolar and submicromolar range (**Table 4**).

Table 4. *Chemical structures and enzymatic activity (LRRK2wt and LRRK2-G2019S) of triazolo-pyrimidine derivatives synthesized* ***45 - 49****.*

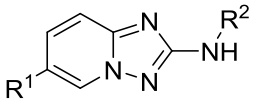

Compound	R^1	R^2	IC_{50} LRRK2wt (μM)	IC_{50} LRRK2 G2019S (μM)
45	H	2-Naph-	3.66	0.26
46	H	1-F,2-Br-Ph-	5.47	1.14
47	Cl	1-F,2-Br-Ph-	4.71	1.03
48	Cl	2-Naph-	0.61	0.11
49	4-CH_2OH-Ph-	1-F,2-Br-Ph-	4.52	0.38

1.1.3. Benzothiazole derivatives

The third approach was the design and synthesis of new LRRK2 inhibitors containing the benzothiazole scaffold. In this case the design was based in previous published hits, compounds **8** and **16,** using a chemical scaffold merge strategy (**Figure 18**)[170].

These results lead the group to start a new family of compounds conserving the [5+6] benzoannelated framework of compound **16** and eliminating the substituted phenol group. Thus, benzoxazole moiety was chosen as central core and with the aim of maintaining the interaction with Leu1949, the phenylamino residue was keept in the molecules. With this idea, a small set of compounds (**50 - 53**) were synthetized and evaluated as LRRK2 inhibitors. However, none of them showed more than 20% of inhibition at 10 μM. In a second step, a morpholino moiety was added to the structure (**Table 5**), as this residue occupied a hydrophobic pocket near the region where the phenylamino binds to ATP-site of LRRK2, in an attempt of combining hits **8** and **16** (**Figure 18**).

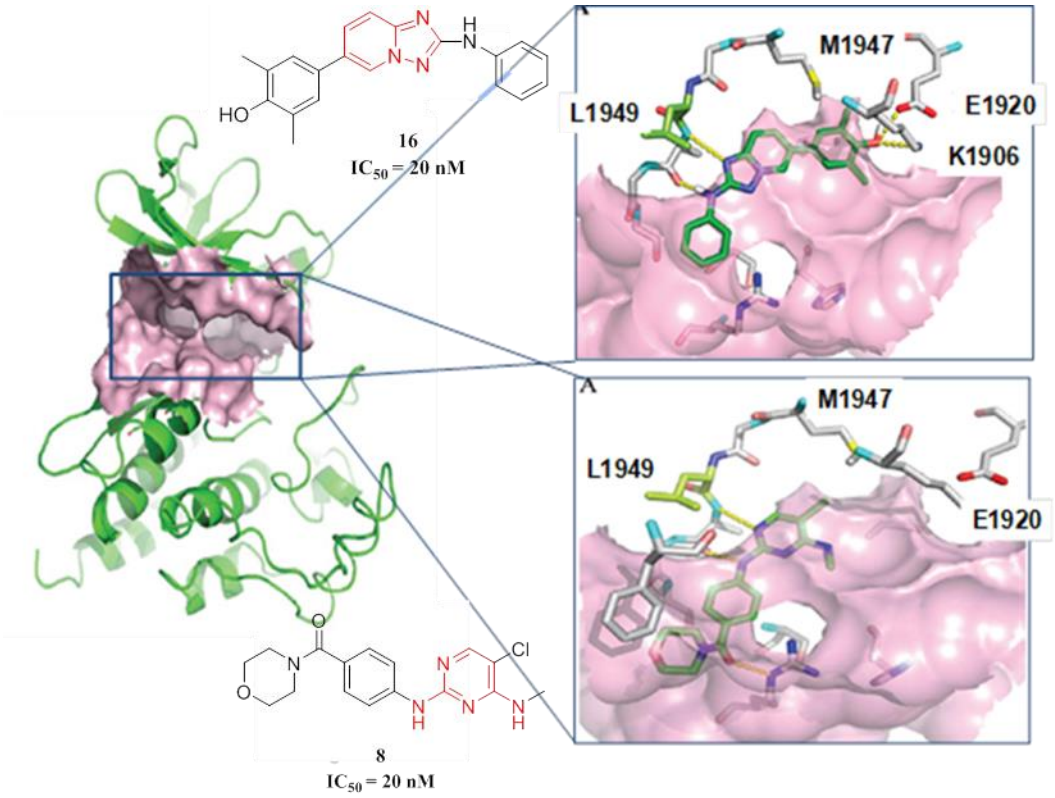

Figure 18. *LRRK2 kinase domain homology model with the N-terminal domain on top and C-terminal domain at bottom. The solvent accessible surface of the ATP-binding site is colored in pink, while the cartoon defining the protein backbone is colored in green. Hit compounds **8** and **16** as new LRRK2 inhibitors and their binding mode in the catalytic site of LRRK2.*

Compound **54** was synthetized and the evaluation of LRRK2 resulted in a 28% of inhibition at 10 μM. A couple more of compounds were then synthesized, varying the heteroatoms in the heterocyclic framework. When the oxygen atom was replaced by an NH (**55**) no activity was found, but when it was replaced by a sulfur atom, promising activity was found. In fact, benzothiazole **56** showed an IC_{50} value of 0.70 μM and could be considered as a new hit for further optimization (**Table 5**).

The selectivity of the active benzothiazole **56** for LRRK2 among other kinases was studied, due to the fact that the catalytic domain of protein kinases is highly conserved along the kinome. Therefore, it is important that new LRRK2 inhibitors have good selectivity among other kinases, in order to avoid problems related to inespecificity. The percentage of inhibition for compound **56** was calculated for 456 kinase proteins, showing a good selectivity as it only interacts with 23 out of 456 kinases evaluated (**Figure 19**).

Table 5. *Chemical structures and enzymatic activity (LRRK2wt) of compounds* ***50 - 56****.*

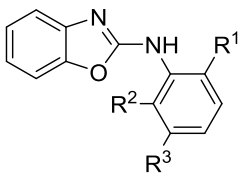

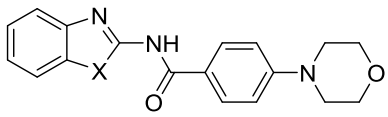

Compound	R^1	R^2	R^3	%Inhibition LRRK2 @10μM	Compound	X	%Inhibition LRRK2 @10μM	IC_{50} LRRK2wt (μM)
50	OMe	H	NO_2	15	**54**	O	28	-
51	OMe	OMe	H	20	**55**	NH	36	-
52	Me	H	H	15	**56**	S	56	0.70
53	OMe	OMe	OMe	-2				

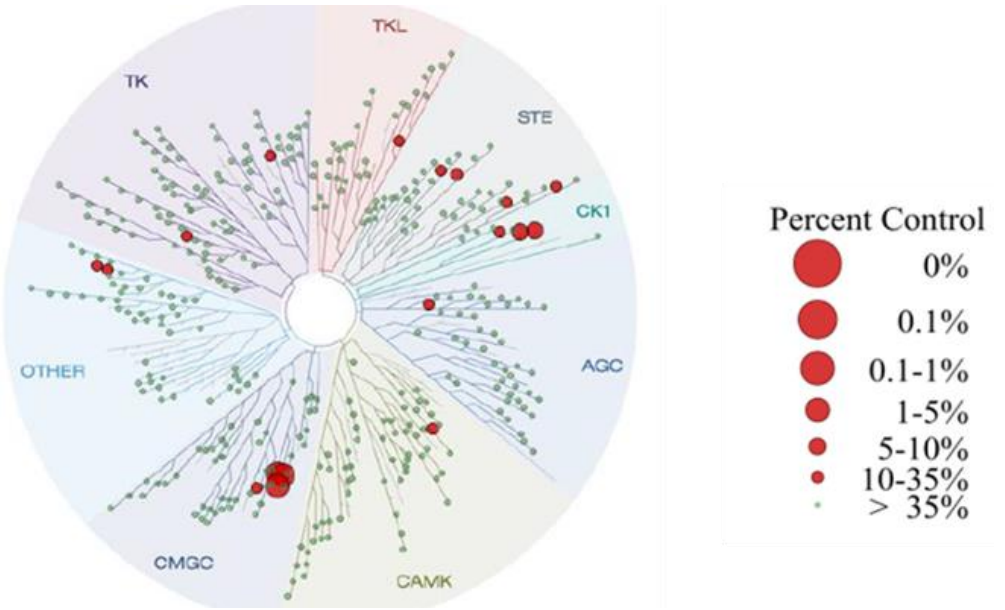

Figure 19. *Protein kinase profile for benzothiazole* ***56****.*

Based on these previous results, compound **56** was proposed as hit compound and the following objectives were planned in order to move from hit to lead step in drug discovery, synthesizing a new family of LRRK2 inhibitors.

1.2. Objectives

The main goal of this chapter is to generate a LRRK2-inhibitor chemolibrary with previous LRRK2 inhibitors described in the group and new ones designed and synthesized

in this work, that can then be used in a chemical genetic approach to study new biological roles of LRRK2.

The specific objectives of this chapter are the following:

- In order to rationalize the biological activity of the family of indolinone derivatives, gain insight into the binding mode of these new potent LRRK2 inhibitors and looking for clues to assist in the lead-to-candidate optimization, docking studies are needed. As the kinase domain of the LRRK2 is not crystallized yet, a homology model needs to be constructed prior to the docking studies. Furthermore, due to the presence of an imino or hydrazine bond directly attached to the heterocycle framework of these indolinone derivatives two different isomers *E* and *Z* are present. Therefore, computational studies will be performed to determine which isomer is the active one and why in each case the isomeric equilibrium is shifted to one of the isomers.
- Design and synthesis of new indolinone derivatives based on the results from the molecular modelling studies.
- Design and synthesis of new LRRK2 inhibitors based on the benzothiazole **56**. The structural modifications here proposed included substituents with different chemical properties (steric and electrostatic) in different positions of the benzothiazole ring and changes in the nature of the morpholino moiety.
- Study of the binding mode of these new benzothiazole LRRK2 inhibitors by computational studies.
- Study of the ADME properties in particular the penetration to the BBB of the triazolo-pyrimidine derivatives previously synthesized and new benzothiazole derivatives (the penetration to the BBB of the indoline derivatives has already been reported)[186].

1.3. LRRK2 Homology model and docking studies

1.3.1. Construction of the homology model

In 2012 a homology model of the kinase domain of LRRK2 was built using the crystal structure of Janus Kinase 2 (JAK2) (PDB code 3JY9[187]) as template[170]. However, the coordinates of this model are not available, thus it needed to be in-house built. Two crystal structures were selected by the online server Swiss-Model[188] to be used as

templates: endothelium-specific tyrosine kinase 2 (TIE2), named as Model 1 and JAK2, named as Model 2. The two models were built and were geometrically and energetically evaluated (**Figure 20**). The work-flow used for the construction of the models was the following: the human LRRK2 sequence was retrieved from Swiss-Prot[189] and aligned to template structure using ClustalW[190]; the models were built using Swiss-Model[188] ; visualized and superimposed with the template using Sybyl-X 2.0[191] and finally were evaluated geometrically using the Ramachandran plot[192] and energetically with the servers Verify3D[193] and ERRAT[194]. The superimposition of the model with the template allows the calculation of the Root Mean Square Deviation (RMSD). The RMSD is the most commonly used quantitative measure of the similarity between two superimposed atomic coordinates. The lower the RMSD between a model and the template used the better, as the model is more similar to the template[195].

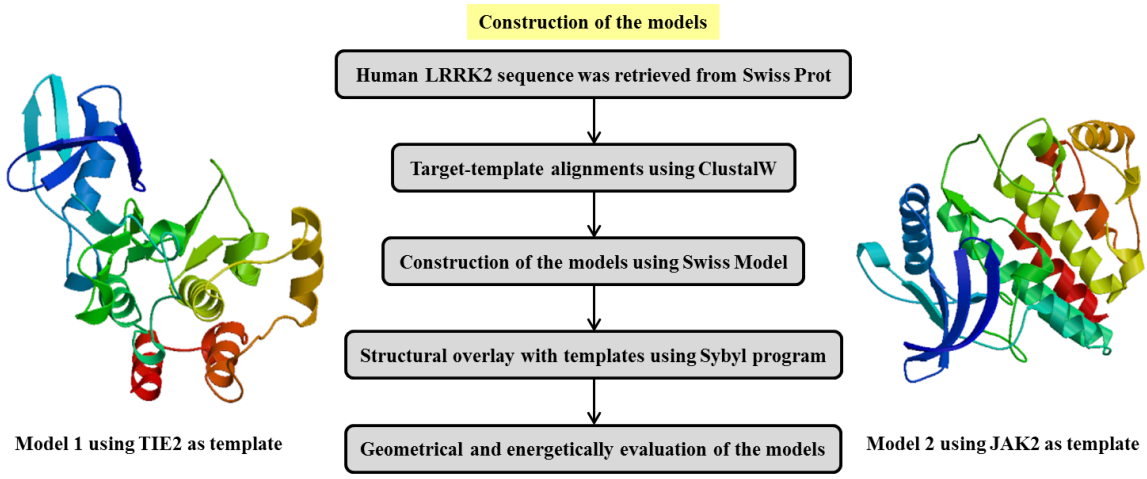

Model	Template	% Identity Kinase domain	% Identity ATP-binding site	% Similarity ATP-binding site	Crystal resolution	RMS (M/T)	Ramachandran			Verify 3D	ERRAT
							Favoured	Allowed	Outlier		
Model 1	TIE2 (1FVR)						97.1%	2.4%	0.5%		94.8
	Model 1	36.4	65	85	2.2Å	3.6	89.1%	6.9%	4.0%	warning	51.6
Model 2	JAK2 (3JY9)						97.6%	2.2%	0.7%		97.9
	Model 2	26.3	65	90	2.1Å	3.12	90.3%	6.6%	3.1%	pass	67.1

Figure 20. *Workflow for the construction of the models and evaluation of the models.*

The Ramachandran plot is a measurement for the geometrical orientation of the amino-acids of a protein. It classifies the *phi* and *psi* angles of the backbone of a protein as favored, allowed and outlier. The higher the percentage of amino-acids in the favored region the better geometrical orientation[192]. The server Verify3D scores the compatibility of the 3D structure of the model with the amino-acid sequence. The proteins are classified in three categories: pass when more than 80% of the amino-acids of the protein have a good

score (colored in green), warning when the rage of percentages is between 65 and 80% (colored in yellow) and error when less than 60% of amino-acids have a good score[193]. The server ERRAT provides an overall energetic quality factor of the 3D structure. The higher the quality factor the better[194].

By comparison of the two models it becomes clear that although TIE2 showed a higher percentage of identity (36.4%), the percentage of identity in the ATP-binding site is the same (65%) for the two templates. Regarding the geometrical evaluation, Model 2 has slightly lower RMS values and most notably it showed better values for the Ramachandran plot (90.3% in the favored region, 6.6% in the allowed region and 3.1% in the outlier region *vs* 89.1%, 6.9% and 4% respectively) (**Figure 21**).

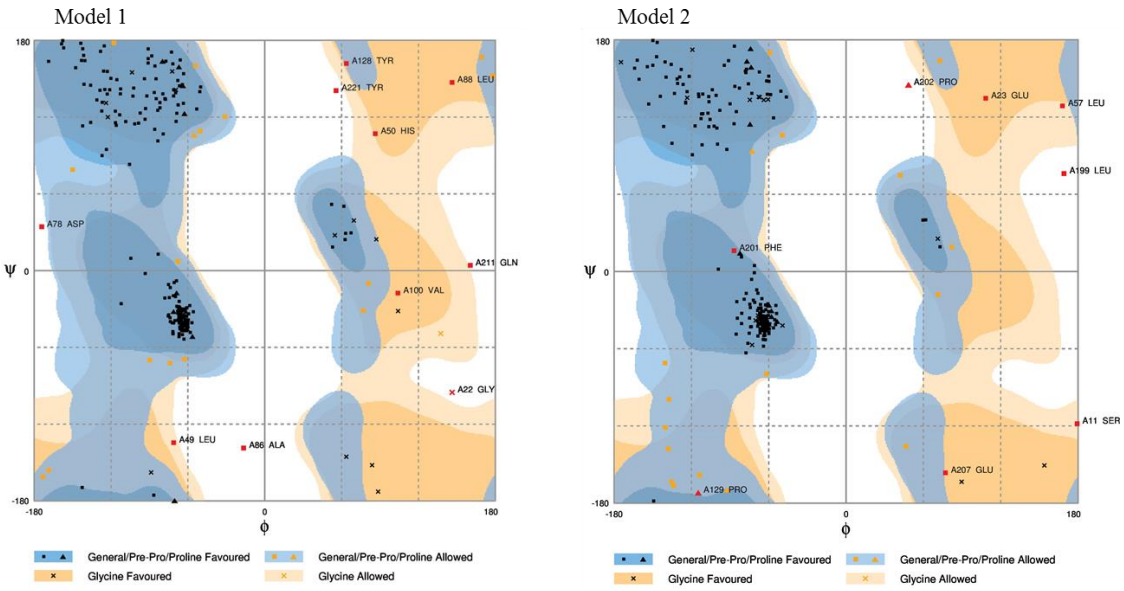

Figure 21. *Ramachandran plots for models 1 and 2 obtained from RAMPAGE*[192].

Analyzing the energetic evaluation with Verify3D server, Model 2 was classified in the pass category whereas Model 1 in the warning one, also Model 2 has a better overall energetic quality factor than Model 1 determined with the ERRAT server. Therefore, Model 2 was the model selected to be used in the following docking studies.

1.3.2. Docking studies

Once the homology model was built, the docking studies were performed using Glide XP (Schrödinger suite program)[196] and the input files were built using the information available about the ATP-binding site[170].

All the compounds showed a similar binding mode in the catalytic site of LRRK2 but the specific interactions found in the different subgroups of indolinone derivatives will be discussed in detail. The most active indolinone derivatives (**21 - 25**) with IC_{50} values in the nanomolar to low submicromolar range (0.01 µM - 0.11 µM for the wt form and 0.03 µM - 0.12 µM for the mutant form) are the ones containing a halogen atom in position 5 of the indolinone and two phenyl rings attached to the nitrogen atom of the hydrazone (**Figure 22**). It is very important to take in consideration that in this particular subgroup of compounds the most prevalent isomer and in one case even the only one, is the *E* isomer. Therefore, the docking studies were performed with the *E* isomer. The most important interaction was governed by the dual hydrogen bond between Lys1906 and two features of the indolinone ring: the carbonyl group in position 2 and the nitrogen atom of the hydrazine attached to the heterocycle. This molecular orientation allowed both the formation of a halogen bond between the Asp1887 and the halide atom in position 5 of the indolinone, and the possibility of a hydrogen bond between the Asp2017 and the heterocyclic NH (**Figure 22**). In Figure 22 the docking of compound **23** is shown, as a representative example.

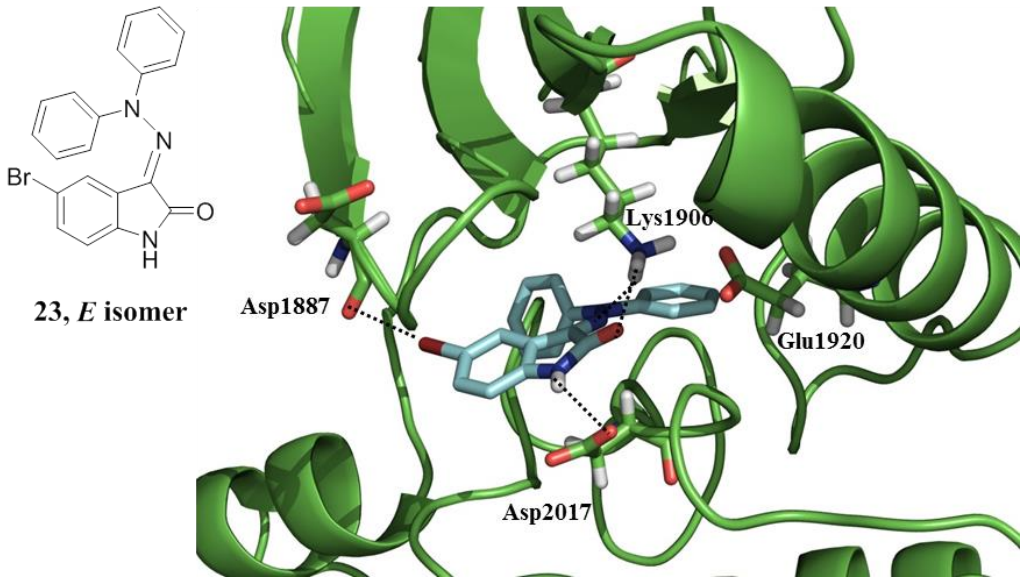

Figure 22. *Binding mode of compound **23** in the homology model. Dashed lines show hydrogen-bonds and halogen-bonds.*

Compounds with piperidine (**27 - 31**) and morpholine (**32 - 38**) in the hydrazone linker resulted in a less potent subgroup with IC_{50} values in the micromolar range (0.28 - 8.74 µM in the wt form and 0.41 - 7.49 µM in the mutant form). In this subgroup the most prevalent isomer is the *Z* one, and therefore, in a first attempt the docking studies were performed with this isomer. With this isomeric conformation, as it orientates in the opposite

direction when binding to the protein only the hydrogen bond between the carbonyl group of the indolinone core and Lys1906 was maintained (**Figure 23 - 24**). Therefore, the residual activity could be explained by the interactions formed by the *E* isomer. In order to prove this hypothesis, in a second attempt docking studies of the *E* isomers were performed. In the *E* isomers the dual hydrogen-bond with Lys1906 as well as the hydrogen bond with Asp2017 and the halogen bond with Asp1887 are kept (**Figures 23 - 24**). In Figures 23 and 24 the dockings of isomers *E* and *Z* of compounds **29** and **34** are shown as representative examples.

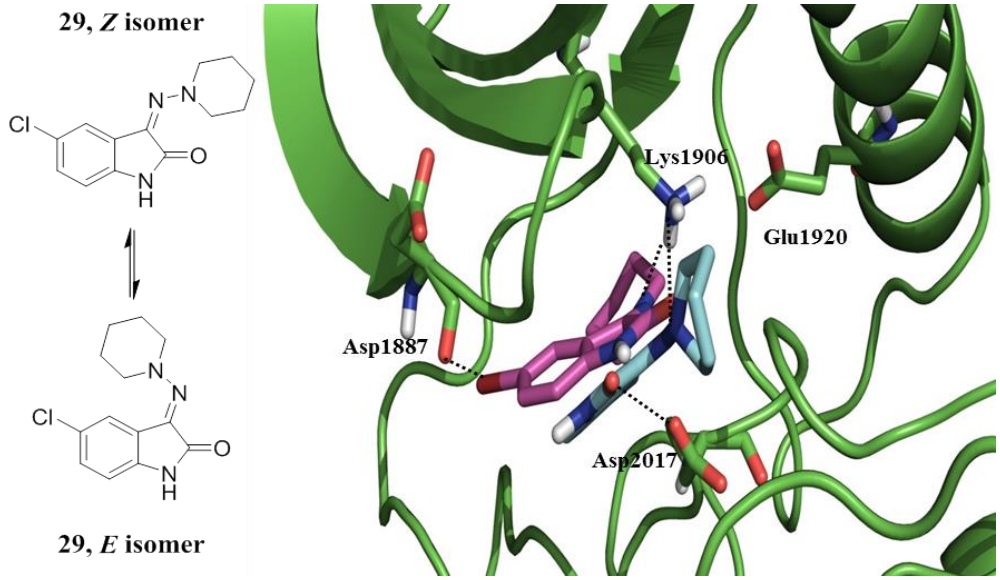

Figure 23. *Overlapped binding modes of compound **29**, E isomer in magenta, Z in cyan in the homology model. Interactions of the E isomer are shown: black dashed lines show hydrogen-bonds and halogen-bonds.*

From these experiments several conclusions can be reached. First of all, these new indolinone derivatives show a similar binding to the kinase domain of LRRK2 in the homology model built. Secondly, the *E* isomer is the biological active one and therefore, the more the isomeric equilibrium is shifted to the *E* isomer, the higher the biological activity. The homology model built and the conclusions from the docking studies found were used in the design of new indolinone derivatives.

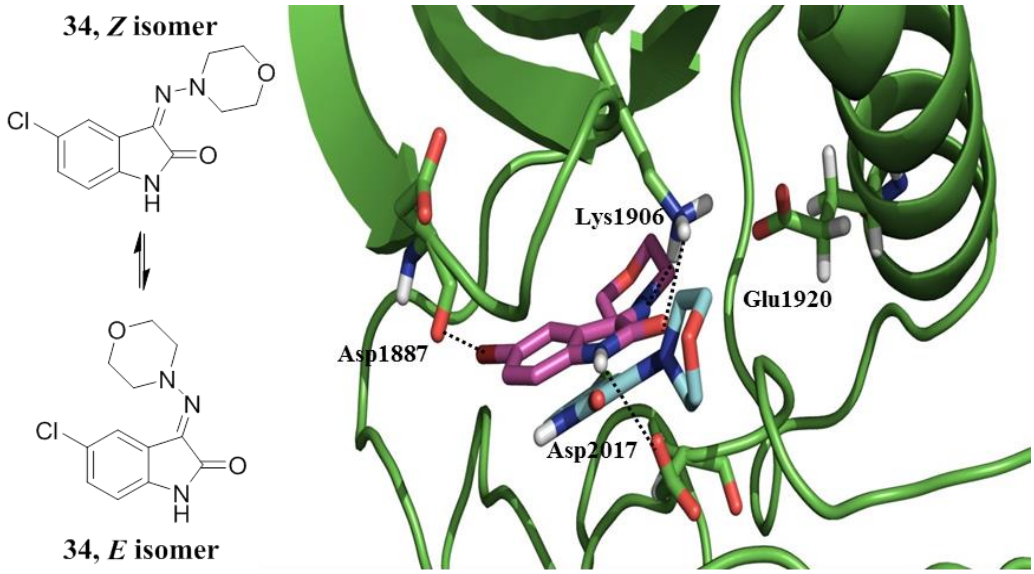

Figure 24. *Overlapped binding modes of compound **34**, E isomer in magenta, Z in cyan in the homology model. Interactions of the E isomer are shown: black dashed lines show hydrogen-bonds and halogen-bonds.*

1.4. Design, synthesis, enzymatic evaluation and SAR of new indolinone derivatives

1.4.1. Design of new indolinone derivatives

In order to guide the design of new indolinone derivatives the protein surface and druggable cavities of the kinase domain of LRRK2 were considered. In the catalytic site there are two pockets where additional van der Waals interactions with the ligand may increase enzymatic potency. The first one at the back of Lys1906 and Glu1920 was fully occupied with one of the phenyl rings of diphenyl amino compounds (**21 - 25**) that may be responsible for the higher potency of these derivatives in comparison with their piperidine (**27 - 31**) and morpholine analogs (**32 - 38**). However, the six-membered ring present in these last compounds was oriented totally towards the second cavity, pointing to a new direction where current molecules may be modified to potentially increase hydrophobic interactions (**Figure 25**).

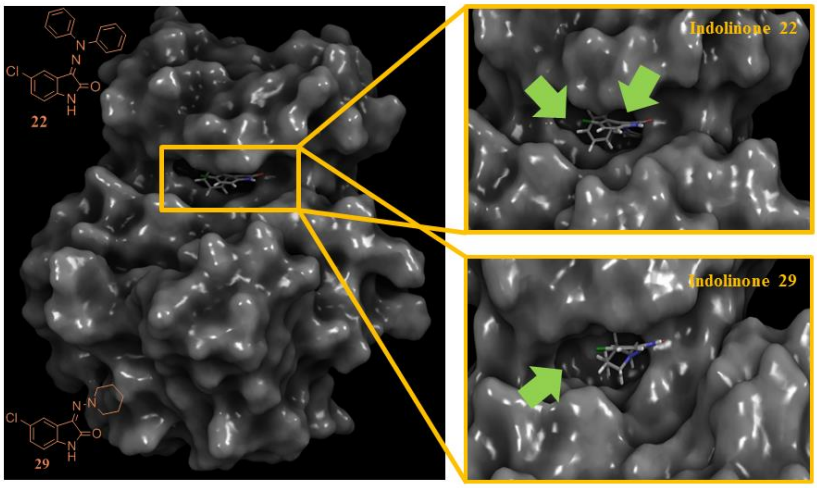

Figure 25. *Indolinones **22** and **29** bound to LRRK2 homology model. Green arrows show the back cavities present in the active site of LRRK2.*

Therefore, it was proposed for the design of new LRRK2 inhibitors to grow the molecules at this point by using different functionalized piperazine derivatives (**Figure 26**).

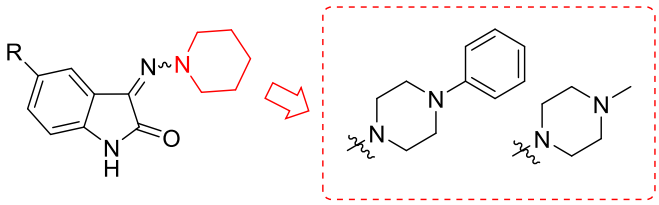

Figure 26. *Proposed modifications for new indolinone-piperazine derivatives.*

1.4.2. Synthesis of new indolinone-piperazine derivatives

The synthesis of 5-halide-3-(piperazin-1-yl)imino)indolin-2-one derivatives was performed using a synthetic methodology optimized in the research group which employs microwave radiation and montmorillonite (MMT-K10) as a surface catalyzer[186]. MMT-K10 is a mixture of silicates in laminar arrangement recently used as inorganic base in organic synthesis. The reactions catalyzed by MMT-K10 are normally performed under mild conditions to obtain high yield and selectivity. MMT-K10 was not only used as a base but also as a solid surface where the reaction took place[197]. Each 5-halide-isatine was dissolved with the corresponding phenyl or methyl 4-amino-piperazine in toluene. MTT-K10 was added and the reaction mixture was heated under microwave irradiation for 2 - 3 hours at 110 ºC. With this procedure it was possible to obtain the corresponding 5-halide-3-(piperazin-1-yl)imino)indolin-2-one derivatives (**57 - 63**) with moderate to high yields. (**Scheme 1**).

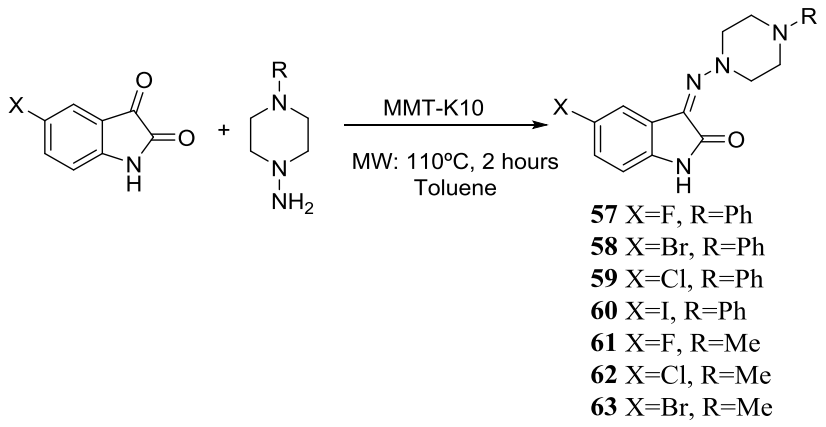

Scheme 1. *Synthesis of 5-halide-3-(piperazin-1-yl)imino)indolin-2-one derivatives,* ***57 - 63****.*

All the compounds here prepared (**57 - 63**) were purified by chromatographic methods. The unequivocal characterization of their chemical structures was done in basis to their analytical and spectroscopic (^{1}H-RMN and ^{13}C-RMN) data which are shown in the experimental part.

The isomeric ratio *Z/E* for each compound was determined using nOe experiments. Due to the presence of an imino or hydrazone bond directly attached to the heterocyclic framework two different isomers *E* and *Z* are present. The two isomers were identified and the isomeric ratio was quantified. In order to determine the main isomer, a 2D Nuclear Overhauser Spectroscopy (NOESY) experiment was performed by which it was possible to determine that proton H4 is not able to show nOe effect with protons H8/H11 of the methylene groups of the piperazine moiety and therefore, the most prevalent isomer is the *Z* one. This methodology was carried out in all the cases to determine the isomers ratio of the compounds (**Table 6**).

The isomeric ratios determined for compounds **57 - 63** are in the same range for the isomeric ratios found in derivatives **27 - 28** in which the most prevalent isomer is the *Z* one. Therefore, in the cases of a saturated cycle (morpholine, piperidine and piperazine) attached to the N of the imino group, the isomeric equilibrium is shifted towards the *Z* isomer.

Table 6. *Isomeric ratio for compounds* ***57 - 63****.*

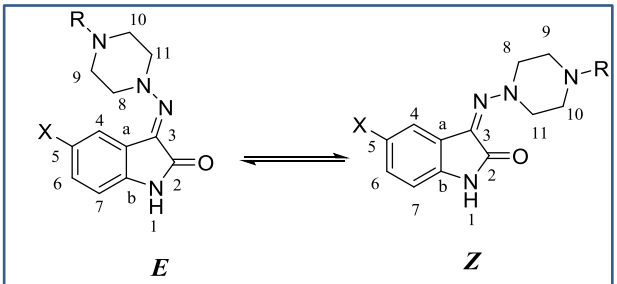

Compound	Ratio *E:Z*
57	17:83
58	17:83
59	9:91
60	17:83
61	17:83
62	17:83
63	9:91

1.4.3. Enzymatic evaluation on LRRK2, SAR and docking studies

Compounds **57 - 63** were evaluated against LRRK2wt and G2019S LRRK2 externally using the Adapta® Specific Kinase Assay. This methodology is a fluorescent based immunoassay for the detection of ADP. In the presence of a kinase inhibitor the amount of free ADP is lower which results in higher fluorescence.

Firstly, all the compounds were tested against LRRK2wt at a fixed concentration of 10µM. Only when the percentage of inhibition was higher than 50, the half inhibitory concentration (IC_{50}) was calculated. Data are reported in **Table 7**.

Table 7. *Enzymatic activities of synthesized compounds,* ***57 - 63****.*

Compound	LRRK2 %inh@10µM	IC_{50} LRRK2wt (µM)	LRRK2 G2019S %inh@10µM	LRRK2 G2019S IC_{50}(µM)
57	39%	47.10	60%	11.20
58	51%	5.19	72%	4.65
59	45%	14.50	71%	12.30
60	65%	4.09	83%	3.75
61	11%	-	18%	-
62	36%	-	36%	-
63	35%	-	42%	-

Some of the new compounds synthesized are LRRK2 inhibitors with lower potency than the previous hits. Preliminary SAR point to a completely lack of activity of the methyl-piperazine derivatives showing that the cavity maybe only occupied in the case of the phenyl-piperazines. In an attempt of explaining the SAR found, docking studies in the homology model previously built were done. For the case of these piperazine derivatives the isomeric equilibrium is shifted towards the *Z* isomer, in concordance to what was seen in the case of piperidine and morpholine analogues (**27 - 38**). The docking studies of the *E* isomers showed that although it was possible to reach the desired cavity (**Figure 27A - B**) and therefore increase the hydrophobic interactions, the phenyl-piperazine derivatives showed a different binding mode than the piperidine and morpholine analogues in which only a hydrogen bond between the carbonyl group of the oxoindol moiety and Lys1906 is formed (**Figure 27C**). From these studies, it becomes clear that a shift in the isomeric equilibrium towards the *E* isomer is of crucial importance for the biological activity. A detailed computational study has been performed in order to understand why the *E* isomer is the most prevalent one in the case of the diphenyl-amino derivatives (**21 - 26**) and why in the case of the morpholine, piperidine and piperazine the most prevalent one is the *Z* isomer.

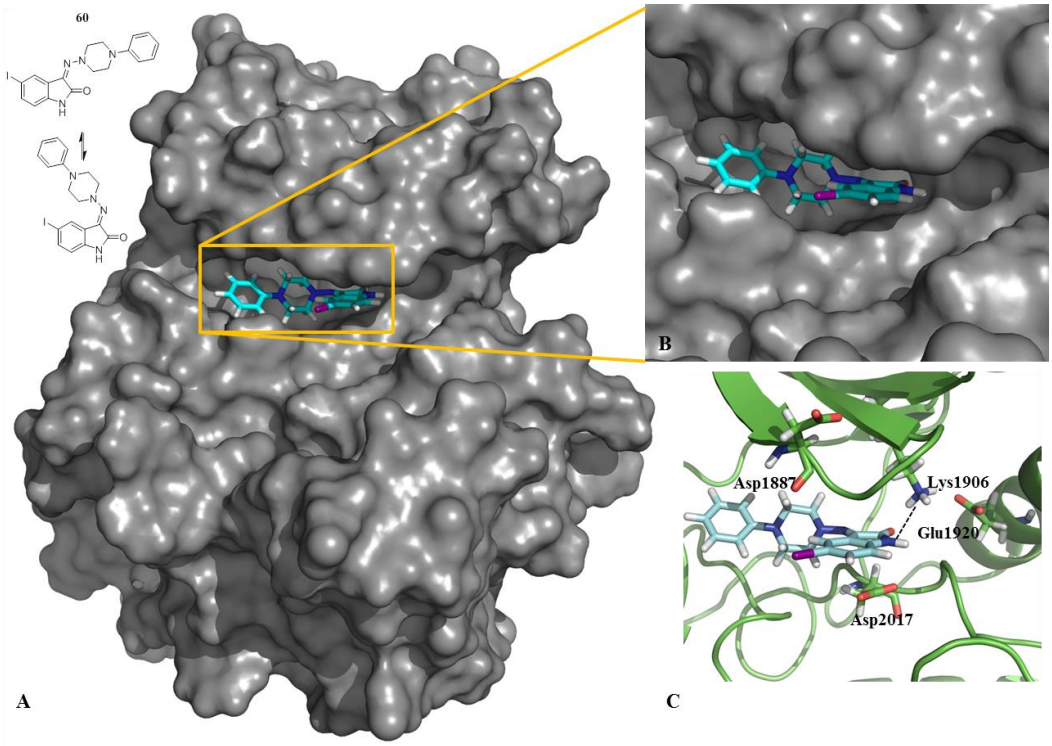

Figure 27. A- *E isomer of* indolinone ***60*** *binds to the ATP-binding site of homology model.* ***B-*** *Close up showing the posterior cavity of the ATP-binding site being occupied by the phenyl-piperazine.* ***C-*** *Binding mode of compound* ***60*** *in the homology model. Dashed lines show hydrogen-bonds.*

1.4.4. Detailed study of the isomeric equilibrium in the indolinone derivatives synthesized

It is very important to take into consideration that due to the presence of an imino or hydrazone bond directly attached to the heterocyclic framework two different isomers *E* and *Z* are present. The *E* isomer seems to be the biological active one, therefore, it is important to study in detail how is the isomeric equilibrium shifted towards one of the isomer in each subgroup of indolinone derivatives.

In the subgroup of indolinone derivatives which have two phenyl groups attached to the hydrazone moiety (**21 - 25**), the main isomer and in one case the only one (compound **24**) is the *E* isomer. This shift in the isomeric equilibrium could be explained theoretically by the formation of a *T-shaped edge-to-face* interaction between the aromatic CH of the oxoindole moiety and the plane of the phenyl ring[198] and a possible intra-molecular hydrogen bond between H4 and the N of the hydrazine (**Figure 28**).

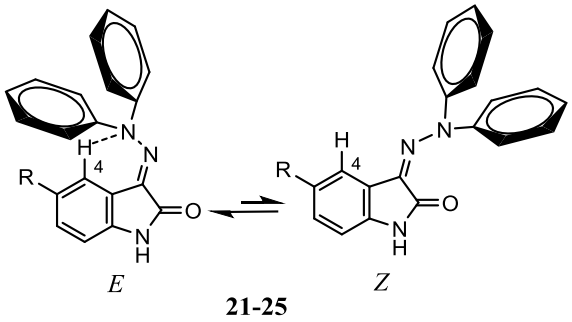

Figure 28. *Different E:Z isomers of the indolinone derivatives* ***21 - 25****.*

In the subgroup of indolinone derivatives which present an aromatic ring attached to the imino moiety (**39 - 44**), the main isomer is the *E* one. This shift in the isomeric equilibrilium could be explained theoretically by the formation of a *T-shaped edge-to-face* interaction between the aromatic CH of the oxoindole moiety and the plane of the phenyl ring[198] (**Figure 29**).

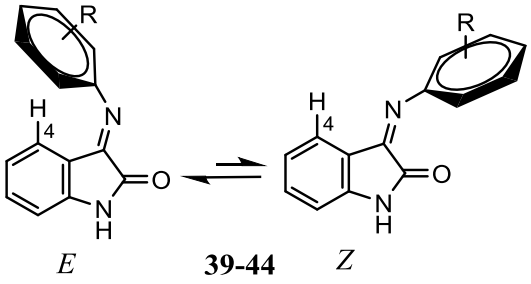

Figure 29. *Different E:Z isomers of the indolinone derivatives* ***39 - 44****.*

Finally, in the case of indolinone derivatives with a piperidine group attached to the hydrazine linker (**27 - 31**) and a morpholine group attached (**32 - 38**), the major isomer is the *Z* one, however, there is not a straight forward explanation for this shift in the isomeric equilibrium.

In order to determine a way to drive the isomeric equilibrium towards the active isomer, which is the *E* one and to explain experimentally why in the case of piperidine and morpholino analogs (**27 - 38**) the most prevalent isomer is the *Z* one, quantum mechanics studies were performed. In these studies both isomers of compounds **22**, **29** and **59** were minimized using Jaguar (Schrödinger suite program) and the force field B3LYP as representative examples.

The minimization of compound **22** showed that the *E* isomer is the most stable one energetically and geometrically. This stability could be explained by the formation of a *T-shaped edge-to-face* interaction between the aromatic CH of the oxoindole moiety and the plane of the phenyl ring[198] and a possible intra-molecular hydrogen bond between H4 and the N of the hydrazine. The distance between the CH of the oxoindole moiety and the plane of the phenyl ring is 3.3 Å and the distance between H4 and the N of the hydrazine of 2.6 Å which is in the range of distances reported to this type of hydrogen bonds[199] (**Figure 30**).

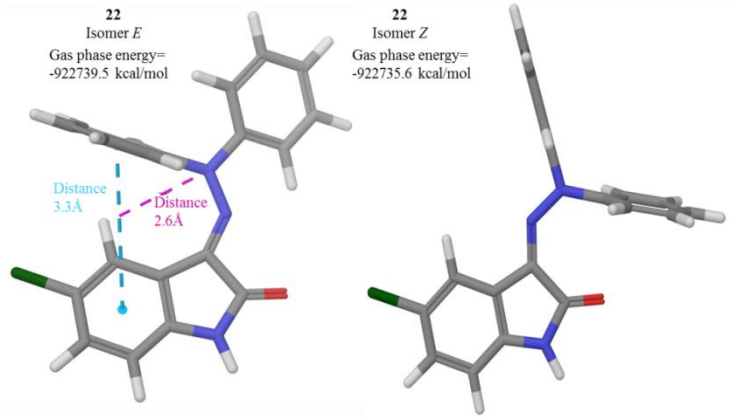

Figure 30. *Minimized structures of isomers E and Z of compound **22**. Blue dashed lines show T-shaped edge-to-face interaction and purple lines the possible hydrogen bond.*

The same minimization was done for isomers *E/Z* of compound **29** in which the most prevalent isomer is the *Z* one. Isomer *Z* is the most stable one energetically and geometrically. These differences in stability between the isomers could be related to steric hindrance in the *E* isomer, as the angle formed between the N of the piperidine ring and the oxoindol moiety is closer and also the diehedral formed between the piperidine ring and the

oxoindole ring has a higher deviation to the plane that in the case of the *Z* isomers (**Figure 31**). This effect observed could explain why in these derivatives the *Z* isomers is the most prevalent one.

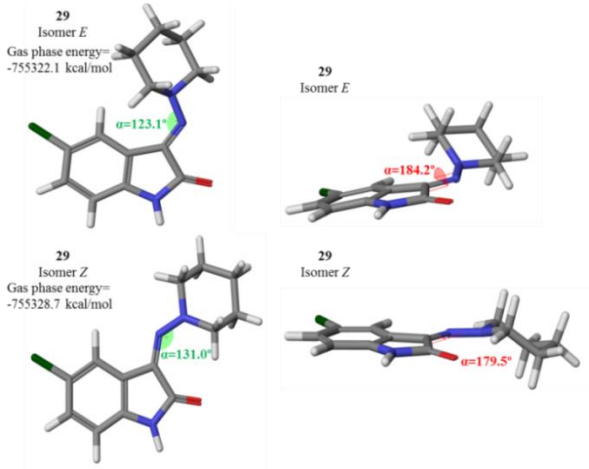

Figure 31. *Minimized structures of both isomers of compound **29** showing the angles and the dihedrals measured between the piperidine ring and the oxoindole moiety.*

The same observations could be done for the piperazine derivative **59**, as similary to compound **29** the most prevalent isomer is the *Z* one. The minimization showed that the *E* isomer is energetically and geometrically less stable than the *Z* one, due to steric hindrance between the functionalized piperazine ring and the oxoindol ring. The angle formed between the N of the piperizine ring and the oxoindol moiety is smaller and also the diehedral formed between the piperidine ring and the oxoindole ring has a higher deviation to the plane that in the case of the *Z* isomer (**Figure 32**).

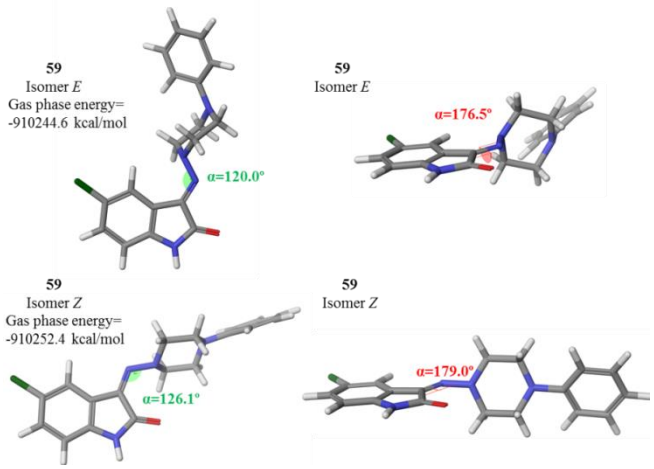

Figure 32. *Minimized structures of both isomers of compound **59** showing the angles and the dihedrals measured between the piperidine ring and the oxoindole moiety.*

From these results and the results obtained from the docking studies for the isomeric equilibrium it becomes clear that regarding the SAR, in order to shift the isomeric equilibrium towards the *E* isomer it is crucial to have an at least one aromatic ring attached to the N of the hydrazine. If that aromatic ring is present, there is *T-shaped edge-to-face* interaction between the aromatic CH of the oxoindole moiety and the plane of the phenyl ring[198] and a possible intra-molecular hydrogen bond between H4 and the N of the hydrazine H-bond, shifting therefore, the isomeric equilibrium towards the *E* isomer. If there is no aromatic ring these interactions will not occur. One possibility that could be studied with the aim of occupying the back cavity of the ATP-binding site in a way similar to the piperazine analogues but maintaining the *E* conformation is by introducing functionalized phenyl groups to the hydrazine moiety.

1.5. Design and synthesis of new LRRK2 inhibitors based on the benzothiazole ring

The design and synthesis of new LRRK2 inhibitors based on the benzothiazole **56** is proposed with the aim of performing structural modifications including substituents with different chemical properties and in different positions of the benzothiazole ring. Furthermore, changes in the nature of the morpholino moiety will also be addressed (**Figure 33**).

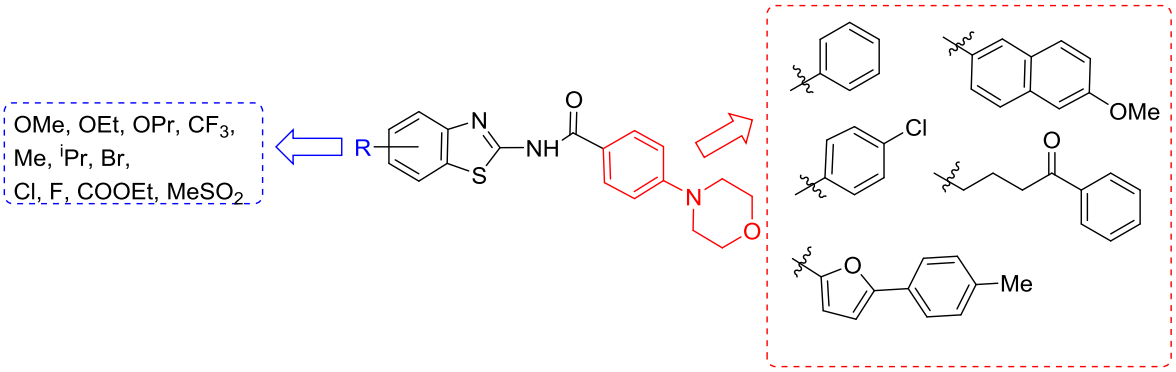

Figure 33.*Proposed modifications for benzothiazole* ***56****.*

1.5.1. Synthesis of *N*-(benzothiazole-2-yl-)-4-morpholinobenzamide derivatives

The synthesis of the *N*-(benzothiazole-2-yl)-4-morpholinobenzamide derivatives was performed by a coupling reaction between the corresponding 2-amino-benzothiazole and the 4-morpholinobenzoic acid. Each 2-amino-benzothiazole was mixed with the 4-morpholinobenzoic acid in the presence of 1-ethyl-3-(3-dimethylaminopropyl) carbodiimide (EDCI) as a coupling agent and 4-dimethylaminopyridine (DMAP) as a basic

catalyzer. Previously, the 4-morpholinobenzoic acid was activated with the coupling agent for a certain time and then the corresponding 2-amino-benzothiazole amine was added. Following this procedure, it was possible to obtain the corresponding *N*-(benzothiazole-2-yl)-4-morpholinobenzamide derivatives with low to moderate yields (**Scheme 2**). A total of thirteen new benzothiazoles (**64 - 76**) were synthesized with different substituents in the benzoannelated ring in order to see the influence of their nature and position in the biological activity.

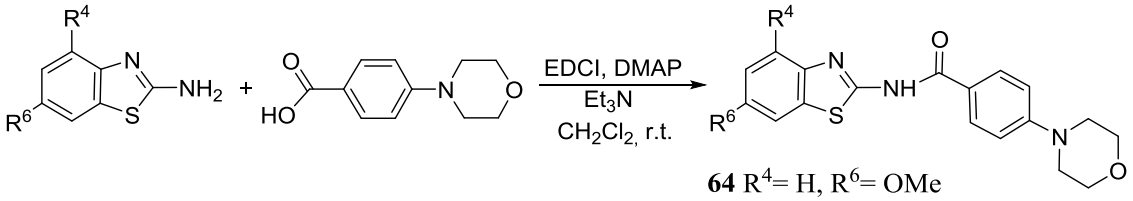

64 R^4= H, R^6= OMe
65 R^4= H, R^6= CF_3
66 R^4= H, R^6= Me
67 R^4= H, R^6= Cl
68 R^4= H, R^6= F
69 R^4= Me, R^6= H
70 R^4= Cl, R^6= H
71 R^4=H, R^6= OEt
72 R^4=H, R^6= Br
74 R^4=H, R^6= OPr
75 R^4=H, R^6= ^{i}Pr
76 R^4=H, R^6= SO_2Me

Scheme 2. *Synthesis of N-(benzothiazole-2-yl)-4-morpholinobenzamide derivatives* ***64 - 72, 74 - 76****.*

In an attempt of trying to increase the yield, a different methodology was tested for compound **73**, using PyBOP and HOBT with the 4-morpholinobenzoic acid, everything dissolved in THF to activate the acid under microwave irradiation (50 ºC) during 1 hour and then adding the corresponding amino-benzothiazole and heating the resulting mixture during 5 hours at 110ºC under microwave irradiation (**Scheme 3**). However, the yield did not increase and the previous methodology with the EDCI and DMAP was continued for derivatives **74 - 76**.

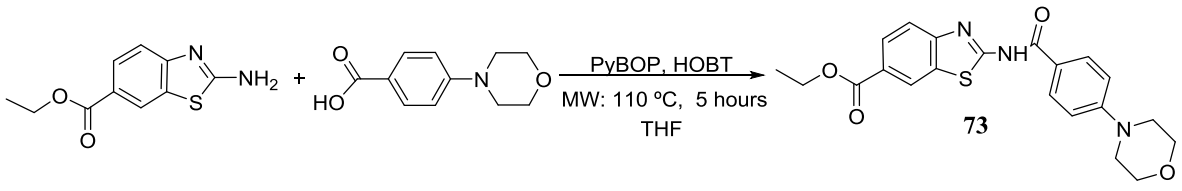

Scheme 3. *Synthesis of N-(6-ethylcarboxylatebenzothiazole-2-yl)-4-morpholinobenzamide,* ***73****.*

1.5.2. Synthesis of *N*-(6-flurobenzothiazol-2-yl-)-aryl derivatives

To study the influence of the morpholino moiety and to confirm the relevance of this chemical fragment in the biological activity, the synthesis of *N*-(6-flurobenzothiazol-2-yl)-benzamide derivatives (**78 - 81**) was proposed. The synthesis performed was done following the same procedure for the previous derivatives (**Scheme 4**) and it is detailed in the experimental part.

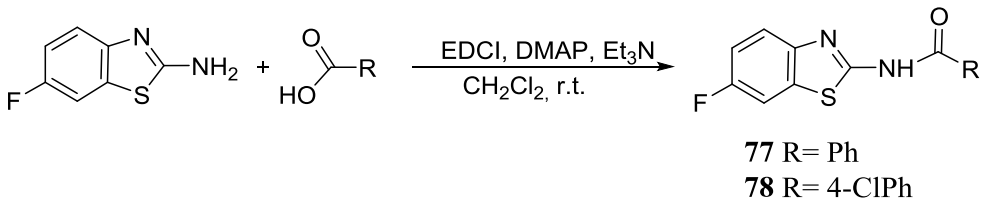

Scheme 4. *Synthesis of N-(6-flurobenzothiazol-2-yl)-aryl derivatives **77 - 78**.*

For compounds **79** – **81**, the same methodology of dissolving the corresponding acid in THF with PyBOP and HOBT for the activation under microwave irradiation at 50 ºC during 1 hour was used. Afterwards, 6-fluoro-2-aminobenxothiazole was added and the resulting mixture was heated during 5 hours at a 110 ºC under microwave irradiation (**Scheme 5**). However, as before the yields did not increase significantly with this methodology.

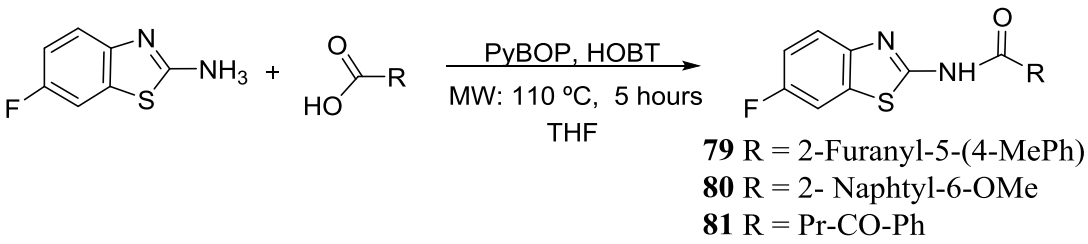

Scheme 5. *Synthesis of N-(6-flurobenzothiazol-2-yl)-aryl derivatives **79 - 81**.*

All the new benzothiazole here prepared (**64 - 81**) were purified by chromatographic methods. The unequivocal characterization of their chemical structures was done in basis to their analytical and spectroscopic (^{1}H-RMN and ^{13}C-RMN) data which are shown in the experimental part.

1.5.3. Enzymatic evaluation on LRRK2, SAR and docking studies

Compounds **64 - 81** were evaluated against LRRK2 and G2019S LRRK2 externally using the Adapta® Specific Kinase Assay as previously described. Data are collected in **Table 8**.

Table 8. *Enzymatic activity of synthesized compounds* ***64 - 81***.

Compound	LRRK2wt %inh@10μM	LRRK2wt IC_{50} (μM)	LRRK2 G2019S %inh@10μM	LRRK2 G2019S IC_{50}(μM)
64	73%	0.37	93%	0.11
65	51%	1.06	69%	0.29
66	61%	0.52	71%	0.33
67	60%	0.78	50%	-
68	66%	0.19	55%	0.43
69	18%	-	-	-
70	32%	-	-	-
71	80%	0.31	85%	0.16
72	75%	0.47	70%	1.39
73	46%	-	37%	-
74	48%	4.00	70%	1.19
75	77%	1.95	80%	1.17
76	22%	-	20%	-
77	81%	0.79	79%	0.51
78	68%	3.92	67%	23.60
79	13%	-	9%	-
80	16%	-	7%	-
81	11%	-	23%	-

The great majority of the prepared compounds were able to inhibit LRRK2 in the submicromolar range. Some preliminary SAR point to a completely lack of activity when a substituent is attached to position 4 of the benzothiazole moiety (see compounds **69 - 70** *vs* **66 - 67**) or when a phenyl ring is not attached to the carbonyl linker (see compounds **79 - 81** *vs* **77 - 78**). In order to throw light into the binding mode of these benzothiazole derivatives a docking study in the homology model previously used was done. All the compounds showed a similar binding mode and the SAR found could be explained. Derivative **68** is the

one that shows the highest activity in the wt form (IC_{50} = 0.19 µM). The nitrogen in the benzothiazole core is able to form a hydrogen bond with Asp2017. Furthermore, the fluorine atom at position 6 of the benzothiazole may form a halogen bond with Glu1920. In addition, the side chain of Arg1957 is flexible and it may, therefore, form a hydrogen bond with the oxygen atom of the morpholino moiety (**Figure 34**).

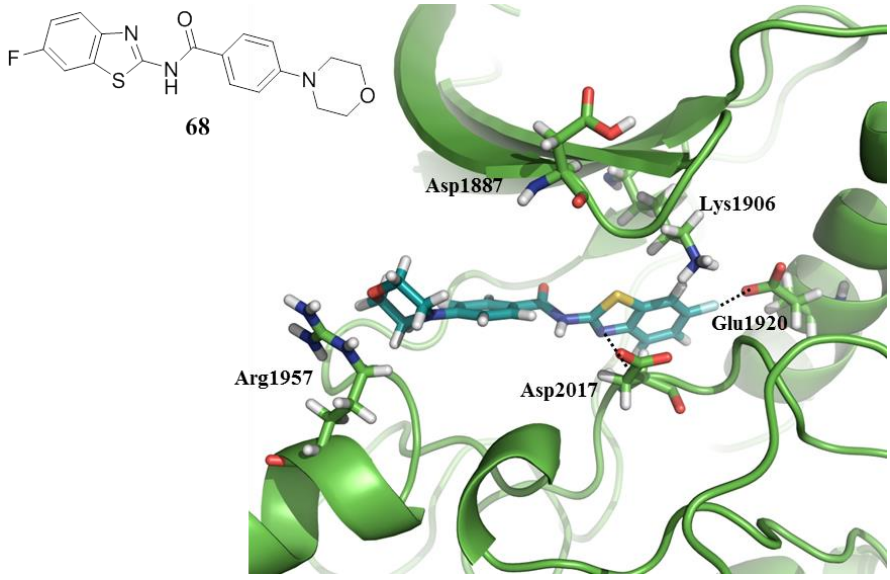

Figure 34. *Docking of compound **68** in the homology model. Dashed lines show hydrogen-bonds and halogen-bonds.*

However, when substitution takes place at position 4 of the benzothiazole moiety instead of position 6, this results in a loose of activity (see **66 - 67** *vs* **69 - 70**). The lack of activity of these compounds could be explained by the fact that due to steric hindrance the benzothiazole core is not able to enter to the interior of the cavity and therefore, in these cases is the phenyl-morpholino moiety the part of the molecule allocated towards the cavity whereas the benzothiazole core is oriented towards the external part that is exposed to the solvent. With this binding mode interactions with Glu1920, Arg1957 and Asp2017 are lost (**Figure 35A**). The docking of compound **69** is shown as an example.

A similar effect is seen in molecules **73** and **76,** in which although the substitution takes place at position 6, the substituents are too bulky and therefore the benzothiazole core is not able to enter properly to the interior of the cavity losing the interactions with Glu1920, Asp2017 and furthermore a potential steric hindrance with Arg1957. Docking of molecule **73** is shown (**Figure 35B**).

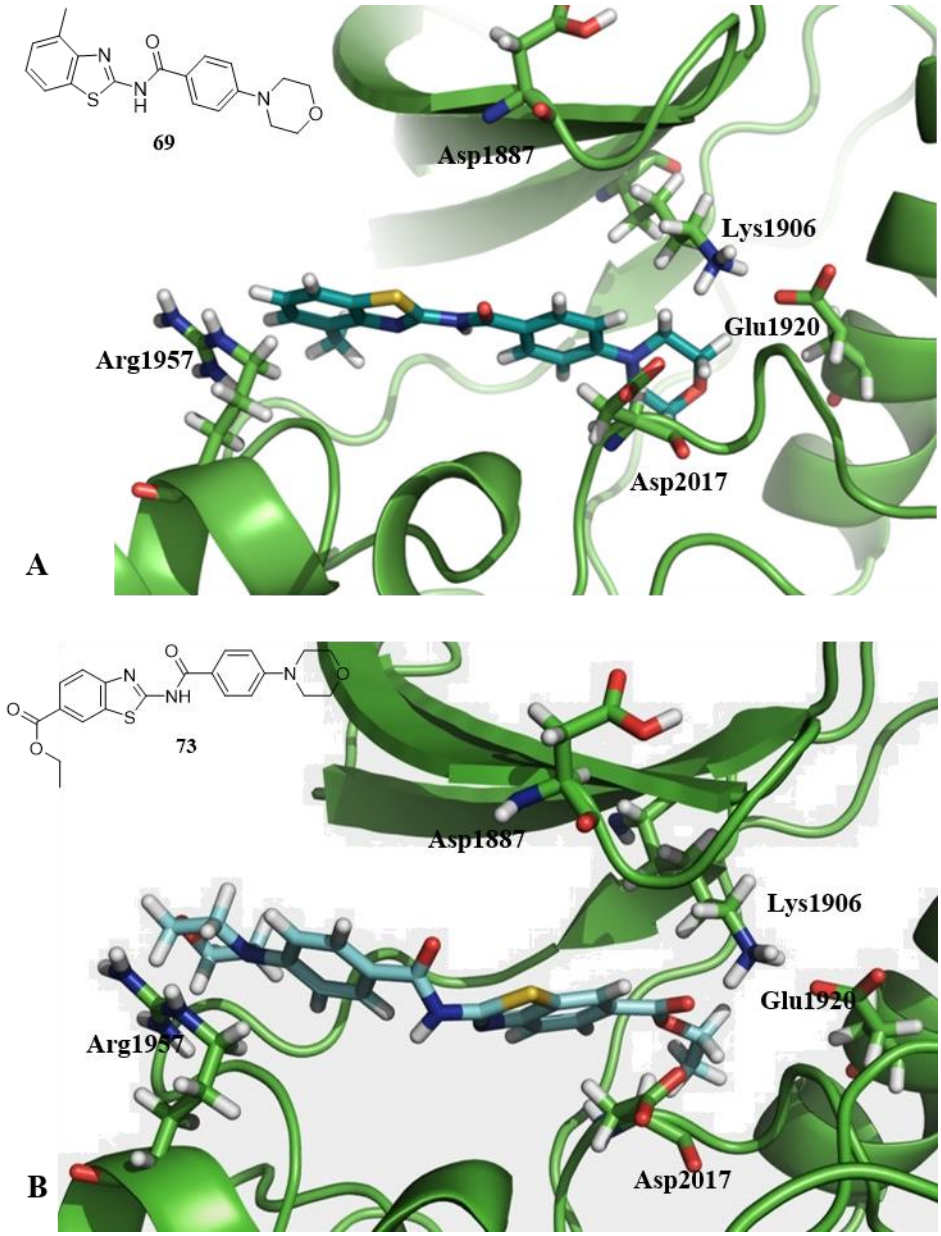

Figure 35. A- *Docking of compound* ***69*** *in the homology model.* ***B-*** *Docking of compound* ***73*** *in the homology model.*

Regarding the nature of the substituent in the exocyclic nitrogen atom, both morpholino or phenyl moieties were allowed by the enzyme (see **77 - 78** *vs* **70**). The docking of **77** is shown as an example (**Figure 36**).

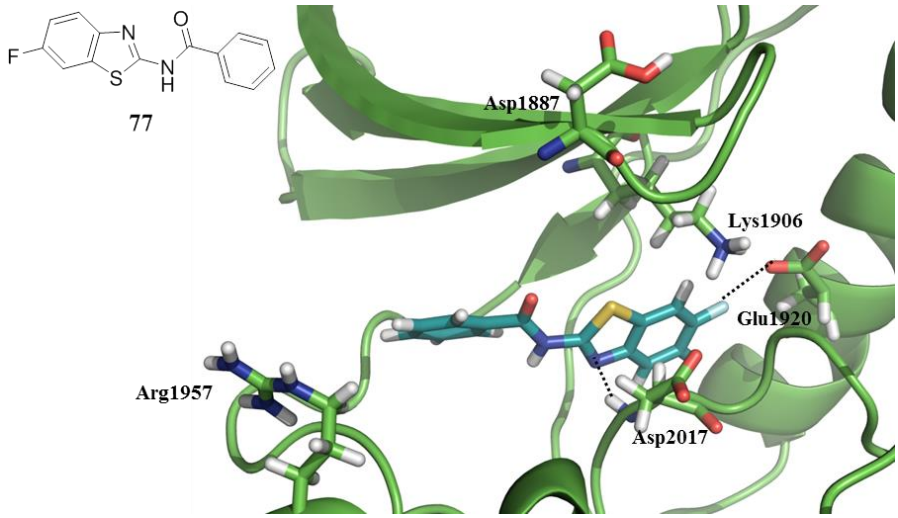

Figure 36. *Docking of compound **77** in the homology model. Dashed lines show hydrogen-bonds and halogen-bonds.*

However, when the moiety attached to exocyclic nitrogen is bigger and/or it contains more than one aromatic ring it results in a lack of activity (see compounds **79 - 81** *vs* **77 - 78**). Docking of compound **79** is shown as an example, an in this case, the loose of activity could be explain that in order to allocate the aliphatic chain attached to the exocyclic nitrogen the benzothiazole core changes its orientation and now the nitrogen atom towards the exterior of the cavity and the sulphur atom towards the interior. With this binding mode, the hydrogen-bond between the nitrogen and Asp2017 is impossible and thus the halogen-bond between the fluorine and Glu1920 (**Figure 37**).

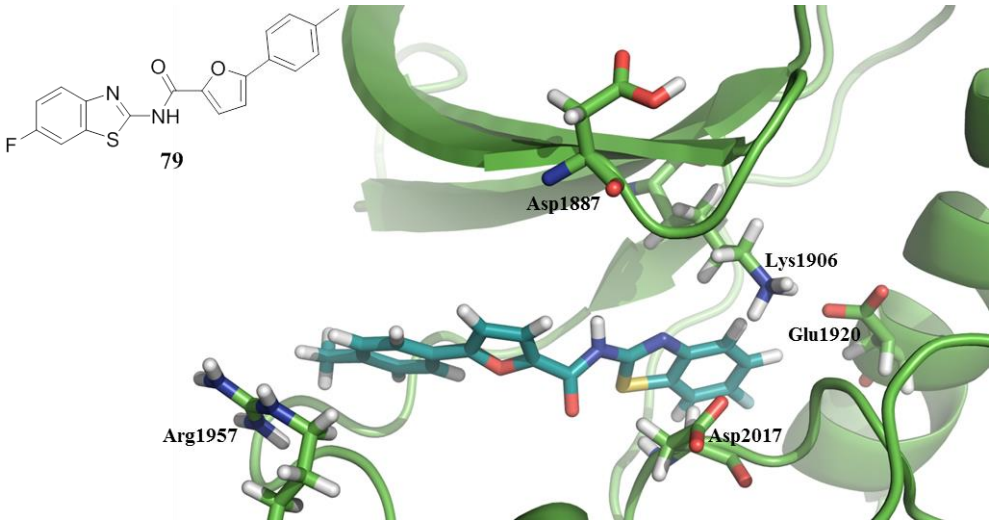

Figure 37. *Docking of compound **79** in the homology model.*

These docking studies performed can be used to further optimize this family of compounds in a lead-to-candidate process. The introduction of halogens in position 5 of the benzothiazole core can be studied in order to determine if two halogen-bonds with the enzyme could be formed, to have a higher enzymatic activity.

To conclude, this series of compound showed good enzymatic activity in the low to submicromolar range. Lastly, regarding the previous hits **8** and **16** that were used in a merge strategy, although the enzymatic activities were higher in these compounds the new synthesized LRRK2 inhibitors combine important structural features in a simpler scaffold that can be further optimized.

1.6. Determination of the blood-brain-barrier permeability

BBB penetration is an essential ADME property for any compound developed to target neurodegenerative and neurological diseases. During the long and complex process for the development of a new drug from the lab to the market, there are several bottleneck steps which one of them relies on the lack of good ADME/Tox properties and in particular CNS penetration in the case of neuro-drugs of the candidate compounds[200]. Thus the next step in development for LRRK2 inhibitors is to determine BBB penetration of the lead compounds found. The BBB is a unique barrier controlling the selective and specific transport of both exogenous and endogenous materials to the brain. Due to its biological structure, lipophilic compounds with low molecular weight (MW< 550 Da) are more likely to cross the BBB and may pass directly through via passive diffusion between the capillary walls. Determination of BBB penetration and other drug like properties at early stages during drug discovery is of utmost importance to select good candidates for *in vivo* studies and further pharmacological development.

1.6.1. *In vitro* parallel artificial membrane permeability assay

Parallel artificial membrane permeability assay (PAMPA) is a high throughput technique developed to predict passive permeability through biological membranes[201] and was the methodology here employed. All new compounds synthesized that showed more than a 50% inhibitory activity were tested. These were:

- Indolinone derivatives: **57 - 59**.
- Triazolopyridine derivatives: **45 - 49**.

- Benzothiazole derivatives: **56**, **64 - 68**, **71 - 72**, **74 - 75**, and **77 - 78**.

The PAMPA-BBB method employing a porcine brain lipid membrane was used. First of all, an assay validation was made comparing the reported permeability values in human BBB of clinical used drugs with the experimental data obtained in this PAMPA methodology. A good correlation between experimental-described values was obtained Pe (exptl) = 1.3711 (bibl) – 1.4509 (R^2= 0.972) (**Figure 38**). Then, for the first round of this assay, the *in vitro* permeabilities (Pe) of derivatives: **45 - 49**, **56 - 59**, **64 - 68**, **71 - 72**, **74 – 75**, and **77 - 78** were determined and described in **Table 9**. From this correlation equation obtained with the commercial compounds and following the pattern established in the literature for BBB permeation prediction, compounds could be classified as CNS + when they present a permeability > 4.03 x 10-6 cm s^{-1}. Based on these results compounds **45 - 49**, **56 - 59**, **66 - 68**, **74 - 75** and **77** are able to cross the BBB by passive permeation (**Table 9**). Whereas compounds **64 - 65**, **71 - 72** and **78** precipitate in the experimental conditions employed or there was not a clear UV spectrum after filtration so it was not possible to determine the BBB permeability using this methodology.

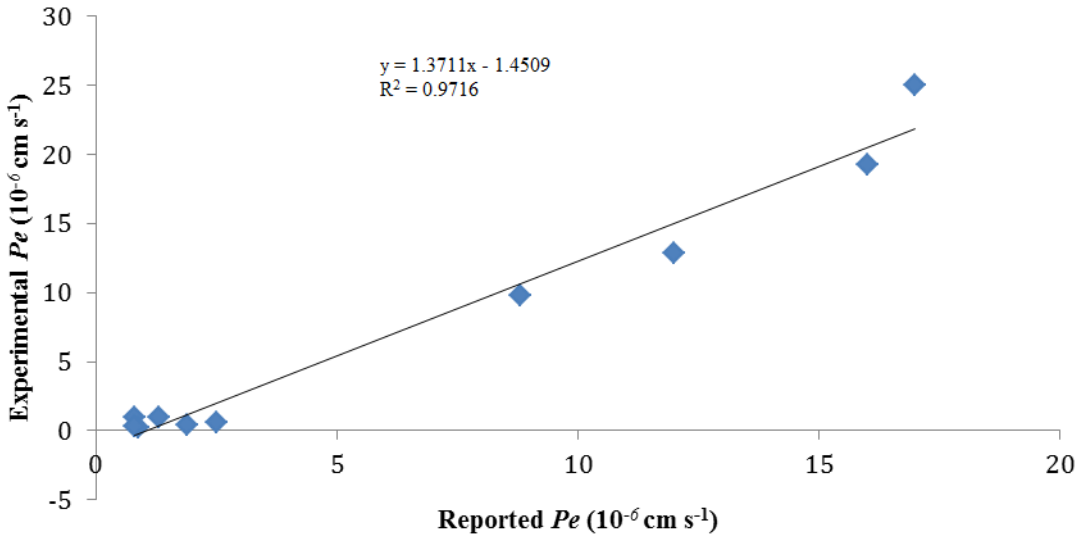

Figure 38. Linear correlation between experimental and reported permeability of commercial drugs using the PAMPA-BBB assay.

Table 9. *Permeability (Pe 10^{-6} cm.s^{-1}) in the PAMPA-BBB assay for commercial drugs and different LRRK2 inhibitors with their predictive penetration in the CNS*[a].

Compound	Bibll.	Pe (10^{-6} cm. s^{-1})[b]	Prediction
Atenolol	0.8	1.0 ± 0.6	
Caffeine	1.3	1.0 ± 0.8	
Desipramine	12	12.9 ± 0.4	
Enoxacin	0.9	0.2 ± 0.2	
Hydrocortisone	1.9	0.4 ± 0.1	
Ofloxacin	0.8	0.3 ± 0.3	
Piroxicam	2.5	0.6 ± 0.2	
Promazine	8.8	9.8 ± 0.5	
Testosterone	17	25.0 ± 0.2	
Verapamil	16	19.3 ± 0.7	
45		14.9 ± 5.23	CNS+
46		8.95 ± 2.77	CNS+
47		10.59 ± 2.25	CNS+
48		6.95 ± 0.91	CNS+
49		n.d.	
56		13.4 ± 2.4	CNS+
57		12.40 ± 0.98	CNS+
58		7.18 ± 0.71	CNS+
59		12.89 ± 3.72	CNS+
64		n.d.	
65		n.d.	
66		19.0 ± 2.6	CNS+
67		3.42 ± 1.26	CNS-/CNS+
68		5.1 ± 0.1	CNS +
71		n.d.	
72		n.d.	
74		4.28 ± 3.45	CNS+
75		4.27±2.7	CNS+
77		15.0 ± 1.3	CNS+
78		n.d.	

[a]PBS:EtOH (70:30) was used as solvent. [b]Data are the mean ± SD of 2 independent experiments. n.d. Not determined under these experimental conditions.

1.7. Conclusions

In this chapter a chemically diverse LRRK2 inhibitor chemolibrary has been completed starting by different hits of three different chemical families (indolinone, triazolo-pyrimidine and benzothiazole derivatives) that were in a different point of development.

In particular, in this present work new chemically diverse LRRK2 inhibitors containing indolinone and benzothiazole scaffolds have been synthesized for the first time. For the design and synthesis of these new inhibitors a homology model of the kinase domain of LRRK2 was built and it was used for docking studies of a family of LRRK2 inhibitors previously synthesized in the group containing the indolinone scaffold. Furthermore, new indolinone derivatives were designed synthesized and also a new family of LRRK2 inhibitors the benzothiazole scaffolds respectively. In addition, the enzymatic activity was determined and a potential binding mode of these new molecules was studied through the homology model built. Finally the ability of all the active compounds to penetrate the BBB was determined using the *in vitro* PAMPA assay.

These new chemically diverse LRRK2 inhibitors will be further used for the interrogation of new biological functions of LRRK2 with special emphasis on: adult neurogenesis, tauopathies and retinitis pigmentosa

2. LRRK2 inhibitors as pro-neurogenic agents

2.1. Introduction

Till the pioneer discovery of adult neurogenesis by Joseph Altman in 1962, the CNS was thought to be considered as a complex static structure unable to undergo any regenerative process. The fact that new neurons are born in the adult brain has profound implications for our understanding of brain function and pathology as it raises the possibility that the nervous system has an intrinsic repair capacity[202]. Therefore, nowadays, neuro-regenerative medicine is one of the most innovative therapeutic approaches for the treatment of different neurological pathologies including neurodegenerative diseases and psychiatric disorders[203].

Neuro-regenerative medicine can be broadly divided in two branches[204]: the first one implies the use of cell-based therapies. Research activities in neural transplantation have steadily increased since the initial reports of fetal tissue transplants in rodent PD-models[205] untill the only clinical study of two patients who, 15 and 18 years after transplantation of fetal cells, show positive clinical improvements in their condition along with abandonment of any pharmacological dopaminergic therapy[206]. Despite this therapeutic promise, the presumed mechanism of action of donor cell populations often remains insufficiently validated and also this approach has a high risk for side-effects specially regarding tumor formation[207]. The second approach involves pharmacological stimulation of endogenous neurogenesis. Since the discovery of the adult neurogenesis, much research effort has been devoted to study its mechanisms and to determine whether they can be pharmacologically modulated or not. Many druggable mechanisms are involved

in the endogenous generation of newborn neurons in the adult brain. The most important ones are followed listed: serotonin and melatonin pathways, Wnt/β-catenin signaling, activation of sigma receptors, nicotinamide phosphoribosyltransferase cascade and activation nuclear erythroid 2-related factor[208].

As it has been explained in detail in the introduction, LRRK2 is implicated in adult neurogenesis at different levels but mainly due to its role in Wnt/β-catenin pathway and, therefore, it may seem possible that the pharmacological inhibition of LRRK2 may have positive effects by activating adult neurogenesis.

2.2. Objectives

The main objective of this chapter is to test the hypothesis if the pharmacological inhibition of LRRK2 has any pro-neurogenic effect using either iPSC-neural derived assays or neurosphere assays. The LRRK2-inhibitor chemolibrary generated previously will be used for those means.

The specific objectives of this chapter are the following (**Figure 39**):

- To screen our LRRK2-inhibitor chemolibrary in Wnt/β-catenin assay using NPC obtained from iPSC of adult healthy volunteers.
- To test if positive hits of the Wnt assay are able to increase the proliferation of neurospheres of the SVZ from adult mice.
- To test if positive hits from the proliferation neurosphere assay are able to induce the differentiation of neurons and oligodendrocytes.

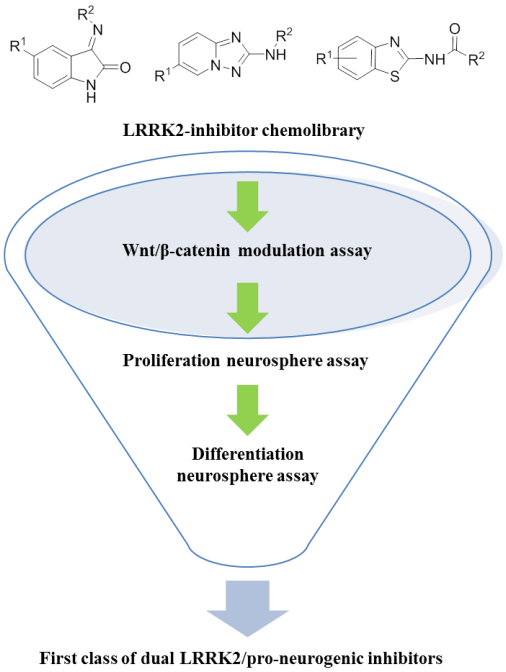

Figure 39. *Workflow of the experiments followed in this chapter.*

2.3. Wnt signaling modulation

2.3.1. Background of the assay employed

Given the dramatic differences between mice and humans, methods that recapitulate paradigms of human brain both in healthy and pathological conditions *in vitro* have an enormous potential for disease modelling and thus drug discovery. In 2006, an outstanding outbreak in science was reported by Takhashi and Yamanaka, who were able to generate human stem-like cells from a somatic cell source and were named as induced-pluripotent stem cells (iPSC)[209]. Therefore, iPSCs can be defined as adult cells genetically reprogrammed to an embryonic stem cell–like state by forcing the expression of genes and factors important for maintaining the defining properties of embryonic stem cells. iPSCs have become a powerful tool for cell modeling of human diseases as patient-derived iPSCs can further be differentiated into specific cell lineages that recapitulate processes of the disease and pathogenesis. The use of these cells has had an extremely high impact in the context of neurological disorders, where access to physiologically active and relevant cell types of the central nervous system for research is very limiting[210]. Patient iPSC–derived neuronal lines now allow for laboratory-grown accurate human neuronal cell models for disease modeling and drug discovery (**Figure 40**)[211].

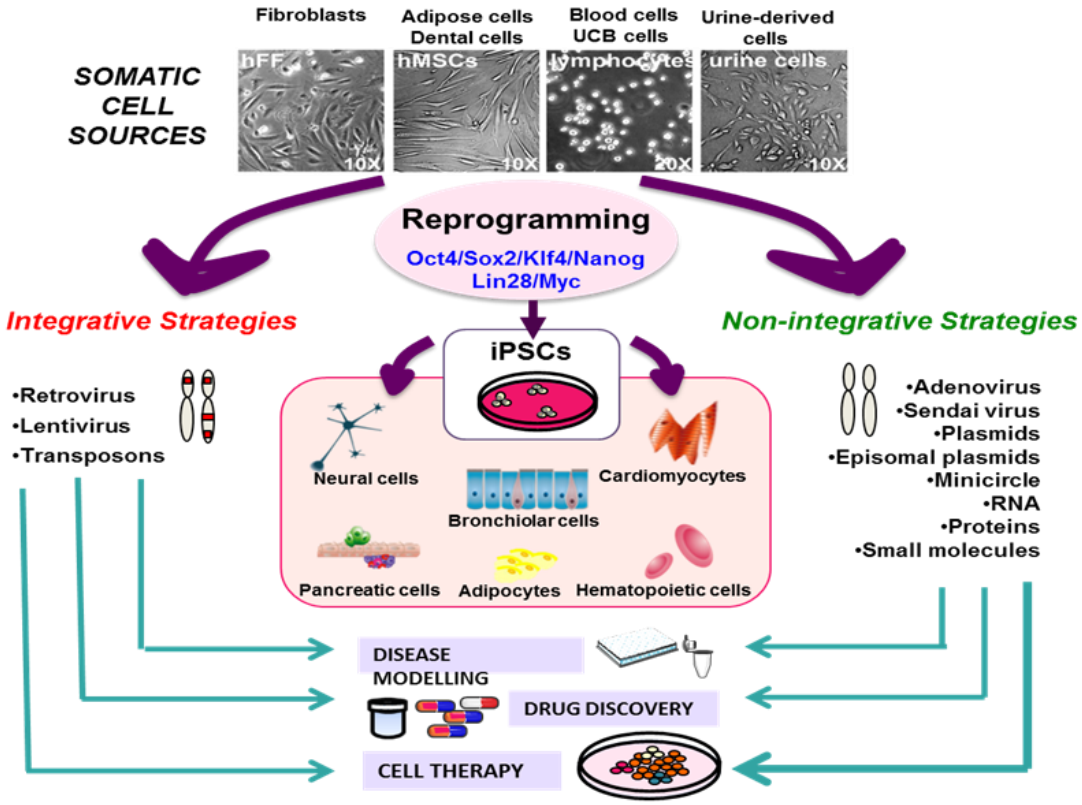

Figure 40. *Schematic representation for the generation and use of iPSCs.*

Along the duration of this work, a 6-month research fellow at the Chemical Neurobiology Laboratory of Dr. Stephen Haggarty at the Massachusetts General Hospital-Harvard University was performed. The main goal of the Haggarty Laboratory is the development of patient iPSC–derived neuronal models that allow the screening of new drugs for neurological disorders. During that time it was possible to evaluate if our LRRK2 inhibitor chemolibrary could modulate Wnt signaling. Potential modulation of Wnt signaling by pharmacological inhibition of LRRK2 was determined in iPSC-derived NPCs from healthy adult volunteers in high-throughput screening way (HTS). The NPC line expressing a TCF/LEF-luciferase reporter that has already been established in the Haggarty Laboratory was used[212].

2.3.2. Results and discussion

- *LRRK2* expression

Before the compounds were tested, the expression of LRRK2 in the cell type of interest was confirmed by quantitative PCR (**Figure 41**).

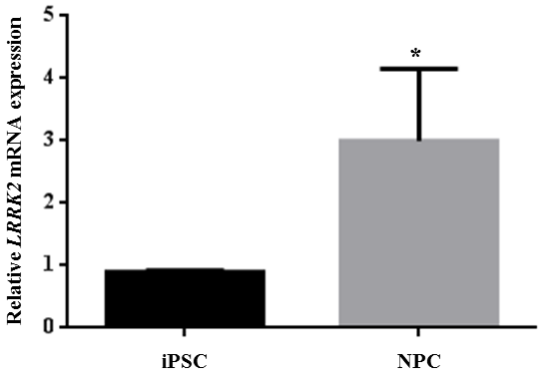

Figure 41. *Quantitative-PCR of LRRK2 expression in iPSC and NPC. Ct values were normalized to iPSC (set to 1) and GAPDH. Bars represent values averages of triplicates ± SD. *p≤ 0.05.*

By this experiment it was possible to confirm that the levels of LRRK2 mRNA in NPC line that will be used for the assay are significantly higher than for iPSC. Therefore, these results suggest that the cell line of interest expresses enough quantity of *LRRK2* gene and thus it is feasible that our inhibitors will bind their target.

- Wnt modulation assay

This assay has been developed in a HTS-manner and thus cells are cultured in 384-well plates which allow the possibility to test a high number of compounds[212]. For this reason all LRRK2 inhibitors from our focused library that showed more than a 50% inhibitory activity were tested. The compounds tested can be classifies in the following categories according to their chemical structure:

- Indolinone derivatives: **21 - 44**.
- Tryazolopyrimidine derivatives: **45 - 49**.
- Benzothiazole derivatives: **56**, **64 - 68**, **71 - 72**, **74 - 75** and **77 - 78**.

CHIR-99021 a known GSK-3β inhibitor and a known positive modulator of Wnt signaling was used as positive control[212].

The NPC line used is a cell line that expresses the luciferase reporter lymphoid enhanced factor/T cell factor (LEF/TCF) which corresponds to one of the endpoints of the Wnt/β-catenin pathway. The LEF/TCF luciferase reporter used contains the firefly luciferase gene under control of tandem repeats of the LEF/TCF. Thus, when the pathway is activated, there is higher luminescence[212]. By these means, luminescence can be used as

read out in order to determine if small molecules cultured with the cells are able or not to positively modulate this pathway (**Figure 42**).

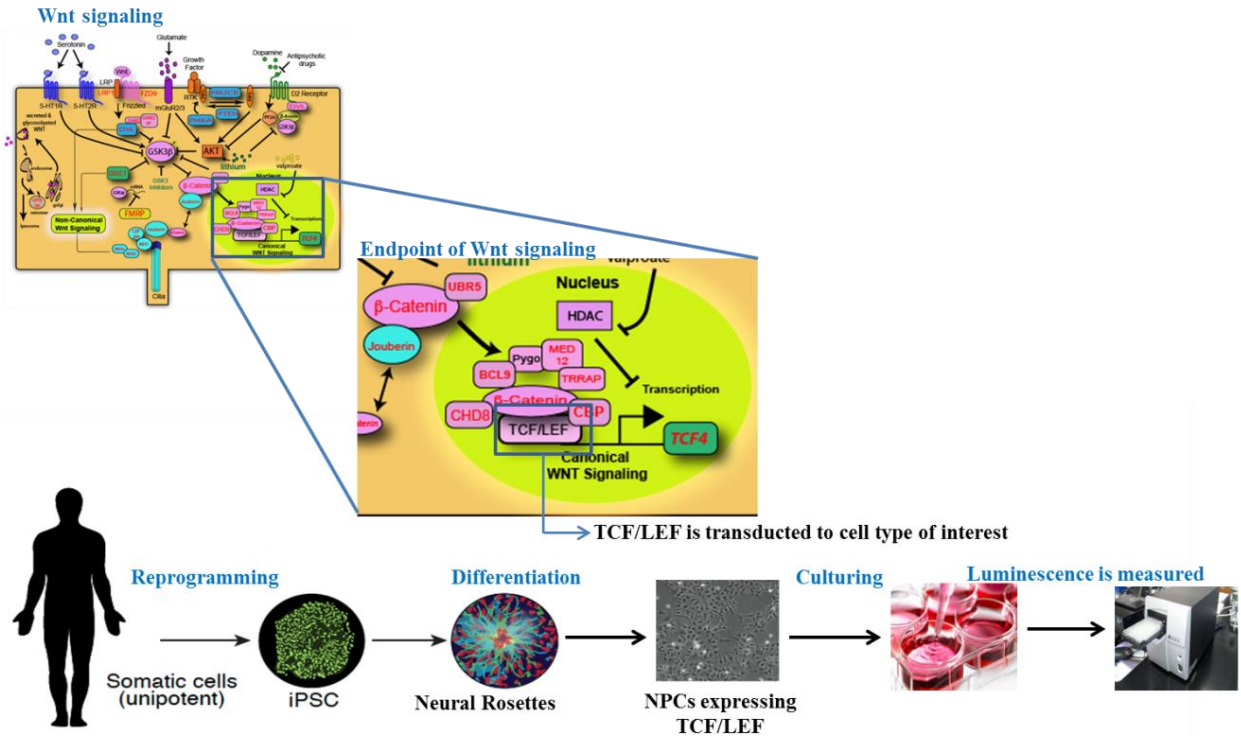

Figure 42. *Schematic representation of the Wnt modulation assay.*

Cells were seeded in 384-well plates at a density of 6000 cells/well and were left overnight in an incubator. The next day cells were treated 24 hours with 10% Wnt3a-conditioned media and the LRRK2 inhibitors at 1 µM and 10 µM. After that time luminescence was measured. Results are expressed in fold increase of TCF/LEF reporter activity of DMSO as the vehicle (**Table 10**).

Table 10. *Wnt signal enhancement expressed as normalized fold change to DMSO.*

Compound	Fold Wnt increase 1µM	Fold Wnt increase 10µM	Compound	Fold Wnt increase 1µM	Fold Wnt increase 10µM
21	0.83	1.11	**42**	1.37	1.70
22	0.66	0.80	**43**	0.85	1.06
23	0.74	0.80	**44**	1.21	2.69
24	0.66	0.92	**45**	1.31	2.23
25	0.72	0.95	**46**	2.14	2.56
26	1.73	1.88	**47**	2.48	2.45
27	0.67	1.06	**48**	2.17	2.56
28	1.10	1.19	**49**	1.76	1.79
29	1.07	1.10	**56**	3.25	2.20
30	0.77	0.92	**64**	0.77	1.04
31	1.10	1.19	**65**	0.83	0.72
32	0.80	0.88	**66**	1.76	1.97
33	0.80	0.83	**67**	0.78	0.83
34	1.28	1.55	**68**	1.58	2.00
35	0.66	0.72	**71**	0.89	1.07
36	0.98	1.10	**72**	1.25	2.00
37	1.73	1.88	**74**	1.19	1.22
38	0.89	0.89	**75**	1.85	2.41
39	1.06	1.42	**77**	1.43	2.29
40	0.77	1.03	**78**	2.00	2.12
41	1.01	1.08	**CHIR-99021**	2.57	11.82

In view of these results, it is feasible to conclude that some of our LRRK2 inhibitors could positively modulate Wnt signaling and the fact that this effect is observed in chemically diverse inhibitors suggests that is indeed LRRK2 inhibition which drives this effect. The fact that this effect does not easily correlate with LRRK2 enzymatic activity does not have a straight forward explanation. A possible explanation could be related to the different physicochemical properties of the compounds and thus to cell penetration.

Compounds **44**, **45**, **47**, **56**, **68**, **72**, **77** and **78** that show more than two fold change in Wnt activity were selected to perform dosage-curves starting at 0.01 µM and finishing at 20.00 µM to confirm that the effect was dose-dependent. The assay was performed in the same way as before but this time serial dilutions of the compounds were used and each concentration of each compound was repeated eight times. Results are expressed in average

fold increase of TCF/LEF reporter activity of DMSO ± SD and plotted in dose-dependent curves. As previously, CHIR-99021 was used as positive control (**Figure 43**).

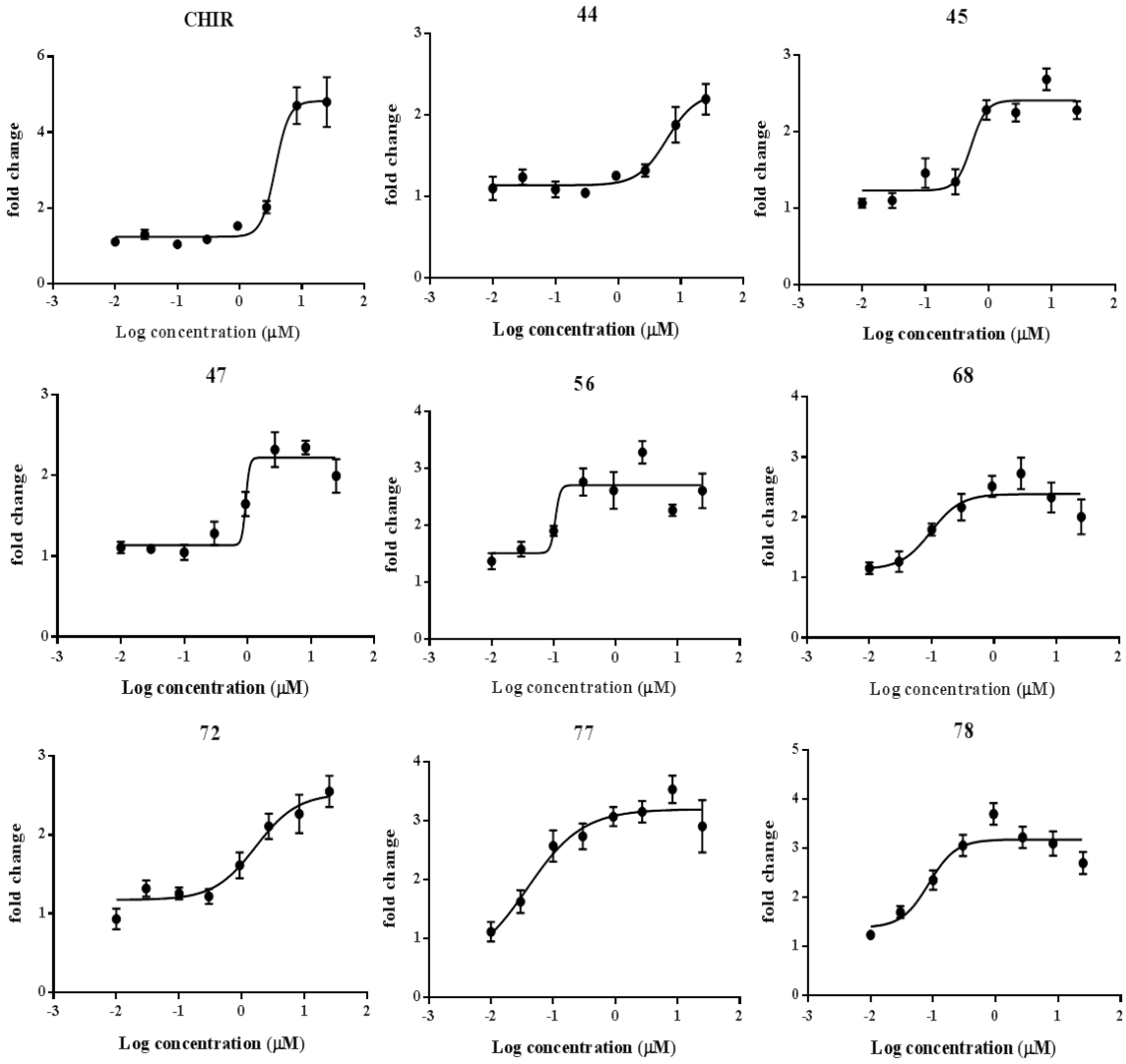

Figure 43. *Dose-dependent curves of Wnt modulation (y axis represents fold change and x axis compound concentration) of compounds* ***44***, ***45***, ***47***, ***56***, ***68***, ***72***, ***77***, ***78***, *and CHIR as positive control.*

With these experiments it is possible to observe a clear correlation between the concentration of the compound and the fold-change observed in Wnt activity. In these chemically diverse compounds a modest increase of Wnt signaling was observed, showing that cellular modulation of LRRK2 produced a dose-dependent increase of Wnt/β-catenin signaling. The fact that this effect is maintained in the three families of compounds may enhance the idea that indeed is LRRK2 inhibition the driving cause of this effect.

2.4. Neurosphere proliferation assay

2.4.1. Background of the assay employed

NSCs present in the SVZ and SGZ in the adult mammalian brain continuously generate new neurons that are functionally integrated into neural circuits[72]. These areas of continuous neurogenesis harbor stem cells that retain the capacity to proliferate, self-renew over an extended period of time, and differentiate into the three primary cell types of the brain (neurons, astrocytes and oligodendrocytes)[213].

In 1992, Reynolds and Weiss first cultured cells that exhibit stem cell properties as free-floating spheres, called neurospheres, from the adult brain of mice. They dissected striatal tissue, which included the SVZ, enzymatically dissociated the tissue to single cells and plated them in non-adherent conditions in serum-free medium in the presence of epidermal growth factor (EGF). A small population of cells began to divide, initially adhering to the plate, and after a few days detaching and forming spheres of proliferating cells[214].

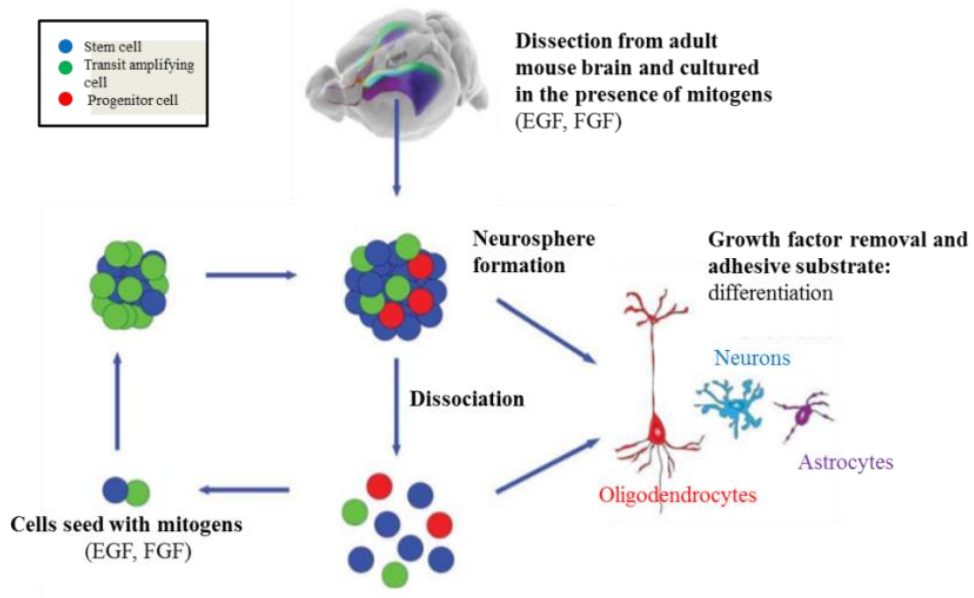

Figure 44. *Schematic representation of the neurosphere assay.*

Since these early experiments, the neurosphere assay has evolved[215]. It is now accepted that to demonstrate multipotency, individual neurospheres must give rise to neurons, astrocytes and oligodendrocytes upon withdrawal of growth factors. In addition, although at first neurospheres were considered to be a homogeneous population, it is now

clear that individual neurospheres contain NSCs, neural progenitor cells (NPCs) and differentiated cells in different phases of the cell cycle arranged in a three-dimensional complex organized by the extracellular matrix[213]. Therefore, the neurosphere assay is now commonly used to test self-renewal, survival or proliferation and differentiation upon different conditions (**Figure 44**).

However, some limitations of this assay need to be taken into consideration. One of the most important concepts in this assay is that each sphere is derived from a single cell and is therefore clonal. Cell density has a critical impact on clonalty. It has been stablished by several groups that platting the cells at a single cell status anywhere between 0.2 to 20 cells per µl is considered appropriate for clonal conditions of growth[216, 217]. Higher densities lead to fusion of the spheres and therefore it is impossible to consider that each spheres emerged from the same single cell. Furthermore, movement of the plate also leads to the fusion of the spheres in the center of the plate[218]. As such, true clonalty can only be guaranteed by plating single cells per well within the established range and without any movement[215].

Sphere-size is the measurement most commonly used as read out of proliferation as smaller spheres could be a result of decreased self-renewal, or altered responsiveness to growth factors. However, significant heterogeneity exists in the size of individual spheres, independent of the problem of merging. Some authors, believe that NSCs are believed to give rise to large spheres, and NPCs to smaller spheres[213]. Therefore, there is a criterion regarding what sized spheres to quantify, which typically ranges from 40 - 150 µm in diameter, in order to include both cell-populations.

2.4.2. Results and discussion

- LRRK2 expression

Although LRRK2 expression has been described in different brain regions such as cortex, *substantia nigra*, caudate putamen, olfactory bulb and hippocampus, among others[219], it has been poorly described in neurogenic niches[220]. To clarify which cells of the SVZ niche of the adult brain could express LRRK2, immunohistochemical analysis in 2.5 months olds mice brain coronal sections were performed. Within the SVZ, it is possible to

observe two populations of cells: glial fibrillary acidic protein (GFAP)-positive type B cells also known as NSCs and neuroblasts posisitve double cortin (Dcx) or type A cells[221].

LRRK2 is clearly expressed in most of the NSCs or type B cells with radial-like morphology expressing GFAP and Sox2 (**Figure 45**) while only a subpopulation of neuroblasts or type A cells, doublecortin (Dcx) positive cells expresses LRRK2. These results suggest a possible involvement of this kinase in the control of the neurogenic process in the VZ neurogenic niche and thus neurospheres isolated from the SVZ are useful to test LRRK2 inhibitors.

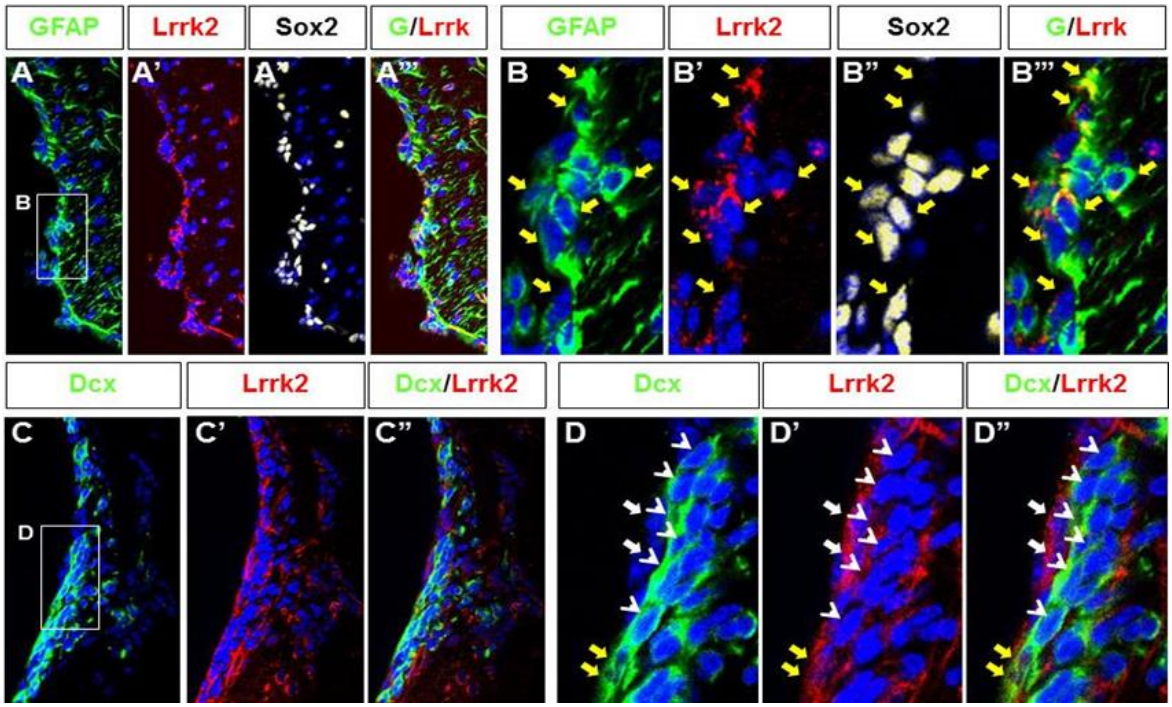

***Figure 45. A/B**-Coronal sections of a 2.5 months old brain mouse showing expression of GFAP (green) and Sox2 (white) in radial glia-like NSCs in the SVZ of the lateral ventricles. The majority of those cells coexpress LRRK2 (red, yellow arrows). **C/ D**-Similar sections showing Dcx expression (green cells, arrowheads) in neuroblasts cells. LRRK2 is expressed in the same neurogenic area (red cells, white arrows) but only in few neuroblasts is coexpressed with Dcx (yellow arrows). The nuclei are stained with bisbenzimide (blue) in all the panels.*

- Compound selection

The eight chemically diverse LRRK2 inhibitors that showed good correlation in dose-response curves in the previous Wnt modulation assay were selected. This group of compounds includes:

- Indolinone derivative: **44**
- Triazolo-pyrimidine derivatives: **45** and **47**

- Benzothiazole derivatives: **56**, **68**, **72**, **77** and **78**.

The commercial LRRK2 inhibitor **19** (PF-06447475) which has a pyrrolopyrimidine-benzonitrile scaffold was also used.

- Proliferation assay

First of all, SVZ neurospheres were prepared from young adult (6 weeks old) C57BL/6 mice and induced to proliferate using established passaging methods to achieve optimal cellular expansion according to published protocols[222]. Cells were plated in 96-well plates at a density of 5000 cells per cm^2. The question asked with these experiments was whether the addition of these chemically diverse LRRK2 inhibitors impacted the formation of neurospheres by increasing the proliferation rate after the dissociated NSCs and NPCs grown for 4 days in the presence of mitogens (fibroblast growth factor (FGF) and EGF). Compounds were used at 1 and 5 µM. As it has been already explained in detail, the size of the neurosphere can be used as an indirect read out of cell proliferation. Therefore, on the 4th day of culture, photographs were taken by bright field microscopy using an automatic platten, taken 6 pictures of different areas of each well with the 10X objective. The area of neurospheres bigger than 400 μm^2 cell area was measured using a macro software for Image J, (NIH, Bethesda, MD) designed at the Cajal Institute-CSIC particularly for this assay. Quantitative analyses were carried out in three separate experiments, calculating the mean ± SEM and using a two-tailed Student's *t*-test to determine statistically relevant changes.

As shown in Figure 46, the size of neurospheres (estimated as total area of the neurospheres) was higher in those cultures treated with the selected small molecules, **44, 45**, **47**, **56**, **68**, **72**, **77**, **78** and commercial LRRK2 inhibitor **19** compared to controls treated with DMSO. Only in compound **68** there is a tendency to increase in the neurosphere size compared to DMSO but it did not reach statistical significance.

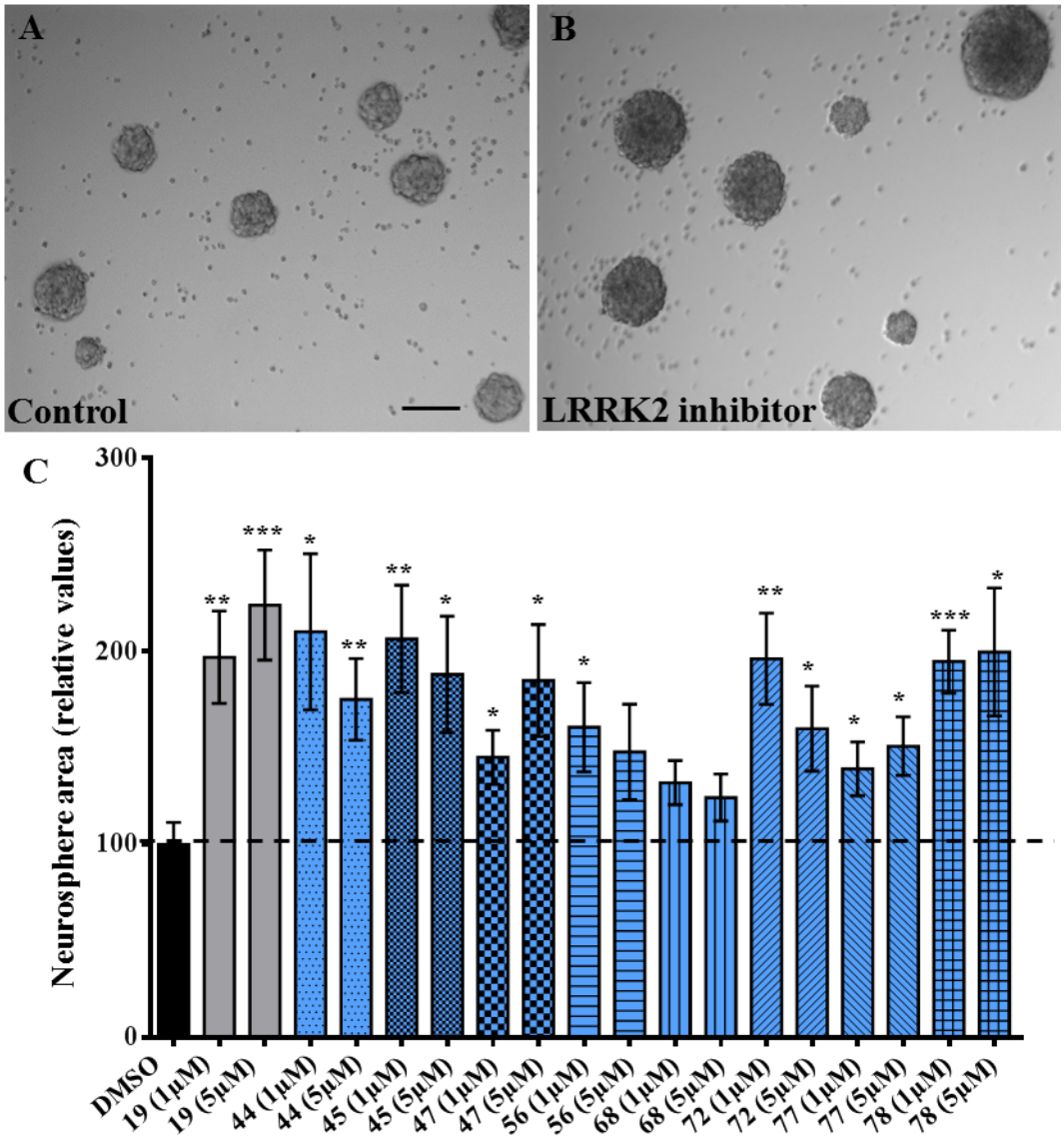

Figure 46. A/B- *Representative bright field micrographs showing the size of primary neurospheres after 3 days in culture in the presence of DMSO as a control (**A**) or LRRK2 inhibitor **78** (**B**). **C-** Quantitative analysis of the neurospheres in culture. The total neurosphere area was measured in each field using an especially designed macro for IMAGE J. Results are mean values ± standard error of the mean (SEM), represented as relatives to control value (=100), of 6 different fields each one from triplicates and from three independent experiments. *p≤0.05; **p≤0.005, ***p≤0.0005.*

This increase in the total area of the formed neurospheres could be related to an increase in the size of individual neurospheres due to an increase in proliferation or to an increase in the number of neurospheres caused by an increase in the number of cells with the ability to form neurospheres. Thus, the inhibition of LRRK2, using chemically diverse inhbitors, promotes the proliferation of NSCs and NPCs from adult SVZ grown as neurospheres.

2.5. Neurosphere differentiation assay

2.5.1. Background of the assay employed

It has been reported that upon mitogen withdrawal, NSC and NPC in neurospheres cultures are able to differentiate into the three primary cell types of the brain (neurons, astrocytes and oligodendrocytes)[213]. With the aim of finding disease-modifying drugs for neurodegenerative diseases as neurogenic probes, it is of crucial importance that these agents not only increase the proliferation rate of NSCs and NPCs in the SVZ niche but also influence in the differentiation of these pluripotent cells to generate mature neurons or oligodendrocytes that could migrate to functioning brain structures in order to compensate the ones that are dying as the disease develops[203]. Therefore, it is important to find *in vitro* compounds that are able to change the differentiation fate of neurospheres towards neuronal and/or oligodendrocitic destinies.

2.5.2. Results and discussion

- Compound selection

For these experiments the most active compounds from the previous proliferation assay were selected:

- Indolinone derivative: **44**
- Triazolo-pyrimidine derivative: **45**
- Benzothiazole derivatives: **56**, **72** and **78**.

In addition, commercial LRRK2 inhibitor **19**, was also used.

- Differentiation assay

Neurospheres were cultured for 6 days with the compounds at a concentration of 1μM without mitogens. On the 7th day cells were fixed and immuno-stained using β3-tubulin as a neuronal marker, CNPase as an oligodendrocytic marker, GFAP for astrocytes and Dapi for nuclei. Images were taken by confocal microscopy and the number of positive cells for each marker was counted. The addition of chemically diverse LRRK2 increases the number of differentiated CNPase positive oligodendrocytes (images of inhibitor **45** are

shown as representative example) (**Figure 47**). Quantification was done by calculating relative values for CNPase posite cells and total number of cells (**Figure 48**).

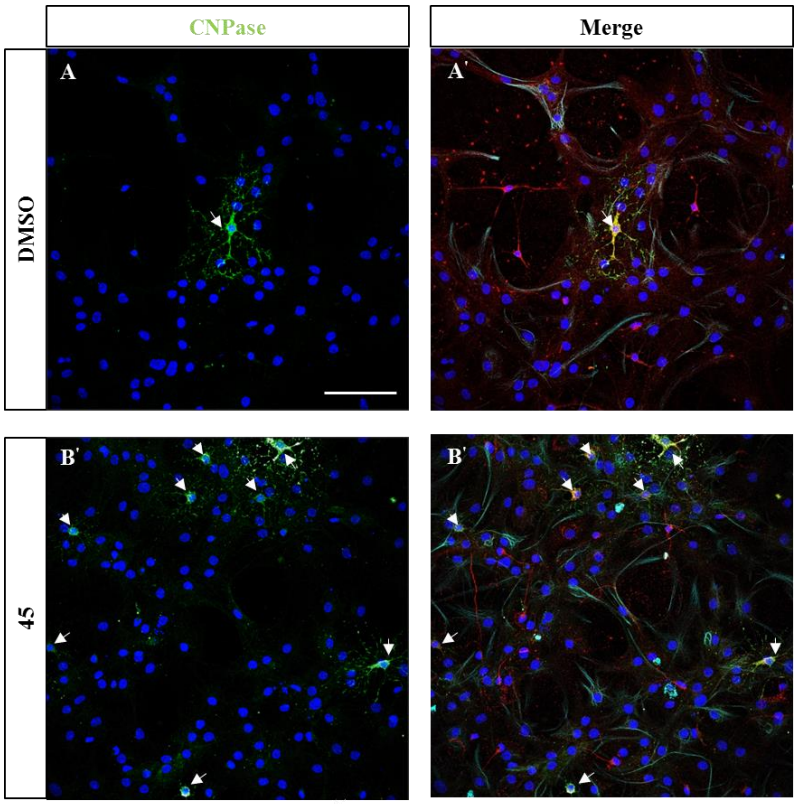

Figure 47. AA´/BB´- *Dissociated cells from adult SVZ neurospheres grown for 7 days without mitogens in the presence of control (DMSO; **AA´**) or a LRRK2 inhibitor (**BB´**). Representative inmunofluorescent field of oligodendrocytes expressing CNPase (green).The nuclei are stained with bisbenzimide (blue) in all the panels. Bar in A :50 µm.*

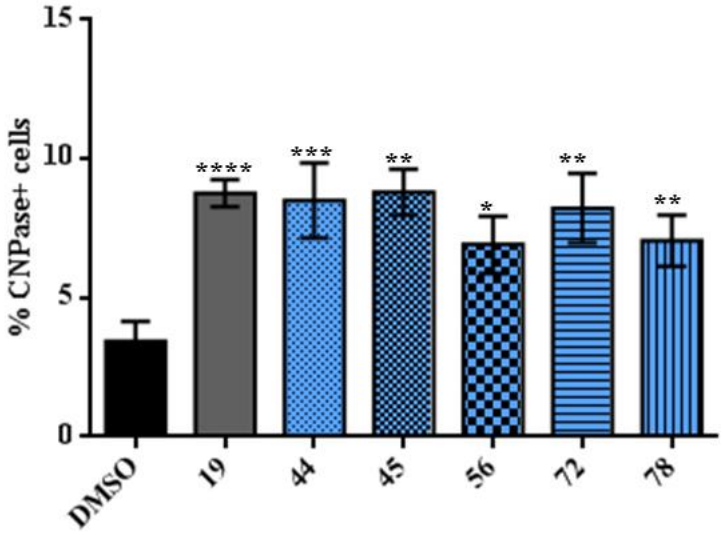

Figure 48. *Differentiation towards oligodendrocytes: quantification analysis of the differentiated cells in culture. Results are mean value ± SEM, represented as relatives to control value (=100), of 4 different fields each one from triplicates and from three independent experiments. *p<0.05,**p<0.005, ***p<0.0005, ****p<0.00005.*

In the case of neurons although there is a constant tendency to increase the number of positive cells compared to control (images of inhibitor **45** are shown as an example (**Figure 49**) only compounds **45** and **19** reached statistical significance (**Figure 50**).

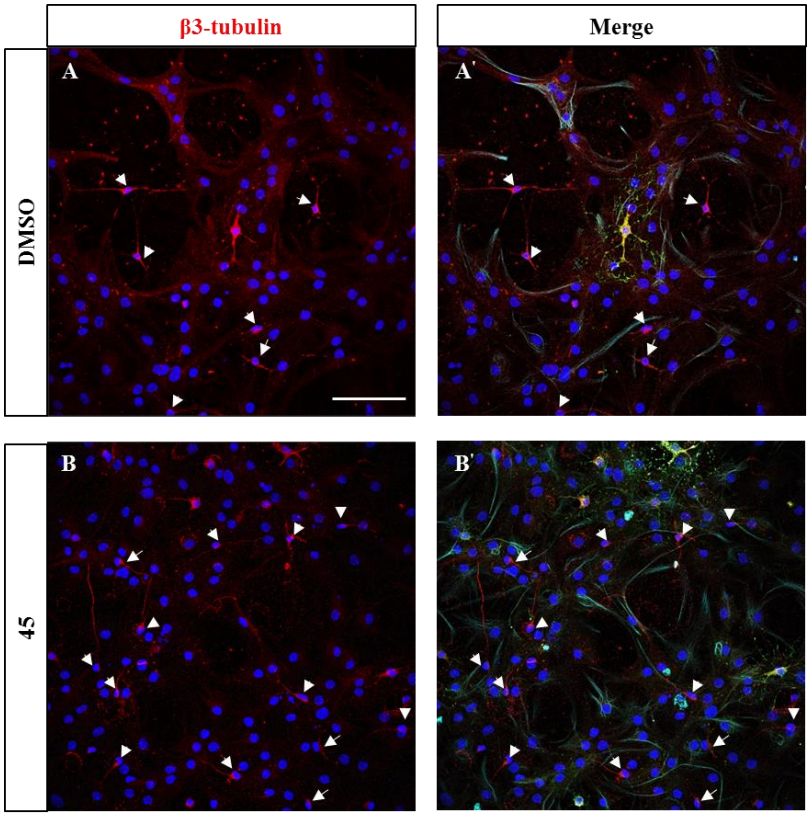

Figure 49. AA´/BB´- *Dissociated cells from adult SVZ neurospheres grown for 7 days without mitogens in the presence of control (DMSO; **AA´**) or a LRRK2 inhibitor (**45**, (**BB´**). Representative inmunofluorescent field micrographs of neurons expressing beta3-tubulin (red).The nuclei are stained with bisbenzimide (blue) in all the panels. Bar in A : 50 µm*

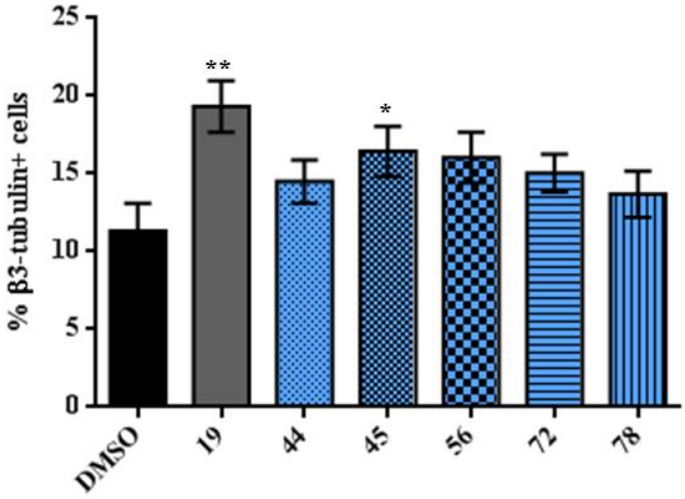

Figure 50. *Differentiation towards neurons: quantification analysis of the differentiated cells in culture. Results are mean value ± SEM, represented as relatives to control value (=100), of 4 different fields each one from triplicates and from three independent experiments. *p<0.05,**p<0.005, ***p<0.0005, ****p<0.00005.*

However, the number of differentiated astrocytes did not change in the LRRK2 inhibitor-treated cells (**Figures 51 - 52**).

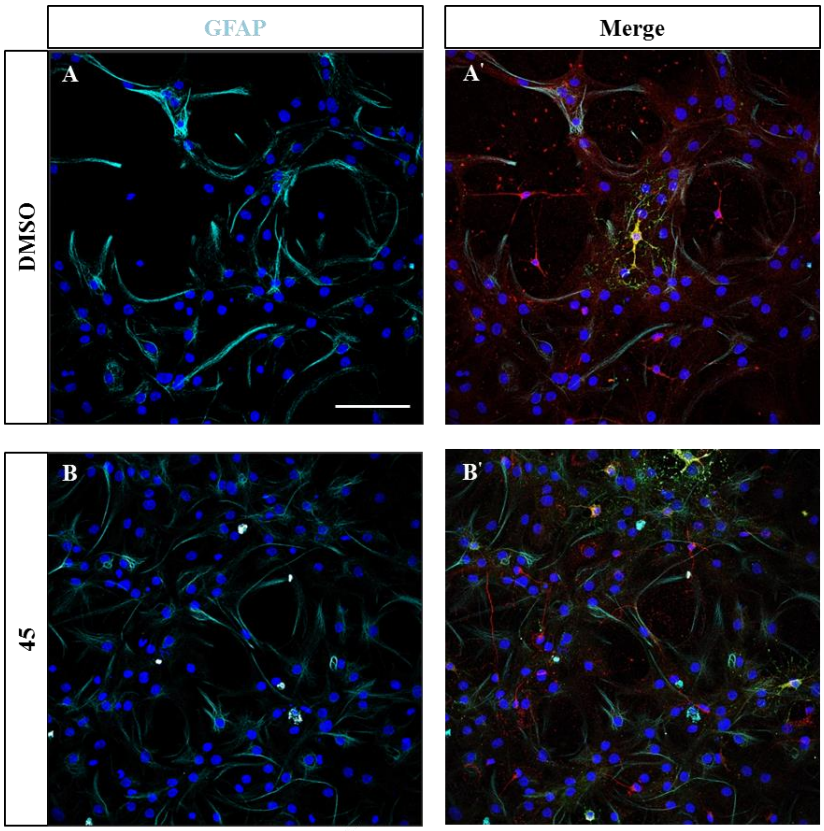

Figure 51. AA´/BB´- *Dissociated cells from adult SVZ neurospheres grown for 7 days without mitogens in the presence of control (DMSO;* ***AA´****) or a LRRK2 inhibitor (****45****, (****BB´****). Representative inmunofluorescent field micrographs of astrocytes GFAP (cyan).The nuclei are stained with bisbenzimide (blue) in all the panels. Bar in A : 50 µm*

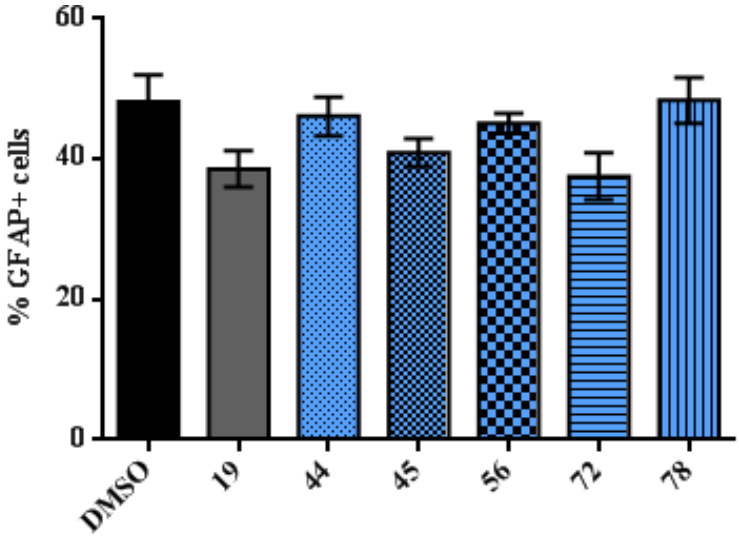

Figure 52. *Differentiation towards astrocytes: quantification analysis of the differentiated cells in culture. Results are mean value ± SEM, represented as relatives to control value (=100), of 4 different fields each one from triplicates and from three independent experiments. *p<0.05,**p<0.005, ***p<0.0005, ****p<0.00005.*

These results suggest that LRRK2 inhibition has the potential to drive differentiation of neural stem cells toward neuronal and oligodendrocytic cell fates. These last set of experiments (proliferation and differentiation) showed for the first time a class of dual LRRK2/pro-neurogenic inhibitors.

2.6. Conclusions

In this present chapter the hypothesis that LRRK2 inhibition may promote adult neurogenesis is addressed. First of all, using an HTS assay it was possible to determine if the LRRK2-inhibitor chemolibrary generated could modulate Wnt signiling. Eight hits from the three chemical families: indolinone derivatives, triazolo-pyrimidine derivatives and benzothiazole derivatives were found that then, were evaluated in a dose-dependent manner. The activation of Wnt/β-catenin cascade is modest but is maintained by chemically diverse LRRK2 inhibitors. This fact suggests that, LRRK2 inhibition is indeed the cause of the activation of this pathway.

These eight LRRK2-inhibitors were then evaluated in a proliferation assay of neurospheres prepared from the SVZ of adult mice. Using the size of the neurosphere measured as total area of the sphere as a read out of proliferation, it was found that LRRK2 inhibition by chemically-diverse inhibitors promoted the proliferation of NSCs and NPCs.

Finally differentiation experiments were carried out in which it was possible to determine that upon the addition of a LRRK2 inhibitor the number of neurons and olygodendrocytes increases whereas the number of astrocytes remains constant. These results suggest that LRRK2 inhibition has the potential to drive differentiation of neural stem cells toward neuronal and oligodendrocytic cell fates.

Taking in consideration all of these findings and bearing in mind that in all of the different assays chemically diverse LRRK2 inhibitors have shown similar effects, which suggests that is indeed LRRK2 the driving cause. The results here reported may open a new field for the clinical application of LRRK2 inhibitors. From what it can be seen in these experiments, the pharmacological inhibition of LRRK2 has the potential to activate Wnt-signaling, promote the proliferation of NSCs and NPCs and drive the differentiation towards neuronal and oligodendrocytic cell fates. This is of crucial importance in the neurodegeneration field as these inhibitors may act as multifactorial drugs that in one hand

they reduce the direct effect that LRRK2 overexpression has and on the other they promote adult neurogenesis. Last but not least, the fact that chemically diverse LRRK2 inhibitors are able to promote the differentiation towards oligodendrocytes opens the venue for the application of these inhibitors in multiple sclerosis or other demyelinating diseases in which oligodendrocyte cell-death is one of the features of the pathology.

3. LRRK2 inhibitors as anti phospho-tau agents

3.1. Introduction

There is a renewed interest in tau protein in the neurodegeneration field. This burgeoning interest can be explained mainly by two reasons. Firstly, the fact that most amyloid centered therapies for AD and related disorders have failed and secondly new facets of tau pathology have been discovered[223]. These new discoveries are of significance importance: it is now known that, PTMs such us acetylation, glycosylation, phosphorylation and truncation are key in the aggregation of tau[224]. Furthermore, the discovery of families with highly penetrant, dominant mutations within the tau gene have shown that tau dysfunction including its alternative splicing is sufficient to cause neurodegeneration and clinical dementia[225]. And finally, all the research that is being done at the moment to study the propagation of tau, which has emerged in the "prion-like" hypothesis[226], in which tau is believed to propagate from cell to cell through anatomically connected brain regions[227]. Thus, focusing on tau as a drug target can have a profound bearing on disease-modification for several neurodegenerative conditions facing our ageing society today.

Among others biological activities of LRRK2, it may play an important role in the phosphorylation of tau. Therefore, to determine if LRRK2 inhibitors are able to reduce tau phosphorylation could be a very interesting therapeutic strategy, as these inhibitors could behave as multi-target drugs addressing two important pathological pathways in neurodegeneration: neuroinflammation and tau hyper-phosphorylation.

3.2. Objectives

The main aim of this chapter is to test our hypothesis: pharmacological inhibition of LRRK2 has effect in decreasing tau phosphorylation. Different cellular and *in vivo* assays together with the LRRK2-inhibitor chemolibrary generated previously will be used.

The specific objectives of this chapter are the following (**Figure 53**):

- To screen our LRRK2-inhibitor chemolibrary in tau-neuroprotective assay using a human neuroblastoma cell line (SH-SY5Y).
- To test if positive hits of the tau-neuroprotective assay are able to decrease tau phosphorylation detected by immucytochemistry using Ngn2-transfected-A152T-derived neurons from iPSCs of a patient carrying the MAPT2 mutation A152T.
- To test if positive hits from the previous assay are able to reduce tau phosphorylation detected by Western Blot in 6-weeks-differentiated-A152T-derived neurons obtained from the same iPSC of the patient carrying the MAPT2 mutation A152T.
- To confirm the efficacy of some positive hits in two different *in vivo* models of tauopathy.

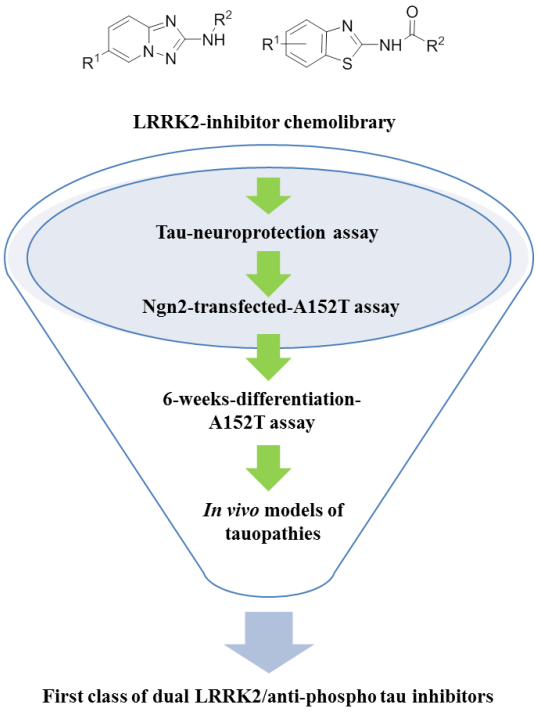

Figure 53. *Workflow of the experiments followed in this chapter.*

3.3. Tau-neuroprotection assay

3.3.1. Validation of the assay

The methodology chosen to test the influence of LRRK2 inhibitors on tau pathology was reverse chemical genetic approach. The first step in this process was already done as a subset of small molecules with LRRK2 inhibition properties has been synthesized. The second step involved the development of a cellular assay in which a phenotypic change could easily be detected.

Different tau-hyperphosphorylation cellular assays have been developed and there are different commercial kits. Recently, okadaic acid (OA)-induced tau hyperphosphorylation model has been successfully established in different cell lines and primary neuronal cultures due to its characteristic of rapid time and dose-dependent action[228]. OA is a monocarboxylic acid isolated from the sponge *Halichondria*[229]. OA is a protein phosphatase 2A (PP2A) inhibitor that has been proved to induce tau protein hyperphosphorylation, microtubules instability and neuronal cell death[230, 231]. With OA stimulation, many AD-related tau epitopes were hyperphosphorylated, which results in further microtubules instability and neuronal cell death[230, 232]. For these reasons, the OA-induced tau hyperphosphorylation cellular model was selected to test the neuroprotective effects of our compounds. The human neuroblastoma cell line SH-SY5Y was used for these means. The potential neuroprotective effect of our inhibitors will be determined by an increase in cell viability after drug treatment measured by the 3-(4,5-dimethylthiazol-2yl)-2,5-diphenyltrtrazolium bromide (MTT) assay.

The first step was to determine which concentration of OA is needed to cause statistical significant differences in the viability of control cells and OA-treated cells. Therefore, cells were seeded in 96-well plates and were grown for 24 hours. After that time cells were treated for another 24 hours with OA at 20, 30, 40 and 50 nM and each condition was repeated five times. On the next day viability was measured by the MTT assay. Results are expressed as relative percentages to the mean value of control cells in Figure 54.

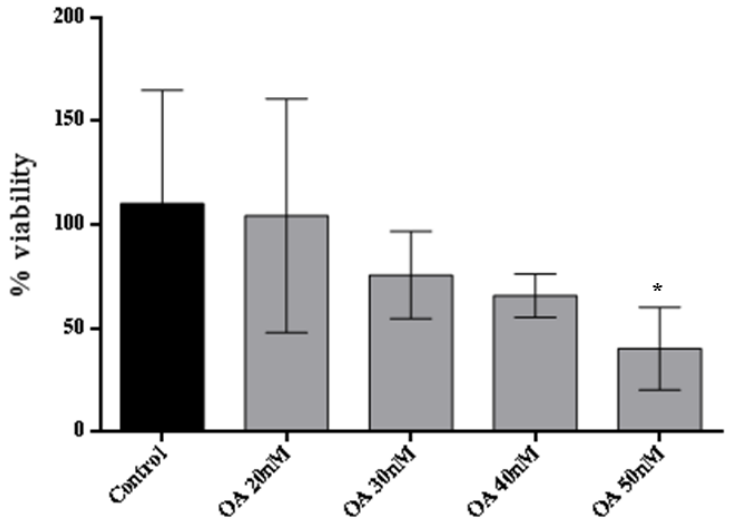

Figure 54. *Results of tau neuroprotection assay. Bars represent Mean values ± standard deviations (SD).*p<0.05.*

With these results it becomes clear that a concentration of OA of 20 nM is not enough to cause neuronal death and the percentages of viability for 30 nM and 40 nM are similar. Therefore, concentrations of 30 nM and 50 nM were selected in the next step. In that case, a reference compound with a well-known anti-phospho activity was added to the cell culture to observe a neuroprotective activity and to be used as a control. The ATP non-competitive GSK-3β inhibitor TDZD8[233] was selected. The experiments were performed exploring three different concentrations of TDZD8 (1, 5 and 10 μM) in two different conditions of OA toxicity. Results are depicted in Figure 55.

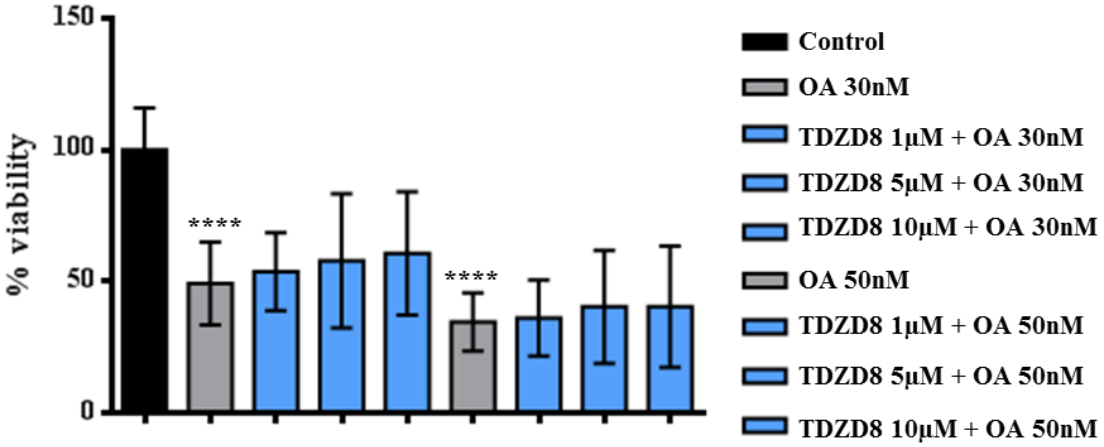

Figure 55. *Results of tau neuroprotection assay. Bars represent Mean values ±SD ****p<0.00005.*

It becomes evident that 50 nM is too toxic for the cells and no neuroprotective effect is observed with the standard reference treatment. However, when 30 nM is used a neuroprotective effect is observed with TDZD8 in a dose-dependent fashion. As it was observed that during the 24 hours in which the cells are growing before compound treatment the level of growth was slightly different even though the cells are seeded at the same density, the time of the cell culture was increased in a way of trying to achieve homogeneity. After 48 hours before treatment with OA, cells were incubated with TDZD8 at different concentrations for 1 hour and then with OA at 30 nM for another 24 hours. Following these conditions three independent experiments were performed (**Figure 56**).

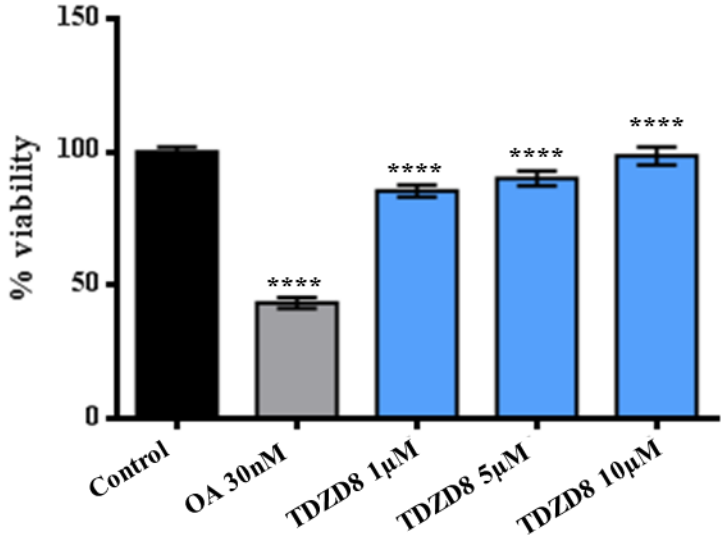

Figure 56. *Global statistical analysis. Bars represent Mean values (of 3 independent experiments) ±SEM,****p<0.00005.*

With these conditions, it was possible to develop a robust enough assay that can be used to test the LRRK2-inhibitor chemolibrary. The conclusions reached in order to have a replicative assay are the following:

- Cells should be seeded for 48 hours in 96 well-plates, after that time cells are pre-incubated with the compounds for 1 hour and then incubated for another 24 hours with OA at a concentration of 30 nM. The next day the MTT assay is performed.
- TDZD8 at a concentration of 10 µM will always be used as a positive control. In order to consider the assay as valid, statistical significant differences must be found between the control cells and the cells treated with OA at 30 nM and between cells treated with OA and 30 nM and TDZD8 at 10 µM.

- Three independent biological replicates will be performed for each compound and only the global statistical analysis will be reported.

3.3.2. Tau neuroprotection assay for triazolo-pyrimidine and benzothiazole LRRK2 inhibitors.

Three different chemical scaffolds of LRRK2 inhibitors have been evaluated in this tau-neuroprotective assay. Triazolo-pyrimidine derivatives and benzothiazole derivatives that showed more than 50% inhibition will be used. This group of compounds includes the following:

- Triazolo-pyrimidine derivatives: **45 - 49**
- Benzothiazole derivatives: **56**, **64 - 68**, **71 - 72**, **74 - 75** and **77-78**.
- The commercial LRRK2 inhibitor **19** (PF-06447475) which has a pyrrolopyrimidine-benzonitrile scaffold.

The assay was performed following the previously stablished guidelines and each compound was tested at 1, 5 and 10 µM except for the case of **19** that due to its high IC_{50} (3 nM in the wt form and 11 nM in the mutant one) was tested at 0.1, 1 and 5 µM. Results are depicted in Figures 57-59 and show a consistent neuroprotective profile for all the compounds assayed.

With these experiments it becomes clear that neuroprotective effect is observed in all of the LRRK2-inhitors tested when OA is used as a neurotoxic agent. In compounds **46**, **47**, **49** and **64** there is a clear correlation between the dose and the effect observed. In an attempt of determining if the mechanism of this neuroprotective effect is directly related to a decrease in tau phosphorylation, these compounds were tested again in different cellular models.

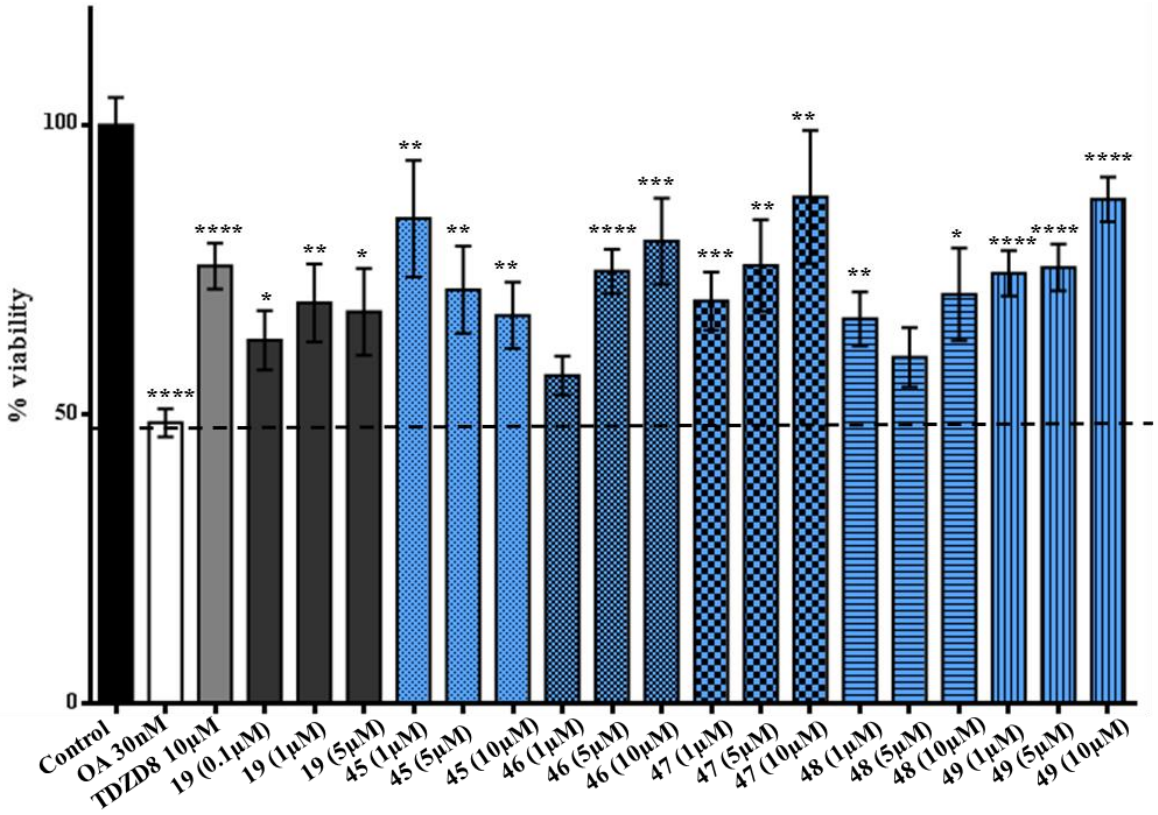

Figure 57. *Tau neuroprective assay for compounds* ***19, 45 - 49.*** *Bars represent Mean values (of 5 independent experiments) ±SEM,*p<0.05, **p<0.005, ***p<0.0005, ****p<0.00005.*

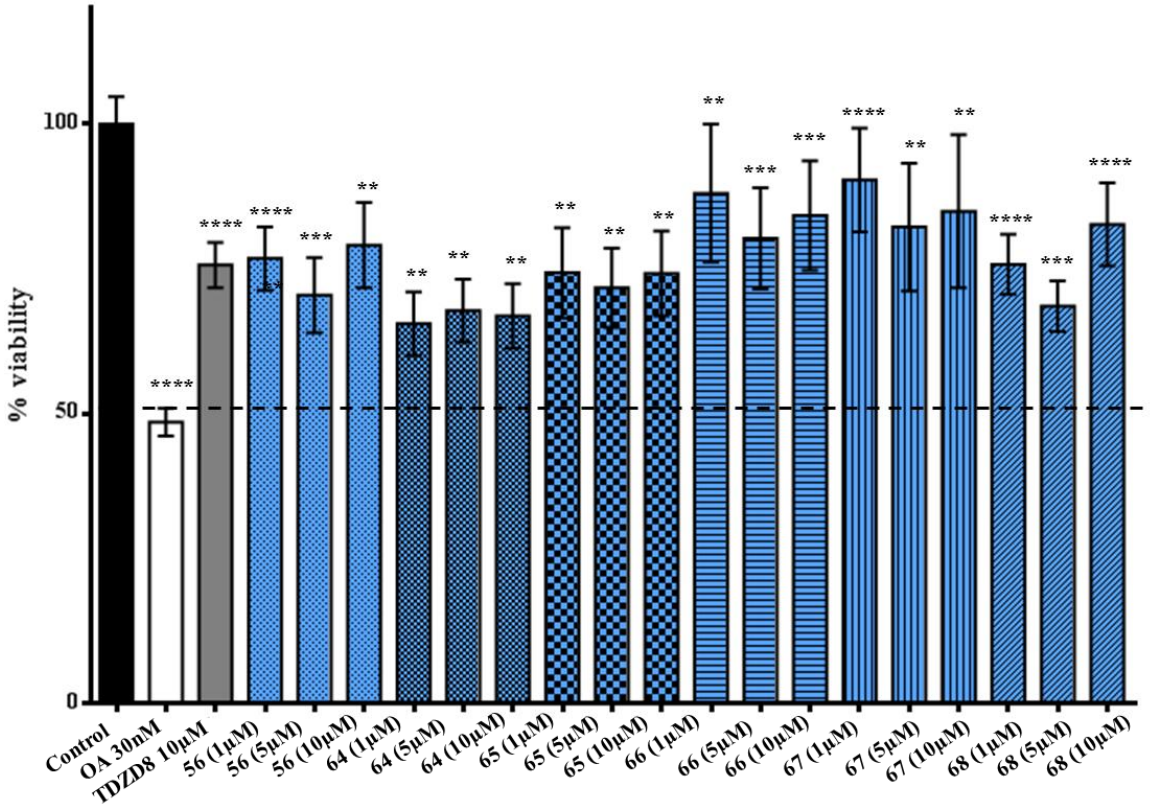

Figure 58. *Tau neuroprective assay for compounds* ***56, 64 - 68.*** *Bars represent Mean values (of 5 independent experiments) ±SEM,*p<0.05, **p<0.005, ***p<0.0005, ****p<0.00005.*

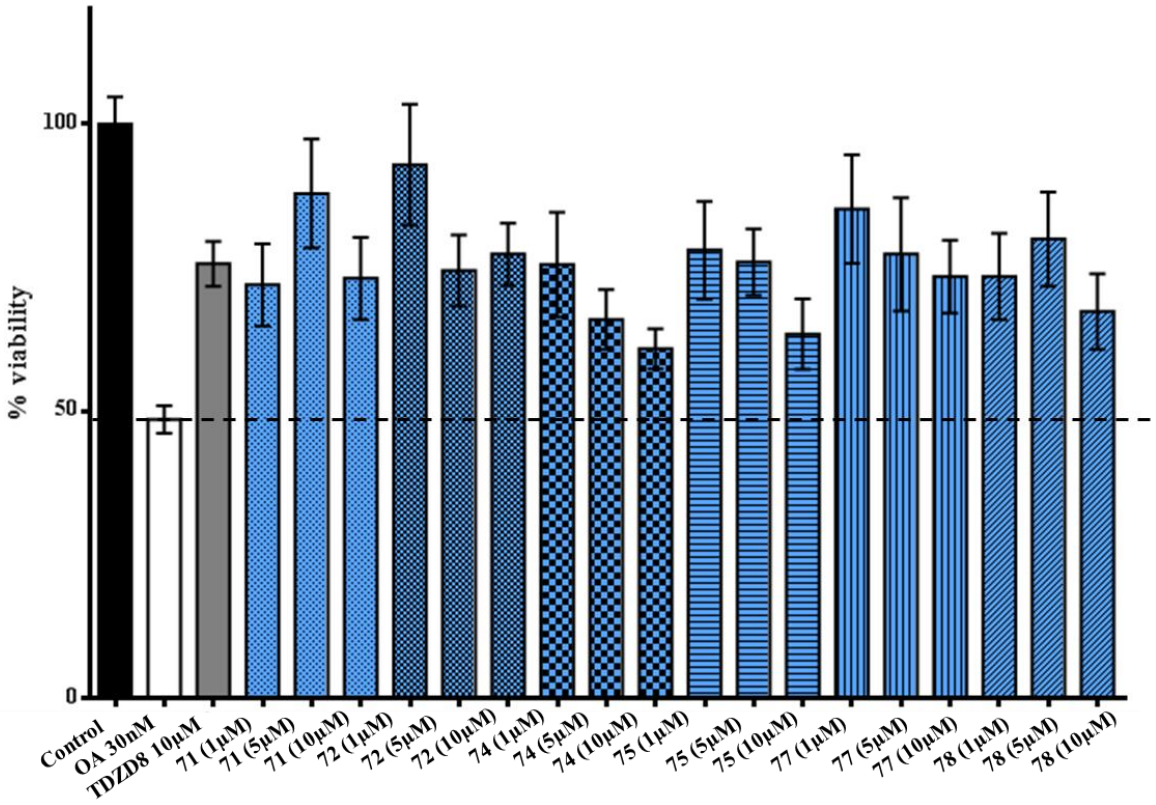

Figure 59. *Tau neuroprective assay for compounds* ***71 - 72, 74 - 75, 77 - 78.*** *Bars represent Mean values (of 5 independent experiments) ±SEM,*p<0.05, **p<0.005, ***p<0.0005, ****p<0.00005.*

3.4. Ngn2-transfected-A152T-derived neurons assay

3.4.1. Background of the assay employed

IPSC-derived neuronal models are very useful for drug discovery and several strategies have been applied to provide efficient platforms for drug screening. One of this, is the use of a doxycycline-inducible Neurogenin 2 (Ngn2) expression cassette that is stably incorporated into NPC to generate in a rapidly and efficiently manner. In this Ngn2 cassette, the gene for puromycin resistance is also incorporated to select the cells in which transfections have succeeded. Ngn2 is a transcription factor that belongs to the family of neurogenenins that are basic-helix-loop-helix transcription factors that regulate many aspects of neural development[234]. Ngn2 regulates the commitment of neural progenitors to neuronal fate during development by inhibiting the expression of glial cells[235]. This method of transfection of the Ngn2-cassette by lentiviral infection to NPCs for neural induction has several advantages (**Figure 60**):

- Phenotypically similar neurons are produced from distinct iPSc-derived NPC line which allows the growth of a homogenic culture.

- Cells acquire neuronal gene expression patterns and morphology mainly as glutamatergic forebrain neurons in only 2 weeks.
- Cultures grown to large scale can be easily differentiated by doxycycline treatment; avoiding to deliver the iNgn2 construct to a large number of naive NPC which allows the screen of multiple compounds[236].

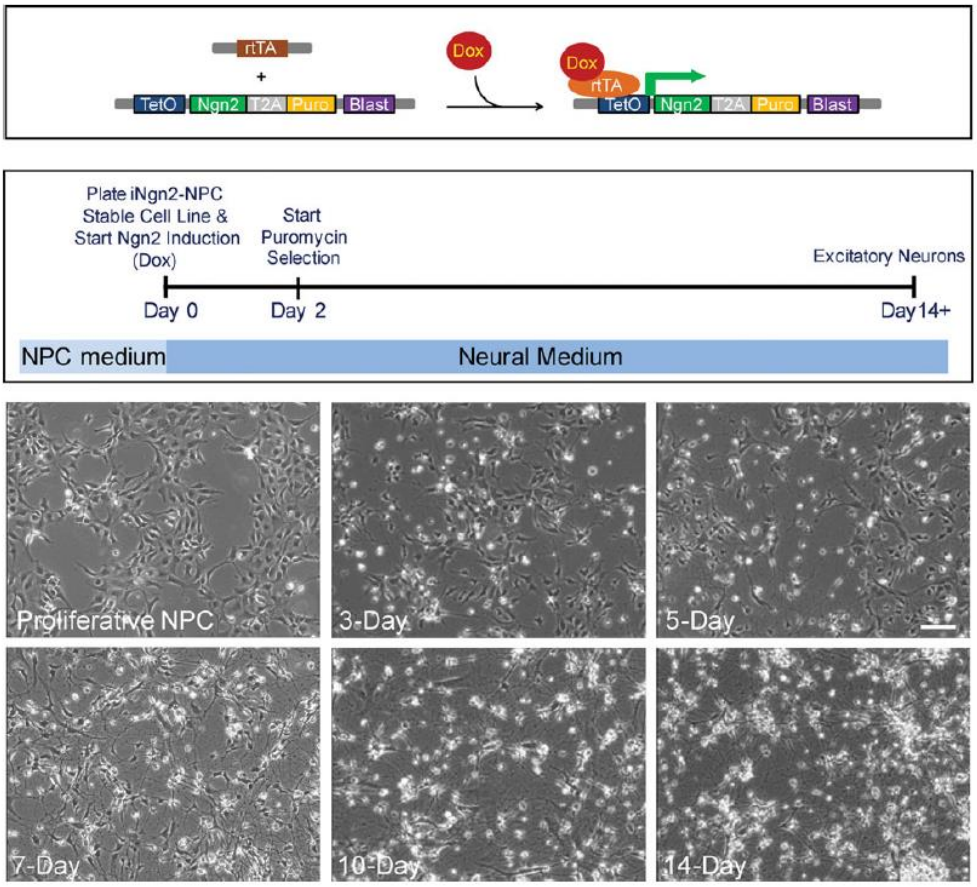

Figure 60. *Development of neurons from iNgn2-NPC stable cell lines. Top panel is a schematic representation of the action of the transgenes in inducing expression of the Ngn2 cassette. The bottom panel contains the timeline of induced Ngn2 neuron generation, as well as phase-contrast images of live induced Ngn2-NPC stable cells at various time points.*

This methodology was implemented in NPCs obtained from iPSCs of a patient carrying the A152T mutation in the gene encoding for tau (MAPT). Although the role of tau A152T in disease is still debated, it has been shown to affect tau function and PTMs[237], promote oligomerization and postmortem detection of inclusions with cognitive decline in rodent models[238], cause neuronal dysfunction in animal models[239], and increase significantly the risk for FTD and other neurodegenerative diseases[240].

These induced-Ngn2 neurons generated from the NPCs of the patient carrying the A152T mutation represent an *ex vivo* model of human neurons where endogenous tau expression reaches relevant levels in the context of the genomic background associated with disease. One of the effects that become clear by comparing the patient cells lines with a relative control is an increase in tau phosphorylation. Therefore, these cells can be immunostained with different tau antibodies and neuronal markers and can be used in a high-content imaging assay for the screening of drug candidates[236]. In this particular case this assay has been employed to test if our LRRK2 inhibitors are able to reduce tau phosphorylation during my research stage at Harvard University-Massachusetts General Hospital under the supervision of Dr. Haggarty (**Figure 61**).

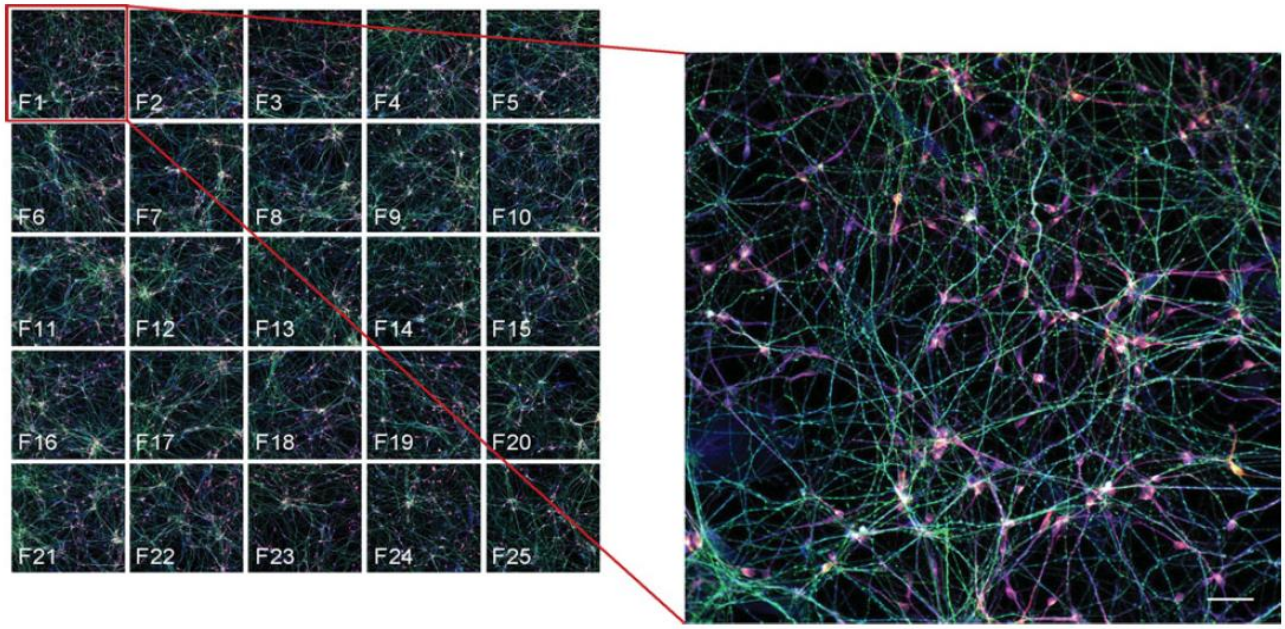

Figure 61. *An example of using the iNgn2 neurons in a high-content imaging assay. Left image illustrates the acquisition of 25 fields (F1 to F25) per each well in a 96-well plate. Right image is zoomed in composite image of a field (F1) of cells immunostained for phosphorylated Tau (PHF-1, green), total Tau (K9JA, red), and neurons (βIII-Tubulin, blue).*

3.4.2. Results and discussion

- LRRK2 expression

Before the compounds were tested in this neuronal model derived from iPSC from patients the expression of LRRK2 was analyzed by quantitative PCR showing that mRNA LRRK2 levels increase with the differentiation stage of the neurons acquiring significant levels after 14 days of culture (**Figure 62**).

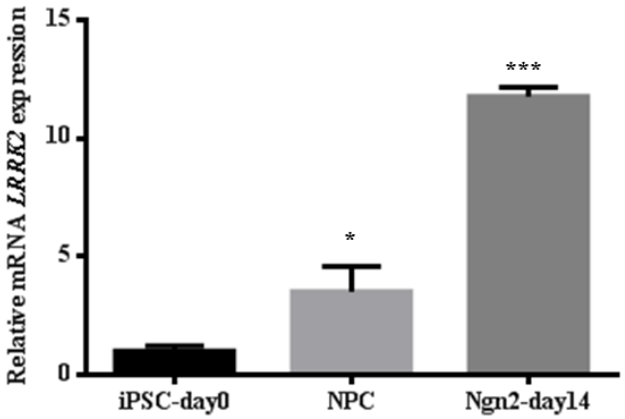

Figure 62. *Quantitative-PCR of LRRK2 expression in iPSC, NPC and Ngn2-neurons at day 14. Ct values were normalized to iPSC (set to 1) and GAPDH. Values represent averages of triplicates. Error bars indicate Mean values ± SD. *p< 0.05,***p<0.0005.*

- Ngn2-transfected-A152T-derived neurons assay

All of the triazolo-pyrimidine and benzothiazole LRRK2 inhibitors showed a neuroprotective effect in the previous assay and therefore, they were used again for this experiment. This group of compounds includes the following:

- Triazolo-pyrimidine derivatives: **45 - 49**
- Benzothiazole derivatives: **56**, **64 - 68**, **71 - 72**, **74 - 75** and **77 - 78**.

The small molecule named, CHIR-99021, a known GSK-3β inhibitor able to decrease tau phosphorylation was used as positive control in the assay[241].

Both neurons derived from iPSC from the patient and a healthy control were seeded in 96 well-plates and each compound was tested at a fixed concentration of 10 µM. CHIR-99021 was tested at 1 and 10 µM. Additionally, a negative control was also used and the neurons were treated with DMSO. Each compound was tested in duplicates in two biological independent experiments.

Neurons were incubated with the compounds for 24 hours and on the next day cells were fixed and immunostained with different tau antibodies such as PHF-1 (p-tau antibody at Ser396 and Ser404), K9JA (total tau antibody), β3-tubulin (neuronal marker) and Hoechst (nuclei marker). Neurons were photographed by automated confocal microscopy, photographing 25 fields per well. Data analysis was performed by an automated pipeline developed at Haggarty Laboratory in which by a segmentation algorithm, the program

differentiates between cell bodies and neurites and is able to measure the intensity of each antibody in both cell bodies and neurites (**Figure 63**).

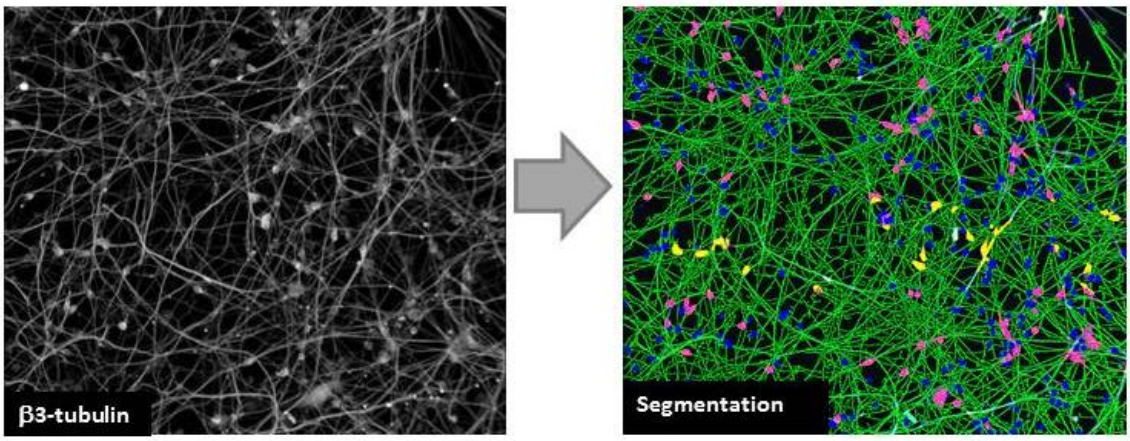

Figure 63. *Schematic representation of the segmentation algorithm.*

Furthermore, different quality control parameters are included in this automated pipeline in order to confirm that there are significant differences between patient cells and healthy control cells, significant differences between negative control cells (cells treated with DMSO) and positive control cells (cells treated with 10 µM CHIR-99021) and confirmation with the neural marker and the nuclei marker (β3-tubulin and Hoechst) that whatever the segmentation algorithm considered as neurite and cell bodies are indeed neurite and cell bodies. If the assay does not fulfill these quality control criteria the assay is rejected.

This pipeline allows this assay to be developed in a high-content way in which with a single experiment a lot of information is obtained. Different measurements can be used as readouts: nuclei cell count, intensity of PHF-1 in the neurites, intensity of K9JA in the neurites, intensity of β3-tubulin in the neurites, intensity of PHF-1 in the cell bodies, intensity of K9JA in the cell bodies and percent of activity of PHF-1 in the neurites. This assay can be quite variable, therefore the coefficient of variation (CV) between plates is calculated for each of these read outs (**Figure 64**).

From this figure it becomes clear that the most robust readouts (CVs closer to 0) are Z-score of the intensity of K9JA in cell bodies and percent activity of neurite PHF-1. From now on, the focus is placed in these two readouts and in the results obtained in the patient cell line.

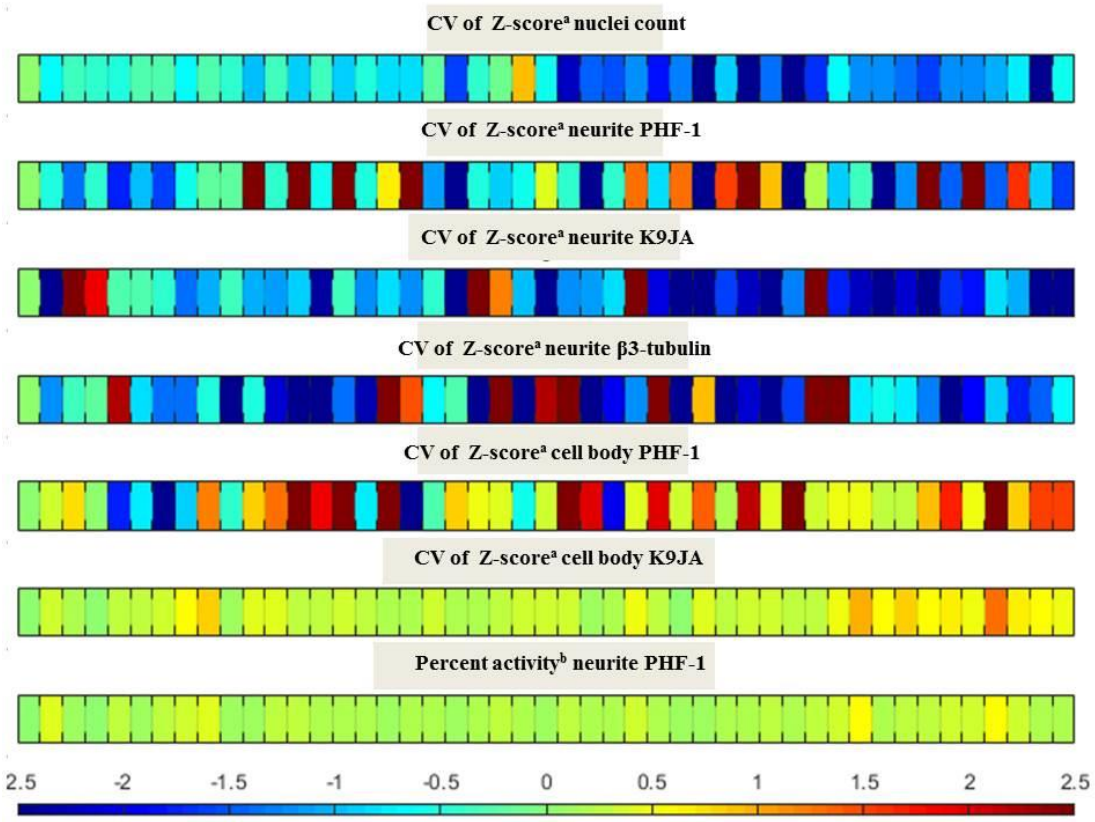

Figure 64. *Coefficient of plate to plate variation for the possible readouts. [a]Z-score is a normalization correction factor calculated by subtracting each data point the average value for negative control (DMSO) of the 25 fields of each well and dividing the result by the standard deviation of the negative control. [b]Percent activity is a normalization correction factor calculated by assigning the value of 100 to the intensity of PHF-1 in the neurites in negative control (DMSO) cells and 0 to the positive control cells (10μM CHIR-99021)*

It is desirable that the LRRK2 inhibitors tested are able to have a low Z-score for cell body K9JA (the more negative the better) which will mean that the inhibitors are able to clear the accumulation of total tau in the cell bodies. Accumulation of total tau in the cell bodies, also known as somatodendritic redistribution of tau has been reported to be pathological in tauopathies[87]. Furthermore, it is also desirable that our LRRK2 inhibitors have a value of percent activity neurite PHF-1 closer to 0 which will mean that there is a decrease in p-tau in the neurites at Ser396 and Ser404. The results are plotted in a volcano plot graph (**Figure 65**).

From these results it becomes clear that compounds **46**, **48**, **49** and **77** can be selected as the best candidates able to modulate both accumulation of tau in the cell bodies and a decrease of p-tau at Ser396. Derivatives **64**, **65** and **68** may also be selected with good result for one parameter and in the border line for the second one.

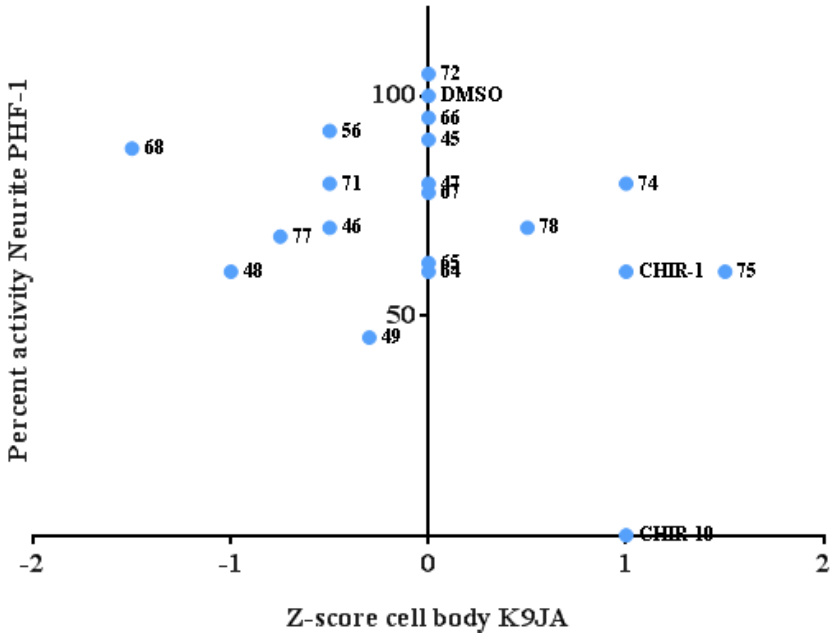

Figure 65. *Volcano plot for data obtained for the Percent activity neurite PHF-1 and Z-score of cell body K9JA for compounds* ***45 - 49***, ***56***, ***64 - 68***, ***71 - 72***, ***74 - 75***, ***77 - 78***, *CHIR-99021 (at 1 µM and 10 µM) and DMSO as negative control.*

For these compounds a detailed statistical analysis of the percent activity of neurite PHF-1 is performed (**Figure 66**).

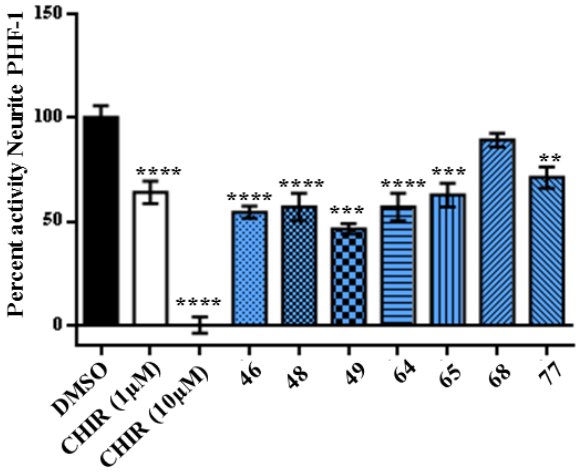

Figure 66. *Statistical analysis of percent activity neurite PHF-1 of compounds* ***46***, ***48 - 49***, ***64 - 65***, ***68***, ***77***, *CHIR (at 1 and 10µM) and DMSO as negative control.*

These compounds (**46**, **48**, **49**, **64**, **65**, **68** and **77**) are able to reduce the phosphorylation of tau in epitopes Ser396 and Ser404 at the neurites of induced Ngn2-derived neurons from a patient carrying the A152T mutation. This decrease in the phosphorylation of tau can be related to the indirect effect that LRRK2 has by activating

GSK-3β as Ser396 is a specific GSK-3 phosphorylation epitope. These compounds were selected to be tested in a more complex cellular model of tauopathy.

3.5. 6-weeks differentiation A152T assay

3.5.1. Background of the assay employed

The induction of Ngn2 into iPSCs drives mainly the differentiation towards a glutamatergic lineage. However, it is important to test if in other neuronal types such as cholinergic or dopaminergic neurons, the pharmacological inhibition of LRRK2 has any effect on tau phosphorylation. The differentiation protocols currently available produce cultures that are heterogeneous to variable extents, whether they contain a wide variety of neural cell types or they can be designed for more fate-restricted neural lineages such as the case of the previous assay[242]. A strategy commonly used for the generation of heterogeneous neuronal cultures is growth factor withdrawal for an extended period of time[243]. That strategy was followed by the Haggarty Laboratory and EGF and FGF were withdrawn of NPC obtained again from iPSCs of a patient carrying the A152T mutation. As a result an heterogeneous culture was developed in which glutamatergic, cholinergic, GABAergic, dopaminergic, adrenergic, serotonergic neurons as well as glial cells were present[237]. This new cellular model of tauopathy showed different tau pathological hallmarks that are following summarized[237]:

- Significant upregulation of p-tau measured by western blot (WB) with the following antibodies: AT8 (p-Ser202/Thr205), AT180 (p-Thr231/Ser235), PHF-1(p-Ser396/Ser404), and S396 (p-Ser396).
- Somatodendritic redistribution of tau to the cell bodies detected by immunofluorescence.
- Accumulation of p-tau oligomeric species of reduced solubility.
- Disruption of the ubiquitin proteasome system, autophagy pathways and oxidative stress induction.
- Increased sensitivity leading to higher cell death to exogenous stressors that are present in a neurodegeneration context: environmental toxins that inhibit the mitochondrial electron transport chain, excitotoxic glutamate, proteotoxic proteasome inhibitors and Aβ(1 - 42) amyloid peptide.

Therefore, this assay is a very powerful technique to determine if the selected LRRK2 inhibitors are able to reduce the phosphorylation of tau at different epitopes measured by western blot (WB).

3.5.2. Results and discussion

Promising compounds form the previous experiment were selected for this assay from the benzothiazole and tryazolo-pyrimidine subfamilies from the previous assay were used: **48**, **49**, **64**, **65**, **68** and **77.** In addition, the commercial LRRK2 inhibitor GSK2578215A (**17**), which is an arylbenzamide derivative was also included in the assay.

6-weeks differentiated neurons obtained from iPSC from a patient carrying A152T mutation were seeded in 6-well-plates and treated with the compounds for 24 hours at a fixed concentration of 10 µM. Each compound was tested by duplicate. On the next day, pellets were collected and the levels of protein were quantified. The effect of the compounds on tau phosphorylation was measured by WB using the following antibodies (**Figure 67**):

- TAU5 which detects total tau.
- S396 which detects p-tau at Ser396.
- TAU1 which detects un-P-tau at Ser199/Ser202/Thr205
- S422 which detects p-tau at Ser422

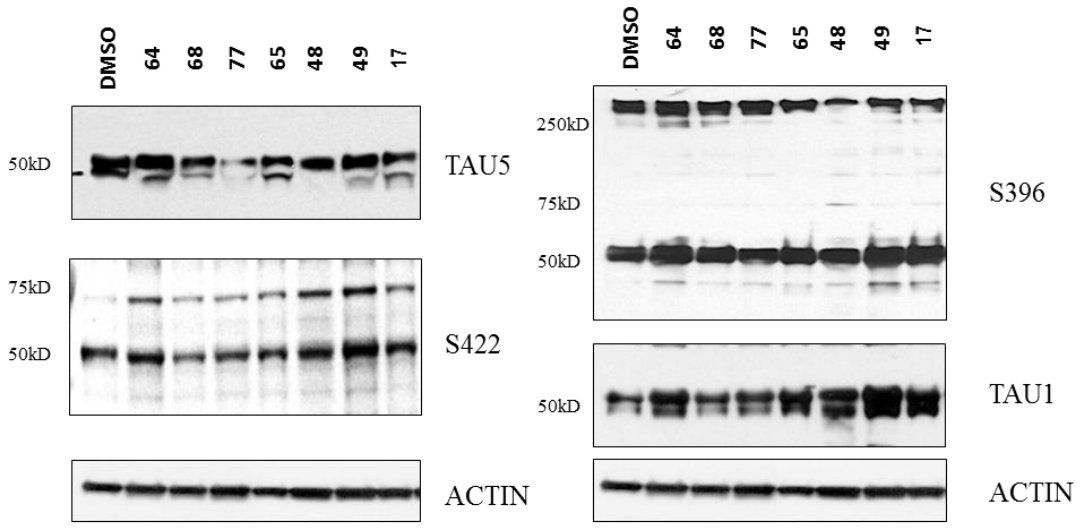

Figure 67. *P-tau expression by western blot analysis of 6-weeks differentiated A152T neurons treated with the LRRK2 inhibitors selected. ACTIN is used as loading control.*

Quantification analysis of the bands was performed with Adobe Photoshop and the relative band intensive intensity was calculated respectively to loading control (actin) (**Figure 68**).

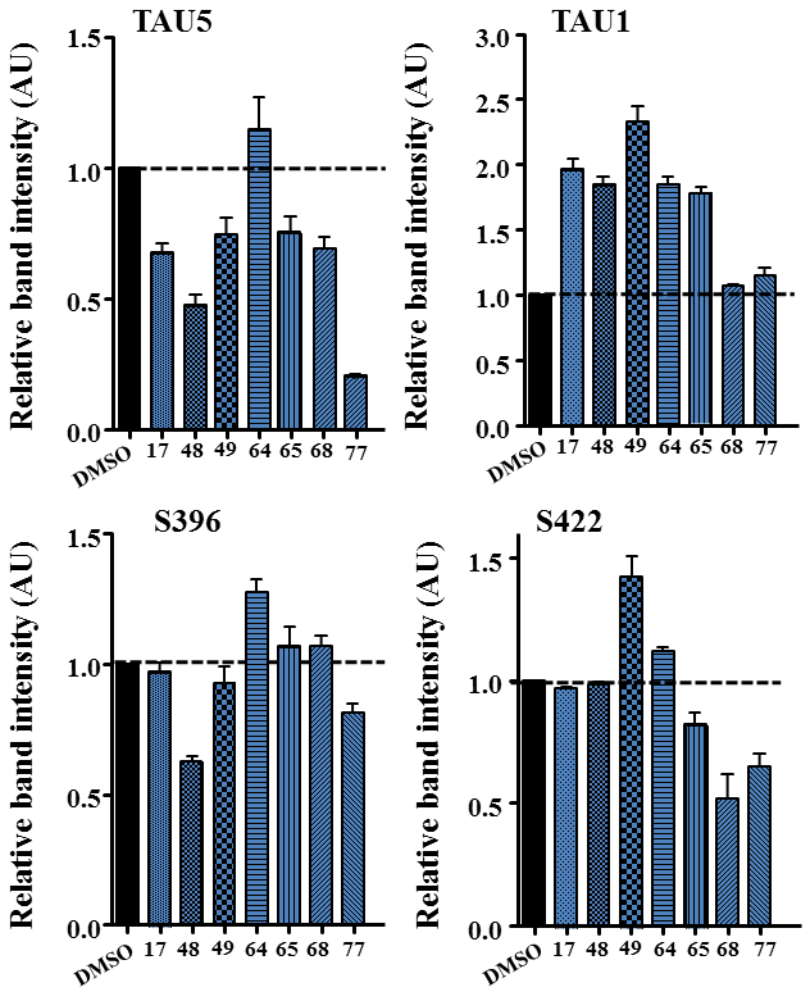

Figure 68. *Quantitative band analysis for the different antibodies used.*

From these results several conclusions are reached:

- Regarding the effect on total tau compounds **48**, **49**, **65**, **68** and **77** together with the reference compound **17** were able to reduce the levels compared to DMSO treated cells. This effect could be a confirmation of the anti somatodendritic redistribution of tau that was already seen in the previous assay, although with this experiment total tau is not specifically measured in the cell bodies.
- In the context of TAU1, up regulation of this un-phospho antibody means downregulation of phosphorylation of tau at Ser199/Ser202/Thr205. Derivatives **48**, **49**, **64**, **65**, the standard compound **17** and very modestly **68** and **77**

downregulate phosphorylation of tau at Ser199/Ser202/Thr205. Thr205 is a direct epitope for LRRK2 phosphorylation on tau. This decrease observed shows that the pharmacological inhibition of LRRK2 has a direct effect on tau phosphorylation.

- According to the data obtained for the antibody of S422, inhibitors **65**, **68** and **77** were able to reduce the phosphorylation at this epitope. Ser422 is a known phospho epitope for another kinase known as Tau-Tubulin Kinase 1 (TTBK1)[244]. Compounds **65**, **68** and **77** were tested for activity against TTBK1 and were found not be active. These results suggest that there may be a possible interaction between LRRK2 and TTBK1 that merits further study.
- Finally, taking in consideration the results obtained for S396 only compounds **48**, **77** and modestly **49** are able to reduce tau phosphorylation at Ser396. This epitope is a site if indirect phosphorylation by GSK-3β activation. Although with the previous Ngn2-transfected A152T assay all of these derivatives did indeed show this indirect effect on tau phosphorylation, in this assay only **48**, **77** and slightly **49** showed the expected effect.

Altogether, it becomes evident that the pharmacological inhibition of LRRK2 does indeed have an effect in decreasing tau phosphorylation. The fact that this effect was observed in chemically diverse inhibitors of LRRK2: benzothiazole derivatives (**64**, **65**, **68** and **77**), triazolo-pyrimidine compounds (**48** and **49**) and an aryl-benzamide derivative (**17**) enhances this hypothesis.

3.6. *In-vivo* models of tauopathies

3.6.1. GMR-MAPT.V337M *Drosophila melanogaster* model

- Background of the model employed

Recent advances in the understanding of the molecular basis of neurodegeneration and *Drosophila* genetics have enabled engineering of the fruit fly to create models that have shed light on the pathophysiological basis of neurological disorders[245]. Another key aspect of *Drosophila* anatomy is that any change in the eye phenotypes of the fly is very easy to detect, but also unlike most organs of the fly, the eye is tolerant of genetic disruption of basic biological principles as it is a dispensable organ under laboratory conditions[246]. These

properties of the eye have enabled the development of different neurodegenerative models in which a genetic eye promoter is used in order to direct the expression of the specific gene of study to the eye of the fly.

The GMR-MAPT.V337M *Drosophila* model, is a model in which an eye promoter (*GMR-Gal4*) is used to drive the expression of the mutant form of human tau V337M in all retinal cell types. The expression of this gene in the retina causes a rough eye phenotype at room temperature characterized by the loss of the mechanosensory bristles and disordered and dysfunctional photoreceptor cells (a phenomenon known as disordered ommatidia) (**Figure 69**)[247].

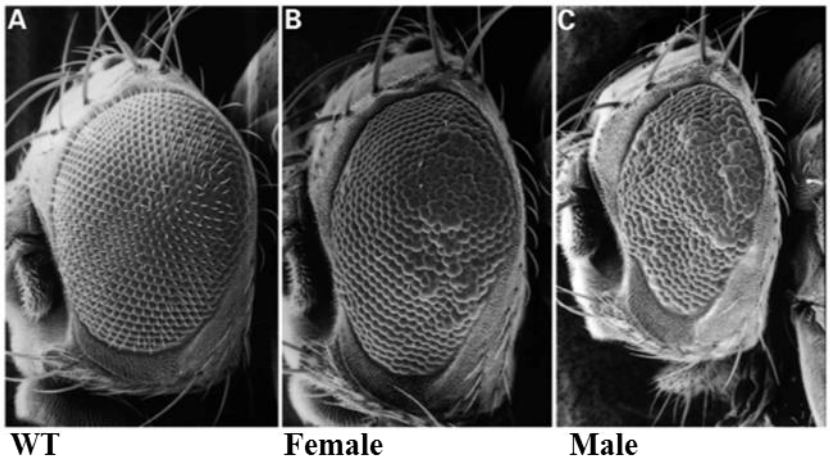

Figure 69. *Scanning electron microscopy (SEM) images of transgenic flies expressing h-tau^{v337M} under the control of the eye-specific promoter (GMR-Gal4)* ***A****-wt,* ***B****-female,* ***C****-male.*

The V337M mutation has been originally described in a family suffering from FTDP-17 dementia[109]. This mutation is associated with predominantly neuronal loss and neurofibrillary tangles composed of aggregated forms of p-tau. In *Drosophila*, the expression of this gene leads to an accumulation of abnormally phosphorylated and folded tau, age-dependent neurodegeneration and early death, as well as, the characteristic eye-phenotype previously explained[248].

- Results and discussion

The GMR-MAPT.V337M *Drosophila* was acquired by Dr. James Walker from the Massachusetts General Hospital-Harvard Medical School where I have worked in collaboration during my research stay in Boston. The strategy followed was to determine if

the systemic administration of a selection of some of our LRRK2 inhibitors is able to alter the characteristic eye phenotype of this model.

Three different chemical scaffolds of LRRK2 inhibitors have been evaluated in this tau-neuroprotective assay. Triazolo-pyrimidine derivatives and benzothiazole derivatives that showed more than 50% inhibition will be used. This group of compounds includes the following:

- Triazolo-pyrimidine derivatives: **45 - 49**
- Benzothiazole derivatives: **56**, **64 - 68**, **71 - 72**, **74 - 75** and **77 - 78**.
- The commercial LRRK2 inhibitor GSK2578215A (**17**), which is an arylbenzamide derivative (DMSO was used as negative control).

A set of adult couples were placed in egg collection cages in order to collect the embryos. 70 embryos per treatment were kept in individual cages at room temperature. The LRRK2 inhibitors selected were tested at a fixed concentration of 10 µM in melted food at 55 ºC. After the drugs were dissolved in the melted food, each food plate was left at room temperature to allow solidification and finally each plate was allocated to each individual cage containing the embryos (**Figure 70A**). With this protocol a set of 70 embryos per treatment will be fed with each LRRK2 inhibitor for 15 days (the foot plates will be replaced every 3 days to ensure adequate amounts of drug reach the flies). After that time the flies will have reached the adulthood (**Figure 70B**) in which the eye phenotype will be studied and photographs will be taken.

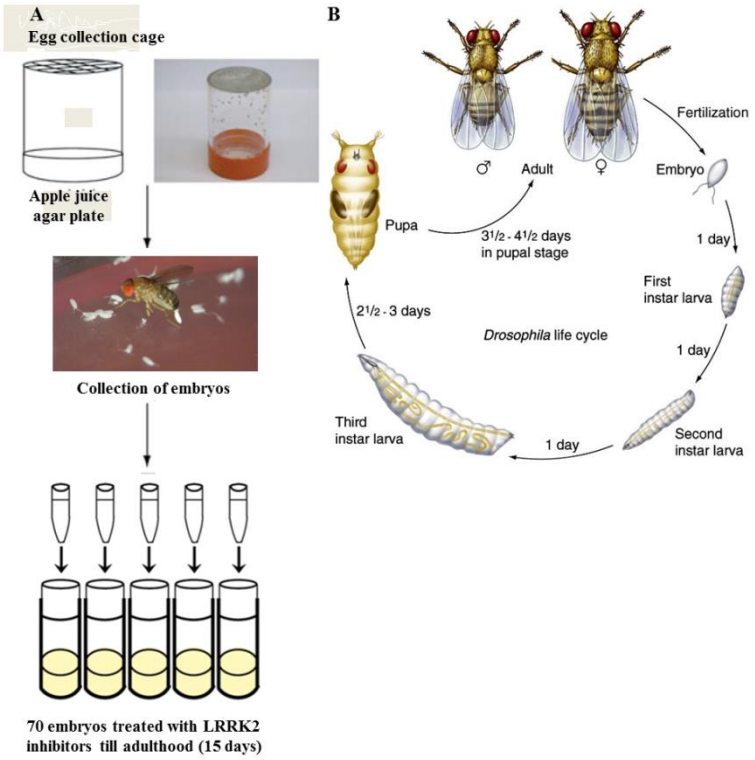

***Figure 70. A**-Schematic representation of the protocol followed. **B**- Life cycle of Drosophila melanogaster.*

Pictures of the eye of adults were taken on day 15 and it was to determine that from all the chemically diverse LRRK2 inhibitors tested, the triazolo-pyrimidine derivative **48**, was able to restore the eye phenotype compared to the wt form. This effect is particularly remarkable in the case of males (**Figure 71**).

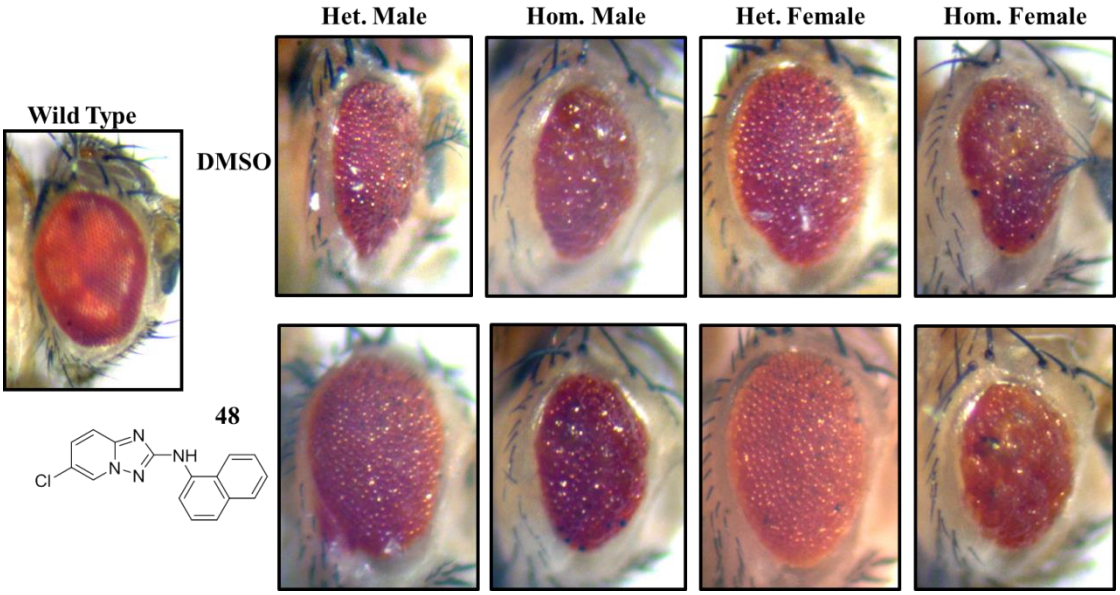

***Figure 71.** Images of the eye of adult flies treated with DMSO (negative control) and compound **48**. The eye phenotype is restored closely to the wt form especially in males with compound treatment.*

From this experiment it becomes evident that treatment with the LRRK2 inhibitor **48**, has an *in vivo* tau neuroprotective effect, as it was able to restore to wt levels the aberrant eye phenotype found in transgenic GMR-MAPT.V337M *Drosophila.*

3.6.2. Tauopathy rodent model

- Background of the model employed

Recombinant adeno-associated viruses (AAVs) are widely used viral vectors in development of novel models for neurodegenerative diseases. AAV vectors expressing full length, mutant or truncated forms of tau demonstrate early and robust pathology characterized by an increase in tau phosphorylation, NFT formation, motor and cognitive deficits. The advantage of these models is that using AAVs as delivery system, is the site specific expression of tau mostly in the hippocampus and the cortex[249]. A collaboration was established with the laboratory of Isabel Lastres-Becker from Instituto de Investigaciones Biomédicas-CSIC, that have followed this strategy to establish a tauopathy rodent model. In this model recombinant AAV vectors of hybrid serotype 1/2 expressing mutant human-tau-P301L under the control of the human synapsin 1 gene promoter[250] were injected into the right hippocampus of wt mice[251]. This model developed allows the analysis of new pharmacological treatments[252].

P301L is a well-known missense MAPT2 mutation that was identified in a family suffering from FTD in which *post mortem* studies showed an increase in tau phosphorylation measured with different antibodies in the frontotemporal lobes, basal ganglia and *substantia nigra*[253].

- Results and discussion

Benzothiazole **77** was selected to be tested in this model because it shows a neuroprotective effect in the tau-neuroprotection assay, is able to reduce tau phosphorylation measured by PHF-1 as well as total tau in the soma measured by K9JA in the Ngn2-transfected A152T assay, is able to reduce tau phosphorylation measured by WB using different p-tau antibodies in 6-week-differentiated-A152T neurons, and finally it is permeable to the BBB by the PAMPA test.

After AAV vector expressing mutant human tau-P301L was injected into the right hippocampus of wt mice, animals were treated daily for three weeks with the benzothiazole derivative **77** at a dose of 10 mg·kg^{-1} intraperitoneally (**Figure 72**). Animals were tested for cognitive impairment and finally animals were euthanized and analyzed for molecular changes regarding tau pathophysiology with different techniques.

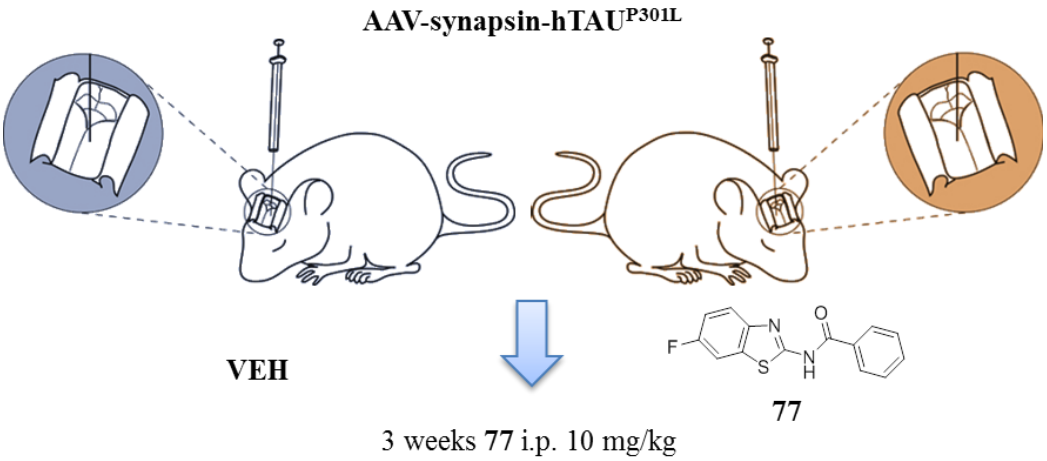

Figure 72. *Schematic representation of the injection protocol.*

A/ Cognitive impairment experiments

Cognitive decline has been widely reported in AD animal models including transgenic models and non-transgenic models[254]. Furthermore, aged animals especially non-human primates develop spontaneously memory loss and other symptoms of cognitive impairment similar to those observed in patients with AD[255]. Therefore, it is of crucial importance to assess if a potential new treatment for neurodegenerative diseases is able to rescue this cognitive dysfunction shown.

One of the most widely used to detect cognitive decline in rodents is the Novel-Object-Recognition (NOR) test. The NOR test evaluates the animal´s ability to recognize a novel object in the environment. Briefly the task procedure consists in two phases: the training phase and the test phase. During the training phase, a single animal is placed for a few minutes in the open-field arena containing two identical objects (A + A). After that time, during the test phase the animal is returned to the open-field arena with one object identical and one new (A + B) (**Figure 73**). Normal animals spend more time exploring the novel object as they recognize that is new and they are familiarized with the old one. Consequently cognitive impaired animals spend equal time in the two objects as they are

not able to remember the old one. Therefore, it is possible to stablish a discrimination ratio if the animal is animal to recognize the novel object or not.

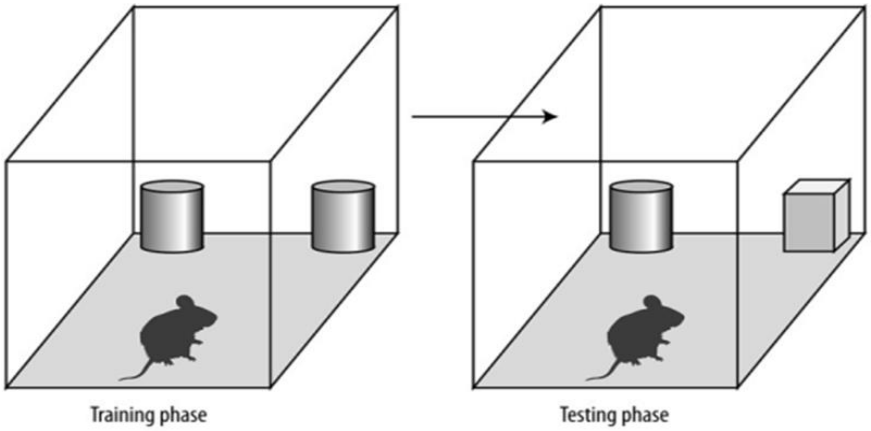

Figure 73. *Schematic representation of the training and testing phase of the NOR.*

With this tauopathy model, animals show an important cognitive decline that is restored after three weeks of treatment with benzothiazole **77**. Furthermore, the values reached in the treated group are closely to the ones obtained in healthy control animals (**Figure 74**).

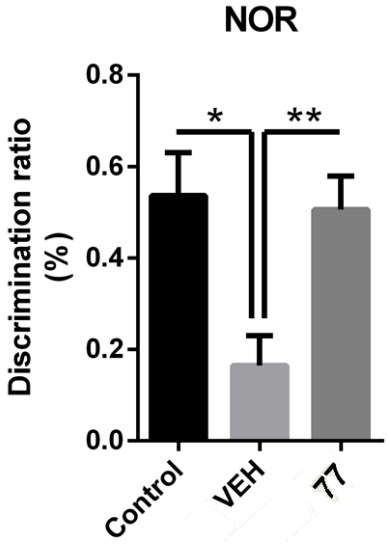

Figure 74. *Discrimination ratio between the novel and the old object in the NOR test. Bars represent mean ± SD of a population of 5 animals per group.*p<0.05, **p<0.005.*

From these results it becomes clear, that the systemic administration of the LRRK2 inhibitor **77** is able to restore to healthy control levels the cognitive decline observed in AAV vector expressing human mutant tau P301L inject mice.

B/ Molecular experiments

In order to correlate the results found at a behavioral level, several experiments were carried out to determine if the cognitive improvement seen is related to a neural preservation of the tauopathy.

1. Immunohistochemical staining with total tau antibody as well as Nissl staining of hippocampi from mice that were injected in the ipsilateral side with AAV-Tau^{P301L}. Immunohistochemical staining of the hippocampus with total tau antibody was performed with the aim of confirming that only the ipsilateral side of the hippocampus was affected by the injection and to determine any beneficial effect with the treatment with the LRRK2 inhibitor **77** by decreasing the number of positive cells. Indeed, it was confirmed that only the ipsilateral side showed a neurodegeneration process as a consequence of the injection and not the contralateral side. However, regarding the effect of benzothiazole **77,** no reduction of the number of tau positive cells was seen (**Figure 75**). On the contrary, regarding the Nitch staining a neuroprotective effect was observed as more positive cells were found in the DG of the hippocampi (**Figure 75,** green box).

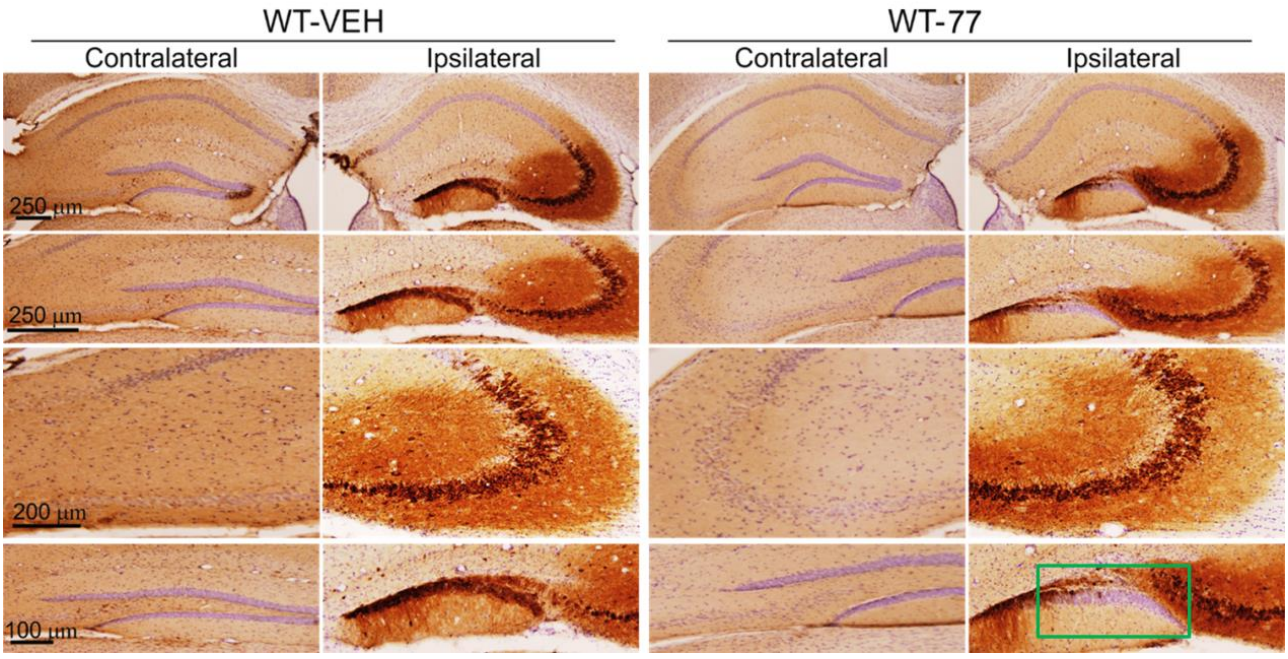

Figure 75. *Immunohistochemical staining with total tau antibody and Nissl staining of hippocampi of mice injected with AAV-Tau^{P301l}. On the left side animals treated with vehicle and on the right side animals treated with benzothiazole **77**.*

2. WB of the hippocampus using p-Thr181 and AT8 Tau antibody.

Thr181 is one of the epitopes in tau that LRRK2 phosphorylates[122, 123]. Therefore, this antibody was used to determine if in the hippocampus of mice treated with benzothiazole **77,** there is any decrease in tau phosphorylation at this epitope. For this specific case, the focus was placed in insoluble tau aggregates. Sarkosyl extraction protocol is a standard procedure for the study of these aggregates. There is a consensus that sarkosyl-insoluble tau correlates with the pathological feautures of tauopathy[256]. Therefore, the sarkosyl extraction was implemented and it was seen that in animals treated with LRRK2 inhibitor **77**, there is a decrease in p-Thr181 tau in the sarkosyl insoluble (SI) fraction and an increase in the sarkosyl soluble (SS) (**Figure 76).** Therefore, with these results it is possible to conclude that the systemic administration of LRRK2 inhibitor **77**, was able to reach the hippocampus and decrease tau phosphorylation at a specific LRRK2 epitope, showing indeed target engagement.

Similar results were found with AT8 (p-tau at Ser 202 and Thr205) antibody that is also a direct epitope of LRRK2 as it has been shown that phosphorylation at these epitopes is increased in LRRK2/P301L transgenic mice[124] (**Figure 77**).

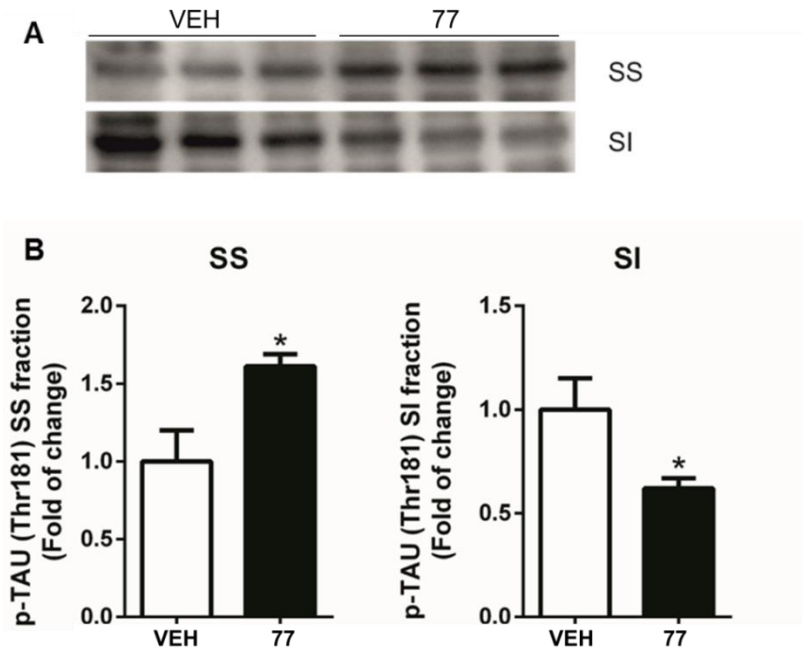

Figure 76. A- *WB of the SS and SI with p-Thr181 tau antibody of animals treated with vehicle and animals treated with derivative **77. B-** Quantification analysis of the bands. Bars represent mean values±SD of three animals per group. *p<0.05*

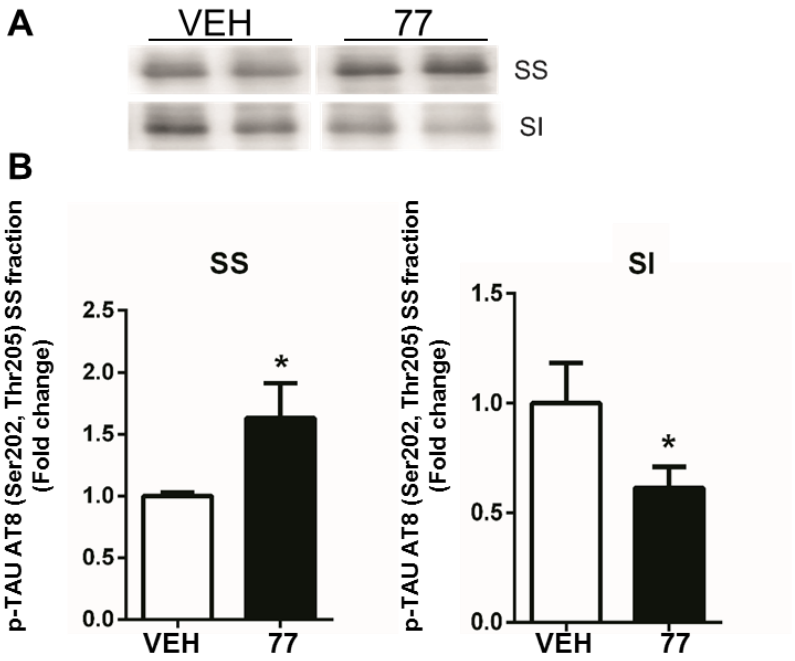

Figure 77. A*- WB of the SS and SI with AT8 tau antibody of animals treated with vehicle and animals treated with derivative* ***77. B****- Quantification analysis of the bands. Bars represent mean values±SD of three animals per group. *p<0.05*

Several important conclusions can be reached after analyzing these results:

- First of all, compound **77** does penetrate *in vivo* the BBB after systemic administration; therefore, it shows excellent ADME properties.
- Secondly, from a molecular point of view, benzothiazole **77** is able to show a neuroprotective effect at the DG of the hippocampus but most worthy is able to reduce tau phosphorylation measured by WB with two different tau antibodies. The fact that this effect was shown at the epitope Thr181 which is a specific tau epitope phosphorylated by LRRK2 and epitopes Ser202/Thr205 which are sites of phosphorylation of both LRRK2 and GSK-3β confirms that LRRK2 phosphorylates *in vivo* tau directly and indirectly.
- Finally but very importantly, the pharmacological inhibition of LRRK2 is able to rescue the cognitive decline observed in these animals showing that the neuroprotective and the anti p-tau effects shown do correlate with improvement at a functional level.

3.7. Conclusions

Our results evidence that the pharmacological inhibition of LRRK2 decreases directly and indirectly tau phosphorylation. This idea is strengthen by the fact that this effect is observed in chemically diverse LRRK2 inhibitors. Therefore, the employ of a chemical genetic approach for the interrogation of a new role for LRRK2 has been successful, showing for the first time anti-phospho tau biological activity together with LRRK2 inhibition.

In particular, an in-house tau neuroprotection assay has been developed in which all of the LRRK2 inhibitors tested have shown promising effects. Secondly, these inhibitors were tested in two different human-based cellular models of tauopathies using A152T-differentiated neurons. Insights in the mechanism of a decrease in tau phosphorylation by pharmacological inhibition of LRRK2 have been accomplished with these two experiments. Finally, a set of compounds was tested two *in vivo* models. Firstly, a set of compounds were tested in a *Drosophila* tau model and one of them was able to rescue the pathogenic phenotype. Secondly, one of the most promising compounds has been tested in a tauopathy rodent model showing an increase in cognitive performance associated to a neuroprotective effect based on the decrease of tau phosphorylation in the brain.

These results showed for the first time that LRRK2 could be a interesting target for tauopathies. Further, *in vivo* experiments using different models of tauopathies are needed, in order to confirm this therapeutic effect and clarify the mechanism of action with the aim of moving LRRK2 inhibitors into the clinic

4. LRRK2 as a therapeutic target for Retinitis pigmentosa

4.1. Introduction

A very innovative application in which LRRK2 may play an interesting role is in retinal neurodegenerations. The relationship between LRRK2 and retina has only been explored in the context of generating a PD animal model in *Drosophila* by Christopher J.H. Elliot and his group. It has been reported that the expression of hG2019S-LRRK2 in dopaminergic neurons of flies lead to visual loss due to mitochondrial abnormalities, apoptosis and disruptions in the autophagic system in the photoreceptors[178, 257, 258]. These flies may provide a useful model for studying LRRK2-linked pathogenesis and for future therapeutic screens[259].

The *rd10* mouse model has been validated as a good model for experimental pharmaceutical-based therapy for RP[260] and it is the one we have used to explore the role that LRRK2 may have in RP. It is described in detail in the following section.

4.1.1. The *rd10* mouse model

The retina of mammals is formed by the neural retina, which contains six types of neurons, the Glia of Müller (GM), and the retinal pigment epithelium (RPE), which is composed of non-neural cells that contain granules of melanine[261]. These neural retinal cells are distributed in three nuclear layers separated by two plexiform layers. The cell bodies of the photoreceptors form the outer nuclear layer (ONL); the soma of horizontal, amacrine and bipolar cells as well as the cell bodies of the GM form the inner nuclear layer

(INL); the cell bodies of the ganglion cells are found in the innermost layer, which is known as the ganglionic cell layer (GCC), where a group of displaced amacrine is also located. On the GCC there is another type of glial cells: astrocytes. The outer plexiform layer (OPL) is the place of synaptic connection between photoreceptors and bipolar cells while the inner plexiform layer (IPL) is the point of contact between bipolar neurons and amacrine neurons and the dendritic spines of the ganglionic cells. Furthermore, beside these cells types microglia cells originated outside the retina can also be found (**Figure 78**).

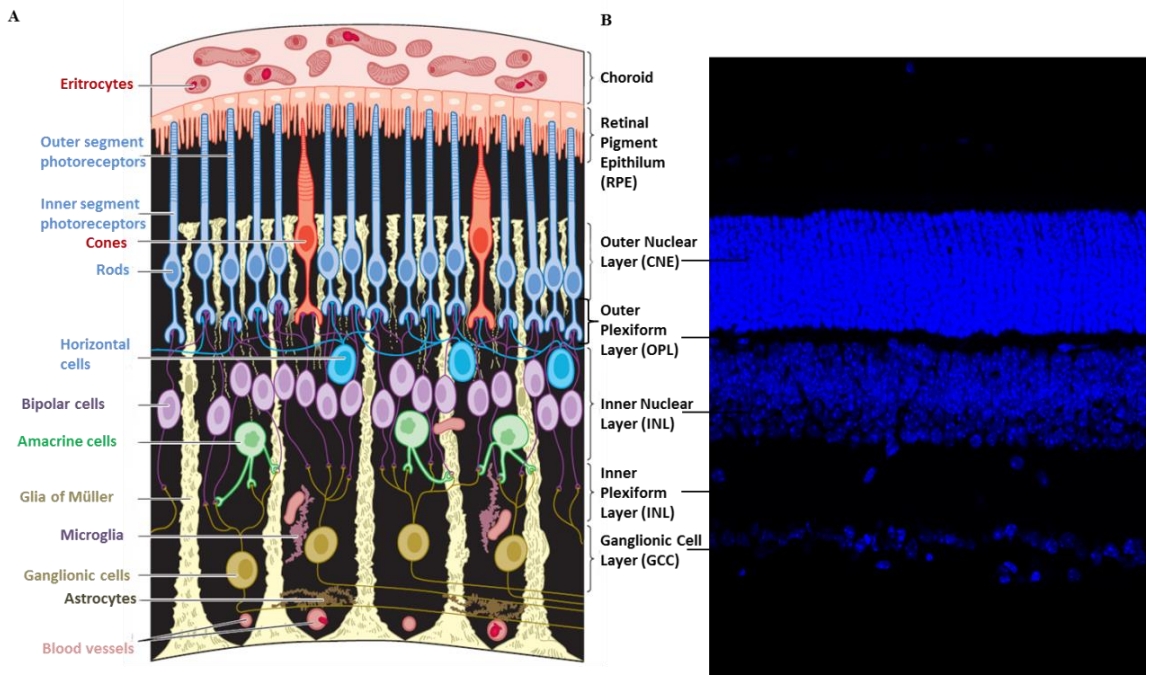

Figure 78. A- *Schematic representation of the retina of mammals.* ***B-*** *DAPI immunostaining of retinal criosections of C57BL/6 mice at postnatal day 21.*

The layer of photoreceptors is formed by cones, responsible for the vision at high light intensity, and rods, in charge of vision at low light intensity[262]. Photoreceptors convert light signal in biochemistry by the cascade of phototransduction (**Figure 79**)[263]. The bipolar cells contact with photoreceptors and ganglion cells, transferring information from one layer to another. The horizontal cells, which contact with photoreceptors in the OPL, and the amacrine cells, which contact the ganglion at the ICL, integrate and require the visual output of the retina. The horizontal cells are involved in the improvement of the contrast, while the amacrine cells collect visual stimuli through feedback between ganglion and bipolar cells. Ganglion cells are the only neurons of the retina emitting their axons out of the eye, forming the optic nerve that connects with the CNS. The GM plays a supporting role and is responsible for the maintenance of the homeostasis of the retina[261].

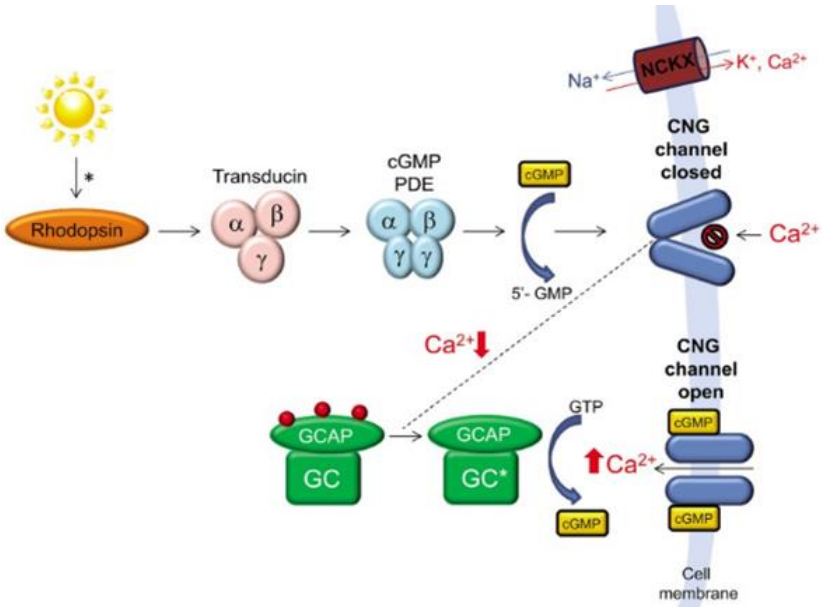

Figure 79. *Schematic representation of the phototransduction mechanism. The rhodopsin in the photoreceptors absorbs a photon, which leads to a conformation change of the rhodopsin form its cis form to a trans form. This conformation change activates G-coupled protein known as transducing, which then interchanges GDP for GTP. GTP now activates phosphodiesterase 6 (PDE6). As a result the hydrolysis of cGMP from GMP is initiated, which causes the closure of the Na/Ca channels leading to a hyperpolarization of the membrane.*

RP comprises a group of genetically heterogeneous retinal disorders in which more than 60 pathogenic genes have been found[154]. Among these pathoghenic genes, mutations in PDE6 gene have been found leading to a hypo- functional enzyme[264]. The loss of function of PDE6 leads to a massive entry of Na+ and Ca^{2+} which result to be toxic leading to photoreceptor cell death[265]. The *rd10* mice presents a mutation in exon 13 of the gene PDE6 leading to a loss of function (**Figure 80**)[266].

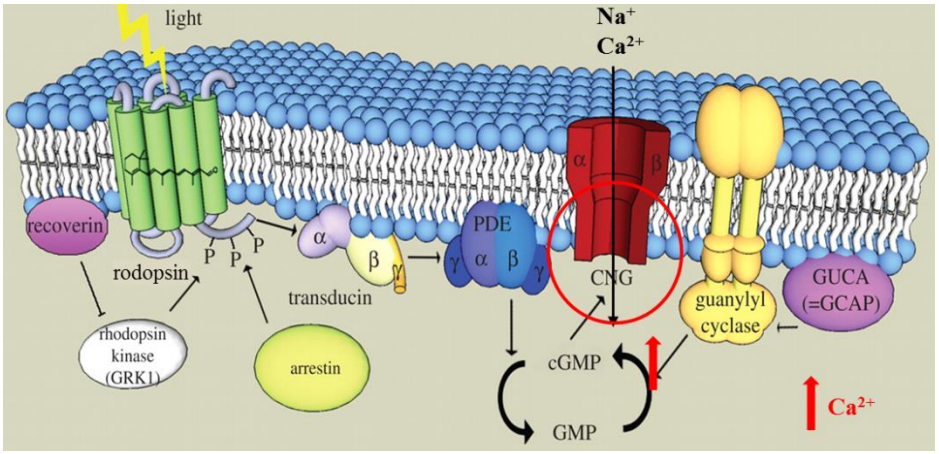

Figure 80. *Schematic representation of retinal neurodegeneration mechanism found in the rd10 model.*

The *rd10* mouse model has been validated as a good model for experimental pharmaceutical-based therapy for RP because of its later onset and milder retinal

degeneration[260]. The histological examination of the retina of the mouse rd10 reveals the progressive death of photoreceptors beginning in the postnatal age of 16 days (P16) in the central retina and P20 in the peripheral. The peak of death of photoreceptors is approximately in P25, leaving a single row of photoreceptors in P35 while the wild type retina has 12 rows (**Figure 81**)[267]. The rest of the layers of the retina are affected later and secondarily to the loss of photoreceptors[267].

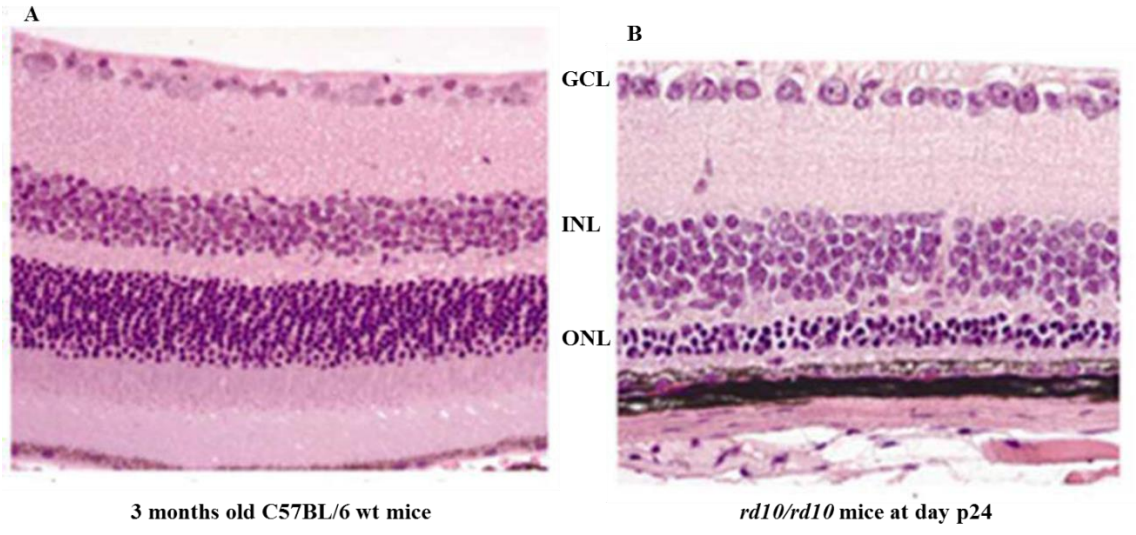

Figure 81. *Histological sections of* ***A-*** *C57BL/6 wt mice and* ***B-*** *rd10 mice.*

In the retina in addition to the two types of glia (GM and astrocytes), there are microglial cells that are macrophages of the CNS (**Figure 78**). The GM and the astrocytes, besides having an important role in the conservation of the structure and the functional integrity of the retina, are also involved in the development of retinal pathologies[268]. An activation of the GM is characterized by an increase of the expression of GFAP which occurs in various dystrophy and retinal lesions and is considered as a sign of identity of reactive gliosis (**Figure 82**). Even more, it has been postulated that the activation of the GM contributes to the death of photoreceptors[269].

As the retina is part of the CNS, the microglial cells are the resident innate immune cells which provide the first line of defense. Activation of the microglia is normally a beneficial effect and its action is stopped whenever the homeostasis of the brain has been reestablished. However, in RP as well as in other neurodegenerative diseases, pathological activation of the microglia turns into chronic persistent inflammation that drives progressive neurodegeneration.

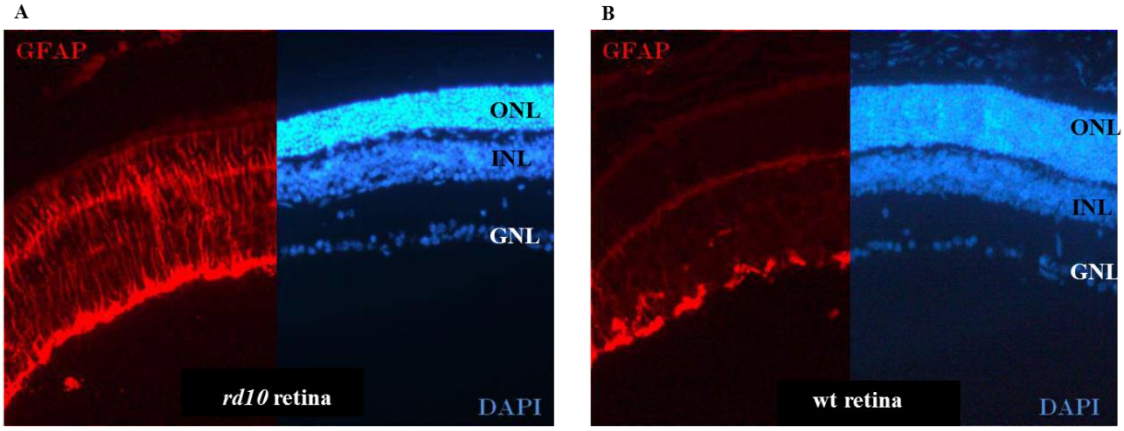

Figure 82.A/B- *Comparison of the expression of GFAP in rd10 retina (**A**) and wild type (**B**). There is an increase of the expression of GFAP in the rd10 retina in the areas where there has been photoreceptors cell death, evidenced by the lower number of rows of the ONL, respectively to the wild type retina. GFAP (is immunostained in red); DAPI (in blue).*

When the microglia is activated it presents an amoeboid phenotype which enhances its phagocytic capacity and also the production of pro-inflammatory cytokines such as tumor necrosis factor-α (TNFα) and interleukin 1-β (IL-1β) among others[270]. Non-activated microglia has a branched morphology and produces anti-inflammatory cytokines (**Figure 83**).

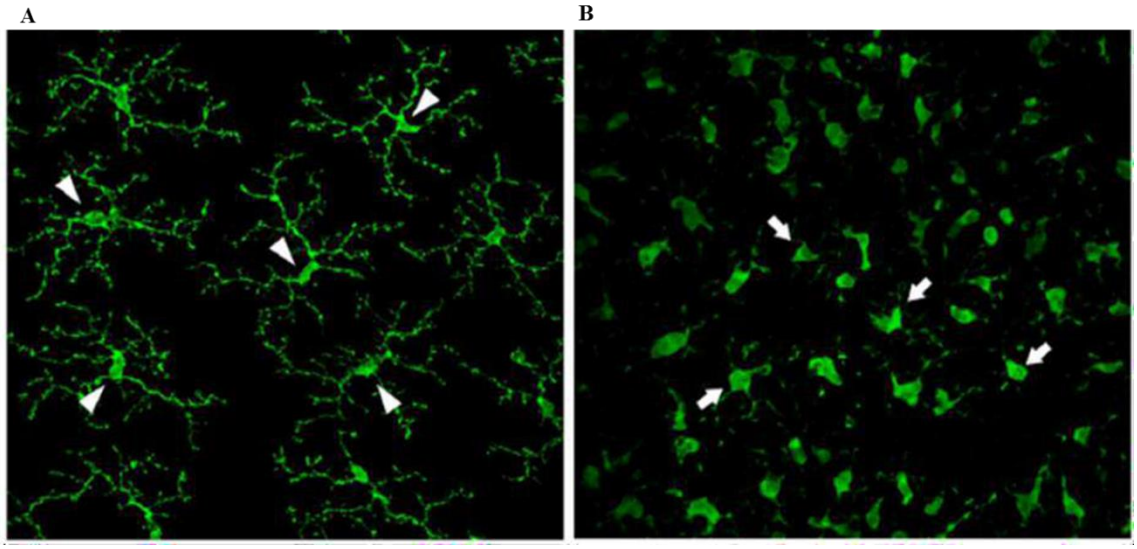

Figure 83.A/B- *Comparison of the morphological differences between non-activated branched microglia (**A**) and activated amoeboid microglia in retinal explants (**B**).*

Finally, but very importantly another aspect that has been described for the pathological role of activated microglia is the migration from the IPL to the ONL. In retinal dystrophies microglia leaves the IPL to infiltrate the ONL causing photoreceptor cell death (**Figure 84**)[271].

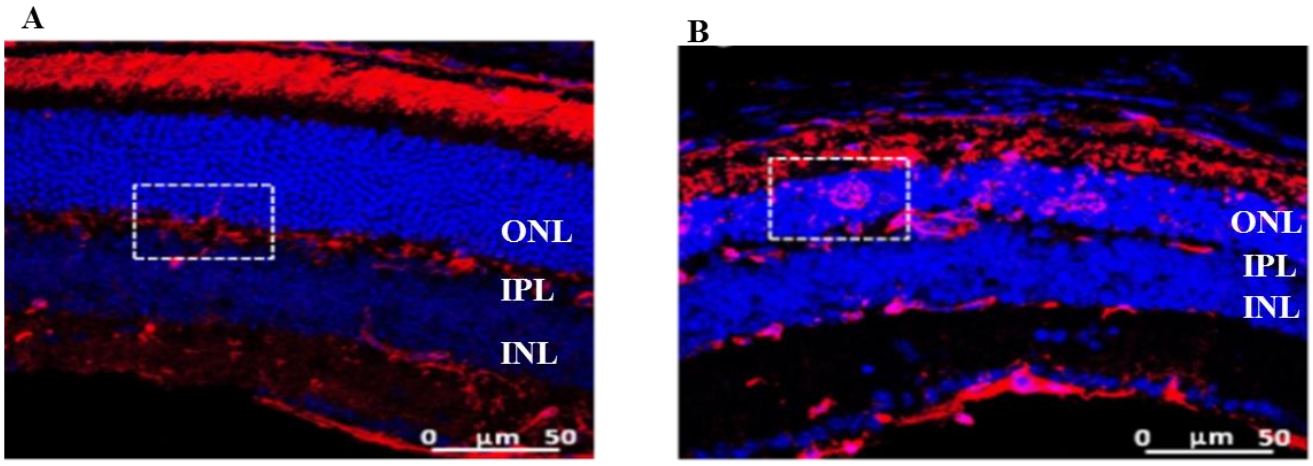

***Figure 84. A**-Branched non-activated microglia in the IPL. **B**-Amoeboid activated microglia infiltrated in the ONL.*

4.2. Background

The retina is a highly specialized sensory tissue that belongs to the central nervous system. It may be considered as an accessible, external part of the brain, as they share identical physiological and pathological molecular pathways. Consequently, diseases of the brain and the retina show similarities. For instance, neuroinflammation appears as a relevant common process for both retina and brain neurodegenerative diseases[152]. Therefore, there can be common molecular targets between retinal dystrophies and neurodegenerative diseases[145].

When looking for a common target between these two types of pathologies, GSK-3β is one that stands out the most. GSK3-β is a constitutively active Ser/Thr kinase ubiquitously expressed in the human body. It is involved in many important biological functions which some of them have been well characterized[233]. In this context, one of the roles of GSK-3β that may be a link between retinal dystrophies and neurodegenerative diseases is the fact that this enzyme plays a key role in neuroinflammation as it regulates the balance between pro-inflammatory and anti-inflammatory cellular responses. Consequently lithium a weak GSK-3β inhibitor has been used in a rat model of glaucoma[272] and valproic acid and indirect inhibitor showed a short-term benefit for RP patients[273, 274].

Following this train of thought, using a chemical genetic approach we decided to test if mechanistically and structurally diverse GSK-3β inhibitors synthesized in our group were able to show a neuroprotective effect in retinal explants. We used retinal explants from wt mice treated with the toxin *N*-methyl-*D*-aspartate (NMDA) which is considered as

an *ex vivo* model of glaucoma[275] and retinal explants from *rd10* mice. The three mechanistically and structurally diverse GSK-3β inhibitors were able to show a neuroprotective effect as they were able to reduce the number of TUNEL positive cells in both types of explants[276]. In a second step, one of GSK-3β inhibitor previously used, the 5-(4-Morpholinethylimino)-2,3-diphenyl-2,5-dihydro-1,2,4-thiadiazole-Dihydrobromide (VP3.15) was tested in an *in vivo* context[277]. The systemic administration of VP3.15 from postnatal day 15 to 21 showed a clear anti-inflammatory effect. VP3.15 treatment significantly decreased the expression of the proinflammatory genes *Il1β* and *α2m* and a trend for *Tnfα* expression. In the case of glial genes *Cd11b* and *Iba1* were also decreased upon VP3.15 treatment, while the activated microglia marker *Cd68* showed a decline trend In parallel, VP3.15 significantly reduced the expression of *Gfap*. Regarding the neuroprotective effect, VP3.15 was able to slow down the neurodegeneration process as the ONL was preserved showing significantly more layers of photoreceptors. This neuroprotective effect was accompanied by an increase in the gene expression of rhodopsin. Finally and most importantly from a physiological point of view, the treatment with VP3.15 decreases visual loss measured by electroretinography.

These results show that GSK-3β is critically involved in the neurodegeneration and neuroinflammation processes in RP. Therefore, the pharmacological inhibition of GSK-3β has an outstanding potential for the treatment of retinal dystrophies. Taking in consideration this new horizon for GSK-3β inhibitors and with the aim of moving forward this inhibitors into the clinic, a personal grant was awarded by the Foundation of orphan drugs and rare diseases (in Spanish Fundación Medicamentos huérfanos y enfermedades raras (MEHUER)) to study Tideglusib (2-naphthyl-4-bencyl-1,2,4-thiadiazolidine-3,5-dione**)**, a GSK3-β inhibitor born in our research group and that has reached phase II clinical trials for AD, in a preclinical model of RP.

In this project it was possible to determine that the *ex vivo* treatment of *rd10* retinas with Tideglusib decreased photoreceptor cell death measured by immunohistochemistry with the TUNEL technique (**Figure 85**). Regarding the anti-inflammatory effect, astrogliosis showed a reduction trend upon Tideglusib treatment (**Figure 86**) but no modulation of microglia (**Figure 87**).

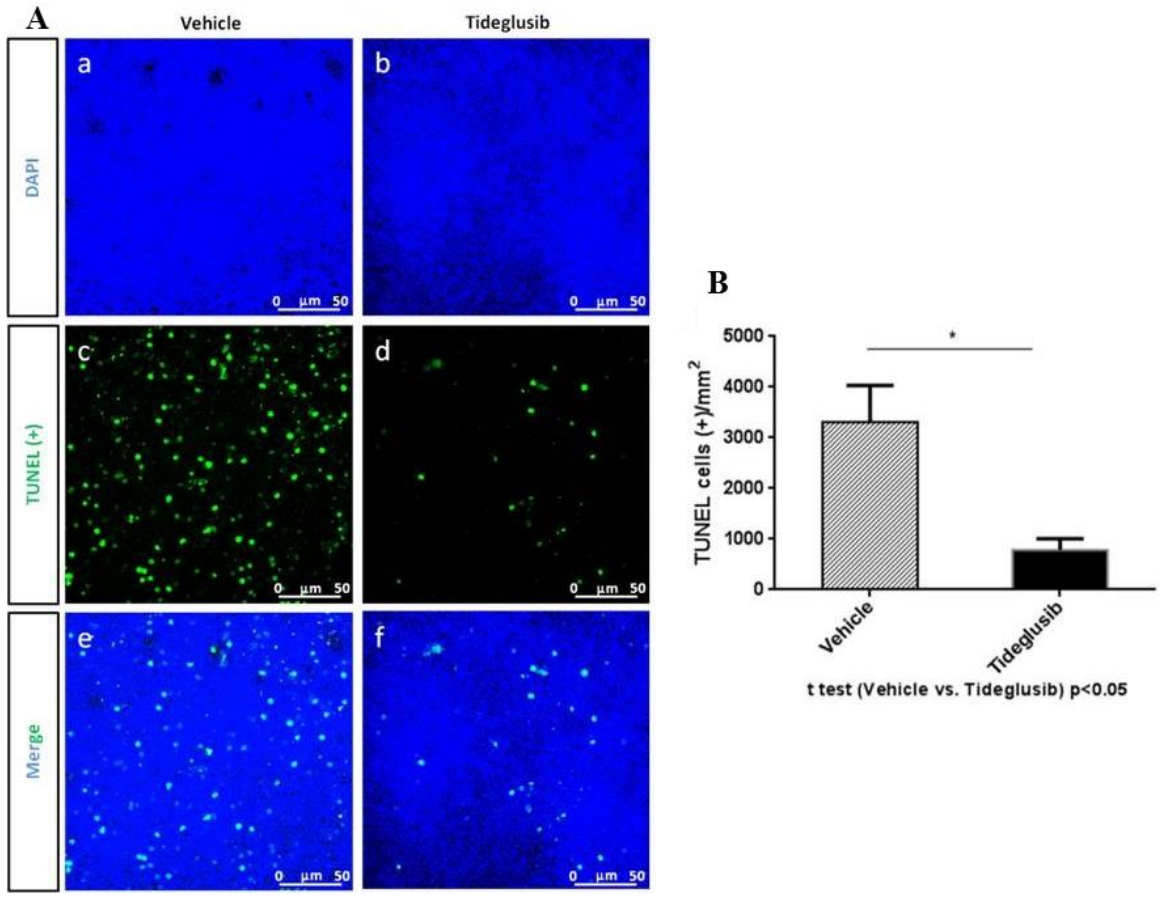

Figure 85. A- *Immunohistochemistry of photoreceptor cell death assessed by TUNEL (green) and nuclei were stained with DAPI (blue) in whole mount retinas. (a-f).* ***B-*** *Quantification of TUNEL-positive nuclei. The results represent the mean ± SD.* p <0.05.*

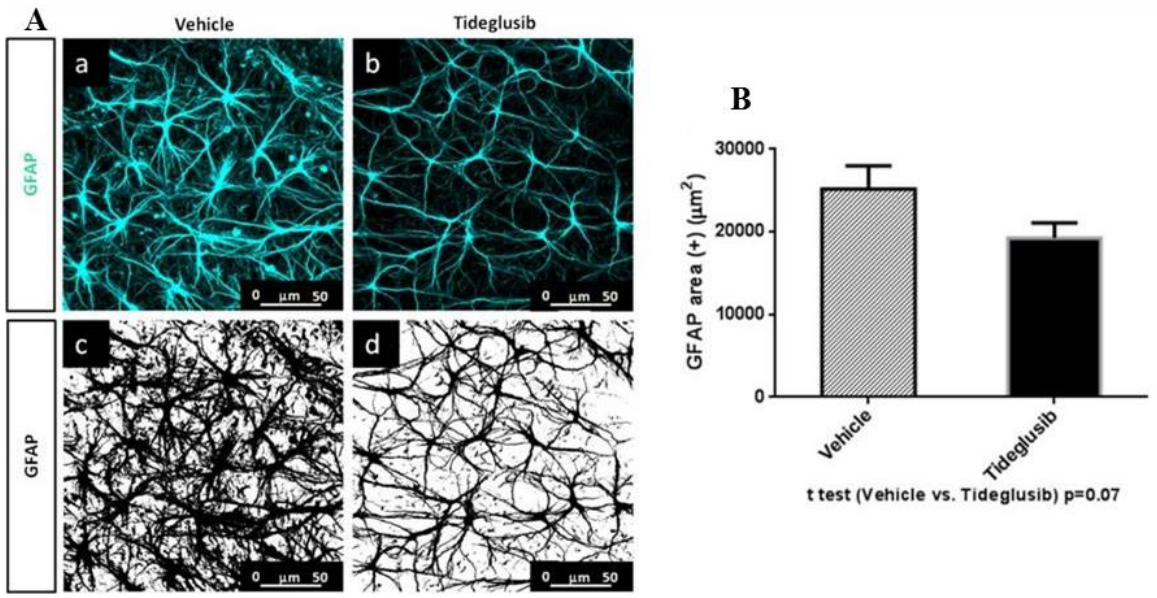

Figure 86. A- *Immunohistochemistry of astrocytes with GFAP in whole mount retinas. (a-b and conversion of the color images to 16 bits images using the ImageJ program (c,d).* ***B-*** *Quantification of of GFAP positive area by ImageJ program. The results represent the mean ± SD. * p <0.05.*

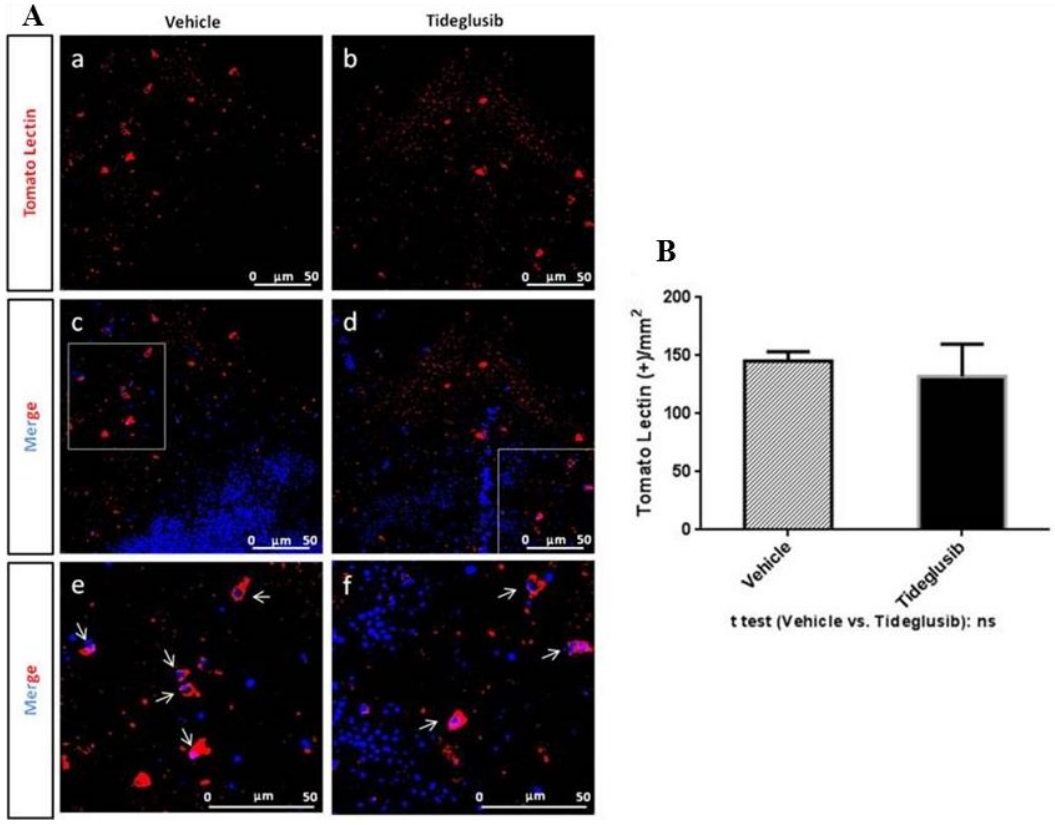

Figure 87. A- *Immunohistochemistry of astrocytes with GFAP in whole mount retinas. (a-b and conversion of the color images to 16 bits images using the ImageJ program (c,d).* ***B-*** *Quantification of of GFAP positive area by ImageJ program. The results represent the mean ± SD. * p <0.05.*

The *in vivo* treatment showed that there was a trend in decreasing the expression of pro-inflammatory cytokines (TNFα and IL1-β) and an increase in rhodopsin measured by qPCR in animals treated systemically with Tideglusib (**Figure 88**).

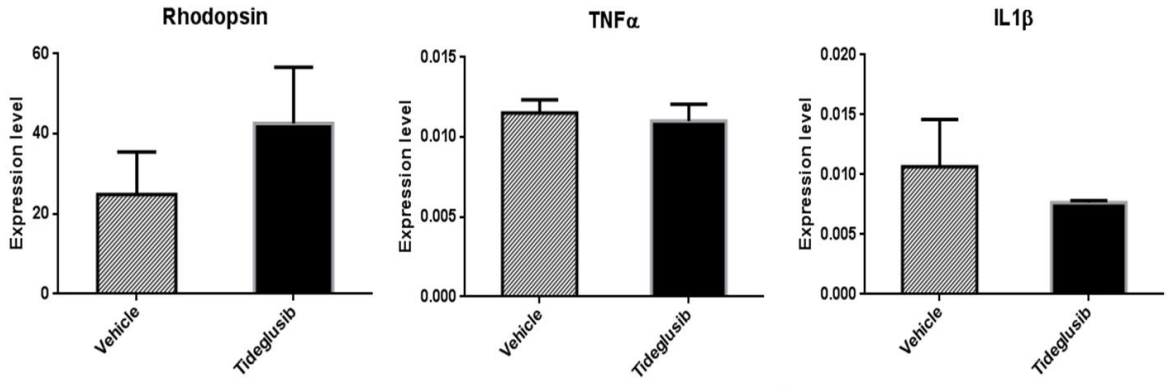

Figure 88. *Quantitative-PCR of Rhodopsin, TNFα and IL1-β. Ct values were normalized to TATA protrein.* *The results represent the mean ± SD.*

Furthermore, the electroretinographic analysis showed that the animals treated with Tideglusib have a trend to increase amplitude for the mixed wave (which measures the

response upon stimulation of rods, cones and bipolar neurons) and for the phototipic wave (which measures the response upon stimulation of the cones) (**Figure 89**). Thus, there is a trend to decrease visual loss.

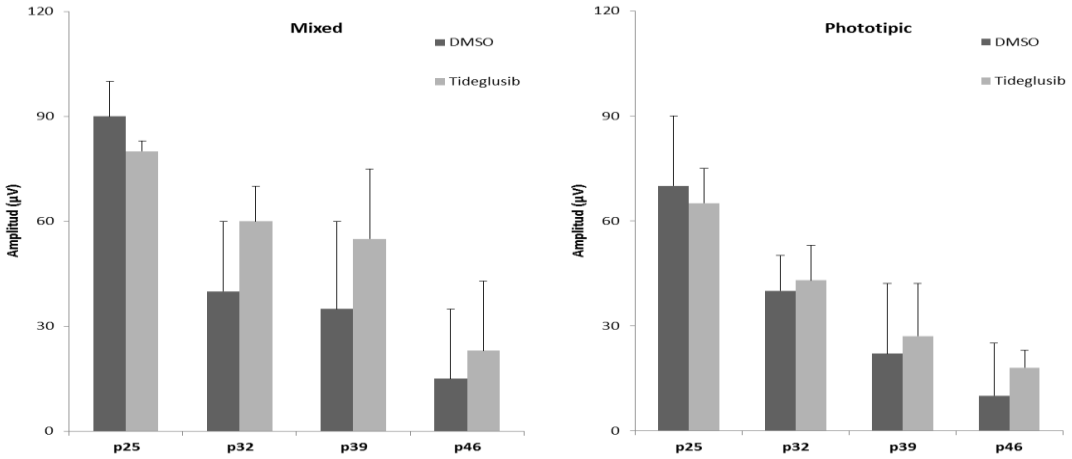

Figure 89. *Electroretinographic analysis of the mixed wave and the phototipic wave. The results represent the mean ± SD.*

These results show that Tideglusib could be used to treat RP, however, the results did not reached statistical significance due to the high variability between the animals. In order to reduce this variability is important to consider that Tideglusib was designed to be administrated orally but because of the small size of the *rd10* mice, this way of administration is not possible. The *P23H* rat model which does indeed allow for orally administration has been acquired in order to repeat these experiments to find a more robust neuroprotective effect with the aim of moving forward this drug into the clinic.

Having seen this important role of GSK-3β in retinal dystrophies, the role of LRRK2 may also be considered in this context. GSK-3β and LRRK2 are very closely related due to the indirect phosphorylation of tau by LRRK2 through GSK-3β activation. Moreover, not only it has been reported that LRRK2 plays a role in the Wnt signaling cascade but also it has been reported that activation of the Wnt signaling may induce functional and morphological rescue of photoreceptors in the *rd10* mouse model of retinal degeneration[278]. We therefore, decided to explore the therapeutic potential of LRRK2 inhibitors in RP.

4.3. Objectives

The main objective of this chapter is to test if inhibition of LRRK2 may be a new interesting therapeutic strategy for the treatment of RP.

The specific objectives of this chapter are the following:

- Analyze the expression of *LRRK2* in *rd10* retinal explants along the neurodegeneration process.
- Determine if the systemically administration of a LRRK2 inhibitor has any neuroprotective effect in the *rd10* model using as a readout the width of the ONL.
- Determine if the systemically administration of a LRRK2 inhibitor has any anti-inflammatory effect

4.4. Analysis of the expression of LRRK2 in retina

In order to analyze the expression of LRRK2 in the retina and characterize this enzyme in RP, it was decided to quantify the levels of LRRK2 in healthy mice and *rd10* mice. To do this, quantitative polymerase chain reaction (qPCR) experiments were performed which enable to follow the progression of the levels of mRNA of LRRK2 from postnatal day 14 till day 21 when the neurodegeneration peak occurs (p16). The results depicted in figure 84 showed that wild-type mice have basal levels of LRRK2 which remain constant over time. Unlike these, *rd10* mice have similar concentrations of LRRK2 mRNA till postnatal day 16, when it starts to manifest the degeneration of the tissue, it increases to doubling levels with respect to normal mice (**Figure 90**).

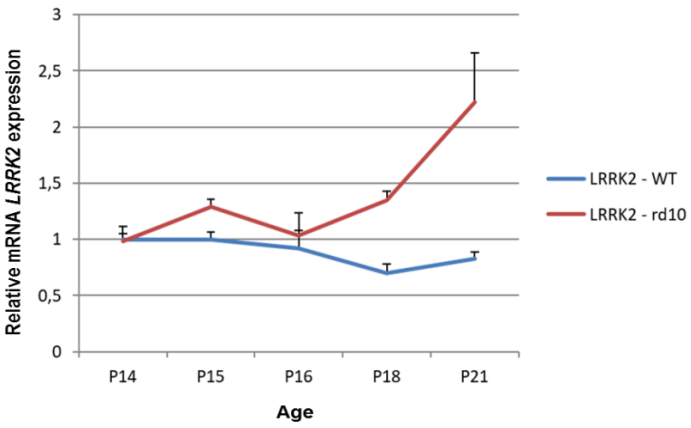

Figure 90. *Quantitative-PCR of LRRK2 expression in WT retina (red) and rd10 retina (blue). Ct values were normalized to GAPDH. Values represent averages of triplicates ± SD.*

These experiments make evident that the expression of LRRK2 increases along the neurodegeneration process. Thus, we can hypothesize that this expression increase could be related to a direct pathogenic role of LRRK2 in RP.

4.5. Determination of the neuroprotective effect of indolinone 23 in the photoreceptor layer in *rd10* mice

To assess the therapeutic effect of a LRRK2 inhibitor in RP, it was decided to administrate systemically one of our LRRK2 inhibitors in the *rd10* mice model.

Among our chemically diverse LRRK2-inhibitor chemolibrary, compound **23** an indolinone derivative was selected due to its high enzymatic activity (20 nM in LRRK2wt and 30 nM in the mutant LRRK2-G2019S). Compound **23** was administered daily at a dose of 10 mg kg^{-1} intraperitoneally (compound **23** was dissolved at a concentration of 1mg/mL and inject as 10 µL g^{-1}) from postnatal day 15 which is previous to the degeneration peak till postnatal day 24 when there is a clear degeneration of the photoreceptor layer. The animals were euthanized and samples were collected on day 25 (**Figure 91**).

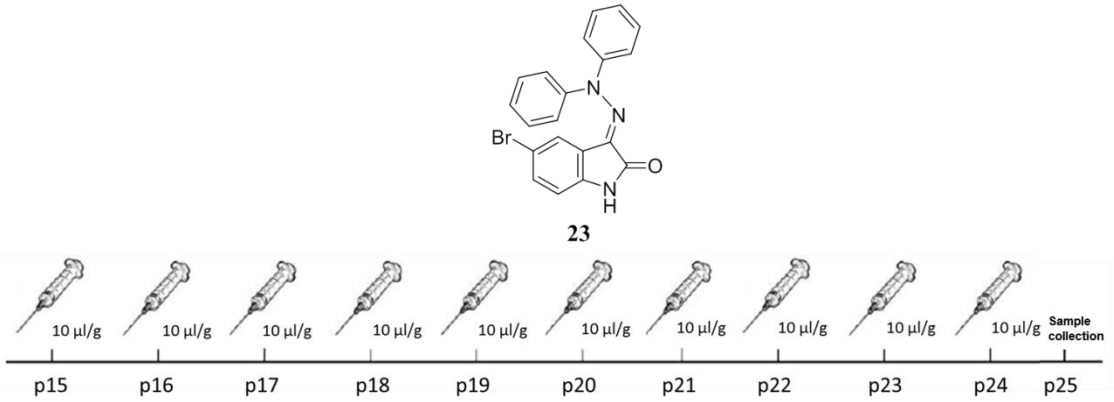

Figure 91. *Schematic representation of injection protocol.*

The eyes were cryosected in sections of 12 µm. Seven central sections in which the optic nerve was visible were selected for each animal. Sections were immunostaining with DAPI (nuclear marker). Photographs were taken by confocal microscopy at 4 different points from the optic nerve at each side. This is an important fact because the neurodegeneration process starts first at central retina (closer to the optic nerve) than in peripheral retina (**Figure 92**).

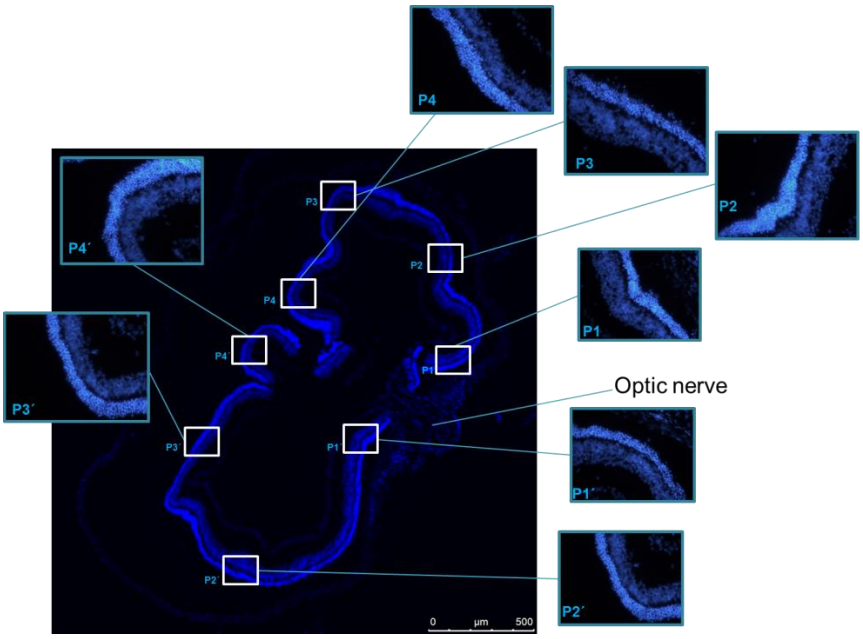

Figure 92. *Photograph of the whole retina to highlight the 4 equidistant points at each side of the optic nerve that were photographed.*

The width of the ONL and the INL of each point of each section of each animal was measured. The ratio between the width of the ONL and INL was calculated and was used as a normalization factor as the width of the INL remains constant (**Figure 93**).

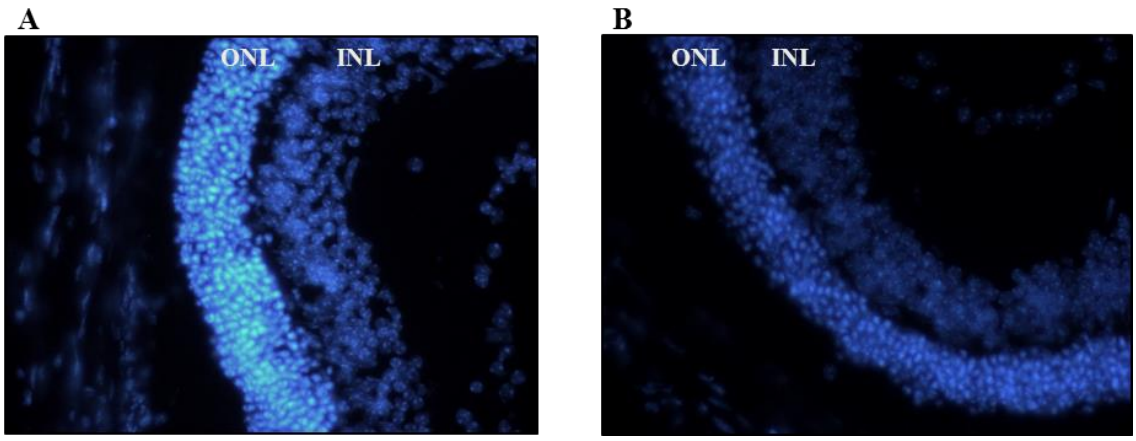

Figure 93. A/B- *Immunohistochemistry of criosections of mice rd10 retinae treated with compound **23(A)** or vehicle from postnatal day 15 to 24 (**B**). Nuclear labelling with DAPI in blue.*

Data was plotted in a spider-graph plot in which one-way ANOVA test was performed in order to determine if there are statistical significant differences between the ONL of treated animals (**Figure 94**). The higher the width of the ONL means that more photoreceptors are preserved and therefore, there is neuroprotective effect.

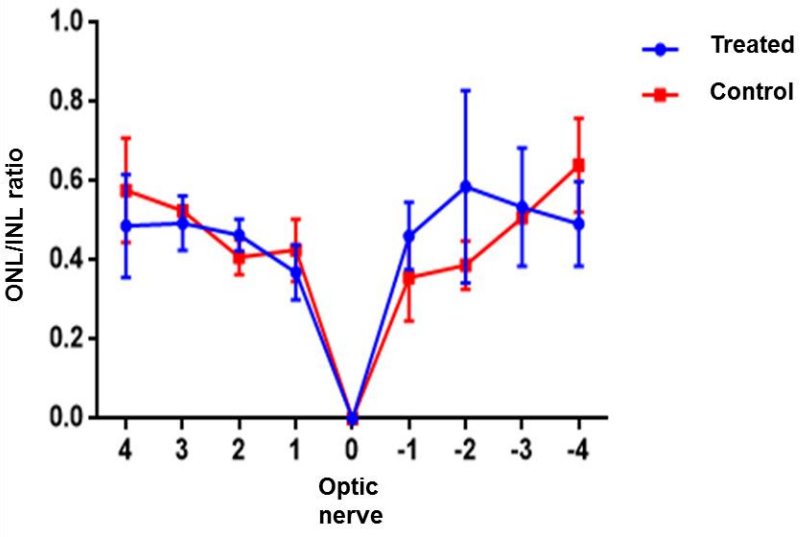

Figure 94. *Spider-graph plot in which the ratio between the width of the ONL and INL are represented for treated animals with compound **23** and for control animals (injected with the vehicle). Arbitrary points in the X-axis represent the 4 equidistant points from each side of the optic nerve in which the width was measured, showing that as expected neurodegeneration starts in central retina (closer to the optic nerve) than peripheral retina.*

These results show that there is a potential neuroprotective effect especially in peripheral retina but it did not reach statistical significance. The lack of a stronger neuroprotective effect could be attributed to the solubility issues encountered. Compound **23,** did not show high aqueous solubility and therefore, 5% of tocrosilve (a cosolvent used to increase water solubility) was used. This low aqueous solubility could mean that compound **23** could not penetrate well enough into the retina.

4.6. Determination of the anti-inflammatory effect of indolinone 23 on activated microglia

Associated with the photoreceptor loss process activation of microglial cells occurs which is made clear by the migration of these cells from the plexiform layers to the INL. The same cryosections from the previous assay were immunostained with ionized calcium-binding adapter molecule 1 (IBA-1) which is a microglia marker. Photographs were taken by confocal microscopy and microglial cells infiltrated in the INL were manually counted. Microglia, in mice injected with **23** was located preferably in plexiform layers and the INL while in animals injected with vehicle; microglia had infiltrated the ONL (**Figure 95**).

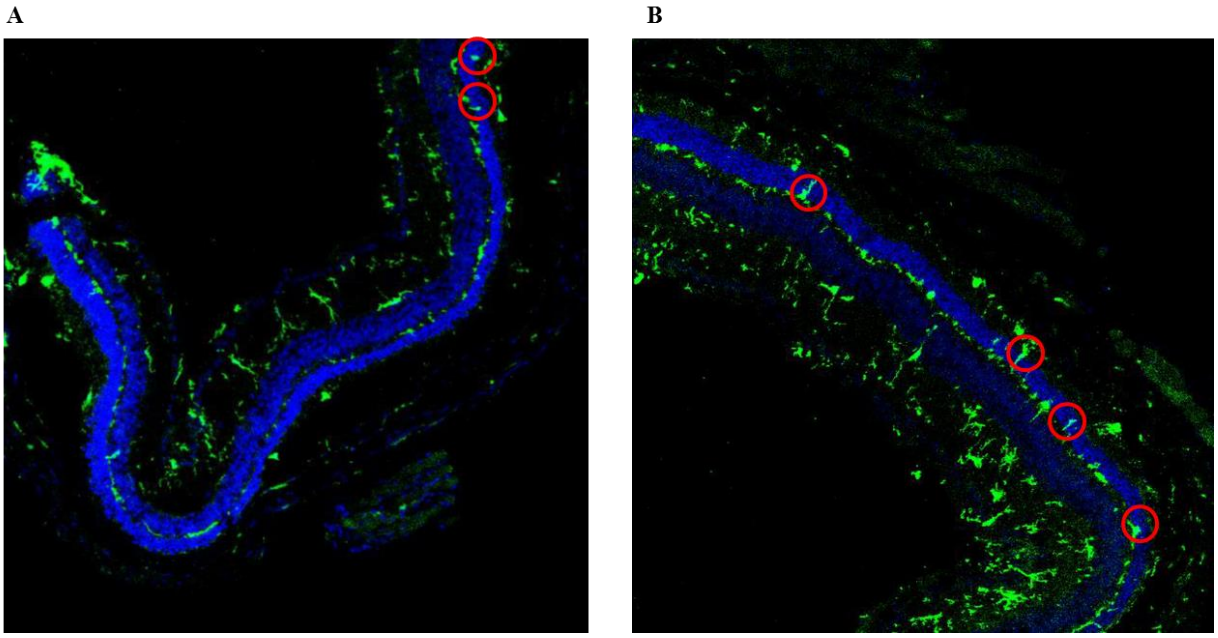

Figure 95. A/B- *Immunohistochemistry of criosections of mice rd10 retinae treated in vivo with **23(A)** or vehicle **(B)** from p15 to p24.Dapi is immunostained in blue –IBA- 1 in green. Red circles indicate the microglia infiltrated in the ONL.*

The statistical analysis of the number of microglia cells in the ONL, which has migrated from lower layers shows significant differences between the two groups of mice. In the case of mice treated with compound **23**, there is a high decrease in the number of microglia cells infiltrated in the ONL (**Figure 96**).

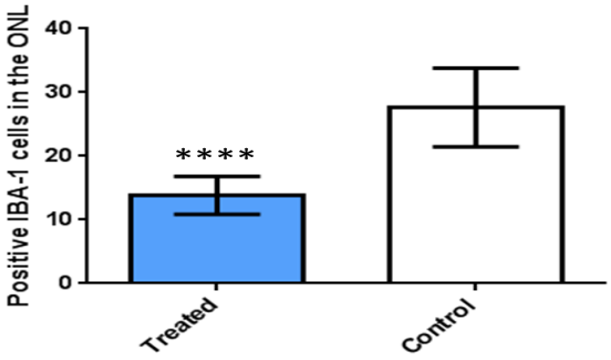

Figure 96. *Statistical analysis of the number of IBA-1 positive cells infiltrated in the ONL in treated animals with compound **23** and animals treated with vehicle. Bars represent the mean value of each cryosection ±SD).****p<0.00005.*

From these results it becomes clear that the pharmacological inhibition of LRRK2 with compound **23,** has an anti-inflammatory effect and may therefore, prevent from the neurodegeneration of the photoreceptors. Furthermore, morphological changes in the microglia were observed between control and treated animals changing from an activated

state with its characteristically amoeboid shape to a non-activated branched shape (**Figure 97**).

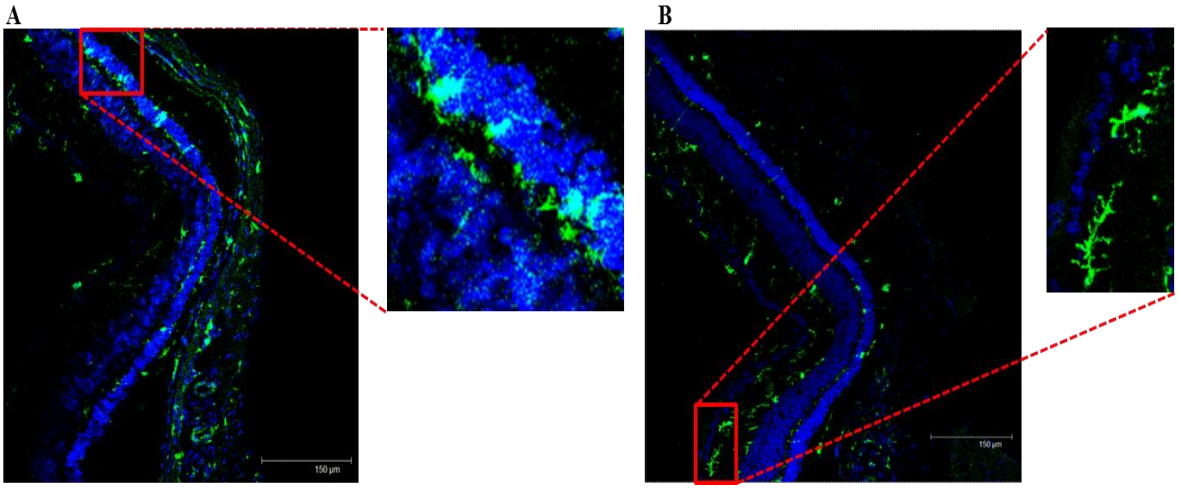

***Figure 97. A**- Amoeboid activated microglia infiltrated in the ONL of control animals. **B**-branched non-activated microglia allocated in the IPL of treated animals.*

4.7. Conclusions

In this chapter it has been shown a potential role of LRRK2 in RP. First of all, we showed that the expression of LRRK2 mRNA increases in *rd10* mice along with the neurodegeneration process.

Moreover, it has been shown that the systemically administration of a LRRK2 inhibitor, indolinone **23,** shows a trend to have neuroprotective effect with a potent anti-inflammatory effect as it reduces the number of positive IBA-1 cells infiltrated in the ONL. At this point in the study we do not know what is the direct consequence of the inhibition of LRRK2, so it would be interesting to study whether the inhibition of the enzyme acts by reducing the death of photoreceptors and this leads to less inflammatory response or by the contrary, if it reduces the inflammatory environment of the retina decreasing the damage on the photoreceptors. It is also possible that LRRK2 inhibitors act at both levels independently giving rise to a general improvement.

In next studies, different chemically diverse LRRK2 inhibitors, if possible, with better aqueous solubility (in order to avoid the use of tocrisolve) will be used to validate this enzyme as a therapeutic target, innovative in the treatment of RP.

CONCLUSIONS

In this work a chemical genetic approach for the interrogation of new biological roles of LRRK2 outside the Parkinson´s disease spectrum has addressed. For these means a chemically diverse LRRK2 inhibitor chemolibrary has been generated using compounds already synthesized in the research group and newly synthesized derivatives. The focus on new functions for LRRK2 has been placed in three fields: adult neurogenesis, tauopathies and retinal degenerations. By different *in vitro* and *in vivo* assays it has been possible to show that LRRK2 may be an interesting target for increasing adult neurogenesis, for ameliorate tauopathies and for improvement in retinal degenerations. These results show new horizons for different therapeutic indications rather than PD that LRRK2 inhibitors could be further developed.

The most important findings of this work are further summarized:

- A homology model of the kinase domain of LRRK2 was built and it was used to study the binding mode of a family of LRRK2 inhibitors containing the indolinone scaffold and to design new inhibitors.
- Design and synthesis of new indolinone derivatives and a new family of LRRK2 inhibitors containing a benzothiazole scaffold.
- Determination of the BBB penetration of the LRRK2 inhibitors chemolibrary.
- HTS to determine if the LRRK2 inhibitor chemolibrary could modulate Wnt signaling using NPC obtained from iPSC of human healthy volunteers. Eight hits were found which were then evaluated in a proliferation assay using neurospheres prepared

from the SVZ of adult mice showing a neurogenic effect by promoting the proliferation of NSCs and NPCs.

- Those chemically-diverse LRRK2 inhibitors were further tested in a differentiation assay showing that the pharmacological inhibition of LRRK2 has the potential to drive differentiation towards neuronal and oligodendrocytic cell fates.
- An in-house tau neuroprotection assay has been developed in which all of the LRRK2 inhibitor chemolibrary has shown promising neuroprotective effects.
- In a second assay these chemically diverse LRRK2 inhibitors were tested in two different human-based cellular models of tauopathies using A152T-differentiated neurons. Some hits were found in which the phosphorylation of tau was decreased with different antibodies in the two models employed.
- In an *in vivo* context a set of LRRK2 inhibitors were tested in a tauopathy *Drosophila* model in which a pathogenic eye phenotype is described. LRRK2 inhibitor **48** was able to restore this phenotype. Furthermore, inhibitor **77** was tested in a tauopathy murine model showing an increase in cognitive performance associated with a decrease of tau phosphorylation in the brain.
- A potential role for LRRK2 in RP has been shown as the expression of LRRK2 mRNA increases in a validated rodent model of RP (*rd10*) along with the neurodegeneration process.
- The systemically administration of LRRK2 inhibitor **23** in *rd10* mice shows a trend to have a neuroprotective effect but it did show a potent anti-inflammatory effect.

The completion of this work has been successful from the scientific and the educational point of view. From a scientific perspective it has been possible to show that LRRK2, one of the most-highly pursued targets in the PD, field is also a very interesting target for tauopathies, for RP and for increasing adult neurogenesis. Furthermore, we have shown for the first time LRRK2 inhibitors that also have pro-neurogenic and anti-phospho tau activity, which could then be used as multifunctional drugs. Regarding RP, we are the first ones to show that there may be a connection between this target and RP and the pharmacological inhibition of LRRK2 could be a new could be a new therapeutic indication for LRRK2 inhibitors.

DIFUSSION OF RESULTS

The results obtained along the different phases of the development of this work have been published till present time in the following papers.

Publications directly related to the work of this thesis:

- Marchena, M.; Villarejo-Zori, B.; **Zaldivar-Diez, J.**; Palomo, V.; Gil, C.; Hernandez-Sanchez, C.; Martinez, A.; de la Rosa, E.J. Small molecules targeting Glycogen Synthase Kinase 3 as potential drug candidates for the treatment of retinitis pigmentosa. *J. Enz. Inh. Med. Chem*., **2017**, *32*, 522 - 526.

- Salado, I.G^{+}.; **Zaldivar-Diez, J**$^{+}$.; Sebastian, V., Li, L.; Geiger, L.; González, S.; Campillo, N.E.; Gil, C.; Morales, A.V.; Perez, D.I.; Martinez, A. Leucine rich repeat kinase 2 (LRRK2) inhibitors based on indolinone scaffold: Potential pro-neurogenic agents. *Eur. J. Med. Chem.*, **2017**, *138*, 328 – 342.

- Sánchez-Cruz, A.; Villarejo-Zori, B.; Marchena, M.; **Zaldivar-Diez, J.**; Palomo, V.; Gil, C.; LIzasoain, I.; de la Villa P.; Martinez, A.; de la Rosa, E.J.; Hernández-Sánchez, C. Modulation of GSK-3 provides cellular and functional neuroprotection in the rd10 mouse model of retinitis pigmentosa. *Mol. Neurodegener.*, **2018**, *13* (1), 19.

- Castro-Sánchez, S^{+}.; **Zaldivar-Diez, J**$^{+}$.; Luengo, E.; López, M.G.; Gil, C.; Martínez, A.; Lastres-Becker, I. Effects of kinase LRRK2 inhibition in a tauopathy mouse model. *Alzheimer´s Res. Ther.*, **2018** (Submitted)

Other publications:

- Tyler, M.W.; **Zaldivar-Diez, J.**; Haggarty, S.J. Classics in Chemical Neuroscience: Haloperidol. *ACS Chem. Neurosci.*, **2017**, *8*, 444 – 453.

- Gandini, A.; Petralla, S.; Bartolini, M.; Zuccheri, G.; Martinez-Gonzalez, L.; Roca, C.; Campillo, N.E.; **Zaldivar-Diez, J.**; Perez, C.; Rossi, M.; Moda, F.; Monti, B.; Legname, G.; Martinez, A.; Bolognesi, M.L. Tau-centric multi-target approach for Alzheimer's disease: development of first-in-class dual glycogen synthase kinase 3β and tau-aggregation inhibitors. *J. Med. Chem.*, **2018**, *(under revision).*

EXPERIMENTAL SECTION

1. Computational studies

1.1. Homology models

The human LRRK2 sequence was retrieved from Swiss-Prot[189]. In order to produce the most accurate model, different structures retrieved from the PDB: JAK2 (PDB code: 3JY9) and TIE2 (PDB code: 1FVR) were used as templates (selected by the server Swiss-Model[188]). The next step was the sequential alignment of the LRRK2 sequence with the two templates using ClustalW[190]. The alignment results showed that the sequence of JAK2 and TIE2 were adequate to be used as templates. Then the models were built using the on-line server Swiss-Model[188]. Once the models were built, an indispensable part of every modeling procedure includes the estimation of a protein's model accuracy; here, model quality is assessed with different metrics, as follows. First, they were visualized and superimposed with the template using Sybyl-X 2.0[191] and the RMS values were calculated (the lower the RMSD between a model and the template used the better, as the model is more similar to the template[195]). Geometric evaluation of the models was performed using the Ramachandran plot[192] available from the on-line server Rampage. The Ramachandran plot is a measurement for the geometrical orientation of the amino-acids of a protein. It classifies the *phi* and *psi* angles of the backbone of a protein as favored, allowed and outlier. Finally the models were energetically evaluated with the servers Verify3D[193] (that scores the compatibility of the 3D structure of the model with the amino-acid sequence) and ERRAT[194] (that provides an overall energetic quality factor of the 3D structure).

1.2. Docking studies

Docking studies are experiments that allow determining the binding mode of a small organic molecule or ligand and a macromolecule or target. For these means molecular mechanics force fields that contain the necessary parameters (such as atomic charges, bond distances, bond angles, dihedrals, and atomic geometries among others) are used to predict the chemical behavior of the ligand and the macromolecule.

In order to carry out these studies both 3D-structures from the macromolecule and the ligand need to be prepared and adjusted according to the force field used. The target structure was prepared using Protein Preparation Wizard[279] implemented on Maestro[280]. Hydrogen atoms were added. The protein was ionized at pH = 7.2, refined carrying out H-bond assignment and restrain minimization using OPLS2005 force field[281].

Ligands were built using the 2D Sketcher module implemented in Maestro. LigPrep[282] was used in order to prepare the ligands for the docking process. LigPrep builds a 3D-structure for each ligand, ionizing them at pH = 7.2 ± 0.2, searching for one lower energy ring conformation for the aliphatic rings and calculating atomic charges using OPLS2005.

A rigid-receptor docking study was carried out using Glide[196] in the extra precision (XP) mode. The grid for the following docking process was centered on the centroid of the residues Lys1906 and Glu1920. For this docking study, OPLS2005 force field was used and a maximum number of 50 poses per ligand were reported. The best energetically ranked poses for each ligand were analyzed visually.

1.3. Quantum mechanics minimizations

Quantum mechanics calculations take into account the electronic nature of the molecules. Optimizations using quantum mechanics calculations are the best methodology for the study of the stable geometry of a small organic molecule. In our case, quantum mechanics calculations were carried out using Jaguar v9.0 software[283, 284] implemented in Maestro. Full geometry optimizations for each species studied were carried out using the density functional theory (DFT) methodology and in particular the Becke, three-parameter-Lee-Yang-Parrusing (B3LYP) with the as 6-31+G* basis set[285]. B3LYP is one of the DFT methods and is very commonly used for this type of calculations as it can predict molecule

physicochemical properties and reaction barriers with accuracy comparable to some wave function based methods but with much improved computational efficiency[285]. In addition to these calculations, distances, angles and dihedrals were measured for the optimized structures.

2. Chemistry

Substrates were purchased from commercial sources (Sigma Aldrich, Acros, Fluorochem and TCI-Europe) and used without further purification. The microwave equipment used was an Initiator TM from Biotage®. Crude residues were purified with the indicated solvent as eluent by column chromatography carried out at medium pressure using silica gel (E. Merck, Grade 60, particle size 0.040 – 0.063 mm, 230 – 240 mesh ASTM) or by IsoleraOne flash purification system from Biotage® using columns SF10-4g Si 50 AX1368-8 from Agilent Technologies and KP-Sil 10 from Biotage®. Thin Layer Chromatography was done in chromatographic sheets (Merck type 60 F254 with a width of 0.2 mm). Compounds were detected with UV light (254 nm). ^{1}H-NMR spectra were obtained on the Bruker AVANCE-300 spectrometer from the CAI-UCM working at 300 MHz. Typical spectral parameters: spectral width 16 ppm, pulse width 9 μs (57°), data size 32 K. ^{13}C-NMR experiments were carried out on the Bruker AVANCE-300 spectrometer operating at 75 MHz or on a Bruker AV 500 MHz spectrometer working at 125 MHz from the CAI-UCM. The acquisition parameters: spectral width 16 kHz, acquisition time 0.99 s, pulse width 9 μs (57°), data size 32 K. Chemical shifts are reported in values (ppm) relative to internal Me_4Si and *J* values are reported in Hz. The multiplicity of the signals (s: singlet, d: doublet, dd: doublet of doublets, t: triplet, td: triplet of doblets, q: quadruplet, qt: quintuplet, m: multiplet), the coupling constants (*J*) and the specific characterization of each compound are shown. HPLC analyses were performed on Alliance Waters 2690 equipment, with a UV detector photodiode array Waters 2996 with MS detector MicromassZQ (Waters), using an Sunfire column C18, 3.5 μm (50 mm × 4.6 mm) and acetonitrile and MilliQ water (with 0.1% formic acid) as mobile phase or in an HPLC-MS equipment form Thermo Fisher coupled to a Finnigan TM LXQ TM detector using an Sunfire column C18, 3.5 μm (50 mm × 4.6 mm) and acetonitrile and MilliQ water (with 0.1% formic acid) as mobile phase. The standard gradient consisted of a 10 min run from 0% to 100% of acetonitrile at a flow rate of 1 $mL \cdot min^{-1}$. Melting points were determined with a Buchi M560 apparatus. High resolution mass spectrometry (HRMS) was done in a

spectrometer LC/MSD 100 Hewlett Packard using positive Electro Spray techniques (ESI). Values are expressed in mass units (m/z). Elemental analyses were performed by the analytical department at CENQUIOR (CSIC) and CAI-UCM, and the results obtained were within ± 0.5% of the theoretical values using the analyzer Heraeus CHN-O-rapid.

2.1. Synthesis of indolinone derivatives

General synthetic procedure for compounds 57 - 63: The procedure described by Pandey *et al*[286] was followed with some modifications. A mixture of the isatin derivative (1 eq), the corresponding amine derivative (1 eq), MMT-K10 (20 mg for 1 mmol of the isatin derivative) and 1mL of toluene were heated under microwave irradiation at 110 ºC during 2 - 3 hours (detailed in each case). After cooling to room temperature, AcOEt (50 mL) was added and the mixture was extracted with a saturated solution of $NaHCO_3$ (50 mL x 3). Finally, the organic phase was dried over magnesium sulfate and the solvent evaporated under reduced pressure. The crude was purified as indicated in each case obtaining the desired product as a solid.

(*E*,*Z*)-5-fluoro-3-((4-phenylpiperazin-1-yl)imino)indolin-2-one (57):

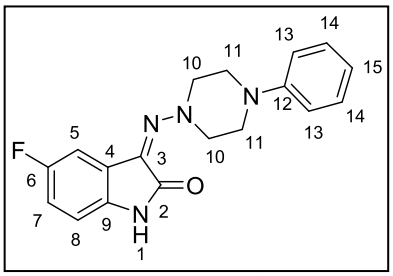

Reagents: 5-fluoroisatine (232.8 mg, 1.4 mmol), 1-amine-4-phenylpiperazine (250.0 mg, 1.4 mmol) and MMT-K10 (28.2 mg). Reaction time: 2 hours. Purification: column chromatography using Hex/AcOEt (1:2) as eluents. Yield: 304.8 mg, 65%, orange solid. *E/Z* ratio*:* 17:83. M.p.: 207 - 208 ºC. Isomer Z: ^{1}H-NMR (300 MHz, DMSO-d_6): δ 10.69 (s, 1 H, H-1), 7.30 - 7.18 (m, 2H, H-14), 7.07 (dd, *J* = 8.7, 2.6 Hz, 1H, H-7), 7.03 - 6.98 (m, 2H, H-13), 6.95 - 6.89 (m, 1H, H-5), 6.85 - 6.80 (m, 1H, H-15), 6.80 - 6.73 (m, 1H, H-8), 4.22 - 4.12 (m, 4H, H-11), 3.43 - 3.35 (m, 4H, H-10). Isomer *E*: ^{1}H-NMR (300 MHz, DMSO-d_6): δ 10.74 (s, 0.2H, H-1), 7.30 - 7.18 (m, 0.4H, H-14), 7.07 (dd, *J* = 8.7, 2.6 Hz, 0.2H, H-7), 6.97 - 6.96 (m, 0.4H, H-13), 6.95 - 6.89 (m, 0.2H, H-5) 6.85 - 6.80 (m, 0.2H, H-15), 6.80 - 6.73 (m, 0.2H, H-8), 4.22 - 4.12 (m, 0.8H, H-11) 3.45 - 3.35 (m, 0.8H, H-10). ^{13}C-NMR (75 MHz, DMSO-d_6): δ 159.0 (C-2), 150.6 (C-3), 135.3 (C-9), 129.3 (C-14), 128.0 (d, J_{C-F} = 196.0 Hz, C-6), 126.6 (C-12), 125.0 (d, J_{C-F} = 3.2 Hz, C-4), 119.5 (C-15), 116.0 (C-13), 113.4 (d, J_{C-F} = 23.9 Hz, C-5), 110.3 (d, J_{C-F} = 8.6 Hz, C-8), 105.4 (d, J_{C-F} = 25.0 Hz, C-7), 56.5 (C-11), 48.5 (C-10).

Purity HPLC: >98%. MS (ESI+): *m/z* 325.23 $[M+H]^+$. HRMS (ESI+) ($C_{18}H_{17}FN_4O$) $[M+H]^+$: Calculated: 325.14592, Found: 325.14588.

(*E,Z*)-5-bromo-3-((4-phenylpiperazin-1-yl)imino)indolin-2-one (58):

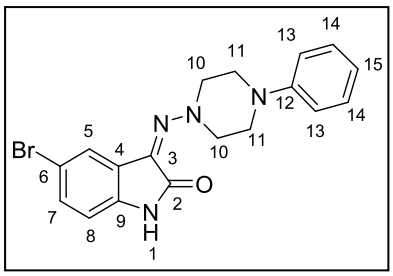

Reagents: 5-bromoisatine (250.0 mg, 1.1 mmol), 1-amine-4-phenylpiperazine (250.0 mg, 1.4 mmol) and MMT-K10 (28.2 mg). Reaction time: 2 hours. Purification: column chromatography using Hex/AcOEt (1:2) as eluents. Yield: 203.4 mg, 48%, yellow solid. *E/Z* ratio*:* 17:83. M.p.: 181 - 183 ºC. Isomer *Z*: ^{1}H-NMR (300 MHz, DMSO-d_6): δ 10.81 (s, 1H, H-1), 7.42 - 7.39 (m, 1H, H-7), 7.31 - 7.21 (m, 3H, H-5 and H-14), 7.01 (d, *J* = 7.9 Hz, 2H, H-13), 6.86 - 6.79 (m, 1H, H-15), 6.76 (d, *J* = 8.2 Hz, 1H, H-8), 4.24 - 4.15 (m, 4H, H-11), 3.44 - 3.35 (m, 4H, H-10). Isomer *E*: ^{1}H-NMR (300 MHz, DMSO-d_6): δ 10.87 (s, 0.2H, H-1), 7.52 - 7.50 (m, 0.2H, H-7), 7.31 - 7. 21 (m, 0.6H, H-5 and H-14), 7.01 (d, *J* = 7.9 Hz, 0.4H, H-13), 6.81 - 6.79 (m, 0.2H, H-15) 6.76 (d, J = 8.2 Hz, 0.2H, H-8), 4.24 - 4.15 (m, 0.8H, H-11), 3.44 - 3.35 (m, 0.8H, H-10). ^{13}C-NMR (75 MHz, DMSO-d_6): δ 158.3 (C-2), 150.3 (C-3), 137.7 (C-9), 129.0 (C-14), 127.2 (C-6), 123.4 (C-7), 120.3 (C-12), 119.3 (C-15), 115.7 (C-13), 115.6 (C-4), 113.0 (C-5), 111.1 (C-8), 56.3 (C-11), 48.2 (C-10). Purity HPLC: >98%. MS (ESI+): *m/z* 387.17 [M+2]. HRMS (ESI+) ($C_{18}H_{17}BrN_4O$) $[M+H]^+$: Calculated: 385.06585, Found: 385.06469.

(*E,Z*)-5-chloro-3-((4-phenylpiperazin-1-yl)imino)indolin-2-one (59):

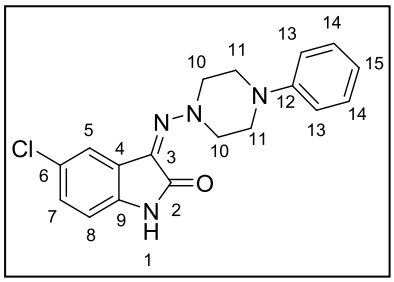

Reagents: 5-chloroisatine (250.0 mg, 1.4 mmol), 1-amine-4-phenylpiperazine (243.9 mg, 1.4 mmol) and MMT-K10 (28.2 mg). Reaction time: 2 hours. Purification: column chromatography using Hex/AcOEt (1:2) as eluents. Yield: 304.8 mg, 65%, orange solid. *E/Z* ratio*:* 9:91. M.p.: 207 - 208 ºC. Isomer *Z*: ^{1}H-NMR (300 MHz, DMSO-d_6): δ 10.79 (s, 1H, H-1), 7.29 - 7.19 (m, 3H, H-5 and H-14), 7.13 (dd, *J* = 8.2, 2.2 Hz, 1H, H-7), 7.00 (d, *J* = 7.9 Hz, 2.35H, H-13), 6.81 (m, 2H, H-8 and H-15), 4.24 - 4.14 (m, 4H, H-11), 3.43 - 3.30 (m, 4H, H-10). Isomer *E*: ^{1}H-NMR (300 MHz, DMSO-d_6): δ 10.85 (s, 0.1H, H-1), 7.29 - 7.19 (m, 0.3H, H-5 and H-14), 7.13 (dd, *J* = 8.2, 2.2Hz, 0.1 H, H-7), 7.00 (d, *J* = 7.9 Hz, 0.2H, H-13), 6.92 (m, 0.2H, H-8 and H-15), 4.24 - 4.14 (m, 0.4H, H-11), 3.43 - 3.30 (m, 0.4H, H-10). ^{13}C-NMR (75 MHz, DMSO-d_6): δ 158.4 (C-2), 150.3 (C-3), 137.3 (C-9),

129.0 (C-14), 126.8 (C-6), 126.2 (C-7), 125.3 (C-4), 123.6 (C-12), 119.3 (C-15), 117.6 (C-5), 115.8 (C-13), 110.7 (C-8), 56.3 (C-11), 48.2 (C-10). Purity HPLC: >98%. MS (ESI+): *m/z* 341.15 $[M+H]^+$. HRMS (ESI+) ($C_{18}H_{17}ClN_4O$) $[M+H]^+$: Calculated: 341.11637, Found: 341.11568.

(*E,Z*)-5-iodo-3-((4-phenylpiperazin-1-yl)imino)indolin-2-one (60):

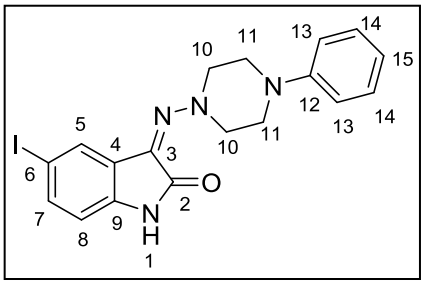

Reagents: 5-iodoisatine (144.7 mg, 0.5 mmol), 1-amine-4-phenylpiperazine (93.7 mg, 0.5 mmol) and MMT-K10 (10.6 mg). Reaction time: 2 hours. Purification: column chromatography using Hex/AcOEt (1:2) as eluents. Yield: 68.7 mg, 30%, orange solid. *E/Z* ratio*:* 17:83. M.p.: 195 - 198 ºC Isomer *Z:* ^{1}H-NMR (300 MHz, DMSO-d_6): δ 10.79 (s, 1H, H-1), 7.56 (s, 1H, H-5), 7.43 (dd, *J* = 8.1, 1.7 Hz, 1H, H-7), 7.28 - 7.21 (m, 2H, H-14), 7.00 (m, 2H, H-13), 6.84 - 6.79 (m, 1H, H-15), 6.65 (d, *J* = 8.1 Hz, 1H, H-8), 4.22 - 4.13 (m, 4H, H-11), 3.44 - 3.35 (m, 4H, H-10). Isomer *E*: ^{1}H-NMR (300 MHz, DMSO-d_6): δ 10.84 (s, 0.2H, H-1), 7.67 (s, 0.2H, H-5), 7.43 (dd, *J* = 8.1, 1.7 Hz, 0.2 H, H-7), 7.28 - 7.21 (m, 0.4H, H-14), 7.00 (m, 0.4H, H-13) 6.79 - 6.75 (m, 0.2H, H-15), 6.64 (d, *J* = 8.1 Hz, 0.2H, H-8), 4.22 - 4.13 (m, 0.8H, H-11), 3.44 - 3.35 (m, 0.8 H, H-10). ^{13}C-NMR (75 MHz, DMSO-d_6): δ 158.0 (C-2), 150.3 (C-3), 138.2 (C-9), 134.9 (C-6), 129.0 (C-14), 127.5 (C-7), 126.0 (C-4), 123.4 (C-12), 119.2 (C-15), 115.7 (C-13), 115.6 (C-5), 111.7 (C-8), 59.8 (C-11), 48.2 (C-10). Purity HPLC: >98% MS (ESI+): *m/z* 433.13 $[M+H]^+$. HRMS (ESI+) ($C_{18}H_{17}IN_4O$) $[M+H]^+$: Calculated: 433.05198, Found: 433.05241.

(*E,Z*)-5-fluoro-3-((4methylpiperazin-1-yl)imino)indolin-2-one (61):

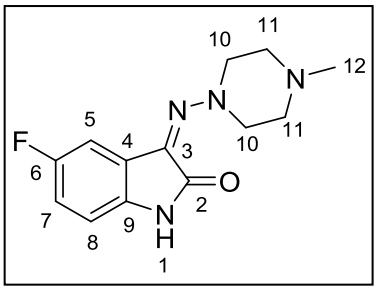

Reagents: 5-fluoroisatine (250.0 mg, 1.5 mmol), 1-amine-4-methylpiperazine (173.9 mg, 1.5 mmol) and MMT-K10 (30.2 mg). Reaction time: 3 hours. Purification: recrystallization from Hex/CH_2Cl_2 (9:1). Yield: 316.9 mg, 80%, orange solid. *E/Z* ratio*:* 17:83. M.p.: 150 - 152 ºC. Isomer *Z:* ^{1}H-NMR (300 MHz, $CDCl_3$): δ 7.90 (s, 1H, H-1), 7.13 (dd, *J* = 8.6, 2.6 Hz, 1H, H-5), 6.75 (td, *J* = 9.2, 2.6 Hz, 1H, H-7), 6.69 - 6.71 (m, 1H, H-8), 4.20 - 4.10 (m, 4H, H-10), 2.70 - 2.57 (m, 4H, H-11), 2.36 (s, 3H, H-12). Isomer *E:* ^{1}H-NMR (300 MHz, $CDCl_3$): δ 8.77 (s, 0.2H, H-1), 7.13 (dd, *J* = 8.6, 2.6 Hz, 0.2H, H-5), 6.75 (td, *J* = 9.2, 2.6 Hz, 0.2H, H-7), 6.69 - 6.71 (m, 0.2H, H-8), 3.56 - 3.48 (m, 0.8H, H-

10), 2.70 - 2.57 (m, 0.8H, H-11), 2.39 (s, 0.6H, H-12).^{13}C-NMR (75 MHz, DMSO-d_6): δ 158.7 (C-2), 139.6 (C-3) 134.8 (C-9), 125.6 (d, J_{C-F} = 218.3 Hz, C-6), 123.7 (C-4), 112.9 (d, J_{C-F} = 23.9 Hz, C-5), 109.9 (d, J_{C-F} = 8.34 Hz, C-8), 104.7 (d, J_{C-F} = 25.4 Hz, C-7), 56.4 (C-10), 54.4 (C-11), 45.3 (C-12). Purity HPLC: >98%. MS (ESI+): *m/z* 263.12 $[M+H]^+$. HRMS (ESI+) ($C_{13}H_{15}FN_4O$) $[M+H]^+$: Calculated: 263.13027, Found: 263.13015.

(*E,Z*)-5-chloro-3-((4-methylpiperazin-1-yl)imino)indolin-2-one (62):

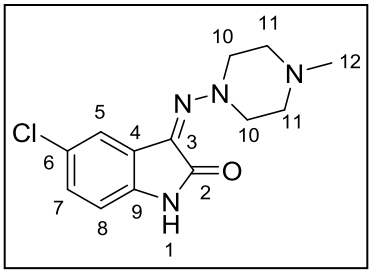

Reagents: 5-chloroisatine (250.0 mg, 1.4 mmol), 1-amine-4-methylpiperazine (158.5 mg, 1.4 mmol) and MMT-K10 (27.5 mg). Reaction time: 2 hours. Purification: recrystallization from Hex/CH_2Cl_2 (9:1). Yield: 326.0 mg, 80%, orange solid. *E/Z* ratio*:* 17:83. M.p.: 173 - 174 ºC. Isomer *Z:* ^{1}H-NMR (300 MHz, DMSO-d_6) δ 10.73 (s, 1H, H-1), 7.24 (d, *J* = 2.0 Hz, 1H, H-5), 7.12 (dd, *J* = 8.2, 2.0 Hz, 1H, H-7), 6.79 (d, *J* = 8.3 Hz, 1H, H-8), 4.14 - 3.98 (m, 4H, H-10), 2.56 - 2.47 (m, 4H, H-11), 2.24 (s, 3H, H-12). Isomer *E*: ^{1}H-NMR (300 MHz, DMSO-d_6): δ 10.80 (s, 0.2H, H-1), 7.38 (dd, *J* = 8.2, 2.0 Hz, 0.2H, H-7), 7.28 (d, *J* = 2.0 Hz, 0.2H, H-5), 6.91 (d, *J* = 8.3 Hz, 0.2H, H-8), 4.14 - 3.98 (m, 0.8H, H-10), 2.56 - 2.47 (m, 0.8H, H-11), 2.26 (s, 0.6H, H-12). ^{13}C-NMR (75 MHz, DMSO-d_6): δ 158.6 (C-2), 137.4 (C-3), 127.2 (C-9), 126.2 (C-5), 125.5 (C-4), 123.0 (C-6), 117.6 (C-7), 110.7 (C-8), 56.7 (C-10), 54.7 (C-11), 45.5 (C-12). Purity HPLC: >98%. MS (ESI+): *m/z* 279.15 $[M+H]^+$. HRMS (ESI+) ($C_{13}H_{15}ClN_4O$) $[M+H]^+$: Calculated: 279.1007, Found: 279.1016.

(*E,Z*)-5-bromo-3-((4-methylpiperazin-1-yl)imino)indolin-2-one (63):

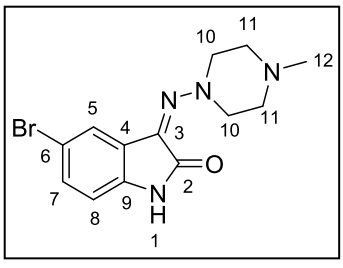

Reagents: 5-bromoisatine (250.0 mg, 1.2 mmol), 1-amine-4-methylpiperazine (133.1 mg, 1.2 mmol) and MMT-K10 (23.2 mg). Reaction time: 2 hours. Purification: recrystallization from Hex/CH_2Cl_2 (9:1). Yield: 326.0 mg, 70%, orange solid. *E/Z* ratio*:* 9:91. M.p.: 179 - 180 ºC. Isomer *Z:* ^{1}H-NMR (300 MHz, DMSO-d_6) δ 10.73 (s, 1H, H-1), 7.35 (d, *J* = 2.0Hz, 1H, H-5), 7.24 (dd, *J* = 8.3, 2.0Hz, 1H, H-7), 6.73 (d, *J* = 8.3 Hz, 1H, H-8), 4.11 - 3.99 (m, 4H, H-10), 2.55 - 2.45 (m, 4H, H-11), 2.23 (s, 3H, H-12). Isomer *E:* ^{1}H-NMR (300 MHz, DMSO-d_6): δ 10.80 (s, 0.1H, H-1), 7.49 (dd, *J* = 8.3, 2.0 Hz, 0.1H, H-7), 7.40 (d, *J* = 2.0 Hz, 0.1H, H-5), 6.85 (d, *J* = 8.3 Hz, 0.1 H, H-8), 4.11 - 3.99 (m, 0.4H. H-10), 2.55 - 2.45 (m, 0.4H. H-11), 2.25 (s, 0.3H, H-12). ^{13}C-NMR (75 MHz, DMSO-d_6): δ 158.2 (C-2), 137.5 (C-3), 128.7 (C-9), 127.4 (C-5), 122.5 (C-

4), 120.1 (C-6), 112.9 (C-7), 111.0 (C-8), 56.5 (C-10), 54.4 (C-11), 45.3 (C-12). Purity HPLC: >98%. MS (ESI+): *m/z* 325.14 [M+2]. HRMS (ESI+) ($C_{13}H_{15}BrN_4O$) $[M+H]^+$: Calculated: 323.0502, Found: 323.05025.

2.2. Synthesis of benzothiazole derivatives

General synthetic procedure for compounds 64 - 81: The synthesis of the *N*-(benzothiazole-2-yl)-aryl-amide derivatives was performed by a coupling reaction between the corresponding 2-amino-benzothiazole and the corresponding aromatic acid. Each 2-amino-benzothiazole was mixed with the aromatic acid in CH_2Cl_2 or THF (specified for each case) at the specific temperature and time detailed for each compound and in the presence of the corresponding coupling agent and the corresponding basic catalyst. Previously, the aromatic acid was activated with the coupling agent and the basic catalyst for a certain time and temperature and then the corresponding 2-amino-benzothiazole was added. After the indicated time, the reaction mixture was washed with different inorganic solutions, detailed in each case. Finally, the organic phase was dried over magnesium sulfate and the solvent was evaporated under reduced pressure. The crude was purified as indicated for each compound obtaining the desired product as a solid.

***N*-(6-methoxybenzothiazol-2-yl)-4-morpholinobenzamide (64):**

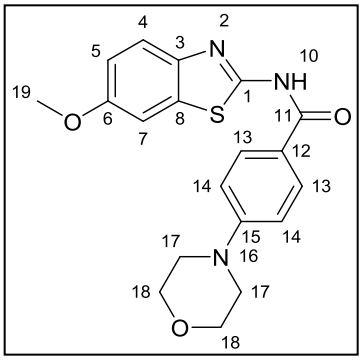

Reagents: 4-morpholinobenzoic acid (230.0 mg, 1.1 mmol), EDCI (276.6 mg, 1.4 mmol), DMAP (24.4 mg, 0.2 mmol), triethylamine (248 µL, 1.8 mmol) and 2-amino-6-methoxybenzothiazole (200.0 mg, 1.1 mmol) dissolved in CH_2Cl_2. Activation reaction: 1 hour at r.t. Coupling reaction: overnight at r.t. Work-up: washes with saturated $NaHCO_3$ and saturated NaCl solutions. Purification: column chromatography using CH_2Cl_2/MeOH (50:1) as eluents. Yield: 36.0 mg, 9%, yellow solid. M.p.: 237.6 - 240.0 ºC. ^{1}H-NMR (300 MHz, $CDCl_3$) δ 9.47 (s, 1H, H-10), 7.88 (d, *J* = 9.0 Hz, 2H, H-13), 7.64 (d, *J* = 8.8 Hz, 1H, H-4), 7.33 (d, *J* = 2.6 Hz, 1H, H-7), 7.04 (dd, *J* = 8.8, 2.6 Hz, 1H, H-5), 6.94 (d, *J* = 9.0 Hz, 2H, H-14), 3.93 - 3.83 (m, 7H, H-18 and H-19), 3.36 - 3.31 (m, 4H, H-17). ^{13}C-NMR (75 MHz, DMSO-d_6) δ 164.8 (C-11), 156.9 (C-1), 156.0 (C-15), 153.8, (C-3), 142.7 (C-6), 132.8 (C-8), 129.8 (C-13), 120.8 (C-5), 120.5 (C-4), 114.80 (C-7), 113.1 (C-14), 104.6 (C-12), 65.8 (C-18), 55.6 (C-19), 46.8 (C-17). Purity

HPLC: 95%. MS (ESI+): *m/z* 370 $[M+H]^+$. HRMS (ESI+) ($C_{19}H_{19}N_3O_3S$) $[M+H]^+$: Calculated: 370.12199, Found: 370.12218.

N-(6-trifluoromethylbenzothiazol-2-yl)-4-morpholinobenzamide (65):

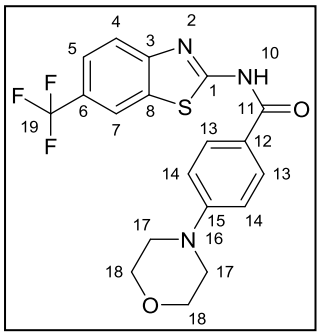

Reagents: 4-morpholinobenzoic acid (189.9 mg, 0.9 mmol), EDCI (228.5 mg, 1.4 mmol), DMAP (22.4 mg, 0.2 mmol), triethylamine (223 μL, 1.8 mmol) and 2-amino-6-trifluoromethylbenzothiazole (200.0 mg, 0.9 mmol) dissolved in CH_2Cl_2. Activation reaction: 1 hour at r.t. Coupling reaction: overnight at r.t. Work-up: washes with saturated $NaHCO_3$ and saturated NaCl solutions. Purification: column chromatography using Hex/AcOEt (50:1) as eluents. Yield: 79.0 mg, 26%, yellow solid. M.p. : 218.5 - 218.5 ºC. ^{1}H-NMR (300 MHz, $CDCl_3$) δ 8.14 (s, 1H, H-7), 7.96 (d, *J* = 8.9 Hz, 2H, H-13), 7.73 - 7.57 (m, 2H, H-4 and H-5), 6.89 (d, *J* = 8.9 Hz, 2H, H-14), 3.92 - 3.81 (m, 4H, H-18), 3.36 - 3.27 (m, 4H, H-17). ^{13}C-NMR (125 MHz, $CDCl_3$) δ 163.8 (C-11), 160.8 (C-1), 153.5 (C-15), 149.4 (C-3), 131.2 (C-8), 128.6 (C-13), 124.9 (q, J_{C-F} = 32.5 Hz, C-6), 123.3 (q, J_{C-F} = 272.1 Hz, C-19), 122.1 (q, J_{C-F} = 3.4 Hz, C-5) 119.8 (C-4), 119.6 (C-12), 118.04 (q, J_{C-F} = 4.4 Hz, C-7), 112.7 (C-14), 65.4 (C-18), 46.3 (C-17). Purity HPLC: 95%. MS (ESI+): *m/z* 408 $[M+H]^+$. Elemental analysis ($C_{19}H_{16}F_3N_30_2S$) Calculated: C 56.01%, H 3.96%, N 10.31%, S 7.87%. Found: C 56.13%, H 3.98%, N 10.38%, S 7.59%.

N-(6-methylbenzothiazol-2-yl)-4-morpholinobenzamide (66):

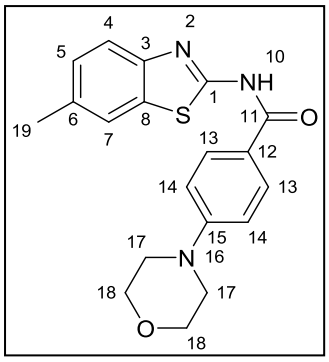

Reagents: 4-morpholinobenzoic acid (252.4 mg, 1.2 mmol), EDCI (303.5 mg, 1.6 mmol), DMAP (20.1 mg, 0.2 mmol), triethylamine (272 μL, 1.9 mmol) and 2-amino-6-methylbenzothiazole (200.0 mg, 0.9 mmol) dissolved in CH_2Cl_2. Activation reaction: 6 hours at r.t. Coupling reaction: overnight at r.t. Work-up: washes with HCl (0.1M), saturated $NaHCO_3$ and saturated NaCl solutions. Purification: automatic chromatographic system (Biotage®Isolera One) using Hex/AcOEt as eluents. Yield: 43.0 mg, 10%, yellow solid. M. p.: 287.7 - 288.8 ºC. ^{1}H-NMR (300 MHz, $CDCl_3$) δ 10.56 (s, 1H, H-10), 7.89 (d, *J* = 8.9 Hz, 2H, H-13), 7.63 (s, 1H, H-7), 7.42 (d, *J* = 8.3 Hz, 1H, H-4), 7.16 (dd, *J* = 8.3, 1.7 Hz, 1H, H-5), 6.85 (d, *J* = 8.9 Hz, 2H, H-14), 3.87 - 3.83 (m, 4H, H-

18), 3.29 - 3.26 (m, 4H, H-17), 2.46 (s, 3H, H-19). ^{13}C-NMR (75 MHz, $CDCl_3$) δ 164.7 (C-11), 158.5 (C-1), 154.2 (C-15), 146.1 (C-3), 133.7 (C-6), 132.3 (C-8), 129.4 (C-13), 127.5 (C-5), 121.3 (C-12), 121.1 (C-7), 120.3 (C-4), 113.8 (C-14), 66.5 (C-18), 47.5 (C-17), 21.4 (C-19). Elemental analysis ($C_{19}H_{19}N_3O_2S$) Calculated: C 64.57%, H 5.42%, N 11.89%, S 9.07%. Found: C 64.33%, H 5.38%, N 11.85%, S 8.96%.

_N_-(6-chlorobenzothiazol-2-yl)-4-morpholinobenzamide (67):

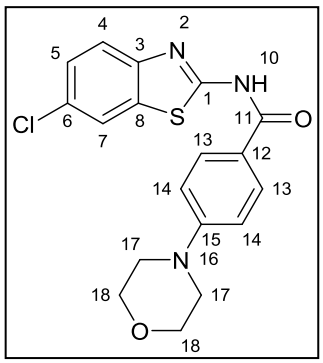

Reagents: 4-morpholinobenzoic acid (224.4 mg, 1.1 mmol), EDCI (269.9 mg, 1.4 mmol), DMAP (26.4 mg, 0.2 mmol), triethylamine (242 μL, 1.7 mmol) and 2-amino-6-chlorobenzothiazole (200.0 mg, 1.1 mmol) dissolved in CH_2Cl_2. Activation reaction: 1 hour at r.t. Coupling reaction: overnight at r.t. Work-up: washes with HCl (0.1M), saturated $NaHCO_3$ and saturated NaCl solutions. Purification: automatic chromatographic system (Biotage®Isolera One) using Hex/AcOEt as eluents. Yield: 96.0 mg, 24%, white solid. M.p.: 245.4 - 246.4 ºC. ^{1}H-NMR (300 MHz, $CDCl_3$) δ 10.25 (s, 1H, H-10), 7.89 (d, *J* = 8.9 Hz, 2H, H-13), 7.81 (d, *J* = 2.1 Hz, 1H, H-7), 7.52 (d, *J* = 8.7 Hz, 1H, H-4), 7.33 (dd, *J* = 8.7, 2.1 Hz, 1H, H-5), 6.89 (d, *J* = 9.0 Hz, 2H, H-14), 3.92 - 3.82 (m, 4H, H-18), 3.33 - 3.30 (m, 4H, H-17). ^{13}C-NMR (75 MHz, $CDCl_3$) δ 164.5 (C-11), 159.3 (C-1), 154.4 (C-15), 146.9 (C-3), 133.5 (C-8), 129.4 (C-13), 126.7 (C-5), 121.5 (C-4), 121.0 (C-7), 120.8 (C-12), 113.7 (C-14), 107.0 (C-6), 66.5 (C-18), 47.4 (C-17). Purity HPLC: 97%. MS (ESI+): *m/z* 374 $[M+H]^+$. Elemental analysis ($C_{18}H_{16}ClN_3O_2S$) Calculated: C 57.83%, H 4.31%, N 11.24%, S 8.58%. Found: C 57.56%, H 4.09%, N 11.43%, S 8.40%.

_N_-(6-fluorobenzothiazol-2-yl)-4-morpholinobenzamide (68):

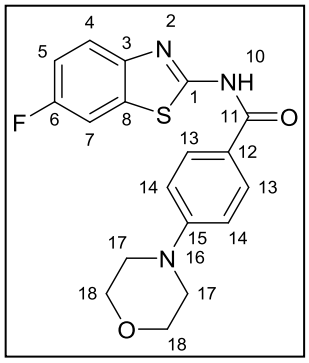

Reagents: 4-morpholinobenzoic acid (168.2 mg, 1.2 mmol), EDCI (296.3 mg, 1.5 mmol), DMAP (29.1 mg, 0.2 mmol), triethylamine (265 μL, 1.9 mmol) and 2-amino-6-fluorobenzothiazole (200.0 mg, 1.2 mmol) dissolved in CH_2Cl_2. Activation reaction: 1 hour at r.t. Coupling reaction: overnight at r.t. Work-up: washes with HCl (0.1M), saturated $NaHCO_3$ and saturated NaCl solutions. Purification: automatic chromatographic system (Biotage®Isolera

One) using Hex/AcOEt as eluents. Yield: 79.0 mg, 19%, white solid. M.p.: 228.3 - 229.3 ºC. ^{1}H-NMR (300 MHz, $CDCl_3$) 7.90 (d, *J* = 8.9 Hz, 2H, H-13), 7.54 (dd, *J* = 8.9, 4.6 Hz, 1H, H-7), 7.48 (dd, *J* = 7.9, 2.6 Hz, 1H, H-4), 7.10 (td, *J* = 7.9, 2.6 Hz, 1H, H-5), 6.85 (d, *J* = 8.9 Hz, 2H, H-14), 3.87 - 3.85 (m, 4H, H-18), 3.34 - 3.30 (m, 4H, H-17). ^{13}C-NMR (125 MHz, $CDCl_3$) δ 165.4 (C-11), 160.0 (d, J_{C-F} = 243.5 Hz, C-6), 159.9 (C-1), 154.7 (C-15), 144.8 (C-3), 133.4 (d, J_{C-F} = 10.5 Hz, C-8), 130.0 (C-13), 121.9 (d, J_{C-F} = 9.0 Hz, C-4), 121.4 (C-12), 114.7 (d, J_{C-F} = 24.5 Hz, C-5), 114.1 (C-14), 108.0 (d, J_{C-F} =26.5 Hz, C-7), 66.9 (C-18), 47.8 (C-17). Purity HPLC: 98%. MS (ESI+): *m/z* 358 $[M+H]^+$. Elemental analysis ($C_{18}H_{16}FN_3O_2S$) Calculated: C 60.49%, H 4.51%, N 11.76%, S 8.97%. Found: C 60.68%, H 4.50%, N 11.55%, S 8.72%.

***N*-(4-methylbenzothiazol-2-yl)-4-morpholinobenzamide (69):**

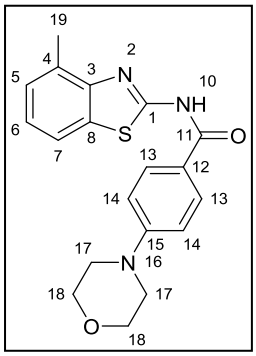

Reagents: 4-morpholinobenzoic acid (252.4 mg, 1.2 mmol), EDCI (303.5 mg, 1.6 mmol), DMAP (24.6 mg, 0.2 mmol), triethylamine (272 μL, 1.9 mmol) and 2-amino-4-methylbenzothiazole (200.0 mg, 1.2 mmol) dissolved in CH_2Cl_2. Activation reaction: 1 hour at r.t. Coupling reaction: overnight at r.t. Work-up: washes with HCl (0.1M), saturated $NaHCO_3$ and saturated NaCl solutions. Purification: automatic chromatographic system (Biotage®Isolera One) using Hex/AcOEt as eluents. Yield: 93.0 mg, 45%, white solid. M.p.: 289 - 290 ºC. ^{1}H-NMR (300 MHz, $CDCl_3$) δ 10.29 (s, 1H, H-10), 7.93 (d, *J* = 9.0 Hz, 2H, H-13), 7.74 (d, *J* = 7.9 Hz, 1H, H-5), 7.47 (d, *J* = 7.9 Hz, 1H, H-7), 7.25 (t, *J* = 7.9 Hz, 1H, H-6) 6.94 (d, *J* = 9.0 Hz, 2H, H-14), 3.90 - 3.86 (m, 4H, H-18), 3.36 - 3.33 (m, 4H, H-17), 2.64 (s, 3H, H-19).^{13}C-NMR (75 MHz, $CDCl_3$) δ 164.3 (C-11), 157.8 (C-1), 154.2 (C-15), 147.5 (C-3), 132.0 (C-6), 130.4 (C-8), 129.2 (C-13), 126.8 (C-4), 123.8 (C-5), 121.2 (C-12), 118.8 (C-7), 113.7 (C-14), 66.5 (C-18), 47.4 (C-17), 18.1 (C-19). Purity HPLC: >99%. MS (ESI+): *m/z* 354 $[M+H]^+$. HRMS (ESI+) ($C_{19}H_{19}N_3O_2S$) $[M+H]^+$: Calculated: 354.12707, Found: 354.12705.

***N*-(4-chlorobenzothiazol-2-yl)-4-morpholinobenzamide (70):**

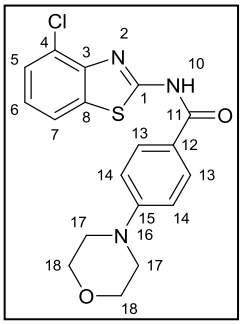

Reagents: 4-morpholinobenzoic acid (224.5 mg, 1.1 mmol), EDCI (269.9 mg, 1.5 mmol), DMAP (24.5 mg, 0.2 mmol), triethylamine (272 µL, 1.9 mmol) and 2-amino-4-chlorobenzothiazole (200.0 mg, 1.2 mmol) dissolved in CH_2Cl_2. Activation reaction: 1 hour at r.t. Coupling reaction: overnight at r.t. Work-up: washes with HCl (0.1M), saturated $NaHCO_3$ and saturated NaCl solutions. Purification: automatic chromatographic system (Biotage®Isolera One) using Hex/AcOEt as eluents. Yield: 29.0 mg, 5%, white solid. M.p.: 148.5 - 150 ºC. ^{1}H-NMR (300 MHz, $CDCl_3$) δ 7.98 (d, *J* = 9.0 Hz, 2H, H-13), 7.75 (dd, *J* = 7.9, 1.0 Hz, 1H, H-5), 7.49 (dd, *J* = 7.9, 1.0 Hz, 1H, H-7), 7.29 (t, *J* = 7.9 Hz, 1H, H-6), 6.95 (d, *J* = 9.0 Hz, 2H, H-14), 3.92 - 3.82 (m, 4H, H-18), 3.40 - 3.30 (m, 4H, H-17). ^{13}C-NMR (75 MHz, $CDCl_3$) δ 163.3 (C-11), 158.6 (C-1), 153.4 (C-15), 144.0 (C-3), 132.3 (C-8), 128.4 (C-13), 125.5 (C-12), 124.0 (C-7) 123.5 (C-6), 119.4 (C-5), 119.0 (C-4), 112.8 (C-14), 65.5 (C-18), 46.4 (C-17). Purity HPLC: >99%. MS (ESI+): *m/z* 374 $[M+H]^+$. Elemental analysis ($C_{18}H_{16}ClN_3O_2S$) Calculated: C 59.83%, H 4.31%, N 11.24%, S 8.58%. Found: C 57.44%, H 4.78%, N 10.84%, S 8.04%.

***N*-(6-ethoxybenzothiazol-2-yl)-4-morpholinobenzamide (71):**

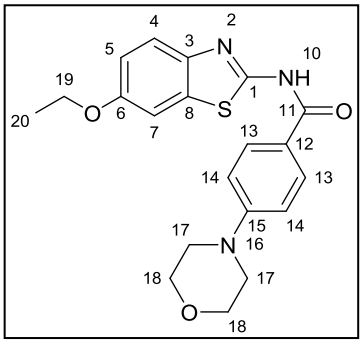

Reagents: 4-morpholinobenzoic acid (213.1 mg, 1.0 mmol), EDCI (256.2 mg, 1.3 mmol), DMAP (25.1 mg, 0.2 mmol), triethylamine (272 µL, 1.9 mmol) and 2-amino-6-ethoxybenzothiazole (200.0 mg, 1.0 mmol) dissolved in CH_2Cl_2. Activation reaction: 6 hours at r.t. Coupling reaction: overnight at r.t. Work-up: washes with HCl (0.1M), saturated $NaHCO_3$ and saturated NaCl solutions. Purification: automatic chromatographic system (Biotage®Isolera One) using Hex/AcOEt as eluents. Yield: 20.0 mg, 5%, white solid. M.p.: 222.8 - 223.8 ºC. ^{1}H-NMR (300 MHz, $CDCl_3$) δ 7.95 (d, *J* = 8.9 Hz, 2H, H-13), 7.49 (d, *J* = 8.9 Hz, 1H, H-4), 7.30 (d, *J* = 2.4 Hz, 1H, H-7), 7.04 (dd, *J* = 8,9, 2.4 Hz, 1H, H-5), 6.89 (d, *J* = 8.9 Hz, 2H, H-14), 4.09 (q, *J* = 6.9 Hz, 2H, H-19), 3.89 - 3.69 (m, 4H, H-18), 3.38 - 3.25 (m, 4H, H-17), 1.43 (t, *J* = 6.9 Hz, 3H, H-20). ^{13}C-NMR (75 MHz, $CDCl_3$) δ 163.4 (C-11), 157.1 (C-1), 155.3 (C-15), 153.3 (C-3), 139.1 (C-6), 131.4 (C-8), 128.6 (C-13), 119.7 (C-5), 119.5 (C-4), 114.9 (C-7), 112.7 (C-14), 104.1 (C-12), 65.5 (C-18), 63.2 (C-19), 46.4 (C-17), 13.8 (C-20). Purity HPLC: 95%. MS

(ESI+): *m/z* 384 $[M+H]^+$. Elemental analysis $C_{20}H_{21}N_3O_3S$: Calculated C 62.64%, H 5.52%, N 10.96%, S 8.36%. Found C 62.05%, H 5.53%, N 10.56%, S 8.09%.

***N*-(6-bromobenzothiazol-2-yl)-4-morpholinobenzamide (72)**:

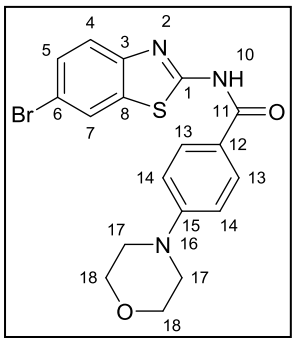

Reagents: 4-morpholinobenzoic acid (180.9 mg, 0.9 mmol), EDCI (217.56 mg, 1.1 mmol), DMAP (21.3 mg, 0.2 mmol), triethylamine (195 μL, 0.9 mmol) and 2-amino-6-bromobenzothiazole (200.0 mg, 1.0 mmol) dissolved in CH_2Cl_2. Activation reaction: 6 hours at r.t. Coupling reaction: overnight at r.t. Work-up: washes with HCl (0.1M), saturated $NaHCO_3$ and saturated NaCl solutions. Purification: automatic chromatographic system (Biotage®Isolera One) using Hex/AcOEt as eluents. Yield: 41.0 mg, 11%, white solid. M.p.: 237.5 - 238.5 ºC. ^{1}H-NMR (300 MHz, $CDCl_3$) δ 10.51 (s, 1H, H-10), 7.96 (d, *J* = 1.6 Hz, 1H, H-7), 7.87 (d, *J* = 9.0 Hz, 2H, H-13), 7.44 (dd, *J* = 8.6, 1.6 Hz, 1H, H-5), 7.38 (d, *J* = 8.6 Hz, 1H, H-4), 6.86 (d, *J* = 9.0 Hz, 2H, H-14), 3.89 - 3.83 (m, 4H, H-18), 3.33 - 3.26 (m, 4H, H-17). ^{13}C-NMR (125 MHz, $CDCl_3$) δ 165.2 (C-11), 160.8 (C-1), 154.9 (C-15), 145.7 (C-3), 133.5 (C-8), 130.3 (C-5), 129.9 (C-13), 124.5 (C-4), 121.6 (C-7), 120.7 (C-12), 117.5 (C-6), 114.1 (C-14), 66.9 (C-18), 47.8 (C-17). Purity HPLC: >99%. MS (ESI+): *m/z* 418 [M+2]. Elemental analysis $C_{18}H_{16}BrN_3O_2S$ Calculated: C 51.68%, H 3.86%, N 10.05%, S 7.55%. Found C 52.18%, H 4.30%, N 9.75%, S 7.05%.

***N*-(6-ethylcarboxylatebenzothiazol-2-yl)-4-morpholinobenzamide (73):**

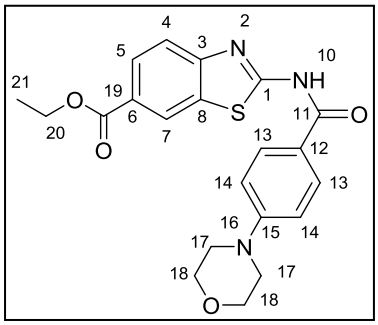

Reagents: 4-morpholinobenzoic acid (279.7 mg, 1.3 mmol), PyBOP (1.5 g, 2.5 mmol), HOBT (350 mg, 2.8 mmol), triethylamine (780 μL, 5.6 mmol) and 2-amino-6-(ethylcarboxylate)benzothiazole (200.0 mg, 1.2 mmol) dissolved in THF. Activation reaction: 1 hour under microwave irradiation at 50 ºC Coupling reaction: 5 hours under microwave irradiation at 110 ºC. Work-up: wash with HCl (0.1M). Purification: recrystallization from CH_2Cl_2/^{i}Pr-OH (99:1). Yield: 50.0 mg, 11%, white solid. M.p: 250.3 - 250.8 ºC. ^{1}H-NMR (300 MHz, $CDCl_3$) δ 10.44 (s, 1H, H-10), 8.56 (d, *J* = 1.4 Hz, 1H, H-7), 8.06 (dd, *J* = 8.5, 1.4 Hz, 1H, H-5), 7.90 (d, *J* = 9.0 Hz, 2H, H-13), 7.58 (d, *J* = 8.5 Hz, 1H, H-4), 6.88 (d, *J* = 9.0 Hz, 2H, H-14), 4.42 (q, *J* = 7.1 Hz, 2H, H-20) 3.90 - 3.81 (m, 4H,

H-18), 3.34 - 3.27 (m, 4H, H-17), 1.43 (t, *J* = 7.1 Hz, 3H, H-21). ^{13}C-NMR (75 MHz, $CDCl_3$) δ 165.2 (C-19), 163.8 (C-11), 161.1 (C-1), 150.5 (C-15), 131.1 (C-6), 128.5 (C-13), 126.5 (C-8), 124.9 (C-5), 122.5 (C-4), 119.7 (C-7), 119.2 (C-12), 112.7 (C-14), 65.5 (C-18), 60.1 (C-20), 46.4 (C-17), 13.4 (C-21). Purity HPLC: >98% MS (ESI+): *m/z* 412 $[M+H]^+$. Elemental analysis ($C_{21}H_{21}N_30_4S$) Calculated: C 61.30%, H 5.14%, N 10.21%, S 7.79%. Found: C 60.96%, H 5.25%, N 9.86%, S 7.53%.

_N_-(6-propoxybenzothiazol-2-yl)-4-morpholinobenzamide (74):

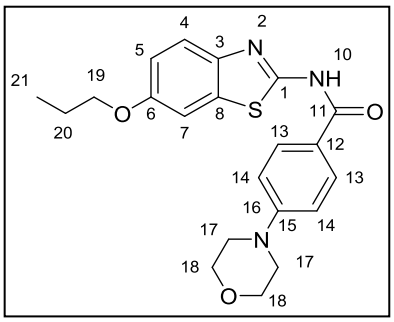

Reagents: 4-morpholinobenzoic acid (248.8 mg, 1.2 mmol), EDCI (299.0 mg, 1.6 mmol), DMAP (30.0 mg, 0.2 mmol), triethylamine (267 μL, 0.9 mmol) and 2-amino-6-propoxybenzothiazole (200.0 mg, 1.0 mmol) dissolved in CH_2Cl_2. Activation reaction: 6 hours at r.t. Coupling reaction: overnight at r.t. Work-up: washes with HCl (0.1M), saturated $NaHCO_3$ and saturated NaCl solutions. Purification: automatic chromatographic system (Biotage®Isolera One) using CH_2Cl_2/MeOH as eluents. Yield: 127.0 mg, 27%, white solid. M.p.: 232.1 - 232.7 ºC. ^{1}H-NMR (300 MHz, $CDCl_3$) δ 10.29 (s, 1H, H-10), 7.88 (d, *J* = 9.0 Hz, 1H, H-13), 7.46 (d, *J* = 8.9 Hz, 1H, H-4), 7.31 (d, *J* = 2.5 Hz, 1H, H-7), 6.96 (dd, *J* = 8.9, 2.5 Hz, 1H, H-5), 6.88 (d, *J* = 9.0 Hz, 1H, H-14), 3.98 (t, *J* = 6.6 Hz, 2H, H-19), 3.89 - 3.83 (m, 4H, H-18), 3.32 - 3.27 (m, 4H, H-17), 1.85 (m, 1H, H-20), 1.06 (t, *J* = 7.4 Hz, 2H, H-21). ^{13}C-NMR (75 MHz, $CDCl_3$) δ 163.6 (C-11), 156.3 (C-1), 155.2 (C-15), 153.3 (C-3), 141.3 (C-6), 132.3 (C-8), 128.4 (C-13), 120.4 (C-5), 120.3 (C-4), 114.55 (C-7), 112.8 (C-14), 103.9 (C-12), 69.25 (C-19), 65.51 (C-18), 46.51 (C-17), 21.62 (C-20), 9.53 (C-21). Purity HPLC: >95%. MS (ESI+): *m/z* 398.25 $[M+H]^+$. HRMS (ESI+) ($C_{19}H_{23}N_3O_3S$) $[M+H]^+$: Calculated: 398.15329, Found: 398.15275.

_N_-(6-isopropylbenzothiazol-2-yl)-4-morpholinobenzamide (75):

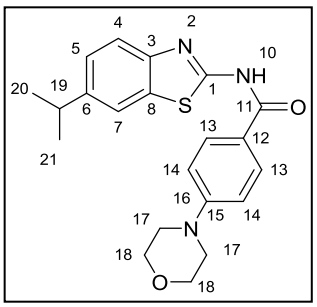

Reagents: 4-morpholinobenzoic acid (269.4 mg, 1.7 mmol), EDCI (324.0 mg, 1.7 mmol), DMAP (32.0 mg, 0.3 mmol), triethylamine (290 μL, 1.9 mmol) and 2-amino-6-isopropylbenzothiazole (250.0 mg, 1.3 mmol) dissolved in CH_2Cl_2. Activation reaction: 6 hours at r.t. Coupling reaction: overnight at r.t. Work-up: washes with HCl (0.1M), saturated

$NaHCO_3$ and saturated NaCl solutions. Purification: automatic chromatographic system (Biotage®Isolera One) using CH_2Cl_2/MeOH as eluents. Yield: 218.4 mg, 44%, white solid. M.p.: 238.2 - 238 ºC. ^{1}H-NMR (300 MHz, $CDCl_3$) δ 10.35 (s, 1H, H-10), 7.89 (d, *J* = 9.0 Hz, 2H, H-13), 7.68 (d, *J* = 1.7 Hz, 1H, H-7), 7.49 (d, *J* = 8.3 Hz, 1H, H-4), 7.26 - 7.22 (m, 1H, H-5), 6.85 (d, *J* = 9.0 Hz, 2H, H-14), 3.89 - 3.81 (m, 4H, H-18), 3.33 - 3.25 (m, 4H, H-17), 3.03 (m, 1H, H-19), 1.31 (d, *J* = 6.9 Hz, 6H, H-20 and H-21). ^{13}C-NMR (75 MHz, $CDCl_3$) δ 163.7 (C-11), 157.7 (C-1), 153.2 (C-15), 145.3 (C-3), 143.9 (C-6), 131.3 (C-8), 128.4 (C-13), 124.0 (C-5), 120.4 (C-12), 119.4 (C-7), 117.5 (C-4), 112.8 (C-14), 65.5 (C-18), 46.5 (C-17), 33.2 (C-19), 23.3 (C-20 and C-21). Purity HPLC: 95%. MS (ESI+): *m/z* 382.25 $[M+H]^+$. HRMS (ESI+) ($C_{19}H_{23}N_3O_2S$) $[M+H]^+$: Calculated: 382.15837, Found: 382.15932.

N-(6-methylsulfonylbenzothiazol-2-yl)-4-morpholinobenzamide (76):

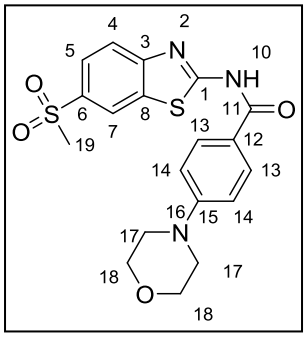

Reagents: 4-morpholinobenzoic acid (227.0 mg, 1.1 mmol), EDCI (274.1 mg, 1.4 mmol), DMAP (37.0 mg, 0.2 mmol), triethylamine (245 μL, 1.8 mmol) and 2-amino-6-methyl-sulfonylbenzothiazole (250.0 mg, 1.1 mmol) dissolved in CH_2Cl_2. Activation reaction: 6 hours at r.t. Coupling reaction: overnight at r.t. Work-up: washes with HCl (0.1M), saturated $NaHCO_3$ and saturated NaCl solutions. Purification: column chromatography using Hex/AcOEt (1:9) as eluents. Yield: 50.0 mg, 18%, white solid. M.p.: 299.7 - 300 ºC. ^{1}H-NMR (300 MHz, DMSO-d_6) δ 12.86 (s, 1H, H-10), 8.66 (s, 1H, H-7), 8.09 (d, *J* = 8.9 Hz, 2H, H-13), 7.97 - 7.91 (m, 2H, H-4 and H-5), 7.06 (d, *J* = 8.9 Hz, 2H, H-14), 3.78 - 3.71 (m, 4H, H-18), 3.36 - 3.29 (s, 4H, H-17), 3.26 (s, 3H, H-19). ^{13}C-NMR (125 MHz, DMSO-d_6) δ 163.0 (C-11), 154.0 (C-1), 149.5 (C-15), 144.6 (C-6), 140.1 (C-3), 135.2 (C-8), 130.1 (C-13), 124.7 (C-5), 121.9 (C-12), 120.4 (C-7), 114.4 (C-4), 113.1 (C-14), 65.8 (C-18), 46.70 (C-17), 44.0 (C-19). Purity HPLC: 95%. MS (ESI+): *m/z* 418.13 $[M+H]^+$. HRMS (ESI+) ($C_{19}H_{23}N_3O_4S$) $[M+H]^+$: Calculated: 418.08897, Found: 418.08802.

***N*-(6-fluorobenzothiazol-2-yl)-benzamide (77):**

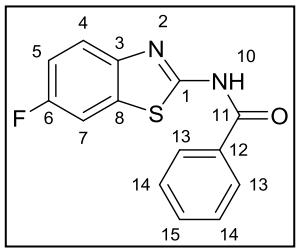

Reagents: benzoic acid (145.3 mg, 1.2 mmol), EDCI (296.3 mg, 1.1 mmol), DMAP (29.3 mg, 0.2 mmol), triethylamine (265 μL, 1.9 mmol) and 2-amino-6-fluorobenzothiazole (200.0 mg, 1.2 mmol) dissolved in CH_2Cl_2. Activation reaction: 6 hours at r.t. Coupling reaction: overnight at r.t. Work-up: washes with HCl (0.1M), saturated $NaHCO_3$ and saturated NaCl solutions. Purification: automatic chromatographic system (Biotage®Isolera One) using Hex/AcOEt as eluents Yield: 90.0 mg, 28%, white solid. M.p.: 262.8 - 264 ºC. ^{1}H-NMR (300 MHz, DMSO-d_6) δ 12.91 (s, 1H, H-10), 8.12 (d, J = 8.6 Hz, 2H, H-13), 7.93 (dd, J = 8.7, 2.8 Hz, 1H, H-7), 7.79 (dd, J = 8.7, 2.7 Hz, 1H, H-4), 7.66 (t, J = 8.5, 2H, H-15), 7.56 (t, J = 8.5 Hz, 2H, H-14), 7.31 (td, J = 8.5, 4.8 Hz, 1H, H-5). ^{13}C-NMR (75 MHz, DMSO-d_6) δ 165.9 (C-11), 158.8 (C-12), 158.7 (d, $J_{C\text{-}F}$ = 234.7 Hz, C-6), 155.7 (C-1), 145.3 (d, $J_{C\text{-}F}$ = 18.2 Hz, C-8) 132.9 (C-15), 131.7 (C-3), 128.6 (C-13), 128.3 (C-14), 121.5 (C-4), 114.3 (d, J = 24.5 Hz, C-5), 108.1 (d, J = 26.9 Hz, C-7). Purity HPLC: >99%. MS (ESI+): *m/z* 273 $[M+H]^+$. HRMS (ESI+) ($C_{14}H_9FN_2OS$) $[M+H]^+$: Calculated: 273.04924 Found: 273.04788.

***N*-(6-fluorobenzothiazol-2-yl)-4-chlorobenzamide (78):**

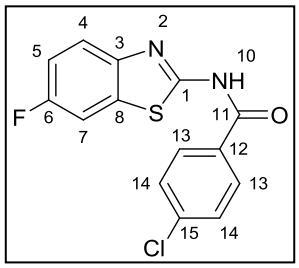

Reagents: 4-chlorobenzoic acid (146.2 mg, 1.2 mmol), EDCI (296.3 mg, 1.1 mmol), DMAP (29.3 mg, 0.2 mmol), triethylamine (265 μL, 1.9 mmol) and 2-amino-6-fluorobenzothiazole (200.0 mg, 1.2 mmol) dissolved in CH_2Cl_2. Activation reaction: 6 hours at r.t. Coupling reaction: overnight at r.t. Work-up: washes with HCl (0.1M), saturated $NaHCO_3$ and saturated NaCl solutions. Purification: automatic chromatographic system (Biotage®Isolera One) using Hex/AcOEt as eluents Yield: 25.0 mg, 28%, white solid. M.p.: 262.8 - 264 ºC. ^{1}H-NMR (300 MHz, DMSO-d_6) δ 13.00 (s, 1H, H-10), 8.15 (d, J = 8.6 Hz, 2H, H-13), 7.95 (dd, J = 8.7, 2.8 Hz, 1H, H-7), 7.86 - 7.74 (m, 1H, H-4), 7.56 (d, J = 8.5 Hz, 2H, H-14), 7.31 (td, J = 8.5, 4.8 Hz, 1H, H-5). ^{13}C NMR (75 MHz, DMSO-d_6) δ 165.9 (C-11), 158.8 (C-12), 158.7 (d, $J_{C\text{-}F}$ = 240.7 Hz, C-6), 154.6 (C-1), 145.2 (d, $J_{C\text{-}F}$ = 13.8 Hz, C-8) 132.9 (C-15), 131.7 (C-3), 128.6 (C-13), 128.3 (C-14), 121.5 (C-4), 114.3 (d, $J_{C\text{-}F}$ = 24.6 Hz, C-5), 108.2 (d, $J_{C\text{-}F}$ = 26.9 Hz, C-7). Purity HPLC:

>99%. MS (ESI+): *m/z* 307 $[M+H]^+$. HRMS (ESI+) ($C_{14}H_8FClN_2OS$) $[M+H]^+$: Calculated: 307.01027, Found: 307.01053.

***N*-(6-fluorobenzothiazol-2-yl)-5-(p-tolyl)furan-2-carboxamide (79):**

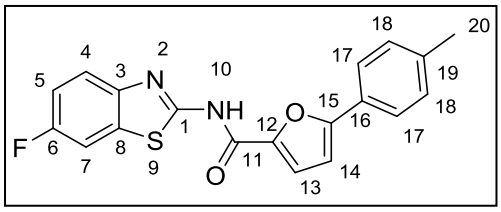

Reagents: 5-(*p*-tolyl)furan-2-carboxylic acid (300.6 mg, 1.5 mmol), PyBOP (296.3 mg, 1.1 mmol), DMAP (29.3 mg, 0.2 mmol), triethylamine (265 µL, 1.9 mmol) and 2-amino-6-fluorobenzothiazole (200.0 mg, 1.2 mmol) dissolved in CH_2Cl_2. Activation reaction: 6 hours at r.t. Coupling reaction: overnight at r.t. Work-up: washes with HCl (0.1M), saturated $NaHCO_3$ and saturated NaCl solutions. Purification: automatic chromatographic system (Biotage®Isolera One) using Hex/AcOEt as eluents Yield: 25.0 mg, 28%, white solid. M.p: 245.1 - 245.7 ºC ^{1}H-NMR (300 MHz, $CDCl_3$) δ 7.67 (dd, *J* = 8.9, 4.6 Hz, 1H, H-7), 7.57 (d, *J* = 8.2 Hz, 2H, H-17), 7.51 (dd, *J* = 8.9, 2.6 Hz, 1H, H-4), 7.48 (d, *J* = 3.7 Hz, 1H, H-13), 7.23 (d, *J* = 8.2 Hz, 2H, H-18), 7.13 (td, *J* = 8.9, 2.6 Hz, 1H, H-5), 6.79 (d, *J* = 3.7 Hz, 1H, H-14), 2.40 (s, 3H, H-20). ^{13}C-NMR (75 MHz, $CDCl_3$) δ 164.9 (C-11), 158.6 (d, J_{C-F} = 243.7 Hz, C-6) 156.9 (C-1), 156.3 (C-3), 154.4 (C-15), 143.1 (C-12), 138.7 (C-16), 132.3 (d, J_{C-F} = 10.7 Hz, C-8), 128.62 (C-17), 125.1 (C-19), 123.8 (C-18), 120.7 (d, J_{C-F} = 9.4 Hz, C-4), 119.2 (C-13 and C-14), 113.6 (d, J_{C-F} = 24.6 Hz, C-5), 106.6 (d, J_{C-F} = 26.1 Hz, C-7), 20.4 (C-20). Purity HPLC: >99%. MS (ESI+): *m/z* 353$[M+H]^+$. HRMS (ESI+) ($C_{19}H_{13}FN_2O_2S$) $[M+H]^+$: Calculated: 353.07545, Found: 353.07641.

***N*-(6-fluorobenzothiazol-2-yl)-6-methoxy-2-naphthamide (80)**

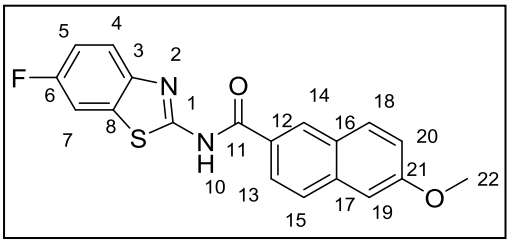

Reagents: 6-methoxy-2-naphtoic acid (201.2 mg, 1.8 mmol), PyBOP (1.9 g, 3.7 mmol), HOBT (502.0 mg, 3.7 mmol), triethylamine (1.04 mL, 7.4 mmol) and 2-amino-6-fluorobenzothiazole (250.0 mg, 1.5 mmol) dissolved in CH_2Cl_2. Activation reaction: 1 hour at r.t. Coupling reaction: overnight at r.t. Work-up: wash with HCl (0.1M) solution. Purification: recrystallization from: CH_2Cl_2:^{i}Pr-OH (99:1). Yield: 36.5 mg, 7%, white solid. M.p,: 248.5 - 248.8 ºC. ^{1}H-NMR (300 MHz, DMSO-d_6) δ 12.94 (s, 1H, H-10), 8.76 (d, *J* = 1.8 Hz, 1H, H-7), 8.12 (dd, *J* = 8.9, 1.9 Hz, 1H, H-4), 8.03 - 7.91 (m, 3H, H-14, H-15 and H-20), 7.80 (dd, *J* = 8.9, 4.8 Hz, 1H, H-5), 7.45 - 7.43 (m, 1H, H-19), 7.35 - 7.26

(m, 2H, H-13 and H-18), 3.92 (s, 3H, H-22). ^{13}C-NMR (125 MHz, DMSO-d_6) δ 159.6 (C-11), 159.3 (C-21), 158.7 (d, J_{C-F} = 240.0 Hz, C-6), 145.3 (C-3), 136.6 (C-1), 132.8 (d, J_{C-F} = 8.7 Hz, C-8), 130.9 (C-17), 129.4 (C-14), 129.1 (C-12), 127.3 (C-18), 127.0 (C-15), 126.5 (C-16) 124.8 (C-13), 121.5 (C-4), 119.7 (C-20), 114.2 (d, J_{C-F} = 24.5 Hz, C-5), 108.1 (d, J_{C-F} = 26.8 Hz, C-7), 105.9 (C-19), 55.4 (C-22). Purity HPLC: >99%. MS (ESI+): *m/z* 353[M+H]$^+$. HRMS (ESI+) ($C_{19}H_{13}FN_2O_2S$) [M+H]$^+$: Calculated: 353.07545, Found: 353.07641.

***N*-(6-fluorobenzothiazol-2-yl)-5-oxo-5-phenylpentamide (81)**

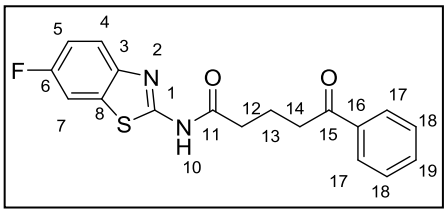

Reagents: 5-oxo-5-phenylpentanoic acid (342.7 mg, 1.8 mmol), PyBOP (1.9 g, 3.7 mmol), HOBT (502.0 mg, 3.7 mmol), triethylamine (1.04 mL, 7.4 mmol) and 2-amino-6-fluorobenzothiazole (250.0 mg, 1.5 mmol) dissolved in CH_2Cl_2. Activation reaction: 1 hour at r.t. Coupling reaction: overnight at r.t. Work-up: wash with HCl (0.1M) solution. Purification: recrystallization from: CH_2Cl_2/^{i}Pr-OH (99:1). Yield: 200.0 mg, 48%, white solid. M.p.: 212.4 - 213.1 ºC. ^{1}H-NMR (300 MHz, DMSO-d_6) δ 12.38 (s, 1H, H-10), 8.00 - 7.95 (m, 2H, H-17), 7.88 (dd, *J* = 8.7, 2.7 Hz, 1H, H-7), 7.73 (dd, *J* = 8.9, 4.8 Hz, 1H, H-4), 7.67 - 7.60 (m, 1H, H-19), 7.55 - 7.50 (m, 2H, H-18), 7.27 (td, *J* = 9.1, 2.7 Hz, 1H, H-5), 3.12 (t, *J* = 7.1 Hz, 2H, H-14), 2.59 (t, *J* = 7.4 Hz, 2H, H-12), 1.98 (qt, *J* = 7.2 Hz, 2H, H-13). ^{13}C-NMR (125 MHz, DMSO-d_6) δ 199.8 (C-11), 172.43 (C-15), 158.9 (d, J_{C-F} = 239.7 Hz, C-6), 158.2 (C-1), 145.5 (C-3), 136.9 (C-16), 133.5 (C-19), 133.0 (d, J_{C-F} = 11.1 Hz, C-8), 129.0 (C-17), 128.2 (C-18), 121.9 (d, J_{C-F} = 9.17 Hz, C-4), 114.4 (d, J_{C-F} = 24.5 Hz, C-5) 108.4 (d, J_{C-F} = 26.9 Hz, C-7), 48.9 (C-13), 37.4 (C-14), 34.6 (C-12). Purity HPLC: >99%. MS (ESI+): *m/z* 343 [M+H] $^+$. Elemental analysis ($C_{18}H_{15}FN_2O_2S$) Theoretical: %C: 63.14, %H: 4.42, %N: 8.18, %S: 9.36. Found: %C: 62.93, %H: 4.40, %N: 8.26, %S: 9.38.

3. Biology

3.1. *In vitro* experiments

3.1.1. Enzymatic activity

$LRRK2_{wt}$ and LRRK2-G2019S kinase activity was measured externally using Adapta® Screen technology from Life Technologies™ (Invitrogen) consisting of a fluorescent-based immunoassay for the detection of ADP[287].

3.1.2. CNS Penetration: *in vitro* parallel artificial membrane permeability assay (PAMPA).

Prediction of the brain penetration was evaluated using the PAMPA methodology[201]. Ten commercial drugs (Sigma, Acros organics, Merck, Aldrich and Fluka), dodecane (Sigma) and porcine polar brain lipid (PBL) (Avanti Polar Lipids) were purchased. The donor plate used was a 96-well filtrate plate (Multiscreen®) and the acceptor plate was an indented 96-well plate (Multiscreen®). Filter PDVF membrane units (Symta) were used to filtered the samples. A 96-well plate UV reader (Thermoscientific, Multiskan spectrum) was used for the UV measurements. Test compounds: caffeine, enoxacine, hydrocortisone, desipramine, ofloxacine, piroxicam, testosterone, promazine, verapamile and atenolol were weighted and dissolved in EtOH to a final concentration of 100 µM. 100 µL of this compound stock solution was taken and 1400 µL of EtOH and 3500 µL of PBS (pH = 7.4) were added to reach 30% of EtOH concentration in the experiment. These solutions were then filtered. The acceptor 96-well microplate was filled with 180 µL of PBS:EtOH (7:3). The donor 96-well plate was coated with 4 µL of porcine brain lipid in dodecane (20 $mg \cdot mL^{-1}$) and after 5 minutes, 180 µL of each compound solution was added to the donor 96-well plate. Then the donor plate was carefully put on the acceptor plate to form a "sandwich", which was left undisturbed for 2 h and 30 min at 25 °C. During this time the compounds diffused from the donor plate through the brain lipid membrane into the acceptor plate. After that time, the donor plate was removed. UV plate reader determined the concentration of compounds and commercial drugs in the acceptor and the donor wells. Every sample was analyzed at three to five wavelengths, in triplicates and in two independent runs. Results are given as the mean of the two runs ± SD. Ten quality control compounds (previously mentioned) of known BBB permeability were included in each experiment to validate the analysis set.

3.1.3. Neural progenitor cells (NPCs) experiments

- Real time RT-PCR for LRRK2 expression in NPCs

Culturing human iPSC-NPCs was performed as previously described[212]. 6-well plates were used in this assay. Plates were prepared with polyornithine/laminin coating. Polyornithine (Sigma) was dissolved in distilled water to a final concentration of 10 $mg \cdot mL^{-1}$ and was finally diluted 1:500 and dispensing it in each well. The polyornithine solution was left at least for 2 hours at r.t. Laminin (Sigma) was dissolved in PBS at a $1mg \cdot mL^{-1}$ and finally diluted 1:200 to be dispensed into the wells prior removing the polyornithine solution. The plates were then left with the laminin solution overnight at the incubator. Before cell seeding, coating reagent was removed through a wash with NPC media (350 mL DMEM (Gibco), 150 mL Hams-F12 (MediaTech), 5 mL of 100X penicillin/streptomycin and 10 mL of B27 (Thermo Fisher). Single-cell suspensions in NPC media were prepared from the human iPSC-NPCs 8330-8 cell line and dispensed into 6-well plates at the seeding density of 2000000 cells per well. After confluency RNA was isolated from the cells using the Direct-zol™ RNA Kit (Zymo Research). The concentration of total RNA was measured using a NanoDrop and cDNA was synthesized using the cDNA Kit (Zymo Research). Real time PCR reactions were performed using the *LRRK2* Taqman Probe (Thermo Fisher) and monitored quantification using the LightCycler® 480 Instrument. Cycle threshold (Ct) values were normalized to iPSC (set to 1) and *GAPDH* expression. Values represent the relative quantification from three biological replicates.

- Wnt modulation assay

Derivation of human iPSC-NPCs, culturing human iPSC-NPCs, creation of the TCF/LEF reporter line, and the production of NPC-compatible Wnt3a-conditioned media was performed as previously described[212]. White 384-well microplates were used in this assay. Plates were prepared with the polyornithine/laminin coating procedure described above with robotic handling, including aspiration with a Power Washer PW384 (Tecan) and dispensing with a Matrix WellMate microplate dispenser (Thermo Scientific), to provide standardized operation. For 384-well plates, 20 µL of coating reagents were used. A quick spin step was included after dispensing of each coating reagent and later cell suspension for 384-well plates to ensure that all liquid was brought down to the bottom of wells. Before

cell seeding, coating reagent was removed through a wash with NPC media (previously described). For these experiments, single-cell suspensions in NPC media were prepared from the human iPSC-NPCs, stably integrated with the TCF/LEF luciferase reporter, and dispensed into 384-well plates at the seeding density of 6000 cells per well, using a Matrix WellMate (Thermo Scientific) microplate dispenser. The next day, cells were treated for 24 hours with 10% Wnt-conditioned media (prepared previously from mouse L cells[288]) and the LRRK2 inhibitors at 1 µM and 10 µM using a CyBio liquid handling system (CyBio®). Just prior to the luminescence reading, the plates were taken out of a 37 °C incubator and equilibrated to room temperature for 30 min before the SteadyGlo reagent (Promega) was dispensed (volume equal 1:1 SteadyGlo:culture medium). Luminescence was measured after a 10 min incubation using an EnVision multilabel plate reader (PerkinElmer). For the dose-dependent experiments the same protocol was followed but in this case concentrations of 0.01, 0.03, 0.10, 0.30, 0.93, 2.70, 8.30 and 20 µM of the selected LRRK2 inhibitors were used.

3.1.4. Neurosphere cultures

- Immunohistochemistry of LRRK2 in the SVZ of adult mice

All animal care and handling was carried out in accordance with European Union guidelines (directives 86/609/EEC and 2010/63/EU) and Spanish legislation (Law 32/2007 and RD 53/2013), and the protocols were approved by the Ethical Committee of the Consejo Superior de Investigaciones Cientificas (CSIC) and Comunidad de Madrid. All efforts were made to ameliorate the suffering of the animals and to reduce the number of animals used to a minimum.

2.5 months old mice were perfused intracardially with 4% paraformaldehyde (PFA) and their brain was post-fixed, cryoprotected, frozen and then serial coronal cryostat sections (15 µM) were obtained. The sections were first blocked in 0.2 - 0.3% Triton X-100, 10% Normal Goat Serum (NGS) dissolved in PBS and they were then incubated for 24 - 72 hours with the following primary antibodies:

Antibody	Animal	Dilution	Commercial source
Anti-DCX	Guinea-pig	1:3000	Millipore
Anti-GFAP	Chicken	1:1000	Abcam
Anti-SOX2	Mouse	1:1000	Abcam
Anti-LRRK2	Rabbit	1:1000	Millipore

The sections were then washed with PBS and followed with incubation for 1 hour at r.t. with the following secondary antibodies:

Fluorophore	Animal	Dilution	Commercial source
Alexa-555	Rabbit	1:1000	Invitrogen
Alexa-488	Guinea-pig	1:1000	Invitrogen
Alexa-647	Mouse	1:1000	Invitrogen
Bisbenzimide		1:1000	Sigma

Afterwards, the sections were mounted in Fluromont-G solution (SouthernBiotech). Images were obtained using confocal microscopy (Leica TCSP5). Quantification was undertaken with LASX software.

- Neurosphere cultures and proliferation assays

Neurosphere (NS) cultures were derived from the subventricular zone of 4 young adult (6 weeks old) C57BL/6 mice and induced to proliferate using established passaging methods to achieve optimal cellular expansion according to published protocols[222]. Briefly, mice were euthanized with CO_2, brains were removed and the subventricular zone was dissected, cut up into pieces and digested using 0.7 $mg \cdot mL^{-1}$ papain (Sigma), 0.2 $mg \cdot mL^{-1}$ cysteine (Sigma) and 0.2 $mg \cdot mL^{-1}$ EDTA (Sigma) before it was gently disaggregated. The resulted cell suspension was plated into 8 wells of a 12-wells plates containing DMEM-F12 (Gibco) supplemented with 10 $mg \cdot mL^{-1}$ of N2 (Thermo Fisher), and B27 (Thermo Fisher). The cells were passaged by mechanical procedures and were maintained until passage 3 for the first experiments, with alternative daily addition of both 10 $ng \cdot mL^{-1}$ of FGF (Peprotech) and 2 $ng \cdot mL^{-1}$ of EGF (Peprotech). Cell proliferation assays were performed on floating neurospheres in 96-well plates at a density of 5000 cells per cm^2. LRRK2 inhibitors were diluted in DMSO at a concentration of 10 mM and then added to the dissociated cells to a final concentration of 5 µM and 0.1% DMSO was used as a control. Each treatment was

repeated by triplicate and the cells were left to grow at 37 ˚C and 5% of CO_2 in an incubator for 4 days. On the fourth day, for the measurement of the size and number of the neurospheres, photographs were taken by bright field microscopy (Leica DMI 6000) using an automatic platten, taken 6 pictures of different areas of each well with the 10X objective. The total number and area of neurospheres bigger than 400 μm^2 cell area was measured using a macro software for Image J, (National Institute of Health) designed at the Cajal Institute. Quantitative analyses were carried out in three separate experiments, calculating the mean ± SEM and using a two-tailed Student's *t*-test to determine statistically relevant changes.

- Differentiation experiments

For the differentiation experiments, cells were initially expanded as neurospheres, then cultured on polyornithine and fibronectin (Sigma) coated glass coverslips in DMEM/F12 (Gibco) supplemented with B27 (Thermo Fisher) for 7 days in the absence of mitogens (density at plating: 100000 cells per cm^2), 0.1% DMSO as a control or the indicated LRRK2 inhibitor at 10 µM was added to the media. Cells were then fixed with 4% PFA and immunostained. Immunocytochemistry**:** the differentiated cells adhered to glass coverslips were washed with PBS, and then permeabilized with 0.1% Triton X-100 for 1 hour at r. t. Cells were incubated overnight at 4 ˚C with the corresponding primary antibodies:

Antibody	**Animal**	**Dilution**	**Commercial source**
Anti-β-III-tubulin	Chicken	1:1000	Abcam
Anti-CNPase	Mouse	1:300	Covance
Anti-GFAP	Rabbit	1:2000	Dako

The cells were then washed with PBS and incubated for 1 hour at r.t. with the following secondary antibodies:

Fluorophore	**Animal**	**Dilution**	**Commercial source**
Alexa-555	Chicken	1:1000	Invitrogen
Alexa-488	Mouse	1:1000	Invitrogen
Alexa-647	Rabbit	1:1000	Invitrogen
Bisbenzimide		1:1000	Sigma

The coverslips were then mounted with Fluromont-G solution (SouthernBiotech). Images were obtained using confocal microscopy (Leica TCSP5). Quantification was undertaken with LASX software. The results are expressed as the mean value of triplicates of the % of positive cells compared to total number of cells ± SEM of three biological independent experiments and using a two-tailed Student's *t*-test to determine statistically relevant changes.

3.1.5. SH-SY5Y cell cultures

Human SH-SY5Y cells were grown in DMEM (Gibco) supplemented with 10% FBS and 1% penicillin/streptocycin at 37 ºC and 5%CO_2 in an incubator. SH-SY5Y cells were seeded onto 96-well plate at 60000 cells per well. 48 hours later, cells were pre-incubated with the compounds at the desired concentration for 1 hour and after that time OA (Sigma) was added at a concentration of 30 nM and incubated for another 24 hours. Afterwards, cells were incubated with 0.5mg·mL^{-1} MTT solution for at least 4 hours at 37 ºC and 5% CO_2. Then culture media was removed and the formazan crystals attached to the bottom of the plate were dissolved with 200 µL of DMSO. Finally, UV-absorbance was measured at 595 nM in a microplate reader (Varioskan Flash Microplate reader, Thermo Scientific). The results are expressed as mean value of triplicates of the % of viability ± SEM of three biological independent experiments and using a two-tailed Student's *t*-test to determine statistically relevant changes.

3.1.6. Ngn2-transfected-A152T-derived neurons

Induced-Ngn2-A152T-NPC stable cells were generated according to the established protocols[236]. Once the NPC line was stable Ngn2 induction was initiated. Cells were seeded on polyornithine and laminin-coated (previously described) 96-well plate at a density of 8.5 x 10^4 cells per cm^2. Cells were grown in N3aM media (48% Neurobasal medium (Gibco), 48% DMEM/F12 (Gibco), 1% B27 (Sigma), 0.5% N2 (Sigma), 0.75% Glutamax (Thermo Fisher) and 1% penicillin/streptomycin, 0.5% Minimum essential media - non essential aminoacid media (Gibco) 50 µM 2-mercaptoethanol (Sigma), 0.2% bovine serum albumin (Sigma), 2 µg·mL^{-1} doxycycline monohydrate (Sigma), 10ng·mL^{-1}, Brain-derived-neurotrofic-factor (Sigma) and 10ng·mL^{-1}, Neurotrofin-3 (Gibco)) which contains doxycycline to induce Ngn2 expression and differentiation. On day 2 and 4 cells were fed with fresh N3aM media containing 1µg·mL^{-1} of puromycin (Sigma) to select the cells

expressing Ngn2. From day 6 onward iNgn2-A152T neurons were fed with fresh N3aM media without puromycin every 2 days until day 14.

- Real time RT-PCR for LRRK2 expression in iNgn2-A152T neurons

On day 14 iNgn2-A152Tneurons were plated on polyornithine and laminin-coated bottom glass-6-well plates (as previously described) (Corning, 3335) at a density of $8.5x10^4$ cells per cm^2. After confluency RNA was isolated from the cells using the Direct-zol™ RNA Kit (Zymo Rsearch). The concentration of total RNA was measured using a NanoDrop and cDNA was synthesized using the cDNA Kit (Zymo Research). Real time PCR reactions were performed using the *LRRK2* Taqman Probe (Thermo Fisher) and monitored quantification using the LightCycler ® 480 Instrument. Ct values were normalized to iPSC (set to 1) and *GAPDH* expression. Values represent the relative quantification from three biological replicates.

- Immunocytochemistry in iNgn2-A152T neurons

On day 13 iNgn2-A152T neurons were treated with the compounds at the desired concentration. On day 14 N3aM media was removed by automated pipette, afterwards iNgn2-A152T neurons were washed with PBS and fixed with 4% PFA. Immunocytochemistry was performed on the same plates. iNgn2-A152T neurons were permeabilized with 0.1% Triton X-100 for 1 hour at r.t. iNgn2-A152T neurons were then incubated overnight at 4 ˚C with the corresponding primary antibodies:

Antibody	**Animal**	**Dilution**	**Commercial Source**
Anti-β-III-tubulin	Chicken	1:1000	Abcam
PHF-1	Mouse	1:500	Alzforum
K9JA	Rabbit1	1:1000	DAKO

iNgn2-A152T neurons were then washed with PBS and then incubated for 1 hour at r.t. with the corresponding conjugated secondary antibodies:

Fluorophore	**Animal**	**Dilution**	**Commercial source**
Alexa-555	Chicken	1:1000	Invitrogen
Alexa-488	Mouse	1:1000	Invitrogen
Alexa-647	Rabbit	1:1000	Invitrogen
Hoechst		1:1000	Sigma

iNgn2-A152T neurons were photograph by automated confocal microscopy (IN Cell Analyzer 6500 HS high content analysis system, GE Health). The intensity of the antibodies was measured by an automated pipeline developed by Surya A. Reis at Haggarty Lab. This automated pipeline generates different read-outs in this case the Z-score for the K9JA intensity in the cell bodies and the percent activity of PHF-1 in the neurites were used. Results represent the mean values of triplicates of two biological experiments and using a two-tailed Student's *t*-test to determine statistically relevant changes.

3.1.7. 6-weeks differentiatied A152T-derived neurons

A152T-NPC stable cells were generated according to the established protocols[212]. Differentiation was achieved by platting A152T-NPCs (passages 30-35) on polyornithine and laminin-coated 6-well plates (as previously described) at a density of 50,000 cells per cm^2 with DMEM/F12 (Gibco) supplemented with B27 (Thermo Fisher) only (no growth factors), and with 50% medium change every 3 days for 6 weeks. After that time A152T-neurons were treated with the compounds at the desired concentration for 24 hours. On the next day cell pellets were collected. Protein Analysis by WB**:** A152T-neurons were washed and collected in PBS, lysed in RIPA buffer (Boston Bio-Products) with 2% SDS (Sigma), protease inhibitors (Roche Complete Mini tablets), and phosphatase inhibitors (Sigma), followed by sonication in a water sonicator (Bransonic Ultrasonic Baths, Thomas Scientific) for 5 min, and centrifugation at 20,000G for 15 min. Supernatants were transferred to new tubes and total protein concentration was quantified with the Pierce BCA Protein Assay Kit (Thermo Fisher). WB lots were performed with the Novex NuPAGE SDS-PAGE Gel System (Invitrogen), by running 10 μg of total protein (pre-boiled for 10 min in SDS-DTT loading buffer (Invitrogen) on pre-cast SDS-PAGE gels (Invitrogen). The proteins were then transferred onto PVDF membranes (EMD Millipore) using standard procedures. Membranes were blocked in 5% nonfat milk (Biorad) in Tris-buffered saline

with Tween-20 (Biorad) for 2.5 h, incubated overnight with the corresponding primary antibodies at 4°C:

Antibody	**Animal**	**Dilution**	**Commercial source**
TAU5	Mouse	1:1000	Invitrogen
S396	Mouse	1:1000	Invitrogen
TAU1	Mouse	1:1000	Millipore
S422	Mouse	1:1000	Abcam

Followed by corresponding HRP-linked secondary antibodies (Cell Signaling Technology), and lastly incubated with SuperSignal West Pico Chemiluminescent Substrate (Thermo Fisher) according to manufacturer's instructions. Membranes were then exposed to autoradiographic film (LabScientific) for different amounts of time, to account for bands of different intensities (and to ensure detection of all relevant bands). Films were scanned using a GS-800 Calibrated Densitometer (Biorad), and band intensities (pixel mean intensity) were quantified using Adobe Photoshop CS5 Histogram function Relative intensity was calculated relative to the respective loading control (actin band).

3.2. *In vivo* experiments

3.2.1. GMR-MAPT.V337M *Drosophila melanogaster* model

The fly stocks were obtained from the Bloomington Drosophila stock center and were raised on standard cornmeal–yeast agar medium (0.5% of d-H_20, 4% agar, 13% of torumel yeast, 25% of cornmeal, 50% of sucrose, 1% of p-Hydroxy benzoic acid methyl ester and 4% EtOH). Fly cultures and crosses were carried out at 25 ºC. 20 couples were placed in egg collection cages in which 70 embryos per treatment were collected and kept in individual cages at 25 ºC. The compounds were dissolved in melted food to reach a final concentration of 10 µM. After solidification, each food plate was placed on the individual cages and was replaced every 3 days till day 15. On day 15 adult flies were collected and photographed. Images were acquired using Motic™ SMZ171 Series Stereo Zoom Microscope equipped with a digital camera.

3.2.2. *Rd10* mouse model

The *rd10* mouse model of retinal neurodegeneration carries a homozygous phosphodiesterase 6b mutation (Pde6brd10/rd10) on a C57BL/6 J background. Mice were provided from The Jackson Laboratory. WT control mice of the same background were also obtained from The Jackson Laboratory. All animals were housed and handled in accordance with the ARVO statement for the Use of Animals in Ophthalmic and Vision Research, European Union guidelines, and those of the local ethics committees of the CSIC and the Comunidad de Madrid. Mice were bred at the CIB core facilities on a 12/12-h light/dark cycle.

- Analysis of the expression of LRRK2 in retina.

RNA isolation and quantitative PCR: Total RNA from individual retinas was extracted using TRIzol Reagent, and 2.5 μg of RNA was typically reverse transcribed using the Superscript III Kit and random primers (all from ThermoFisher Scientific). Quantitative PCR (qPCR) was performed with the ABI Prism 7900HT Sequence Detection System using TaqMan Universal PCR Master Mix, no-AmpErase UNG, and the *LRRK2* Taqman Probe (Thermo Fisher). The relative change in gene expression was calculated using the Ct method, normalizing to expression levels of the Tbp (TATA-binding protein) gene.

- Determination of the neuroprotective and anti-inflammatory effect of compound 23 in the photoreceptor layer in *rd10* mice

Three *rd10* mice were injected intraperitoneally with indolinone **23** from a stock solution of 1 $mg \cdot mL^{-1}$ in 90% NaCl solution with a 10% DMSO and 5% Tocrisol (Tocris), adjusting it to the weight of mice (10 $\mu L \cdot g^{-1}$). As control three *rd10* mice were injected in the same way but without indolinone **23**. Histology and immunostaining: mice were euthanized at the indicated ages and their eyes enucleated. The right eye was processed for histological analyses and the left eye for retinal RNA extraction. For histological analyses, eyes were fixed for 1 h in 4% (w/v) PFA in PBS (pH = 7.4), and then cryoprotected by incubation in increasing concentrations of sucrose (final concentration 50% (w/v) in PBS). The eyes were then embedded in Tissue-Tek OCT (Sakura Finetec) and frozen on isopropanol/dry ice. Cryostat equatorial sections (12 μm) were performed (Leica Microsystems GmbH) and were mounted on Superfrost® Plus slides (Thermo Scientific),

dried at r.t., and stored at -20 °C. Before performing further analyses, sections were fixed in acetone for 10 min at -20 °C and dried at 65 °C for 10 min. After rinsing in PBS and permeation with 1% (w/v) TritonX-100 in PBS, sections were blocked in BGT (2.5 $g \cdot L^{-1}$ BSA, 100 mM glycine, 0.25% (w/v) Triton X-100 in PBS) for 1 h and then incubated overnight at 4 °C with the primary antibody anti-IBA-1 (rabbit, 1:1000, Abcam) diluted in BGT. Sections incubated in the absence of primary antibody were used as specificity controls. After rinsing in PBS and incubation with the secondary antibody Alexa α-Rbb-488 (1:1000, Invitrogen) and finally were stained with DAPI (4′,6-diamidino-2-phenylindole (Sigma). Sections were cover-slipped and mounted with Fluoromont-G (SouthernBiotech). The cover-slips were photographed by confocal microscopy (Leica TCSP5). Image processing and statistical analysis: images were obtained with the program LASX software and were processed with the program ImageJ (National Institute of Health). To assess preservation of the photoreceptor layer, we compared the thickness of the ONL (which primarily contains photoreceptors) with that of the corresponding INL (which contains bipolar, horizontal, amacrine neurons and Müller glial cell bodies). Seven sections per eye were analyzed: for each section, one image was captured for each of the 8 retinal zones (P1, P2, P3, P4, P1´, P2´, P3´and P4´. In each image, three measurements were recorded at random positions to obtain an average value per retinal zone per section. Measurements were performed using the "freehand line" and "measure" tools in the software. The ONL thickness was normalized to that of the INL (not affected by the degeneration at this stage) to correct for possible inclinations of the sectioning plane. For the statistical analysis the program GraphPad Prism (GraphPad Software Inc.) was used. The data were plotted in a spider-graph plot and a 2-way ANOVA test was performed to determine statistical differences between the widths of the ONL in treated animals *vs* control animals. Values represent mean values from each group ± SD. With ImageJ software the number of microglia IBA positive cells was determined. A two-tailed t-test was performed and results are expressed as the mean values from each group ± SD.

REFERENCES

1. Chaudhuri, K. R.; Jenner, P., Two hundred years since James Parkinson's essay on the shaking palsy-have we made progress? Insights from the James Parkinson's 200 years course held in London, March 2017. *Mov Disord* **2017,** *32* (9), 1211-1315.

2. Caselli, R. J.; Beach, T. G.; Knopman, D. S.; Graff-Radford, N. R., Alzheimer disease: scientific breakthroughs and translational challenges. *Mayo Clin Proc* **2017,** *92* (6), 978-994.

3. Forman, M. S.; Trojanowski, J. Q.; Lee, V. M., Neurodegenerative diseases: a decade of discoveries paves the way for therapeutic breakthroughs. *Nat Med* **2004,** *10* (10), 1055-1063.

4. Parkinson, J., An essay on the Shaking Palsy. *London: Sherwood* **1817**.

5. Alzheimer, A., Über eine eigenartige Erkraunkung der Hirnrinde. *Allg Z Psychiatr Psych-Gerichtl Med* **1907,** *64*, 146-148.

6. Dugger, B. N.; Dickson, D. W., Pathology of neurodegenerative diseases. *Cold Spring Harb Perspect Biol* **2017,** *9*:a023549

7. Sanabria-Castro, A.; Alvarado-Echeverria, I.; Monge-Bonilla, C., Molecular pathogenesis of Alzheimer's disease: an update. *Ann Neurosci* **2017,** *24* (1), 46-54.

8. Nixon, R. A., Amyloid precursor protein and endosomal-lysosomal dysfunction in Alzheimer's disease: inseparable partners in a multifactorial disease. *FASEB J* **2017,** *31* (7), 2729-2743.

9. Lewerenz, J.; Maher, P., Chronic glutamate toxicity in neurodegenerative diseases: what is the evidence? *Front Neurosci* **2015,** *9*, (469), 1-20.

10. Schain, M.; Kreisl, W. C., Neuroinflammation in neurodegenerative disorders: a review. *Curr Neurol Neurosci Rep* **2017,** *17* (25), 1-11.

11. Gao, H. M.; Hong, J. S., Why neurodegenerative diseases are progressive: uncontrolled inflammation drives disease progression. *Trends Immunol* **2008,** *29* (8), 357-365.

12. Liu, Z.; Zhou, T.; Ziegler, A. C.; Dimitrion, P.; Zuo, L., Oxidative stress in neurodegenerative diseases: from molecular mechanisms to clinical applications. *Oxid Med Cell Longev* **2017,** *2017* (2525967), 1-11.

13. Shamsi, T. N.; Athar, T.; Parveen, R.; Fatima, S., A review on protein misfolding, aggregation and strategies to prevent related ailments. *Int J Biol Macromol* **2017,** *105* (2017), 993-1000.

14. Alam, P.; Siddiqi, K.; Chturvedi, S. K.; Khan, R. H., Protein aggregation: from background to inhibition strategies. *Int J Biol Macromol* **2017,** *103*, 208-219.

15. Kumar, V.; Sami, N.; Kashav, T.; Islam, A.; Ahmad, F.; Hassan, M. I., Protein aggregation and neurodegenerative diseases: from theory to therapy. *Eur J Med Chem* **2016,** *124*, 1105-1120.

16. Citron, M., Alzheimer's disease: strategies for disease modification. *Nat Rev Drug Discov* **2010,** *9* (5), 387-398.

17. Brundin, P.; Li, J. Y.; Holton, J. L.; Lindvall, O.; Revesz, T., Research in motion: the enigma of Parkinson's disease pathology spread. *Nat Rev Neurosci* **2008,** *9* (10), 741-745.

18. Robberecht, W.; Philips, T., The changing scene of amyotrophic lateral sclerosis. *Nat Rev Neurosci* **2013,** *14* (4), 248-264.

19. Tenreiro, S.; Eckermann, K.; Outeiro, T. F., Protein phosphorylation in neurodegeneration: friend or foe? *Front Mol Neurosci* **2014,** *7* (42), 1-30.

20. Salazar, C.; Hofer, T., Multisite protein phosphorylation--from molecular mechanisms to kinetic models. *FEBS J* **2009,** *276* (12), 3177-3198.

21. Anderson, J. P.; Walker, D. E.; Goldstein, J. M.; de Laat, R.; Banducci, K.; Caccavello, R. J.; Barbour, R.; Huang, J.; Kling, K.; Lee, M.; Diep, L.; Keim, P. S.; Shen, X.; Chataway, T.; Schlossmacher, M. G.; Seubert, P.; Schenk, D.; Sinha, S.; Gai, W. P.; Chilcote, T. J., Phosphorylation of Ser-129 is the dominant pathological modification of alpha-synuclein in familial and sporadic Lewy body disease. *J Biol Chem* **2006,** *281* (40), 29739-29752.

22. Noble, W.; Hanger, D. P.; Miller, C. C.; Lovestone, S., The importance of tau phosphorylation for neurodegenerative diseases. *Front Neurol* **2013,** *4* (83), 1-11.

23. Gunosewoyo, H.; Yu, L.; Munoz, L.; Kassiou, M., Kinase targets in CNS drug discovery. *Future Med Chem* **2017,** *9* (3), 303-314.

24. Manning, G.; Whyte, D. B.; Martinez, R.; Hunter, T.; Sudarsanam, S., The protein kinase complement of the human genome. *Science* **2002,** *298* (5600), 1912-1934.

25. Rask-Andersen, M.; Zhang, J.; Fabbro, D.; Schioth, H. B., Advances in kinase targeting: current clinical use and clinical trials. *Trends Pharmacol Sci* **2014,** *35* (11), 604-620.

26. Chico, L. K.; Van Eldik, L. J.; Watterson, D. M., Targeting protein kinases in central nervous system disorders. *Nat Rev Drug Discov* **2009,** *8* (11), 892-909.

27. Funayama, M.; Hasegawa, K.; Kowa, H.; Saito, M.; Tsuji, S.; Obata, F., A new locus for Parkinson's disease (PARK8) maps to chromosome 12p11.2-q13.1. *Ann Neurol* **2002,** *51* (3), 296-301.

28. Deng, H.; Wang, P.; Jankovic, J., The genetics of Parkinson disease. *Ageing Res Rev* **2017,** *42*, 72-85.

29. Paisan-Ruiz, C.; Jain, S.; Evans, E. W.; Gilks, W. P.; Simon, J.; van der Brug, M.; Lopez de Munain, A.; Aparicio, S.; Gil, A. M.; Khan, N.; Johnson, J.; Martinez, J. R.; Nicholl, D.; Carrera, I. M.; Pena, A. S.; de Silva, R.; Lees, A.; Marti-Masso, J. F.; Perez-Tur, J.; Wood, N. W.; Singleton, A. B., Cloning of the gene containing mutations that cause PARK8-linked Parkinson's disease. *Neuron* **2004,** *44* (4), 595-600.

30. Zimprich, A.; Biskup, S.; Leitner, P.; Lichtner, P.; Farrer, M.; Lincoln, S.; Kachergus, J.; Hulihan, M.; Uitti, R. J.; Calne, D. B.; Stoessl, A. J.; Pfeiffer, R. F.; Patenge, N.; Carbajal, I. C.; Vieregge, P.; Asmus, F.; Muller-Myhsok, B.; Dickson, D. W.; Meitinger, T.; Strom, T. M.; Wszolek, Z. K.; Gasser, T., Mutations in LRRK2 cause autosomal-dominant parkinsonism with pleomorphic pathology. *Neuron* **2004,** *44* (4), 601-607.

31. Li, J. Q.; Tan, L.; Yu, J. T., The role of the LRRK2 gene in parkinsonism. *Mol Neurodegener* **2014,** *9* (47),1-17.

32. Marin, I., Ancient origin of the Parkinson disease gene LRRK2. *J Mol Evol* **2008,** *67* (1), 41-50.

33. Cardona, F.; Tormos-Perez, M.; Perez-Tur, J., Structural and functional in silico analysis of LRRK2 missense substitutions. *Mol Biol Rep* **2014,** *41* (4), 2529-2542.

34. Mata, I. F.; Wedemeyer, W. J.; Farrer, M. J.; Taylor, J. P.; Gallo, K. A., LRRK2 in Parkinson's disease: protein domains and functional insights. *Trends Neurosci* **2006,** *29* (5), 286-293.

35. Deng, J.; Lewis, P. A.; Greggio, E.; Sluch, E.; Beilina, A.; Cookson, M. R., Structure of the ROC domain from the Parkinson's disease-associated leucine-rich repeat kinase 2 reveals a dimeric GTPase. *Proc Natl Acad Sci U S A* **2008,** *105* (5), 1499-1504.

36. Scott, J. D.; DeMong, D. E.; Greshock, T. J.; Basu, K.; Dai, X.; Harris, J.; Hruza, A.; Li, S. W.; Lin, S. I.; Liu, H.; Macala, M. K.; Hu, Z.; Mei, H.; Zhang, H.; Walsh, P.; Poirier, M.; Shi, Z. C.; Xiao, L.; Agnihotri, G.; Baptista, M. A.; Columbus, J.; Fell, M. J.; Hyde, L. A.; Kuvelkar, R.; Lin, Y.; Mirescu, C.; Morrow, J. A.; Yin, Z.;

Zhang, X.; Zhou, X.; Chang, R. K.; Embrey, M. W.; Sanders, J. M.; Tiscia, H. E.; Drolet, R. E.; Kern, J. T.; Sur, S. M.; Renger, J. J.; Bilodeau, M. T.; Kennedy, M. E.; Parker, E. M.; Stamford, A. W.; Nargund, R.; McCauley, J. A.; Miller, M. W., Discovery of a 3-(4-pyrimidinyl) indazole (MLi-2), an orally available and selective leucine-rich repeat kinase 2 (LRRK2) inhibitor that reduces brain kinase activity. *J Med Chem* **2017,** *60* (7), 2983-2992.

37. Guaitoli, G.; Raimondi, F.; Gilsbach, B. K.; Gomez-Llorente, Y.; Deyaert, E.; Renzi, F.; Li, X.; Schaffner, A.; Jagtap, P. K.; Boldt, K.; von Zweydorf, F.; Gotthardt, K.; Lorimer, D. D.; Yue, Z.; Burgin, A.; Janjic, N.; Sattler, M.; Versees, W.; Ueffing, M.; Ubarretxena-Belandia, I.; Kortholt, A.; Gloeckner, C. J., Structural model of the dimeric Parkinson's protein LRRK2 reveals a compact architecture involving distant interdomain contacts. *Proc Natl Acad Sci U S A* **2016,** *113* (30), E4357-E4366.

38. Gotthardt, K.; Weyand, M.; Kortholt, A.; Van Haastert, P. J.; Wittinghofer, A., Structure of the Roc-COR domain tandem of c. tepidum, a prokaryotic homologue of the human LRRK2 Parkinson kinase. *EMBO J* **2008,** *27* (16), 2239-2249.

39. Gilsbach, B. K.; Messias, A. C.; Ito, G.; Sattler, M.; Alessi, D. R.; Wittinghofer, A.; Kortholt, A., Structural characterization of LRRK2 inhibitors. *J Med Chem* **2015,** *58* (9), 3751-3756.

40. Gilsbach, B. K.; Ho, F. Y.; Vetter, I. R.; van Haastert, P. J.; Wittinghofer, A.; Kortholt, A., Roco kinase structures give insights into the mechanism of Parkinson disease-related leucine-rich-repeat kinase 2 mutations. *Proc Natl Acad Sci U S A* **2012,** *109* (26), 10322-10327.

41. Henderson, J. L.; Kormos, B. L.; Hayward, M. M.; Coffman, K. J.; Jasti, J.; Kurumbail, R. G.; Wager, T. T.; Verhoest, P. R.; Noell, G. S.; Chen, Y.; Needle, E.; Berger, Z.; Steyn, S. J.; Houle, C.; Hirst, W. D.; Galatsis, P., Discovery and preclinical profiling of 3-[4-(morpholin-4-yl)-7H-pyrrolo[2,3-d]pyrimidin-5-yl]benzonitrile (PF-06447475), a highly potent, selective, brain penetrant, and in vivo active LRRK2 kinase inhibitor. *J Med Chem* **2015,** *58* (1), 419-432.

42. Williamson, D. S.; Smith, G. P.; Acheson-Dossang, P.; Bedford, S. T.; Chell, V.; Chen, I. J.; Daechsel, J. C. A.; Daniels, Z.; David, L.; Dokurno, P.; Hentzer, M.; Herzig, M. C.; Hubbard, R. E.; Moore, J. D.; Murray, J. B.; Newland, S.; Ray, S. C.; Shaw, T.; Surgenor, A. E.; Terry, L.; Thirstrup, K.; Wang, Y.; Christensen, K. V., Design of leucine-rich repeat kinase 2 (LRRK2) inhibitors using a crystallographic

surrogate derived from checkpoint kinase 1 (CHK1). *J Med Chem* **2017,** *60* (21), 8945-8962.

43. Cookson, M. R., The role of leucine-rich repeat kinase 2 (LRRK2) in Parkinson's disease. *Nat Rev Neurosci* **2010,** *11* (12), 791-797.

44. Kett, L. R.; Dauer, W. T., Leucine-rich repeat kinase 2 for beginners: six key questions. *Cold Spring Harb Perspect Med* **2012,** *2* (3), a009407.

45. Mata, I. F.; Hutter, C. M.; Gonzalez-Fernandez, M. C.; de Pancorbo, M. M.; Lezcano, E.; Huerta, C.; Blazquez, M.; Ribacoba, R.; Guisasola, L. M.; Salvador, C.; Gomez-Esteban, J. C.; Zarranz, J. J.; Infante, J.; Jankovic, J.; Deng, H.; Edwards, K. L.; Alvarez, V.; Zabetian, C. P., Lrrk2 R1441G-related Parkinson's disease: evidence of a common founding event in the seventh century in northern Spain. *Neurogenetics* **2009,** *10* (4), 347-353.

46. Anand, V. S.; Braithwaite, S. P., LRRK2 in Parkinson's disease: biochemical functions. *FEBS J* **2009,** *276* (22), 6428-6435.

47. Schapansky, J.; Nardozzi, J. D.; Felizia, F.; LaVoie, M. J., Membrane recruitment of endogenous LRRK2 precedes its potent regulation of autophagy. *Hum Mol Genet* **2014,** *23* (16), 4201-4214.

48. Steger, M.; Tonelli, F.; Ito, G.; Davies, P.; Trost, M.; Vetter, M.; Wachter, S.; Lorentzen, E.; Duddy, G.; Wilson, S.; Baptista, M. A.; Fiske, B. K.; Fell, M. J.; Morrow, J. A.; Reith, A. D.; Alessi, D. R.; Mann, M., Phosphoproteomics reveals that Parkinson's disease kinase LRRK2 regulates a subset of Rab GTPases. *Elife* **2016,** *5*, 1-28.

49. West, A. B.; Moore, D. J.; Choi, C.; Andrabi, S. A.; Li, X.; Dikeman, D.; Biskup, S.; Zhang, Z.; Lim, K. L.; Dawson, V. L.; Dawson, T. M., Parkinson's disease-associated mutations in LRRK2 link enhanced GTP-binding and kinase activities to neuronal toxicity. *Hum Mol Genet* **2007,** *16* (2), 223-232.

50. Chan, S. L.; Tan, E. K., Targeting LRRK2 in Parkinson's disease: an update on recent developments. *Expert Opin Ther Targets* **2017**, *21*(6), 601-610.

51. Ito, G.; Katsemonova, K.; Tonelli, F.; Lis, P.; Baptista, M. A.; Shpiro, N.; Duddy, G.; Wilson, S.; Ho, P. W.; Ho, S. L.; Reith, A. D.; Alessi, D. R., Phos-tag analysis of Rab10 phosphorylation by LRRK2: a powerful assay for assessing kinase function and inhibitors. *Biochem J* **2016,** *473* (17), 2671-2685.

52. Eyers, P. A., 'Up with the LRRK': a phosphorylated Rab10 assay for evaluation of LRRK2 activity and inhibitor engagement. *Biochem J* **2016,** *473* (18), 2757-2762.

53. Kanao, T.; Venderova, K.; Park, D. S.; Unterman, T.; Lu, B.; Imai, Y., Activation of FoxO by LRRK2 induces expression of proapoptotic proteins and alters survival of postmitotic dopaminergic neuron in drosophila. *Hum Mol Genet* **2010,** *19* (19), 3747-3758.

54. Imai, Y.; Gehrke, S.; Wang, H. Q.; Takahashi, R.; Hasegawa, K.; Oota, E.; Lu, B., Phosphorylation of 4E-BP by LRRK2 affects the maintenance of dopaminergic neurons in drosophila. *EMBO J* **2008,** *27* (18), 2432-2443.

55. Papkovskaia, T. D.; Chau, K. Y.; Inesta-Vaquera, F.; Papkovsky, D. B.; Healy, D. G.; Nishio, K.; Staddon, J.; Duchen, M. R.; Hardy, J.; Schapira, A. H.; Cooper, J. M., G2019S leucine-rich repeat kinase 2 causes uncoupling protein-mediated mitochondrial depolarization. *Hum Mol Genet* **2012,** *21* (19), 4201-4213.

56. Heo, H. Y.; Kim, K. S.; Seol, W., Coordinate regulation of neurite outgrowth by LRRK2 and its interactor, rab5. *Exp Neurobiol* **2010,** *19* (2), 97-105.

57. Gillardon, F., Leucine-rich repeat kinase 2 phosphorylates brain tubulin-beta isoforms and modulates microtubule stability: a point of convergence in parkinsonian neurodegeneration? *J Neurochem* **2009,** *110* (5), 1514-1522.

58. Cirnaru, M. D.; Marte, A.; Belluzzi, E.; Russo, I.; Gabrielli, M.; Longo, F.; Arcuri, L.; Murru, L.; Bubacco, L.; Matteoli, M.; Fedele, E.; Sala, C.; Passafaro, M.; Morari, M.; Greggio, E.; Onofri, F.; Piccoli, G., LRRK2 kinase activity regulates synaptic vesicle trafficking and neurotransmitter release through modulation of LRRK2 macro-molecular complex. *Front Mol Neurosci* **2014,** *7*(49), 1-12.

59. Lee, H.; James, W. S.; Cowley, S. A., LRRK2 in peripheral and central nervous system innate immunity: its link to Parkinson's disease. *Biochem Soc Trans* **2017,** *45* (1), 131-139.

60. Biskup, S.; Moore, D. J.; Celsi, F.; Higashi, S.; West, A. B.; Andrabi, S. A.; Kurkinen, K.; Yu, S. W.; Savitt, J. M.; Waldvogel, H. J.; Faull, R. L.; Emson, P. C.; Torp, R.; Ottersen, O. P.; Dawson, T. M.; Dawson, V. L., Localization of LRRK2 to membranous and vesicular structures in mammalian brain. *Ann Neurol* **2006,** *60* (5), 557-569.

61. Alegre-Abarrategui, J.; Christian, H.; Lufino, M. M.; Mutihac, R.; Venda, L. L.; Ansorge, O.; Wade-Martins, R., LRRK2 regulates autophagic activity and localizes to specific membrane microdomains in a novel human genomic reporter cellular model. *Hum Mol Genet* **2009,** *18* (21), 4022-4034.

62. Vitte, J.; Traver, S.; Maues De Paula, A.; Lesage, S.; Rovelli, G.; Corti, O.; Duyckaerts, C.; Brice, A., Leucine-rich repeat kinase 2 is associated with the endoplasmic reticulum in dopaminergic neurons and accumulates in the core of Lewy bodies in Parkinson disease. *J Neuropathol Exp Neurol* **2010,** *69* (9), 959-972.

63. Fukuzono, T.; Pastuhov, S. I.; Fukushima, O.; Li, C.; Hattori, A.; Iemura, S.; Natsume, T.; Shibuya, H.; Hanafusa, H.; Matsumoto, K.; Hisamoto, N., Chaperone complex BAG2-HSC70 regulates localization of caenorhabditis elegans leucine-rich repeat kinase LRK-1 to the golgi. *Genes Cells* **2016,** *21* (4), 311-324.

64. Westerlund, M.; Belin, A. C.; Anvret, A.; Bickford, P.; Olson, L.; Galter, D., Developmental regulation of leucine-rich repeat kinase 1 and 2 expression in the brain and other rodent and human organs: implications for Parkinson's disease. *Neuroscience* **2008,** *152* (2), 429-436.

65. West, A. B., Achieving neuroprotection with LRRK2 kinase inhibitors in Parkinson disease. *Exp Neurol* **2017,** *298* (2017), 236-245.

66. Chan, S. L.; Tan, E. K., Targeting LRRK2 in Parkinson's disease: an update on recent developments. *Expert Opin Ther Targets* **2017,** *21* (6), 601-610.

67. Altman, J., Are new neurons formed in the brains of adult mammals? *Science* **1962,** *135* (3509), 1127-1128.

68. Frisen, J., Neurogenesis and gliogenesis in nervous system plasticity and repair. *Annu Rev Cell Dev Biol* **2016,** *32*, 127-141.

69. Abdipranoto, A.; Wu, S.; Stayte, S.; Vissel, B., The role of neurogenesis in neurodegenerative diseases and its implications for therapeutic development. *CNS Neurol Disord Drug Targets* **2008,** *7* (2), 187-210.

70. Hollands, C.; Bartolotti, N.; Lazarov, O., Alzheimer's disease and hippocampal adult neurogenesis; exploring shared mechanisms. *Front Neurosci* **2016,** *10*, 178.

71. Lamm, O.; Ganz, J.; Melamed, E.; Offen, D., Harnessing neurogenesis for the possible treatment of Parkinson's disease. *J Comp Neurol* **2014,** *522* (12), 2817-2830.

72. Zhao, C.; Deng, W.; Gage, F. H., Mechanisms and functional implications of adult neurogenesis. *Cell* **2008,** *132* (4), 645-660.

73. Spalding, K. L.; Bergmann, O.; Alkass, K.; Bernard, S.; Salehpour, M.; Huttner, H. B.; Bostrom, E.; Westerlund, I.; Vial, C.; Buchholz, B. A.; Possnert, G.; Mash, D. C.; Druid, H.; Frisen, J., Dynamics of hippocampal neurogenesis in adult humans. *Cell* **2013,** *153* (6), 1219-1227.

74. Noelanders, R.; Vleminckx, K., How Wnt signaling builds the brain: Bridging development and disease. *Neuroscientist* **2017,** *23* (3), 314-329.

75. Azim, K.; Fischer, B.; Hurtado-Chong, A.; Draganova, K.; Cantu, C.; Zemke, M.; Sommer, L.; Butt, A.; Raineteau, O., Persistent Wnt/beta-catenin signaling determines dorsalization of the postnatal subventricular zone and neural stem cell specification into oligodendrocytes and glutamatergic neurons. *Stem Cells* **2014,** *32* (5), 1301-1312.

76. Piccin, D.; Morshead, C. M., Wnt signaling regulates symmetry of division of neural stem cells in the adult brain and in response to injury. *Stem Cells* **2011,** *29* (3), 528-538.

77. Kurimoto, S.; Jung, J.; Tapadia, M.; Lengfeld, J.; Agalliu, D.; Waterman, M.; Mozaffar, T.; Gupta, R., Activation of the Wnt/beta-catenin signaling cascade after traumatic nerve injury. *Neuroscience* **2015,** *294*, 101-108.

78. Libro, R.; Bramanti, P.; Mazzon, E., The role of the Wnt canonical signaling in neurodegenerative diseases. *Life Sci* **2016,** *158*, 78-88.

79. L'Episcopo, F.; Tirolo, C.; Testa, N.; Caniglia, S.; Morale, M. C.; Serapide, M. F.; Pluchino, S.; Marchetti, B., Wnt/beta-catenin signaling is required to rescue midbrain dopaminergic progenitors and promote neurorepair in ageing mouse model of Parkinson's disease. *Stem Cells* **2014,** *32* (8), 2147-2163.

80. Hussaini, S. M.; Choi, C. I.; Cho, C. H.; Kim, H. J.; Jun, H.; Jang, M. H., Wnt signaling in neuropsychiatric disorders: ties with adult hippocampal neurogenesis and behavior. *Neurosci Biobehav Rev* **2014,** *47*, 369-383.

81. Berwick, D. C.; Harvey, K., LRRK2: an eminence grise of Wnt-mediated neurogenesis? *Front Cell Neurosci* **2013,** *7*, 82.

82. Sancho, R. M.; Law, B. M.; Harvey, K., Mutations in the LRRK2 Roc-COR tandem domain link Parkinson's disease to Wnt signalling pathways. *Hum Mol Genet* **2009,** *18* (20), 3955-3968.

83. Berwick, D. C.; Harvey, K., LRRK2 functions as a Wnt signaling scaffold, bridging cytosolic proteins and membrane-localized LRP6. *Hum Mol Genet* **2012,** *21* (22), 4966-4979.

84. Nixon-Abell, J.; Berwick, D. C.; Granno, S.; Spain, V. A.; Blackstone, C.; Harvey, K., Protective LRRK2 R1398H variant enhances GTPase and Wnt signaling activity. *Front Mol Neurosci* **2016,** *9*(18), 1-13.

85. Winner, B.; Melrose, H. L.; Zhao, C.; Hinkle, K. M.; Yue, M.; Kent, C.; Braithwaite, A. T.; Ogholikhan, S.; Aigner, R.; Winkler, J.; Farrer, M. J.; Gage, F. H., Adult neurogenesis and neurite outgrowth are impaired in LRRK2 G2019S mice. *Neurobiol Dis* **2011,** *41* (3), 706-716.

86. Liu, G. H.; Qu, J.; Suzuki, K.; Nivet, E.; Li, M.; Montserrat, N.; Yi, F.; Xu, X.; Ruiz, S.; Zhang, W.; Wagner, U.; Kim, A.; Ren, B.; Li, Y.; Goebl, A.; Kim, J.; Soligalla, R. D.; Dubova, I.; Thompson, J.; Yates, J., 3rd; Esteban, C. R.; Sancho-Martinez, I.; Izpisua Belmonte, J. C., Progressive degeneration of human neural stem cells caused by pathogenic LRRK2. *Nature* **2012,** *491* (7425), 603-607.

87. Arendt, T.; Stieler, J. T.; Holzer, M., Tau and tauopathies. *Brain Res Bull* **2016,** *126* (Pt 3), 238-292.

88. Chin, S. S.; Goldman, J. E., Glial inclusions in CNS degenerative diseases. *J Neuropathol Exp Neurol* **1996,** *55* (5), 499-508.

89. Spillantini, M. G.; Murrell, J. R.; Goedert, M.; Farlow, M. R.; Klug, A.; Ghetti, B., Mutation in the tau gene in familial multiple system tauopathy with presenile dementia. *Proc Natl Acad Sci U S A* **1998,** *95* (13), 7737-7741.

90. Spillantini, M. G.; Goedert, M.; Crowther, R. A.; Murrell, J. R.; Farlow, M. R.; Ghetti, B., Familial multiple system tauopathy with presenile dementia: a disease with abundant neuronal and glial tau filaments. *Proc Natl Acad Sci U S A* **1997,** *94* (8), 4113-4118.

91. Ballatore, C.; Lee, V. M.; Trojanowski, J. Q., Tau-mediated neurodegeneration in Alzheimer's disease and related disorders. *Nat Rev Neurosci* **2007,** *8* (9), 663-672.

92. Ferrer, I.; Legati, A.; Garcia-Monco, J. C.; Gomez-Beldarrain, M.; Carmona, M.; Blanco, R.; Seeley, W. W.; Coppola, G., Familial behavioral variant frontotemporal dementia associated with astrocyte-predominant tauopathy. *J Neuropathol Exp Neurol* **2015,** *74* (4), 370-379.

93. Williams, D. R., Tauopathies: classification and clinical update on neurodegenerative diseases associated with microtubule-associated protein tau. *Intern Med J* **2006,** *36* (10), 652-660.

94. Cairns, N. J.; Bigio, E. H.; Mackenzie, I. R.; Neumann, M.; Lee, V. M.; Hatanpaa, K. J.; White, C. L., 3rd; Schneider, J. A.; Grinberg, L. T.; Halliday, G.; Duyckaerts, C.; Lowe, J. S.; Holm, I. E.; Tolnay, M.; Okamoto, K.; Yokoo, H.; Murayama, S.; Woulfe, J.; Munoz, D. G.; Dickson, D. W.; Ince, P. G.; Trojanowski, J. Q.; Mann, D. M., Neuropathologic diagnostic and nosologic criteria for frontotemporal lobar degeneration: consensus of the consortium for frontotemporal lobar degeneration. *Acta Neuropathol* **2007,** *114* (1), 5-22.

95. Mackenzie, I. R.; Neumann, M.; Bigio, E. H.; Cairns, N. J.; Alafuzoff, I.; Kril, J.; Kovacs, G. G.; Ghetti, B.; Halliday, G.; Holm, I. E.; Ince, P. G.; Kamphorst, W.; Revesz, T.; Rozemuller, A. J.; Kumar-Singh, S.; Akiyama, H.; Baborie, A.; Spina, S.; Dickson, D. W.; Trojanowski, J. Q.; Mann, D. M., Nomenclature and nosology for neuropathologic subtypes of frontotemporal lobar degeneration: an update. *Acta Neuropathol* **2010,** *119* (1), 1-4.

96. Dickson, D. W.; Kouri, N.; Murray, M. E.; Josephs, K. A., Neuropathology of frontotemporal lobar degeneration-tau (FTLD-tau). *J Mol Neurosci* **2011,** *45* (3), 384-389.

97. Seltman, R. E.; Matthews, B. R., Frontotemporal lobar degeneration: epidemiology, pathology, diagnosis and management. *CNS Drugs* **2012,** *26* (10), 841-870.

98. McKee, A. C.; Cantu, R. C.; Nowinski, C. J.; Hedley-Whyte, E. T.; Gavett, B. E.; Budson, A. E.; Santini, V. E.; Lee, H. S.; Kubilus, C. A.; Stern, R. A., Chronic traumatic encephalopathy in athletes: progressive tauopathy after repetitive head injury. *J Neuropathol Exp Neurol* **2009,** *68* (7), 709-735.

99. Hof, P. R.; Bouras, C.; Perl, D. P.; Sparks, D. L.; Mehta, N.; Morrison, J. H., Age-related distribution of neuropathologic changes in the cerebral cortex of patients with Down's syndrome. Quantitative regional analysis and comparison with Alzheimer's disease. *Arch Neurol* **1995,** *52* (4), 379-391.

100. Bugiani, O.; Giaccone, G.; Piccardo, P.; Morbin, M.; Tagliavini, F.; Ghetti, B., Neuropathology of Gerstmann-Straussler-Scheinker disease. *Microsc Res Tech* **2000,** *50* (1), 10-15.

101. Vidal, R.; Revesz, T.; Rostagno, A.; Kim, E.; Holton, J. L.; Bek, T.; Bojsen-Moller, M.; Braendgaard, H.; Plant, G.; Ghiso, J.; Frangione, B., A decamer duplication in the 3' region of the BRI gene originates an amyloid peptide that is associated with dementia in a danish kindred. *Proc Natl Acad Sci U S A* **2000,** *97* (9), 4920-4925.

102. Andreadis, A.; Brown, W. M.; Kosik, K. S., Structure and novel exons of the human tau gene. *Biochemistry* **1992,** *31* (43), 10626-10633.

103. Goedert, M.; Spillantini, M. G.; Potier, M. C.; Ulrich, J.; Crowther, R. A., Cloning and sequencing of the cDNA encoding an isoform of microtubule-associated protein tau containing four tandem repeats: differential expression of tau protein mRNAs in human brain. *EMBO J* **1989,** *8* (2), 393-399.

104. Kovacs, G. G., Molecular pathological classification of neurodegenerative diseases: turning towards precision medicine. *Int J Mol Sci* **2016,** *17* (2), 1-33.

105. Rossi, G.; Tagliavini, F., Frontotemporal lobar degeneration: old knowledge and new insight into the pathogenetic mechanisms of tau mutations. *Front Aging Neurosci* **2015,** *7*(192), 1-15..

106. Lee, V. M.; Goedert, M.; Trojanowski, J. Q., Neurodegenerative tauopathies. *Annu Rev Neurosci* **2001,** *24*, 1121-1159.

107. Hutton, M.; Lendon, C. L.; Rizzu, P.; Baker, M.; Froelich, S.; Houlden, H.; Pickering-Brown, S.; Chakraverty, S.; Isaacs, A.; Grover, A.; Hackett, J.; Adamson, J.; Lincoln, S.; Dickson, D.; Davies, P.; Petersen, R. C.; Stevens, M.; de Graaff, E.; Wauters, E.; van Baren, J.; Hillebrand, M.; Joosse, M.; Kwon, J. M.; Nowotny, P.; Che, L. K.; Norton, J.; Morris, J. C.; Reed, L. A.; Trojanowski, J.; Basun, H.; Lannfelt, L.; Neystat, M.; Fahn, S.; Dark, F.; Tannenberg, T.; Dodd, P. R.; Hayward, N.; Kwok, J. B.; Schofield, P. R.; Andreadis, A.; Snowden, J.; Craufurd, D.; Neary, D.; Owen, F.; Oostra, B. A.; Hardy, J.; Goate, A.; van Swieten, J.; Mann, D.; Lynch, T.; Heutink, P., Association of missense and 5'-splice-site mutations in tau with the inherited dementia FTDP-17. *Nature* **1998,** *393* (6686), 702-705.

108. Jin, S. C.; Pastor, P.; Cooper, B.; Cervantes, S.; Benitez, B. A.; Razquin, C.; Goate, A.; Ibero-American Alzheimer Disease Genetics Group, R.; Cruchaga, C., Pooled-DNA sequencing identifies novel causative variants in PSEN1, GRN and MAPT in a clinical early-onset and familial Alzheimer's disease ibero-american cohort. *Alzheimers Res Ther* **2012,** *4* (4), 1-9.

109. Poorkaj, P.; Bird, T. D.; Wijsman, E.; Nemens, E.; Garruto, R. M.; Anderson, L.; Andreadis, A.; Wiederholt, W. C.; Raskind, M.; Schellenberg, G. D., Tau is a candidate gene for chromosome 17 frontotemporal dementia. *Ann Neurol* **1998,** *43* (6), 815-825.

110. Alonso, A. C.; Zaidi, T.; Grundke-Iqbal, I.; Iqbal, K., Role of abnormally phosphorylated tau in the breakdown of microtubules in Alzheimer disease. *Proc Natl Acad Sci U S A* **1994,** *91* (12), 5562-5566.

111. Feinstein, S. C.; Wilson, L., Inability of tau to properly regulate neuronal microtubule dynamics: a loss-of-function mechanism by which tau might mediate neuronal cell death. *Biochim Biophys Acta* **2005,** *1739* (2-3), 268-279.

112. Chen, J.; Kanai, Y.; Cowan, N. J.; Hirokawa, N., Projection domains of MAP2 and tau determine spacings between microtubules in dendrites and axons. *Nature* **1992,** *360* (6405), 674-677.

113. Janning, D.; Igaev, M.; Sundermann, F.; Bruhmann, J.; Beutel, O.; Heinisch, J. J.; Bakota, L.; Piehler, J.; Junge, W.; Brandt, R., Single-molecule tracking of tau reveals fast kiss-and-hop interaction with microtubules in living neurons. *Mol Biol Cell* **2014,** *25* (22), 3541-3551.

114. Kopke, E.; Tung, Y. C.; Shaikh, S.; Alonso, A. C.; Iqbal, K.; Grundke-Iqbal, I., Microtubule-associated protein tau. Abnormal phosphorylation of a non-paired helical filament pool in Alzheimer disease. *J Biol Chem* **1993,** *268* (32), 24374-24384.

115. Bramblett, G. T.; Goedert, M.; Jakes, R.; Merrick, S. E.; Trojanowski, J. Q.; Lee, V. M., Abnormal tau phosphorylation at Ser396 in Alzheimer's disease recapitulates development and contributes to reduced microtubule binding. *Neuron* **1993,** *10* (6), 1089-1099.

116. Lovestone, S.; Hartley, C. L.; Pearce, J.; Anderton, B. H., Phosphorylation of tau by glycogen synthase kinase-3 beta in intact mammalian cells: the effects on the organization and stability of microtubules. *Neuroscience* **1996,** *73* (4), 1145-1157.

117. Kowall, N. W.; Kosik, K. S., Axonal disruption and aberrant localization of tau protein characterize the neuropil pathology of Alzheimer's disease. *Ann Neurol* **1987,** *22* (5), 639-643.

118. Bancher, C.; Brunner, C.; Lassmann, H.; Budka, H.; Jellinger, K.; Wiche, G.; Seitelberger, F.; Grundke-Iqbal, I.; Iqbal, K.; Wisniewski, H. M., Accumulation of

abnormally phosphorylated tau precedes the formation of neurofibrillary tangles in Alzheimer's disease. *Brain Res Bull* **1989,** *477* (1-2), 90-99.

119. Mandelkow, E. M.; Mandelkow, E., Biochemistry and cell biology of tau protein in neurofibrillary degeneration. *Cold Spring Harb Perspect Med* **2012,** *2* (7), a006247.

120. Kruger, L.; Mandelkow, E. M., Tau neurotoxicity and rescue in animal models of human tauopathies. *Curr Opin Neurobiol* **2016,** *36*, 52-58.

121. Cope, T. E.; Rittman, T.; Borchert, R. J.; Jones, P. S.; Vatansever, D.; Allinson, K.; Passamonti, L.; Vazquez Rodriguez, P.; Bevan-Jones, W. R.; O'Brien, J. T.; Rowe, J. B., Tau burden and the functional connectome in Alzheimer's disease and progressive supranuclear palsy. *Brain* **2017**, 1-18.

122. Kawakami, F.; Yabata, T.; Ohta, E.; Maekawa, T.; Shimada, N.; Suzuki, M.; Maruyama, H.; Ichikawa, T.; Obata, F., LRRK2 phosphorylates tubulin-associated tau but not the free molecule: LRRK2-mediated regulation of the tau-tubulin association and neurite outgrowth. *PLoS One* **2012,** *7* (1), e30834.

123. Ujiie, S.; Hatano, T.; Kubo, S.; Imai, S.; Sato, S.; Uchihara, T.; Yagishita, S.; Hasegawa, K.; Kowa, H.; Sakai, F.; Hattori, N., LRRK2 I2020T mutation is associated with tau pathology. *Parkinsonism Relat Disord* **2012,** *18* (7), 819-823.

124. Bailey, R. M.; Covy, J. P.; Melrose, H. L.; Rousseau, L.; Watkinson, R.; Knight, J.; Miles, S.; Farrer, M. J.; Dickson, D. W.; Giasson, B. I.; Lewis, J., LRRK2 phosphorylates novel tau epitopes and promotes tauopathy. *Acta Neuropathol* **2013,** *126* (6), 809-827.

125. Hamm, M.; Bailey, R.; Shaw, G.; Yen, S. H.; Lewis, J.; Giasson, B. I., Physiologically relevant factors influence tau phosphorylation by leucine-rich repeat kinase 2. *J Neurosci Res* **2015,** *93* (10), 1567-1580.

126. Melrose, H. L.; Dachsel, J. C.; Behrouz, B.; Lincoln, S. J.; Yue, M.; Hinkle, K. M.; Kent, C. B.; Korvatska, E.; Taylor, J. P.; Witten, L.; Liang, Y. Q.; Beevers, J. E.; Boules, M.; Dugger, B. N.; Serna, V. A.; Gaukhman, A.; Yu, X.; Castanedes-Casey, M.; Braithwaite, A. T.; Ogholikhan, S.; Yu, N.; Bass, D.; Tyndall, G.; Schellenberg, G. D.; Dickson, D. W.; Janus, C.; Farrer, M. J., Impaired dopaminergic neurotransmission and microtubule-associated protein tau alterations in human LRRK2 transgenic mice. *Neurobiol Dis* **2010,** *40* (3), 503-517.

127. Wagner, U.; Utton, M.; Gallo, J. M.; Miller, C. C., Cellular phosphorylation of tau by GSK-3 beta influences tau binding to microtubules and microtubule organisation. *J Cell Sci* **1996,** *109 (Pt 6)*, 1537-1543.

128. Kawakami, F.; Shimada, N.; Ohta, E.; Kagiya, G.; Kawashima, R.; Maekawa, T.; Maruyama, H.; Ichikawa, T., Leucine-rich repeat kinase 2 regulates tau phosphorylation through direct activation of glycogen synthase kinase-3beta. *FEBS J* **2014,** *281* (1), 3-13.

129. Lin, C. H.; Tsai, P. I.; Wu, R. M.; Chien, C. T., LRRK2 G2019S mutation induces dendrite degeneration through mislocalization and phosphorylation of tau by recruiting autoactivated GSK3s. *J Neurosci* **2010,** *30* (39), 13138-13149.

130. Ohta, E.; Nihira, T.; Uchino, A.; Imaizumi, Y.; Okada, Y.; Akamatsu, W.; Takahashi, K.; Hayakawa, H.; Nagai, M.; Ohyama, M.; Ryo, M.; Ogino, M.; Murayama, S.; Takashima, A.; Nishiyama, K.; Mizuno, Y.; Mochizuki, H.; Obata, F.; Okano, H., I2020T mutant LRRK2 iPSC-derived neurons in the Sagamihara family exhibit increased tau phosphorylation through the AKT/GSK-3beta signaling pathway. *Hum Mol Genet* **2015,** *24* (17), 4879-4900.

131. Lin, C. H.; Lin, H. I.; Chen, M. L.; Lai, T. T.; Cao, L. P.; Farrer, M. J.; Wu, R. M.; Chien, C. T., Lovastatin protects neurite degeneration in LRRK2-G2019S parkinsonism through activating the Akt/Nrf pathway and inhibiting GSK3beta activity. *Hum Mol Genet* **2016,** *25* (10), 1965-1978.

132. Shanley, M. R.; Hawley, D.; Leung, S.; Zaidi, N. F.; Dave, R.; Schlosser, K. A.; Bandopadhyay, R.; Gerber, S. A.; Liu, M., LRRK2 facilitates tau phosphorylation through strong interaction with tau and cdk5. *Biochemistry* **2015,** *54* (33), 5198-5208.

133. Guerreiro, P. S.; Gerhardt, E.; Lopes da Fonseca, T.; Bahr, M.; Outeiro, T. F.; Eckermann, K., LRRK2 promotes tau accumulation, aggregation and release. *Mol Neurobiol* **2016,** *53* (5), 3124-3135.

134. Khan, N. L.; Jain, S.; Lynch, J. M.; Pavese, N.; Abou-Sleiman, P.; Holton, J. L.; Healy, D. G.; Gilks, W. P.; Sweeney, M. G.; Ganguly, M.; Gibbons, V.; Gandhi, S.; Vaughan, J.; Eunson, L. H.; Katzenschlager, R.; Gayton, J.; Lennox, G.; Revesz, T.; Nicholl, D.; Bhatia, K. P.; Quinn, N.; Brooks, D.; Lees, A. J.; Davis, M. B.; Piccini, P.; Singleton, A. B.; Wood, N. W., Mutations in the gene LRRK2 encoding dardarin (PARK8) cause familial Parkinson's disease: clinical, pathological, olfactory and functional imaging and genetic data. *Brain* **2005,** *128* (Pt 12), 2786-2796.

135. Ross, O. A.; Whittle, A. J.; Cobb, S. A.; Hulihan, M. M.; Lincoln, S. J.; Toft, M.; Farrer, M. J.; Dickson, D. W., Lrrk2 R1441 substitution and progressive supranuclear palsy. *Neuropathol Appl Neurobiol* **2006,** *32* (1), 23-25.

136. Rajput, A.; Dickson, D. W.; Robinson, C. A.; Ross, O. A.; Dachsel, J. C.; Lincoln, S. J.; Cobb, S. A.; Rajput, M. L.; Farrer, M. J., Parkinsonism, Lrrk2 G2019S, and tau neuropathology. *Neurology* **2006,** *67* (8), 1506-1508.

137. Miklossy, J.; Qing, H.; Guo, J. P.; Yu, S.; Wszolek, Z. K.; Calne, D.; McGeer, E. G.; McGeer, P. L., Lrrk2 and chronic inflammation are linked to pallido-ponto-nigral degeneration caused by the N279K tau mutation. *Acta Neuropathol* **2007,** *114* (3), 243-254.

138. Poulopoulos, M.; Cortes, E.; Vonsattel, J. P.; Fahn, S.; Waters, C.; Cote, L. J.; Moskowitz, C.; Honig, L. S.; Clark, L. N.; Marder, K. S.; Alcalay, R. N., Clinical and pathological characteristics of LRRK2 G2019S patients with PD. *J Mol Neurosci* **2012,** *47* (1), 139-143.

139. Puschmann, A.; Englund, E.; Ross, O. A.; Vilarino-Guell, C.; Lincoln, S. J.; Kachergus, J. M.; Cobb, S. A.; Tornqvist, A. L.; Rehncrona, S.; Widner, H.; Wszolek, Z. K.; Farrer, M. J.; Nilsson, C., First neuropathological description of a patient with Parkinson's disease and LRRK2 p.N1437H mutation. *Parkinsonism Relat Disord* **2012,** *18* (4), 332-338.

140. Ruffmann, C.; Giaccone, G.; Canesi, M.; Bramerio, M.; Goldwurm, S.; Gambacorta, M.; Rossi, G.; Tagliavini, F.; Pezzoli, G., Atypical tauopathy in a patient with LRRK2-G2019S mutation and tremor-dominant parkinsonism. *Neuropathol Appl Neurobiol* **2012,** *38* (4), 382-386.

141. Aasly, J. O.; Shi, M.; Sossi, V.; Stewart, T.; Johansen, K. K.; Wszolek, Z. K.; Uitti, R. J.; Hasegawa, K.; Yokoyama, T.; Zabetian, C. P.; Kim, H. M.; Leverenz, J. B.; Ginghina, C.; Armaly, J.; Edwards, K. L.; Snapinn, K. W.; Stoessl, A. J.; Zhang, J., Cerebrospinal fluid amyloid beta and tau in LRRK2 mutation carriers. *Neurology* **2012,** *78* (1), 55-61.

142. Wilson, S. W.; Houart, C., Early steps in the development of the forebrain. *Dev Cell* **2004,** *6* (2), 167-181.

143. Wassle, H., Parallel processing in the mammalian retina. *Nat Rev Neurosci* **2004,** *5* (10), 747-757.

144. Prasad, S.; Galetta, S. L., Anatomy and physiology of the afferent visual system. *Handb Clin Neurol* **2011,** *102*, 3-19.

145. Jindal, V., Interconnection between brain and retinal neurodegenerations. *Mol Neurobiol* **2015,** *51* (3), 885-892.

146. Reynolds, A.; Laurie, C.; Mosley, R. L.; Gendelman, H. E., Oxidative stress and the pathogenesis of neurodegenerative disorders. *Int Rev Neurobiol* **2007,** *82*, 297-325.

147. You, Y.; Gupta, V. K.; Graham, S. L.; Klistorner, A., Anterograde degeneration along the visual pathway after optic nerve injury. *PLoS One* **2012,** *7* (12), e52061.

148. Buhl, E. H.; Schwerdtfeger, W. K.; Germroth, P.; Singer, W., Combining retrograde tracing, intracellular injection, anterograde degeneration and electron microscopy to reveal synaptic links. *J Neurosci Methods* **1989,** *29* (3), 241-250.

149. Gupta, S.; Zivadinov, R.; Ramanathan, M.; Weinstock-Guttman, B., Optical coherence tomography and neurodegeneration: are eyes the windows to the brain? *Expert Rev Neurother* **2016,** *16* (7), 765-775.

150. Hippert, C.; Graca, A. B.; Barber, A. C.; West, E. L.; Smith, A. J.; Ali, R. R.; Pearson, R. A., Muller glia activation in response to inherited retinal degeneration is highly varied and disease-specific. *PLoS One* **2015,** *10* (3), e0120415.

151. London, A.; Benhar, I.; Schwartz, M., The retina as a window to the brain-from eye research to CNS disorders. *Nat Rev Neurol* **2013,** *9* (1), 44-53.

152. Cuenca, N.; Fernandez-Sanchez, L.; Campello, L.; Maneu, V.; De la Villa, P.; Lax, P.; Pinilla, I., Cellular responses following retinal injuries and therapeutic approaches for neurodegenerative diseases. *Prog Retin Eye Res* **2014,** *43*, 17-75.

153. Natarajan, S., Retinitis pigmentosa: a brief overview. *Indian J Ophthalmol* **2011,** *59* (5), 343-346.

154. Daiger, S. P.; Bowne, S. J.; Sullivan, L. S., Perspective on genes and mutations causing retinitis pigmentosa. *Arch Ophthalmol* **2007,** *125* (2), 151-158.

155. Nash, B. M.; Wright, D. C.; Grigg, J. R.; Bennetts, B.; Jamieson, R. V., Retinal dystrophies, genomic applications in diagnosis and prospects for therapy. *Transl Pediatr* **2015,** *4* (2), 139-163.

156. Chang, S.; Vaccarella, L.; Olatunji, S.; Cebulla, C.; Christoforidis, J., Diagnostic challenges in retinitis pigmentosa: genotypic multiplicity and phenotypic variability. *Curr Genomics* **2011,** *12* (4), 267-275.

157. Chizzolini, M.; Galan, A.; Milan, E.; Sebastiani, A.; Costagliola, C.; Parmeggiani, F., Good epidemiologic practice in retinitis pigmentosa: from phenotyping to biobanking. *Curr Genomics* **2011,** *12* (4), 260-266.

158. Walsh, D. P.; Chang, Y. T., Chemical genetics. *Chem Rev* **2006,** *106* (6), 2476-2530.

159. Zheng, X. F.; Chan, T. F., Chemical genomics in the global study of protein functions. *Drug Discov Today* **2002,** *7* (3), 197-205.

160. Zheng, X. S.; Chan, T. F.; Zhou, H. H., Genetic and genomic approaches to identify and study the targets of bioactive small molecules. *Chem Biol* **2004,** *11* (5), 609-618.

161. Fisher, M.; Nelson, A., The chemical genetic approach: the interrogation of biological mechanisms with small molecule probes. In *New Frontiers in Chemical Biology: Enabling Drug Discovery*, Bunnage, M., Ed. Royal Society of Chemistry: Cambridge, UK, 2011; Vol. 5, pp 1-32.

162. Galatsis, P., Leucine-rich repeat kinase 2 inhibitors: a patent review (2014-2016). *Expert Opin Ther Pat* **2017,** *27* (6), 667-676.

163. Covy, J. P.; Giasson, B. I., Identification of compounds that inhibit the kinase activity of leucine-rich repeat kinase 2. *Biochem Biophys Res Commun* **2009,** *378* (3), 473-477.

164. Nichols, R. J.; Dzamko, N.; Hutti, J. E.; Cantley, L. C.; Deak, M.; Moran, J.; Bamborough, P.; Reith, A. D.; Alessi, D. R., Substrate specificity and inhibitors of LRRK2, a protein kinase mutated in Parkinson's disease. *Biochem J* **2009,** *424* (1), 47-60.

165. Deng, X.; Dzamko, N.; Prescott, A.; Davies, P.; Liu, Q.; Yang, Q.; Lee, J. D.; Patricelli, M. P.; Nomanbhoy, T. K.; Alessi, D. R.; Gray, N. S., Characterization of a selective inhibitor of the Parkinson's disease kinase LRRK2. *Nat Chem Biol* **2011,** *7* (4), 203-205.

166. Luerman, G. C.; Nguyen, C.; Samaroo, H.; Loos, P.; Xi, H.; Hurtado-Lorenzo, A.; Needle, E.; Stephen Noell, G.; Galatsis, P.; Dunlop, J.; Geoghegan, K. F.; Hirst, W. D., Phosphoproteomic evaluation of pharmacological inhibition of leucine-rich

repeat kinase 2 reveals significant off-target effects of LRRK-2-IN-1. *J Neurochem* **2014,** *128* (4), 561-576.

167. Ramsden, N.; Perrin, J.; Ren, Z.; Lee, B. D.; Zinn, N.; Dawson, V. L.; Tam, D.; Bova, M.; Lang, M.; Drewes, G.; Bantscheff, M.; Bard, F.; Dawson, T. M.; Hopf, C., Chemoproteomics-based design of potent LRRK2-selective lead compounds that attenuate Parkinson's disease-related toxicity in human neurons. *ACS Chem Biol* **2011,** *6* (10), 1021-1028.

168. Zhang, J.; Deng, X.; Choi, H. G.; Alessi, D. R.; Gray, N. S., Characterization of TAE684 as a potent LRRK2 kinase inhibitor. *Bioorg Med Chem Lett* **2012,** *22* (5), 1864-1869.

169. Choi, H. G.; Zhang, J.; Deng, X.; Hatcher, J. M.; Patricelli, M. P.; Zhao, Z.; Alessi, D. R.; Gray, N. S., Brain penetrant LRRK2 inhibitor. *ACS Med Chem Lett* **2012,** *3* (8), 658-662.

170. Chen, H.; Chan, B. K.; Drummond, J.; Estrada, A. A.; Gunzner-Toste, J.; Liu, X.; Liu, Y.; Moffat, J.; Shore, D.; Sweeney, Z. K.; Tran, T.; Wang, S.; Zhao, G.; Zhu, H.; Burdick, D. J., Discovery of selective LRRK2 inhibitors guided by computational analysis and molecular modeling. *J Med Chem* **2012,** *55* (11), 5536-5545.

171. Estrada, A. A.; Liu, X.; Baker-Glenn, C.; Beresford, A.; Burdick, D. J.; Chambers, M.; Chan, B. K.; Chen, H.; Ding, X.; DiPasquale, A. G.; Dominguez, S. L.; Dotson, J.; Drummond, J.; Flagella, M.; Flynn, S.; Fuji, R.; Gill, A.; Gunzner-Toste, J.; Harris, S. F.; Heffron, T. P.; Kleinheinz, T.; Lee, D. W.; Le Pichon, C. E.; Lyssikatos, J. P.; Medhurst, A. D.; Moffat, J. G.; Mukund, S.; Nash, K.; Scearce-Levie, K.; Sheng, Z.; Shore, D. G.; Tran, T.; Trivedi, N.; Wang, S.; Zhang, S.; Zhang, X.; Zhao, G.; Zhu, H.; Sweeney, Z. K., Discovery of highly potent, selective, and brain-penetrable leucine-rich repeat kinase 2 (LRRK2) small molecule inhibitors. *J Med Chem* **2012,** *55* (22), 9416-9433.

172. Estrada, A. A.; Chan, B. K.; Baker-Glenn, C.; Beresford, A.; Burdick, D. J.; Chambers, M.; Chen, H.; Dominguez, S. L.; Dotson, J.; Drummond, J.; Flagella, M.; Fuji, R.; Gill, A.; Halladay, J.; Harris, S. F.; Heffron, T. P.; Kleinheinz, T.; Lee, D. W.; Le Pichon, C. E.; Liu, X.; Lyssikatos, J. P.; Medhurst, A. D.; Moffat, J. G.; Nash, K.; Scearce-Levie, K.; Sheng, Z.; Shore, D. G.; Wong, S.; Zhang, S.; Zhang, X.; Zhu, H.; Sweeney, Z. K., Discovery of highly potent, selective, and brain-penetrant

aminopyrazole leucine-rich repeat kinase 2 (LRRK2) small molecule inhibitors. *J Med Chem* **2014,** *57* (3), 921-936.

173. Fuji, R. N.; Flagella, M.; Baca, M.; Baptista, M. A.; Brodbeck, J.; Chan, B. K.; Fiske, B. K.; Honigberg, L.; Jubb, A. M.; Katavolos, P.; Lee, D. W.; Lewin-Koh, S. C.; Lin, T.; Liu, X.; Liu, S.; Lyssikatos, J. P.; O'Mahony, J.; Reichelt, M.; Roose-Girma, M.; Sheng, Z.; Sherer, T.; Smith, A.; Solon, M.; Sweeney, Z. K.; Tarrant, J.; Urkowitz, A.; Warming, S.; Yaylaoglu, M.; Zhang, S.; Zhu, H.; Estrada, A. A.; Watts, R. J., Effect of selective LRRK2 kinase inhibition on nonhuman primate lung. *Sci Transl Med* **2015,** *7* (273), 273ra215.

174. Troxler, T.; Greenidge, P.; Zimmermann, K.; Desrayaud, S.; Druckes, P.; Schweizer, T.; Stauffer, D.; Rovelli, G.; Shimshek, D. R., Discovery of novel indolinone-based, potent, selective and brain penetrant inhibitors of LRRK2. *Bioorg Med Chem Lett* **2013,** *23* (14), 4085-4090.

175. Göring, S.; Taymans, J. M.; Baekelandt, V.; Schmidt, B., Indolinone based LRRK2 kinase inhibitors with a key hydrogen bond. *Bioorg Med Chem Lett* **2014,** *24* (19), 4630-4637.

176. Schulz, S.; Göring, S.; Schmidt, B.; Hopf, C., LRRK2 kinase inhibitors as new drugs for Parkinson´s disease? In *Emerging drugs and targets for Parkinson´s disease*, Martinez, A.; Gil, C., Eds. Royal Society of Chemistry: Cambridge, UK, 2013; Vol. 34, pp 266-293.

177. Reith, A. D.; Bamborough, P.; Jandu, K.; Andreotti, D.; Mensah, L.; Dossang, P.; Choi, H. G.; Deng, X.; Zhang, J.; Alessi, D. R.; Gray, N. S., GSK2578215A; a potent and highly selective 2-arylmethyloxy-5-substitutent-N-arylbenzamide LRRK2 kinase inhibitor. *Bioorg Med Chem Lett* **2012,** *22* (17), 5625-5629.

178. Afsari, F.; Christensen, K. V.; Smith, G. P.; Hentzer, M.; Nippe, O. M.; Elliott, C. J.; Wade, A. R., Abnormal visual gain control in a Parkinson's disease model. *Hum Mol Genet* **2014,** *23* (17), 4465-4478.

179. Fell, M. J.; Mirescu, C.; Basu, K.; Cheewatrakoolpong, B.; DeMong, D. E.; Ellis, J. M.; Hyde, L. A.; Lin, Y.; Markgraf, C. G.; Mei, H.; Miller, M.; Poulet, F. M.; Scott, J. D.; Smith, M. D.; Yin, Z.; Zhou, X.; Parker, E. M.; Kennedy, M. E.; Morrow, J. A., MLi-2, a potent, selective, and centrally active compound for exploring the

therapeutic potential and safety of LRRK2 kinase inhibition. *J Pharmacol Exp Ther* **2015,** *355* (3), 397-409.

180. Miklavc, P.; Ehinger, K.; Thompson, K. E.; Hobi, N.; Shimshek, D. R.; Frick, M., Surfactant secretion in LRRK2 knock-out rats: changes in lamellar body morphology and rate of exocytosis. *PLoS One* **2014,** *9* (1), e84926.

181. Baptista, M. A.; Merchant, K. M.; Bharghava, S.; Bryce, D.; Ellis, E.; Estrada, A. A. In *LRRK2 kinase inhibitors of different structural classes induce abnormal, but reversible, accumulation of lamellar bodies in type II pneumocytes in non-huma primates*, Society for Neuroscience, Chicago, Chicago, 2015.

182. Pardridge, W. M., The blood-brain barrier: bottleneck in brain drug development. *NeuroRx* **2005,** *2* (1), 3-14.

183. Lipinski, C. A.; Lombardo, F.; Dominy, B. W.; Feeney, P. J., Experimental and computational approaches to estimate solubility and permeability in drug discovery and development settings. *Adv Drug Deliv Rev* **2001,** *46* (1-3), 3-26.

184. Levin, V. A., Relationship of octanol/water partition coefficient and molecular weight to rat brain capillary permeability. *J Med Chem* **1980,** *23* (6), 682-684.

185. Nies, A. T., The role of membrane transporters in drug delivery to brain tumors. *Cancer Lett* **2007,** *254* (1), 11-29.

186. Salado, I. G.; Zaldivar-Diez, J.; Sebastian-Perez, V.; Li, L.; Geiger, L.; Gonzalez, S.; Campillo, N. E.; Gil, C.; Morales, A. V.; Perez, D. I.; Martinez, A., Leucine rich repeat kinase 2 (LRRK2) inhibitors based on indolinone scaffold: Potential pro-neurogenic agents. *Eur J Med Chem* **2017,** *138*, 328-342.

187. Wang, T.; Duffy, J. P.; Wang, J.; Halas, S.; Salituro, F. G.; Pierce, A. C.; Zuccola, H. J.; Black, J. R.; Hogan, J. K.; Jepson, S.; Shlyakter, D.; Mahajan, S.; Gu, Y.; Hoock, T.; Wood, M.; Furey, B. F.; Frantz, J. D.; Dauffenbach, L. M.; Germann, U. A.; Fan, B.; Namchuk, M.; Bennani, Y. L.; Ledeboer, M. W., Janus kinase 2 inhibitors. Synthesis and characterization of a novel polycyclic azaindole. *J Med Chem* **2009,** *52* (24), 7938-7941.

188. Guex, N.; Peitsch, M. C., SWISS-MODEL and the Swiss-PdbViewer: an environment for comparative protein modeling. *Electrophoresis* **1997,** *18* (15), 2714-2723.

189. Bairoch, A.; Boeckmann, B.; Ferro, S.; Gasteiger, E., Swiss-Prot: juggling between evolution and stability. *Brief Bioinform* **2004,** *5* (1), 39-55.

190. Thompson, J. D.; Higgins, D. G.; Gibson, T. J., CLUSTAL W: improving the sensitivity of progressive multiple sequence alignment through sequence weighting, position-specific gap penalties and weight matrix choice. *Nucleic Acids Res* **1994,** *22* (22), 4673-4680.

191. Ghose, A. K.; Jaeger, E. P.; Kowalczyk, P. J.; Peterson, M. L.; Treasurywala, A. M., Conformational searching methods for small molecules. I. Study of the sybyl search method. *J Comput Chem* **1993,** *14* (9), 1050-1065.

192. Gopalakrishnan, K.; Sowmiya, G.; Sheik, S. S.; Sekar, K., Ramachandran plot on the web (2.0). *Protein Pept Lett* **2007,** *14* (7), 669-671.

193. Eisenberg, D.; Luthy, R.; Bowie, J. U., VERIFY3D: assessment of protein models with three-dimensional profiles. *Methods Enzymol* **1997,** *277*, 396-404.

194. Colovos, C.; Yeates, T. O., Verification of protein structures: Patterns of nonbonded atomic interactions. *Protein Science* **1993,** *2* (9), 1511-1519.

195. Kufareva, I.; Abagyan, R., Methods of protein structure comparison. *Methods Mol Biol* **2012,** *857*, 231-257.

196. Schrödinger Release 2015-4: Glide, v., Schrödinger, LLC, New York, NY, 2015.

197. Kaur, N. K., D., Montmorillonite: an efficient, heterogeneous and green catalyst for organic synthesis. *J Chem Pharm Res* **2012,** *4* (2), 991-1015.

198. Salonen, L. M.; Ellermann, M.; Diederich, F., Aromatic rings in chemical and biological recognition: energetics and structures. *Angew Chem Int Ed* **2011,** *50* (21), 4808-4842.

199. Alekseyeva, E. A. B., A.S.; Boyd, L.A.; Foz, M.A.; Hibbert, T.G.; Howard, JAK.; Hugh MacBride, J.A.; Mackinnon, A.; Wadde, K., Intra-and inter-molecular carbonyl C-H-N nydrogen bonds in pyridyl-containing *ortho* carboranes. *Dalton Trans* **2003**, 475-482.

200. Kola, I.; Landis, J., Can the pharmaceutical industry reduce attrition rates? *Nat Rev Drug Discov* **2004,** *3* (8), 711-715.

201. Di, L.; Kerns, E. H.; Fan, K.; McConnell, O. J.; Carter, G. T., High throughput artificial membrane permeability assay for blood-brain barrier. *Eur J Med Chem* **2003,** *38* (3), 223-232.

202. Abdipranoto, A.; Wu, S.; Stayte, S.; Vissel, B., The role of neurogenesis in neurodegenerative diseases and its implications for therapeutic development. *CNS Neurol. Disord Drug Targets* **2008,** *7* (2), 187-210.

203. Davies, S.; Kennewell, P.; Russell, A.; Silpa, L.; Westwood, R.; Wynne, G., Regenerative Medicine. In *Comprenhinsive Medicinal Chemistry III General Perspective – The Future of Drug Discovery*, Martinez, A.; Gil, C., Ed. Elservier: New York, USA, 2017; Vol. 1, pp 379-428.

204. Felsenstein, K. M.; Candelario, K. M.; Steindler, D. A.; Borchelt, D. R., Regenerative medicine in Alzheimer's disease. *Transl Res* **2014,** *163* (4), 432-438.

205. Dunnett, S. B.; Bjorklund, A.; Stenevi, U.; Iversen, S. D., Behavioural recovery following transplantation of substantia nigra in rats subjected to 6-OHDA lesions of the nigrostriatal pathway. I. Unilateral lesions. *Brain Res* **1981,** *215* (1-2), 147-161.

206. Kefalopoulou, Z.; Politis, M.; Piccini, P.; Mencacci, N.; Bhatia, K.; Jahanshahi, M.; Widner, H.; Rehncrona, S.; Brundin, P.; Bjorklund, A.; Lindvall, O.; Limousin, P.; Quinn, N.; Foltynie, T., Long-term clinical outcome of fetal cell transplantation for Parkinson disease: two case reports. *JAMA Neurol* **2014,** *71* (1), 83-87.

207. Steinbeck, J. A.; Studer, L., Moving stem cells to the clinic: potential and limitations for brain repair. *Neuron* **2015,** *86* (1), 187-206.

208. Herrera-Arozamena, C.; Marti-Mari, O.; Estrada, M.; de la Fuente Revenga, M.; Rodriguez-Franco, M. I., Recent advances in neurogenic small molecules as innovative treatments for neurodegenerative diseases. *Molecules* **2016,** *21*(9), 1-21.

209. Takahashi, K.; Yamanaka, S., Induction of pluripotent stem cells from mouse embryonic and adult fibroblast cultures by defined factors. *Cell* **2006,** *126* (4), 663-676.

210. Haggarty, S. J.; Silva, M. C.; Cross, A.; Brandon, N. J.; Perlis, R. H., Advancing drug discovery for neuropsychiatric disorders using patient-specific stem cell models. *Mol Cell Neurosci* **2016,** *73*, 104-115.

211. Cheng, C.; Fass, D. M.; Folz-Donahue, K.; MacDonald, M. E.; Haggarty, S. J., Highly expandable human iPS cell-derived neural progenitor cells (NPC) and neurons for central nervous system disease modeling and high-throughput screening. *Curr Protoc Hum Genet* **2017,** *92*, 2181-2182

212. Zhao, W.-N.; Cheng, C.; Theriault, K. M.; Sheridan, S. D.; Tsai, L.-H.; Haggarty, S. J., A high-throughput screen for wnt/β-catenin signaling pathway modulators in human iPSC-derived neural progenitors. *J Biomol Screening* **2012,** *17* (9), 1252-1263.

213. Pastrana, E.; Silva-Vargas, V.; Doetsch, F., Eyes wide open: a critical review of sphere-formation as an assay for stem cells. *Cell Stem Cell* **2011,** *8* (5), 486-498.

214. Reynolds, A.; Weiss, S., Generation of neurons and astrocytes from isolated cells of the adult mammalian central nervous system. *Science* **1992,** *255*, 1707-1710.

215. Gil-Perotin, S.; Duran-Moreno, M.; Cebrian-Silla, A.; Ramirez, M.; Garcia-Belda, P.; Garcia-Verdugo, J. M., Adult neural stem cells from the subventricular zone: a review of the neurosphere assay. *Anat Rec (Hoboken)* **2013,** *296* (9), 1435-1452.

216. Gabay, L.; Lowell, S.; Rubin, L. L.; Anderson, D. J., Deregulation of dorsoventral patterning by FGF confers trilineage differentiation capacity on CNS stem cells in vitro. *Neuron* **2003,** *40* (3), 485-499.

217. Chojnacki, A.; Weiss, S., Production of neurons, astrocytes and oligodendrocytes from mammalian CNS stem cells. *Nat Protoc* **2008,** *3* (6), 935-940.

218. Coles-Takabe, B. L.; Brain, I.; Purpura, K. A.; Karpowicz, P.; Zandstra, P. W.; Morshead, C. M.; van der Kooy, D., Don't look: growing clonal versus nonclonal neural stem cell colonies. *Stem Cells* **2008,** *26* (11), 2938-2944.

219. Biskup, S.; Moore, D. J.; Celsi, F.; Higashi, S.; West, A. B.; Andrabi, S. A.; Kurkinen, K.; Yu, S. W.; Savitt, J. M.; Waldvogel, H. J.; Faull, R. L.; Emson, P. C.; Torp, R.; Ottersen, O. P.; Dawson, T. M.; Dawson, V. L., Localization of LRRK2 to membranous and vesicular structures in mammalian brain. *Ann Neurol* **2006,** *60* (5), 557-569.

220. Melrose, H. L.; Kent, C. B.; Taylor, J. P.; Dachsel, J. C.; Hinkle, K. M.; Lincoln, S. J.; Mok, S. S.; Culvenor, J. G.; Masters, C. L.; Tyndall, G. M.; Bass, D. I.; Ahmed, Z.; Andorfer, C. A.; Ross, O. A.; Wszolek, Z. K.; Delldonne, A.; Dickson, D. W.; Farrer, M. J., A comparative analysis of leucine-rich repeat kinase 2 (Lrrk2) expression in mouse brain and Lewy body disease. *Neuroscience* **2007,** *147* (4), 1047-1058.

221. Fuentealba, L. C.; Obernier, K.; Alvarez-Buylla, A., Adult neural stem cells bridge their niche. *Cell Stem Cell* **2012,** *10* (6), 698-708.

222. Nieto-Estevez, V.; Oueslati-Morales, C. O.; Li, L.; Pickel, J.; Morales, A. V.; Vicario-Abejon, C., Brain insulin-like growth factor-I directs the transition from stem cells to mature neurons during postnatal/adult hippocampal neurogenesis. *Stem Cells* **2016,** *34* (8), 2194-2209.

223. Mudher, A.; Brion, J.-P.; Avila, J.; Medina, M.; Buée, L., EuroTau: towing scientists to tau without tautology. *Acta Neuropathol Commun* **2017,** *5* (1), 1-4.

224. Medina, M.; Avila, J., New perspectives on the role of tau in Alzheimer's disease. Implications for therapy. *Biochem Pharmacol* **2014,** *88* (4), 540-547.

225. Andreadis, A., Tau splicing and the intricacies of dementia. *J Cell Physiol* **2012,** *227* (3), 1220-1225.

226. Kaufman, S. K.; Thomas, T. L.; Del Tredici, K.; Braak, H.; Diamond, M. I., Characterization of tau prion seeding activity and strains from formaldehyde-fixed tissue. *Acta Neuropathol Commun* **2017,** *5* (1), 1-12.

227. de Calignon, A.; Polydoro, M.; Suarez-Calvet, M.; William, C.; Adamowicz, D. H.; Kopeikina, K. J.; Pitstick, R.; Sahara, N.; Ashe, K. H.; Carlson, G. A.; Spires-Jones, T. L.; Hyman, B. T., Propagation of tau pathology in a model of early Alzheimer's disease. *Neuron* **2012,** *73* (4), 685-697.

228. Kamat, P. K.; Rai, S.; Swarnkar, S.; Shukla, R.; Nath, C., Molecular and cellular mechanism of okadaic acid (OKA)-induced neurotoxicity: a novel tool for Alzheimer's disease therapeutic application. *Mol Neurobiol* **2014,** *50* (3), 852-865.

229. Tachibana, K.; Scheuer, P. J.; Tsukitani, Y.; Kikuchi, H.; Van Engen, D.; Clardy, J.; Gopichand, Y.; Schmitz, F. J., Okadaic acid, a cytotoxic polyether from two marine sponges of the genus Halichondria. *J Am Chem Soc* **1981,** *103* (9), 2469-2471.

230. Li, R.; Xu, D. E.; Ma, T., Lovastatin suppresses the aberrant tau phosphorylation from FTDP-17 mutation and okadaic acid-induction in rat primary neurons. *Neuroscience* **2015,** *294*, 14-20.

231. Placido, A. I.; Pereira, C. M.; Correira, S. C.; Carvalho, C.; Oliveira, C. R.; Moreira, P. I., Phosphatase 2A inhibition affects endoplasmic reticulum and mitochondria homeostasis via cytoskeletal alterations in brain endothelial cells. *Mol Neurobiol* **2017,** *54* (1), 154-168.

232. Das, V.; Miller, J. H., Microtubule stabilization by peloruside A and paclitaxel rescues degenerating neurons from okadaic acid-induced tau phosphorylation. *Eur J Neurosci* **2012,** *35* (11), 1705-1717.

233. Martinez, A.; Castro, A.; Dorronsoro, I.; Alonso, M., Glycogen synthase kinase 3 (GSK-3) inhibitors as new promising drugs for diabetes, neurodegeneration, cancer, and inflammation. *Med Res Rev* **2002,** *22* (4), 373-384.

234. Yuan, L.; Hassan, B. A., Neurogenins in brain development and disease: an overview. *Arch Biochem Biophys* **2014,** *558*, 10-13.

235. Sun, Y.; Nadal-Vicens, M.; Misono, S.; Lin, M. Z.; Zubiaga, A.; Hua, X.; Fan, G.; Greenberg, M. E., Neurogenin promotes neurogenesis and inhibits glial differentiation by independent mechanisms. *Cell* **2001,** *104* (3), 365-376.

236. Cheng, C.; Fass, D. M.; Folz-Donahue, K.; MacDonald, M. E.; Haggarty, S. J., Highly expandable human iPS cell-derived neural progenitor cells (NPC) and neurons for central nervous system disease modeling and high-throughput screening. *Curr Protoc Hum Genet* **2017,** *92*, 2181-2182.

237. Silva, M. C.; Cheng, C.; Mair, W.; Almeida, S.; Fong, H.; Biswas, H. U.; Zhang, Z.; Huang, Y.; Temple, S.; Coppola, G.; Geschwind, D. H.; Karydas, A.; Miller, B. L.; Kosik, K. S.; Gao, F.; Steen, J. A.; Haggarty, S. J., Human iPSC-derived neuronal model of tau-A152T frontotemporal dementia reveals tau-mediated mechanisms of neuronal vulnerability. *Stem Cell Rep* **2016,** *7* (3), 325-340.

238. Sydow, A.; Hochgräfe, K.; Könen, S.; Cadinu, D.; Matenia, D.; Petrova, O.; Joseph, M.; Dennissen, F. J.; Mandelkow, E. M., Age-dependent neuroinflammation and cognitive decline in a novel Ala152Thr-Tau transgenic mouse model of PSP and AD. *Acta Neuropathol Commun* **2016,** *4* (17), 1-21.

239. Maeda, S.; Djukic, B.; Taneja, P.; Yu, G. Q.; Lo, I.; Davis, A.; Craft, R.; Guo, W.; Wang, X.; Kim, D.; Ponnusamy, R.; Gill, T. M.; Masliah, E.; Mucke, L., Expression of A152T human tau causes age-dependent neuronal dysfunction and loss in transgenic mice. *EMBO Rep* **2016,** *17* (4), 530-551.

240. Coppola, G.; Chinnathambi, S.; Lee, J. J.; Dombroski, B. A.; Baker, M. C.; Soto-Ortolaza, A. I.; Lee, S. E.; Klein, E.; Huang, A. Y.; Sears, R.; Lane, J. R.; Karydas, A. M.; Kenet, R. O.; Biernat, J.; Wang, L.-S.; Cotman, C. W.; DeCarli, C. S.; Levey, A. I.; Ringman, J. M.; Mendez, M. F.; Chui, H. C.; Le Ber, I.; Brice, A.; Lupton, M. K.; Preza, E.; Lovestone, S.; Powell, J.; Graff-Radford, N.; Petersen, R. C.; Boeve, B. F.; Lippa, C. F.; Bigio, E. H.; Mackenzie, I.; Finger, E.; Kertesz, A.; Caselli, R. J.; Gearing, M.; Juncos, J. L.; Ghetti, B.; Spina, S.; Bordelon, Y. M.; Tourtellotte, W. W.; Frosch, M. P.; Vonsattel, J. P. G.; Zarow, C.; Beach, T. G.; Albin, R. L.; Lieberman, A. P.; Lee, V.

M.; Trojanowski, J. Q.; Van Deerlin, V. M.; Bird, T. D.; Galasko, D. R.; Masliah, E.; White, C. L.; Troncoso, J. C.; Hannequin, D.; Boxer, A. L.; Geschwind, M. D.; Kumar, S.; Mandelkow, E.-M.; Wszolek, Z. K.; Uitti, R. J.; Dickson, D. W.; Haines, J. L.; Mayeux, R.; Pericak-Vance, M. A.; Farrer, L. A.; Ross, O. A.; Rademakers, R.; Schellenberg, G. D.; Miller, B. L.; Mandelkow, E.; Geschwind, D. H., Evidence for a role of the rare p.A152T variant in MAPT in increasing the risk for FTD-spectrum and Alzheimer's diseases. *Hum Mol Genet* **2012,** *21* (15), 3500-3512.

241. Selenica, M. L.; Jensen, H. S.; Larsen, A. K.; Pedersen, M. L.; Helboe, L.; Leist, M.; Lotharius, J., Efficacy of small-molecule glycogen synthase kinase-3 inhibitors in the postnatal rat model of tau hyperphosphorylation. *Br J Pharmacol* **2007,** *152* (6), 959-979.

242. Srikanth, P.; Young-Pearse, T. L., Stem cells on the brain: modeling neurodevelopmental and neurodegenerative diseases using human induced pluripotent stem cells. *J Neurogenet* **2014,** *28* (1-2), 5-29.

243. Sandoe, J.; Eggan, K., Opportunities and challenges of pluripotent stem cell neurodegenerative disease models. *Nat Neurosci* **2013,** *16* (780), 1-10.

244. Sato, S.; Cerny, R. L.; Buescher, J. L.; Ikezu, T., Tau-tubulin kinase 1 (TTBK1), a neuron-specific tau kinase candidate, is involved in tau phosphorylation and aggregation. *J Neurochem* **2006,** *98* (5), 1573-1584.

245. Sang, T. K.; Jackson, G. R., Drosophila models of neurodegenerative disease. *NeuroRx* **2005,** *2* (3), 438-446.

246. Bouleau, S.; Tricoire, H., Drosophila models of Alzheimer's disease: advances, limits, and perspectives. *J Alzheimers Dis* **2015,** *45* (4), 1015-1038.

247. Blard, O.; Feuillette, S.; Bou, J.; Chaumette, B.; Frebourg, T.; Campion, D.; Lecourtois, M., Cytoskeleton proteins are modulators of mutant tau-induced neurodegeneration in Drosophila. *Hum Mol Genet* **2007,** *16* (5), 555-566.

248. Wittmann, C. W.; Wszolek, M. F.; Shulman, J. M.; Salvaterra, P. M.; Lewis, J.; Hutton, M.; Feany, M. B., Tauopathy in Drosophila: neurodegeneration without neurofibrillary tangles. *Science* **2001,** *293* (5530), 711-714.

249. Cubinkova, V.; Valachova, B.; Brezovakova, V.; Szabo, R.; Zimova, I.; Kostecka, Z.; Jadhav, S., Next generation tau models in Alzheimer's disease research - virus based gene delivery systems. *Acta Virol* **2017,** *61* (1), 13-21.

250. Lastres-Becker, I.; Innamorato, N. G.; Jaworski, T.; Rabano, A.; Kugler, S.; Van Leuven, F.; Cuadrado, A., Fractalkine activates NRF2/NFE2L2 and heme oxygenase 1 to restrain tauopathy-induced microgliosis. *Brain* **2014,** *137* (Pt 1), 78-91.

251. Sanchez-Guajardo, V.; Febbraro, F.; Kirik, D.; Romero-Ramos, M., Microglia acquire distinct activation profiles depending on the degree of alpha-synuclein neuropathology in a rAAV based model of Parkinson's disease. *PLoS One* **2010,** *5* (1), e8784.

252. Cuadrado, A.; Kugler, S.; Lastres-Becker, I., Pharmacological targeting of GSK-3 and NRF2 provides neuroprotection in a preclinical model of tauopathy. *Redox Biol* **2018,** *14*, 522-534.

253. Mirra, S. S.; Murrell, J. R.; Gearing, M.; Spillantini, M. G.; Goedert, M.; Crowther, R. A.; Levey, A. I.; Jones, R.; Green, J.; Shoffner, J. M.; Wainer, B. H.; Schmidt, M. L.; Trojanowski, J. Q.; Ghetti, B., Tau pathology in a family with dementia and a P301L mutation in tau. *J Neuropathol Exp Neurol* **1999,** *58* (4), 335-345.

254. Neha; Sodhi, R. K.; Jaggi, A. S.; Singh, N., Animal models of dementia and cognitive dysfunction. *Life Sci* **2014,** *109* (2), 73-86.

255. De Felice, F. G.; Munoz, D. P., Opportunities and challenges in developing relevant animal models for Alzheimer's disease. *Ageing Res Rev* **2016,** *26*, 112-114.

256. Ren, Y.; Sahara, N., Characteristics of tau oligomers. *Front Neurol* **2013,** *4* (102), 1-6.

257. Hindle, S. J.; Elliott, C. J., Spread of neuronal degeneration in a dopaminergic, Lrrk-G2019S model of Parkinson disease. *Autophagy* **2013,** *9* (6), 936-938.

258. Hindle, S.; Afsari, F.; Stark, M.; Middleton, C. A.; Evans, G. J.; Sweeney, S. T.; Elliott, C. J., Dopaminergic expression of the Parkinsonian gene LRRK2-G2019S leads to non-autonomous visual neurodegeneration, accelerated by increased neural demands for energy. *Hum Mol Genet* **2013,** *22* (11), 2129-2140.

259. Liu, Z.; Wang, X.; Yu, Y.; Li, X.; Wang, T.; Jiang, H.; Ren, Q.; Jiao, Y.; Sawa, A.; Moran, T.; Ross, C. A.; Montell, C.; Smith, W. W., A Drosophila model for LRRK2-linked parkinsonism. *Proc Natl Acad Sci U S A* **2008,** *105* (7), 2693-2698.

260. Chang, B.; Hawes, N. L.; Hurd, R. E.; Davisson, M. T.; Nusinowitz, S.; Heckenlively, J. R., Retinal degeneration mutants in the mouse. *Vision Res* **2002,** *42* (4), 517-525.

261. Centanin, L.; Wittbrodt, J., Retinal neurogenesis. *Development* **2014,** *141* (2), 241-244.

262. Delyfer, M. N.; Leveillard, T.; Mohand-Said, S.; Hicks, D.; Picaud, S.; Sahel, J. A., Inherited retinal degenerations: therapeutic prospects. *Biol Cell* **2004,** *96* (4), 261-269.

263. Bramall, A. N.; Wright, A. F.; Jacobson, S. G.; McInnes, R. R., The genomic, biochemical, and cellular responses of the retina in inherited photoreceptor degenerations and prospects for the treatment of these disorders. *Annu Rev Neurosci* **2010,** *33*, 441-472.

264. Dvir, L.; Srour, G.; Abu-Ras, R.; Miller, B.; Shalev, S. A.; Ben-Yosef, T., Autosomal-recessive early-onset retinitis pigmentosa caused by a mutation in PDE6G, the gene encoding the gamma subunit of rod cGMP phosphodiesterase. *Am J Hum Genet* **2010,** *87* (2), 258-264.

265. Travis, G. H., Mechanisms of cell death in the inherited retinal degenerations. *Am J Hum Genet* **1998,** *62* (3), 503-508.

266. Chang, B.; Hawes, N. L.; Pardue, M. T.; German, A. M.; Hurd, R. E.; Davisson, M. T.; Nusinowitz, S.; Rengarajan, K.; Boyd, A. P.; Sidney, S. S.; Phillips, M. J.; Stewart, R. E.; Chaudhury, R.; Nickerson, J. M.; Heckenlively, J. R.; Boatright, J. H., Two mouse retinal degenerations caused by missense mutations in the beta-subunit of rod cGMP phosphodiesterase gene. *Vision Res* **2007,** *47* (5), 624-633.

267. Phillips, M. J.; Otteson, D. C.; Sherry, D. M., Progression of neuronal and synaptic remodeling in the rd10 mouse model of retinitis pigmentosa. *J Comp Neurol* **2010,** *518* (11), 2071-2089.

268. Kubrusly, R. C.; Panizzutti, R.; Gardino, P. F.; Stutz, B.; Reis, R. A.; Ventura, A. L.; de Mello, M. C.; de Mello, F. G., Expression of functional dopaminergic phenotype in purified cultured Muller cells from vertebrate retina. *Neurochem Int* **2008,** *53* (3-4), 63-70.

269. Nakazawa, T.; Takeda, M.; Lewis, G. P.; Cho, K. S.; Jiao, J.; Wilhelmsson, U.; Fisher, S. K.; Pekny, M.; Chen, D. F.; Miller, J. W., Attenuated glial reactions and photoreceptor degeneration after retinal detachment in mice deficient in glial fibrillary acidic protein and vimentin. *Invest Ophthalmol Vis Sci* **2007,** *48* (6), 2760-2768.

270. Kaur, C.; Rathnasamy, G.; Ling, E.-A., Roles of activated microglia in hypoxia induced neuroinflammation in the retina. *J Neuroimmune Pharmacol* **2013,** *8* (1), 66-78.

271. Zeng, H.-y.; Zhu, X.-a.; Zhang, C.; Yang, L.-P.; Wu, L.-m.; Tso, M. O. M., Identification of sequential events and factors associated with microglial activation, migration, and cytotoxicity in retinal degeneration in rd Mice. *Invest Ophthalmol Visual Sci* **2005,** *46* (8), 2992-2999.

272. Sun, X. B.; Lu, H. E.; Chen, Y.; Fan, X. H.; Tong, B., Effect of lithium chloride on endoplasmic reticulum stress-related PERK/ROCK signaling in a rat model of glaucoma. *Pharmazie* **2014,** *69* (12), 889-893.

273. Kumar, A.; Midha, N.; Gogia, V.; Gupta, S.; Sehra, S.; Chohan, A., Efficacy of oral valproic acid in patients with retinitis pigmentosa. *J Ocul Pharmacol Ther* **2014,** *30* (7), 580-586.

274. Iraha, S.; Hirami, Y.; Ota, S.; Sunagawa, G. A.; Mandai, M.; Tanihara, H.; Takahashi, M.; Kurimoto, Y., Efficacy of valproic acid for retinitis pigmentosa patients: a pilot study. *Clin Ophthalmol* **2016,** *10*, 1375-1384.

275. Xin, H.; Yannazzo, J. A.; Duncan, R. S.; Gregg, E. V.; Singh, M.; Koulen, P., A novel organotypic culture model of the postnatal mouse retina allows the study of glutamate-mediated excitotoxicity. *J Neurosci Methods* **2007,** *159* (1), 35-42.

276. Marchena, M.; Villarejo-Zori, B.; Zaldivar-Diez, J.; Palomo, V.; Gil, C.; Hernandez-Sanchez, C.; Martinez, A.; de la Rosa, E. J., Small molecules targeting glycogen synthase kinase 3 as potential drug candidates for the treatment of retinitis pigmentosa. *J Enzyme Inhib Med Chem* **2017,** *32* (1), 522-526.

277. Sanchez-Cruz, A.; Villarejo-Zori, B.; Marchena, M.; Zaldivar-Diez, J.; Palomo, V.; Gil, C.; Lizasoain, I.; de la Villa, P.; Martinez, A.; de la Rosa, E. J.; Hernandez-Sanchez, C., Modulation of GSK-3 provides cellular and functional neuroprotection in the rd10 mouse model of retinitis pigmentosa. *Mol Neurodegener* **2018,** *13* (1), 1-10.

278. Patel, A. K.; Surapaneni, K.; Yi, H.; Nakamura, R. E.; Karli, S. Z.; Syeda, S.; Lee, T.; Hackam, A. S., Activation of Wnt/beta-catenin signaling in Muller glia protects photoreceptors in a mouse model of inherited retinal degeneration. *Neuropharmacology* **2015,** *91*, 1-12.

279. Schrödinger Release 2015-4 Protein Preparation Wizard; Epik version 3.4, S., LLC, New York, NY, 2015; Impact version 6.9, Schrödinger, LLC, New York, NY, 2015; Prime version 4.2, Schrödinger, LLC, New York, NY, 2015.

280. Schrödinger Release 2015-4: Maestro, v., Schrödinger, LLC, New York, NY, 2015.

281. Jorgensen, W. L.; Maxwell, D. S.; Tirado-Rives, J., Development and testing of the OPLS all-atom force field on conformational energetics and properties of organic liquids. *J Am Chem Soc* **1996,** *118* (45), 11225-11236.

282. Schrödinger Release 2015-4: LigPrep, S., LLC, New York, NY, 2015.

283. Bochevarov, A.; Harder, E.; Hughes, T.; Greenwood, J.; Braden, A.; Philipp, M.; Rinaldo, D.; Mathew, D.; Zhang, J.; Friesner, R., Jaguar: A high-performance quantum chemistry software program with strengths in life and materials sciences. *Int J Quantum Chem* **2013,** *113* (18), 2110-2142.

284. Schrödinger Release 2015-4: Jaguar, v., Schrödinger, LLC, New York, NY, 2015.

285. Becke, A. D., Density-functional thermochemistry. IV. A new dynamical correlation functional and implications for exact-exchange mixing. *J Chem Phys* **1996,** *104* (3), 1040-1046.

286. Pandey, M.; Raghuvanshi, D. S.; Singh, K. N., Microwave-assisted, solvent-free synthesis of 3′-(aryl/heteroaryl)-1-morpholinomethyl/piperidinomethylspiro[3H-indole-3,2′-thiazolidine]-2,4′(1H)-diones via 3-isatinimines. *J Heterocycl Chem* **2009,** *46* (1), 49-53.

287. Kashem, M. A.; Nelson, R. M.; Yingling, J. D.; Pullen, S. S.; Prokopowicz, A. S.; Jones, J. W.; Wolak, J. P.; Rogers, G. R.; Morelock, M. M.; Snow, R. J.; Homon, C. A.; Jakes, S., Three mechanistically distinct kinase assays compared: measurement of intrinsic ATPase activity identified the most comprehensive set of ITK inhibitors. *J Biomol Screening* **2007,** *12* (1), 70-83.

288. Willert, K.; Brown, J. D.; Danenberg, E.; Duncan, A. W.; Weissman, I. L.; Reya, T.; Yates, J. R., 3rd; Nusse, R., Wnt proteins are lipid-modified and can act as stem cell growth factors. *Nature* **2003,** *423* (6938), 448-452.